Analysis and Design of Annular Dies for Mono- and Multi-Layer Polymer Flows

By

John Perdikoulias, M.Eng, P.Eng

A thesis
presented to the University of Waterloo
in fulfilment of the
thesis requirement for the degree of
Doctor of Philosophy
in
Chemical Engineering

Waterloo, Ontario, Canada, 1997

© John Perdikoulias, 1997

National Library of Canada
Acquisitions and Bibliographic Services
395 Wellington Street
Ottawa ON K1A 0N4
Canada

Bibliothèque nationale du Canada
Acquisitions et services bibliographiques
395, rue Wellington
Ottawa ON K1A 0N4
Canada

Your file Votre référence

Our file Notre référence

The author has granted a non-exclusive licence allowing the National Library of Canada to reproduce, loan, distribute or sell copies of his/her thesis by any means and in any form or format, making this thesis available to interested persons.

The author retains ownership of the copyright in his/her thesis. Neither the thesis nor substantial extracts from it may be printed or otherwise reproduced with the author's permission.

L'auteur a accordé une licence non exclusive permettant à la Bibliothèque nationale du Canada de reproduire, prêter, distribuer ou vendre des copies de sa thèse de quelque manière et sous quelque forme que ce soit pour mettre des exemplaires de cette thèse à la disposition des personnes intéressées.

L'auteur conserve la propriété du droit d'auteur qui protège sa thèse. Ni la thèse ni des extraits substantiels de celle-ci ne doivent être imprimés ou autrement reproduits sans son autorisation.

0-612-21380-3

Canada

BORROWER'S PAGE

The University of Waterloo requires that the signatures of all persons using or photocopying this thesis. Please sign below and give address and date.

Signature	Name	Address	Date

ANALYSIS AND DESIGN OF ANNULAR DIES FOR MONO- AND MULTI-LAYER POLYMER FLOWS

ABSTRACT

A review of the current die designs used to produce annular flows is presented. An analysis of the performance of the two most commonly used designs in the coextrusion industry showed that one design exposed the polymer melt to a much lower wetted surface area thereby resulting in lower pressure and residence time within the die. This analysis lead to the development of a new type of annular die which also minimized the exposed wetted surface area in a multi-layer construction. A mathematical model based on the Control Volume Method (CVM) was developed and used to design a prototype die which was subsequently manufactured and tested. The thickness variation that was predicted by the model was slightly higher than that which was measured from samples obtained experimentally. The prototype die was also successfully used to produce film.

A smaller die was also designed using the CVM and tested. The experimental data were in good agreement with the predictions of the CVM model. The small die was also analysed using a 3D Finite Element Method (FEM) simulation. The isothermal FEM analysis predicted a lower variation than what was experimentally observed. Subsequent non-isothermal analyses could not be performed at the isothermal flow rates, due to solution instability problems, but the predictions at lower flow rates indicated larger thickness variations.

The small die was reproduced from clear acrylic and used in a visualization experiment. The experiment involved the injection of a tracer at certain points within the flow field and observing the flow path. These visualization experiments were then simulated with a particle path analysis from the FEM results. The agreement between the calculated particle paths and the observed tracer paths was good indicating that the FEM analysis was a viable method of analysing and improving the design of this type of die.

A fundamental investigation into the interfacial instability phenomenon was also performed. A series of coextrusion experiments were conducted using a carefully selected set of polymers for the purpose of differentiating the effects of Molecular Weight (MW) and Molecular Weight Distribution (MWD) on the occurrence of an interfacial instability. It was concluded that there are essentially two types of interfacial instability and that the MW had the strongest effect on the occurrence of the 'zig-zag' instability due to high interfacial stress while the MWD had a strong affect on the appearance of the 'wave' instability. The actual source of the wave instability or the mechanism could not be confirmed but the experiments did provide some new insight for future study.

ACKNOWLEDGEMENTS

I would like to thank my supervisors, Dr. Costas Tzoganakis and Dr. Alex Penlidis, for their encouragement, guidance and patience during this work.

I would also like to thank Mr. William Wybenga and Brampton Engineering for providing me with the opportunity to continue my education while pursuing a most interesting and challenging career in a dynamic research environment. A special thank you goes out to all of my co-workers who helped me with various aspects of this thesis and especially Mr. George Wright and Mr. Stephen MacEwen for their assistance with the experiments.

I would also like to acknowledge the assistance of Mr. T. Seketa and Mr. T. Kato of the Kureha Chemical Company, E.I. Du Pont De Nemours and Company, the Dow Chemical Company and Quantum Chemical Corporation for their generous material donations. I would especially like to thank Dr. Harry Mavridis for his assistance with the selection of the materials for the coextrusion experiments.

I would also like to thank Dr. Jiri Vlcek of COMPUPLAST and Dr. John Vlachopoulos of POLYDYNAMICS for donating some of the software that was used during this work.

I would like to thank my parents for their continual support and encouragement to pursue my education.

Finally, I would like to thank my wife, Helen, for her patience and my daughter, Petula, for putting it all into perspective for me.

To my family and my friends ...

TABLE OF CONTENTS

ABSTRACT iv

ACKNOWLEDGEMENTS vi

DEDICATION vii

TABLE OF CONTENTS viii

LIST OF TABLES x

LIST OF FIGURES xi

NOMENCLATURE xv

CHAPTER 1: INTRODUCTION 1
1.1 Polymer Processing 1
1.2 Mono-layer Blown Film 5
1.3 Multi-layer Blown Film 10
1.4 Current Problems 12
1.5 Objectives and Thesis Outline 16

CHAPTER 2: LITERATURE REVIEW 17
2.1 Blown Film Dies 17
2.1.1 Die Development 17
2.1.2 Mathematical Models 26
2.2 Coextrusion 35

CHAPTER 3: RESIDENCE TIME ANALYSIS 44
3.1 Residence Time Distribution 44
3.1.1 Theory 46
3.2 RTD and Pressure Drop In The Block 48
3.2.1 Port Design 48
3.2.2 Annular Design 49
3.2.3 Comparative Analysis 52
3.2.4 RTD and Flow Rate 62
3.3 Residence Time Analysis in Spiral Dies 66
3.3.1 Description of Method 66
3.3.2 Application to a Spiral Die 70
3.4 Discussion 76

CHAPTER 4: NEW FLAT SPIRAL DIE DESIGN 77
4.1 Introduction of Concept 77
4.2 Flat Spiral Modelling 88
4.3 Experimental Verification 95
4.4 Small Die Experiments 108
4.4.1 Thickness variation and CVM comparison 108
4.4.2 Visualization Experiments 115
4.4.3 Visualization Results 120
4.5 Benefits to Coextrusion 131

CHAPTER 5: FINITE ELEMENT METHOD ANALYSIS 139
5.1 FIDAP Overview 139
5.2 FEM Analysis of Small Die Thickness Variation Experiment 146
5.3 FEM Analysis of the Visualization Experiment 162
5.4 FEM and CVM Comparison. 169
5.5 Discussion 175

CHAPTER 6: INTERFACIAL INSTABILITY 181
6.1 Experimental Investigation 181
6.1.1 Equipment. 181
6.1.2 Materials 184
6.1.3 Experimental Procedure 187
6.2 Observations 188
6.3 Analysis and Simulations 196
6.4 Discussion 215

CHAPTER 7: CONCLUDING REMARKS and RECOMMENDATIONS 217
7.1 Die Design 217
7.2 Recommendations 220

REFERENCES 222

APPENDICES 228

LIST OF TABLES

Table 3.2.1 Basic Conditions and Material Properties 52
Table 4.3.1 Material Properties for Experimental Evaluation 95
Table 4.3.2 Input Parameters for the Simulation 96
Table 4.4.1 The small flat spiral design parameters. 108
Table 4.5.1 Pressure Drop and Average Residence Time through a Conventional 5 Layer die 131
Table 4.5.2 Pressure Drop and Average Residence Time through New 5 Layer die .. 134
Table 6.1.1 Molecular weight averages and ratios for the materials used in this study 185
Table 6.1.2 Viscosity characteristics of the materials used in this study. 185
Table 6.2.1 Single material coextrusion experiment with minor flow in 'A' and narrow gap 192
Table 6.2.2 Single material coextrusion experiment with minor flow in 'A' and wide gap 192
Table 6.2.3 Single material coextrusion experiment with minor flow in 'B' and narrow gap 193
Table 6.2.4 Single material coextrusion experiment with minor flow in 'B' and wide gap 193
Table 6.2.5 Two material coextrusion experiment with minor flow in 'B' and narrow gap 194
Table 6.2.6 Two material coextrusion experiment with minor flow in 'B' and wide gap 194

LIST OF FIGURES

Figure 1.1.1 A typical viscosity curve for a polymer melt 3
Figure 1.2.1 US demand for flexible packaging. 6
Figure 1.2.2 A drawing of a Blown Film line (Brampton Engineering) 7
Figure 1.2.3 A spiral mandrel die (Brampton Engineering) 9
Figure 1.3.1 A three layer spiral mandrel die (Brampton Engineering) 13
Figure 2.1.1 Some common annular dies (Michaeli,1984) 18
Figure 2.1.2 Several mandrel support systems (Michaeli,1984) 19
Figure 2.1.3 Two radial spider dies used for pipe production (Top - Richardson,1974 Bottom - Michaeli,1984) 21
Figure 2.1.4 Side fed dies used for film (top) and pipe (bottom) production 22
Figure 2.1.5 A star fed die (Whelan,1982) 23
Figure 2.1.6 A photograph of a spiral mandrel distribution system. 24
Figure 2.1.7 The orientation of weld lines in a plastic pipe produced from a radial spider die and a spiral mandrel die. 25
Figure 2.1.8 A spiral mandrel die with half the body cut away. The arrows give the direction of melt flow. 28
Figure 2.1.9 An unwrapped view of a spiral mandrel surface with 4 zones. 29
Figure 2.1.10 A perspective view of: the actual flow geometry (top) and the approximate geometry (bottom) used by Proctor (1972). 31
Figure 2.2.1 A typical coextrusion flow field. 36
Figure 2.2.2 A FEM grid of a coextrusion flow field. 36
Figure 2.2.3 Streamlines for a 50/50 ratio (top), 75/25 ratio(middle) and a 25/75 ratio (bottom) 37
Figure 2.2.4 Photograph of two coextrusion film samples on pages with writing 39
Figure 2.2.5 Photograph of two coextrusion film samples 80 mm above pages with writing. 40
Figure 2.2.6 Photograph of a magnified cross-section showing a smooth interface (bottom - run # 6) and an unstable interface (top - run # 1). 41
Figure 3.1.1 Geometry of a tube and an annulus 47
Figure 3.2.1 A drawing of a 2 layer die with a port block design 50
Figure 3.2.2 A drawing of a 2 layer die with an annular block design. 51
Figure 3.2.3 A representation of 1 tube and 4 tubes with the same average velocity. . 53
Figure 3.2.4 Pressure drop versus the number of tubes used to convey the polymer. . 54
Figure 3.2.5 A representation of a small annulus and a large annulus with the same average velocity. 56
Figure 3.2.6 Pressure drop versus the nominal annulus diameter. 57
Figure 3.2.7 A comparison of the age distribution for a tube and an annulus. 58
Figure 3.2.8 Pressure drop versus annulus diameter for a constant average velocity . 60
Figure 3.2.9 The age distribution versus nominal annulus diameter for a constant pressure drop. 61
Figure 3.2.10 Various residence times versus nominal annulus diameter. 64

Figure 3.2.11 The RTD versus flow rate for a given system. 65
Figure 3.3.1 A simple flow system divided into 6 control volumes. 68
Figure 3.3.2 The flow geometry of the spiral mandrel die. 71
Figure 3.3.3 Channel flow versus channel length for the 1 mm and 2 mm gap geometry 72
Figure 3.3.4 Average residence time distribution for the 1 mm gap geometry. 74
Figure 3.3.5 Average residence time distribution for the 2 mm gap geometry. 75
Figure 4.1.1 A single layer spiral mandrel blown film die. 78
Figure 4.1.2 A simple representation of a single layer annular die. 79
Figure 4.1.3 A simple representation of a five layer annular die. 80
Figure 4.1.4 A simple representation of a five layer 'stacked' annular die. 82
Figure 4.1.5 A typical side feed distribution system. 85
Figure 4.1.6 A flat spiral die distribution system with 4 spirals. 86
Figure 4.1.7 A cross section of a flat spiral die distribution system. 87
Figure 4.2.1 A representation of one periodic section in flat spiral distribution system 89
Figure 4.2.2 A perspective view of the geometry showing the flow field 90
Figure 4.2.3 A perspective view of the flow field showing the three different types of control volumes. 91
Figure 4.2.4 A representation of the variables associated with a type 3 control volume (flow between flat plates). 92
Figure 4.3.1 The predicted flow rate along the channel of the prototype flat spiral die (Material, Dow 2045). 97
Figure 4.3.2 The predicted pressure along the channel of the prototype flat spiral die (Material, Dow 2045). 98
Figure 4.3.3 The predicted flow variation at the end of the flat spiral distribution system (Material, Dow 2045). 99
Figure 4.3.4 The predicted flow rate along the channel of the prototype flat spiral die for the Dow 2071 and the Dow 607 materials. 100
Figure 4.3.5 The predicted pressure along the channel of the prototype flat spiral die for the Dow 2071 and the Dow 607 materials. 101
Figure 4.3.6 The predicted flow variation at the end of the flat spiral distribution for the Dow 2071 and the Dow 607 materials. 102
Figure 4.3.7 Thickness variation of the parison produced with 2045. 104
Figure 4.3.8 Thickness variation of the parison produced with 2071 and 607. 105
Figure 4.3.9 A photograph of the die with an air ring producing film. 106
Figure 4.3.10 Percent thickness variation of the 40 micron film produced with 2071 and 607. 107
Figure 4.4.1 A photograph of a small flat spiral die. 109
Figure 4.4.2 A perspective view of the small die flat spiral distribution system (above) and a cut-away view (below). 110
Figure 4.4.3 A close up view of half the cross section of the small flat spiral die. .. 111
Figure 4.4.4 The predicted flow rate along the channel. 112

Figure 4.4.5 The predicted pressure along the channel. 113
Figure 4.4.6 The predicted final flow variation. 114
Figure 4.4.7 Measured thickness variation of two parisons. 116
Figure 4.4.8 Measured thickness variation of two film samples. 117
Figure 4.4.9 A photograph of the small die manufacture from clear acrylic. 118
Figure 4.4.10 A schematic of the experimental setup. 119
Figure 4.4.11 The location of the injection points used in this experiments. 121
Figure 4.4.12 Photographs of the tracer path from injection points 1a(4.4.12a-top) and 1b(4.4.12b-bottom) 122
Figure 4.4.13 Photographs of the tracer path from injection points 2a(4.4.13a-top) and 2b(4.4.13b-bottom) 123
Figure 4.4.14 Photographs of the tracer path from injection points 3(4.4.14a-top) and 4(4.4.14b-bottom) 125
Figure 4.4.15 A sequence of photographs showing the distribution of a 'plug' of tracer injected in the right channel (1). 126
Figure 4.5.1 A conventional 5 layer spiral mandrel die. 132
Figure 4.5.2 A new stacked 5 layer flat spiral die 133
Figure 4.5.3 Comparison of wetted surface area in a conventional die with the new die 135
Figure 4.5.4 A drawing of an 8 layer flat spiral die. 137
Figure 4.5.5 A photograph of an 8 layer flat spiral die. 138
Figure 5.2.1 An isometric view of the FEM grid used for the small die 147
Figure 5.2.2 A top view of the FEM grid used for the small die. 148
Figure 5.2.3 A cross section view of the FEM grid. 149
Figure 5.2.4 FEM pressure contour plot of the small die (Isothermal analysis). 152
Figure 5.2.5 FEM pressure drop along the channel in the small die. 153
Figure 5.2.6 FEM speed variation at the exit of the small die. 154
Figure 5.2.7 FEM temperature contour plot for the small die. 155
Figure 5.2.8 FEM temperature along the channel for low, medium and high flow rates 156
Figure 5.2.9 FEM Speed variation at the exit of the small die. (Non-isothermal analysis for low, medium and high flowrates). 157
Figure 5.2.10 FEM speed along the spiral channel centerline (Isothermal conditions) 159
Figure 5.2.11 Velocity vector plots through a cross section of the die. 160
Figure 5.2.12 Closeup view of a velocity vector plot through a cross section of half the die 161
Figure 5.3.1 An isometric view a particle plot for the small die. 164
Figure 5.3.2 FEM particle traces from injection points 1a (top) and 1b (bottom). .. 165
Figure 5.3.3 FEM particle traces from injection points 2a (top) and 2b (bottom). .. 166
Figure 5.3.4 FEM particle traces from injection points 3a (top) and 4b (bottom). .. 167
Figure 5.3.5 FEM particle path of the flow in the right channel. 168
Figure 5.4.1 FEM channel speed for power law index 1.0, 0.7, 0.5 and 0.3. 171

Figure 5.4.2 FEM exit speed variation for power law index 1.0, 0.7, 0.5 and 0.3. . . 172
Figure 5.4.3 CVM channel speed for power law index 1.0, 0.7, 0.5 and 0.3. 173
Figure 5.4.4 CVM exit flow variation for power law index 1.0, 0.7, 0.5 and 0.3. . . . 174
Figure 5.4.5 Particle trace for power law index =1.0. 177
Figure 5.4.6 Particle trace for power law index =0.7. 178
Figure 5.4.7 Particle trace for power law index =0.5. 179
Figure 5.4.8 Particle trace for power law index =0.3. 180
Figure 6.1.1 A representation of the narrow exit gap geometry. 182
Figure 6.1.2 A representation of the wide exit gap geometry. 183
Figure 6.1.3 A comparison of the relative MWD's for the polymers used in this study 184
Figure 6.1.4 A comparison of the shear viscosity for the materials used in this study 186
Figure 6.2.1 A photograph showing a 'zig-zag' interfacial instability. 189
Figure 6.2.2 A photograph of a film sample exhibiting a 'wave' type instability. . . 191
Figure 6.3.1 Shear stress along the interface for a 10/90 ratio of NA957. 197
Figure 6.3.2 Exit shear stress versus layer ratio for broad MWD materials. 199
Figure 6.3.3 Exit shear stress versus layer ratio for narrow MWD materials 200
Figure 6.3.4 Velocity contours for an A:B ratio of 12:88 for NA960 in both layers . 202
Figure 6.3.5 Streamlines for an A:B ratio of 12:88 for NA960 in both layers. 203
Figure 6.3.6 Velocity contours for an A:B ratio of 8:92 for NA960 in both layers . . 204
Figure 6.3.7 Streamlines for an A:B ratio of 8:92 for NA960 in both layers. 205
Figure 6.3.8 Velocity contours for an A:B ratio of 88:12 for NA960 in both layers . 206
Figure 6.3.9 Streamlines for an A:B ratio of 88:12 for NA960 in both layers 207
Figure 6.3.10 Velocity contours for an A:B ratio of 92:8 for NA960 in both layers . . 208
Figure 6.3.11 Streamlines for an A:B ratio of 92:8 for NA960 in both layers 209
Figure 6.3.12 Velocity ratio versus layer ratio with A as the minor layer. 211
Figure 6.3.13 Velocity ratio versus layer ratio with A as the major layer. 212
Figure 6.3.14 A comparison of the elongational viscosity of the materials used in this study 214

NOMENCLATURE

b	viscosity temperature coefficient
D,d	diameter or length
E	exit age distribution
k	radius ratio
m	consistence coefficient
n	power-law index
P	pressure
Q,q	flow rate
R	radius
S	gap
t	time
T	temperature
To	reference temperature
u	velocity vector
V	velocity
$\dot{\gamma}$	shear rate
λ	maximum velocity position ratio
η	viscosity
τ	extra stress tensor
θ	dimensionless time

CHAPTER 1

INTRODUCTION

1.1 Polymer Processing

Polymer processing involves the conversion of virgin polymer into useful products. The polymer producers, (DOW, DUPONT, ESSO etc) supply the polymer in the form of beads, pellets or granules. The polymer processor then converts these into the useful, everyday objects which we are accustomed to or into forms that are used by subsequent converters. The general area of polymer processing can be roughly divided into two categories. One category, often referred to as extrusion, contains the processes which produce products with a constant cross section and infinite length. Examples of such processes include the production of film, sheet, tubing, pipe, automotive trim, vinyl siding, etc. Such processes produce the product on a continuous basis and the product is either wound on a winder or cut to the desired length. The other category contains processes such as injection moulding and blow moulding which are used to make products of irregular shape. The reader is referred to several good texts on the subject of polymer processing (Middleman ,1977; Rauwendaal, 1986; Tadmor and Gogos ,1979). This study will focus on the Tubular or Blown Film process which falls into the extrusion category. However, many of the ideas and concepts presented in this study can be applied to practically all areas of polymer processing.

Polymer melts exhibit complex flow phenomena which make the mathematical

modelling of their flow behaviour very difficult. One of the most important characteristics applicable to this study is the shear thinning nature of polymer melts.

Figure 1.1.1 is a typical plot of the viscosity versus the shear rate for a non-Newtonian fluid (polymer melt). The viscosity of a Newtonian fluid is constant for any shear rate. The viscosity of a non-newtonian fluid however, is a function of the shear rate. Polymers typically exhibit a 'Newtonian plateau' at very low shear rates but are shear thinning at the shear rates encountered during extrusion. The most common method of modelling this behaviour is the so called 'power - law' model. The logarithm of the viscosity versus the logarithm of the shear rate is the most common plot. However, in some instances the shear rate is substituted by the shear stress which is simply the product of the viscosity and that shear rate. Over small ranges of the shear rate (2 or 3 decades), the curve can be approximated by a straight line which follows a power function:

$$\eta = m \dot{\gamma}^{n-1} \qquad (1.1)$$

where η is the viscosity and $\dot{\gamma}$ is the shear rate. The coefficient m is often referred to as the 'consistency index'. The parameter, n, is called the power-law index and indicates the degree of non-Newtonian behaviour exhibited by the polymer melt. The value of the power-law index typically ranges from about 0.3 for polystyrenes to 0.5 for polyethylenes to 0.7 for polyamides. A Newtonian fluid, such as water, would have a power-law index of 1.0. The application of this model also usually involves the specification of a truncation shear rate which is used to represent the constant viscosity plateau that is generally observed at low shear rates.

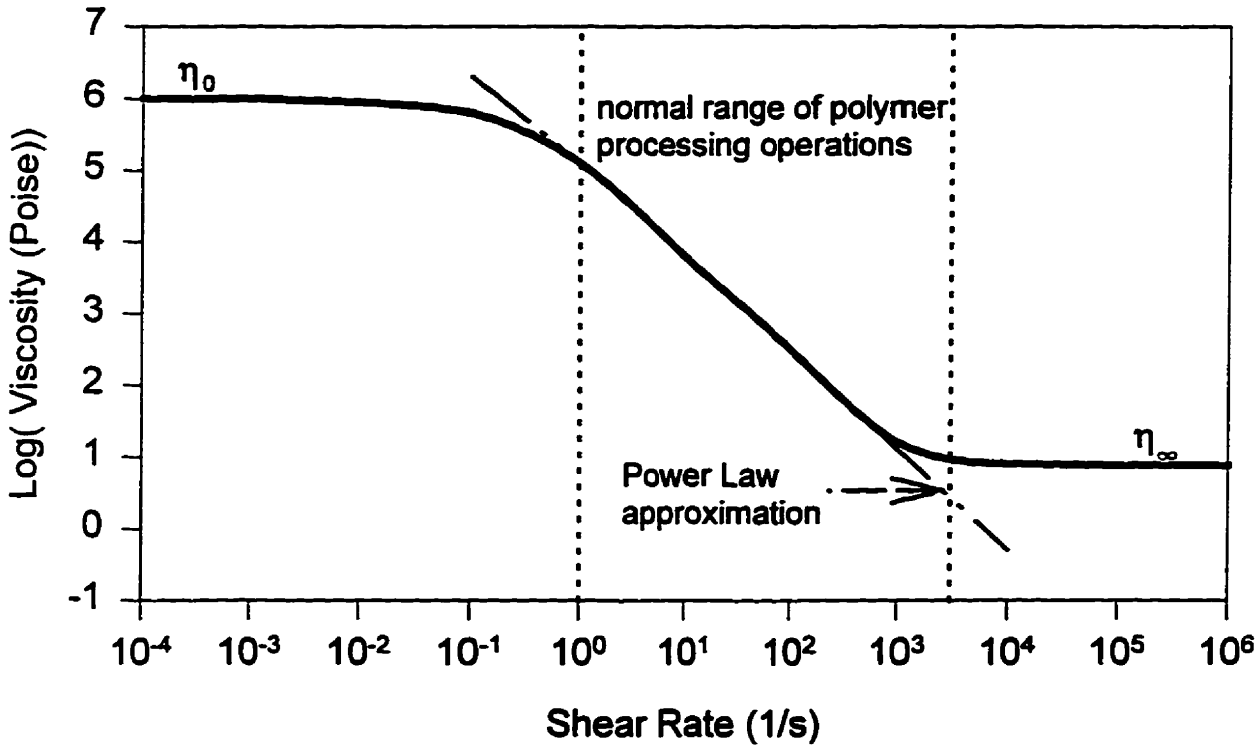


Figure 1.1.1 A typical viscosity curve for a polymer melt

The viscosity of a polymer melt also depends on the temperature. An increase in temperature will lower the viscosity but with only a small effect on the slope of the viscosity curve. That is, for small temperature variation (20-30 C °), the power-law index (n) remains relatively constant. The net effect is a shift in the plot which is commonly taken into account with the equation:

$$m = m_o \, e^{(-b(T - T_o))} \qquad (1.2)$$

where m_o is the consistency index at the reference temperature T_o. The coefficient b describes the magnitude of the effect of temperature on viscosity.

Equations 1.1 and 1.2 are the most commonly used for describing the flow behaviour of polymer melts. They provide satisfactory results when used properly in the analysis of closed channel flows. Of course, there are many other models or constitutive equations that have been proposed for the purposes of modelling the polymer viscosity. The reader is referred to the literature for more details on this subject (Brydson, 1981; Dealy and Wissbrun, 1990; Tadmor and Gogos ,1979). The more complex models may provide a more accurate description of the rheological behaviour of the polymer melt but they are also typically more difficult to apply. However, the increasing use of numerical techniques is making it easier to use more complex constitutive equations.

The viscosity versus shear rate and temperature data should always be used when designing polymer processing equipment and not the **melt index** (M.I.). The melt index is a commonly used, industry developed, method of describing the viscosity of a polymer melt. Although, it has the advantage of being easy, quick and inexpensive, it can be misleading.

The melt index, described by ASTM D1238, is basically the amount of material that will flow through a specific size capillary under a specific force in ten (10) minutes. It represents a single point on the viscosity curve and as such it does not give any indication of the shear thinning nature of the polymer. However, in many cases, the only available information regarding the viscosity of a polymer is the melt index. Shenoy et al (1983) and Shenoy and Saini (1985,1986) have done a substantial amount of work on master viscosity curves, for many different polymers, which can be used to construct a viscosity curve from the melt index.

1.2 Mono-layer Blown Film

The blown film process is the process by which almost all commodity LDPE film is produced. A study by Munstedt and Wolter (1993) indicates that 75% of the 5.5 million tonnes of LLDPE and LDPE consumed in Western Europe in 1992 was used in film or sheet production. It is estimated that 70 - 80% of this was produced by the blown film process. The March 1988 issue of *Paper, Film, & Foil Converter* magazine stated that 2.9 billion kg of polyolefins were sold for film extrusion in the United States in 1987 and that this market consumes one fourth of all polyolefins sold. A *Plastics News* survey of 193 US film and sheet manufacturers published in the September 1996 issue reported that the film market had a least $12.4 billion dollars in sales from a production rate of over 4 billion kg. The May 1996 issue of *Plastics News* reported US demand for flexible packaging which is shown in Figure 1.2.1.

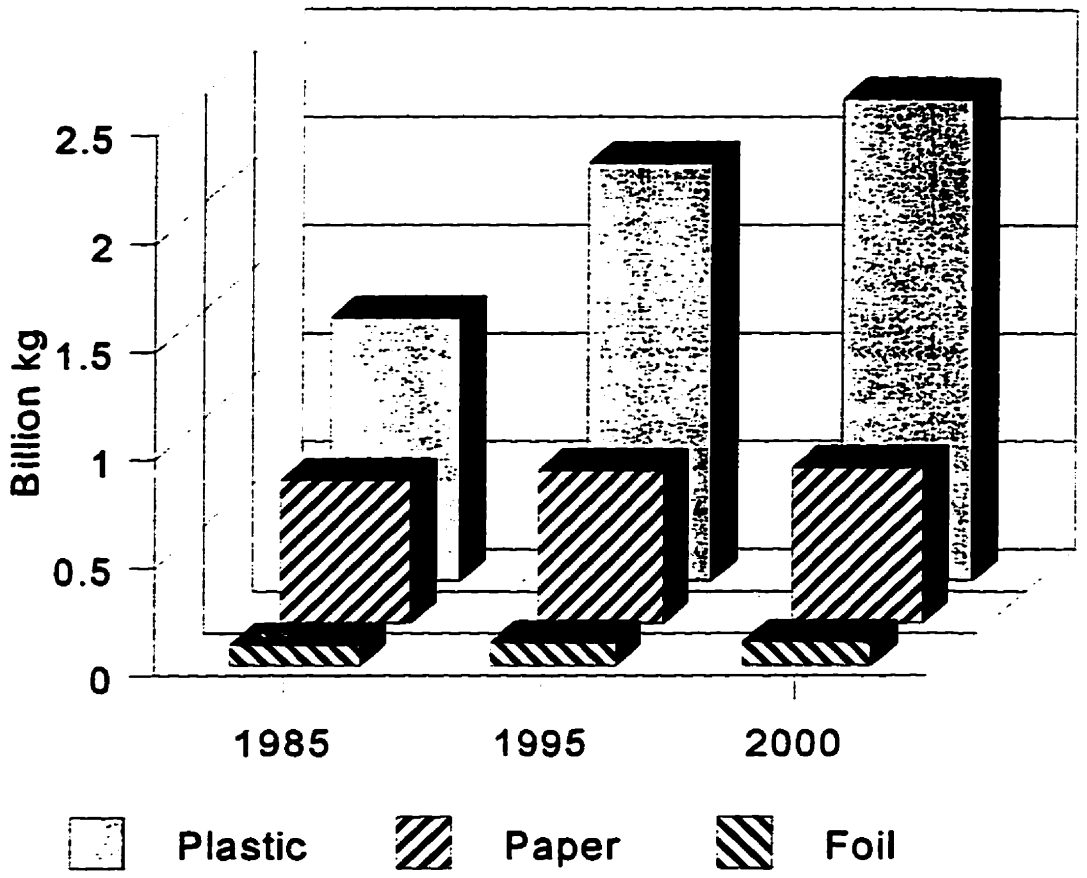


Figure 1.2.1 US demand for flexible packaging.

It is quite evident that plastics is the dominant material and has the strongest growth. The magnitude of these numbers means that even small improvements in the efficiency of the blown film process can lead to significant savings and justifies further research in this area.

A schematic of the blown film process is shown in Figure 1.2.2. The main components of this system are the extruder, die, air ring, upper nip/collapsing frame , and winders. Resin is fed through a hopper into the extruder (screw pump) where it is melted,

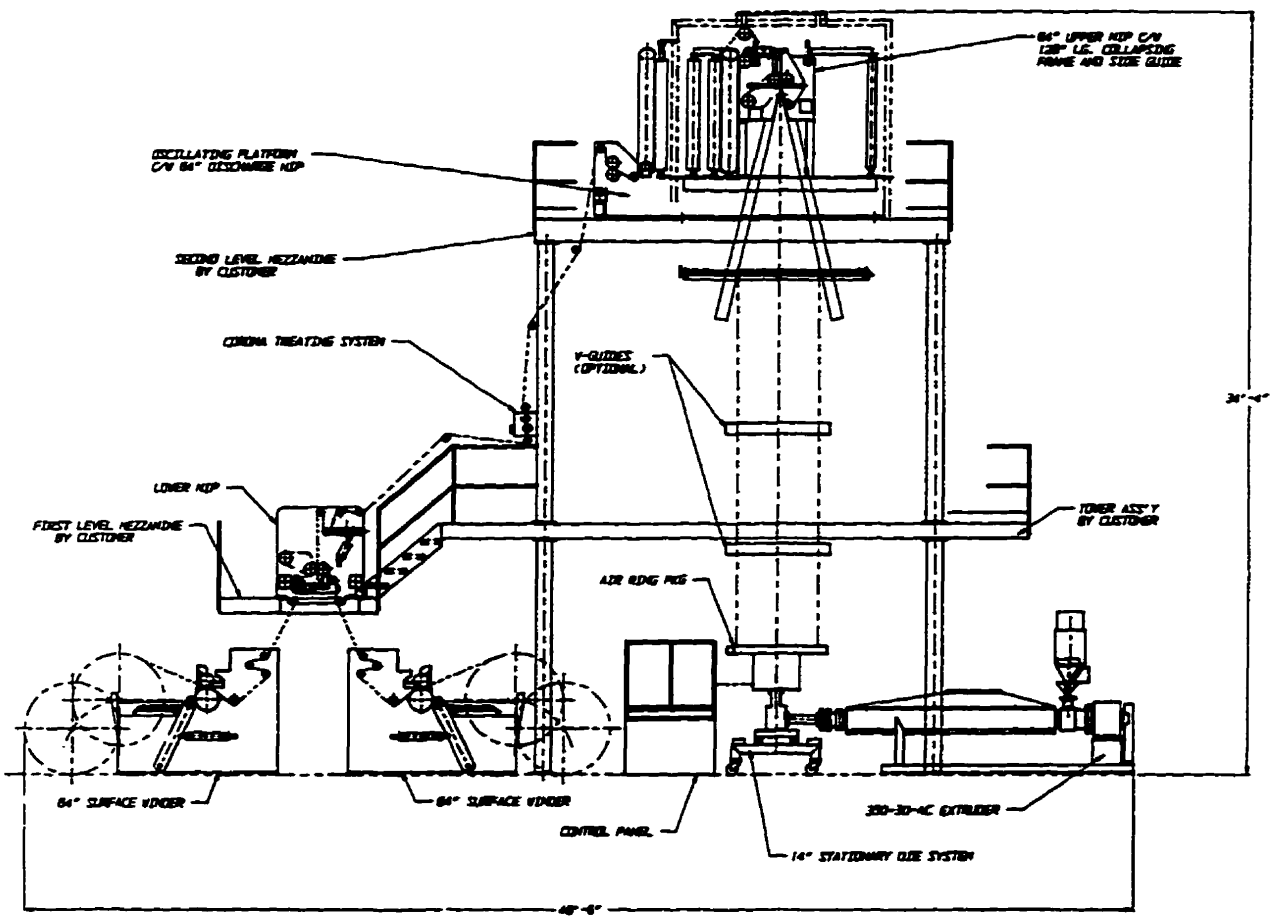


Figure 1.2.2 A drawing of a Blown Film line (Brampton Engineering)

homogenized and pressurized. The pressure then forces the molten polymer through adapters to the block which, in most cases, directs the flow upwards. The polymer melt then flows into the die, which is sitting on top of the block. Figure 1.2.3 is a drawing of a typical spiral mandrel die used in the production of blown film. The ports direct the melt from the centre feed port to the spirals where it is uniformly distributed. The melt flows into a relaxation chamber and then through a small annular gap for sizing before it exits from the die. The rollers or nips at the top of the collapsing frame pull the polymer upwards as it exits the die. The air ring directs large volumes of high velocity air onto the surface of the polymer melt in order to cool it. The point at which the polymer begins to solidify is called the frost line and generally occurs about 2 to 4 die diameters above the die. The height of the tower is determined by the height required for the inner surface of the bubble to reach a low enough temperature so that it will not seal itself when it is pinched at the nips. Tower heights can vary from 5m to 20m. The size of the bubble is controlled by the volume of air that is trapped inside. After the bubble has been flattened at the nips, it is collected on a winder. In some instances, the film is fed directly into printing and bag making machinery.

Extruder sizes refer to the diameter of the screw and are commonly 50 mm to 150 mm. Die sizes refer to the diameter of the final annular gap or "die lips". The sizes that have been manufactured in the past range from about 20 mm to over 2000 mm. The diameter of the lips depends on the size of the bubble to be produced and the corresponding blow-up and draw-down ratios for a particular polymer and application. The blow-up ratio (BUR) is the ratio between the bubble diameter and the diameter of the die lips. The draw-down ratio (DDR) is the ratio between the cross sectional area of the final annular die gap and the

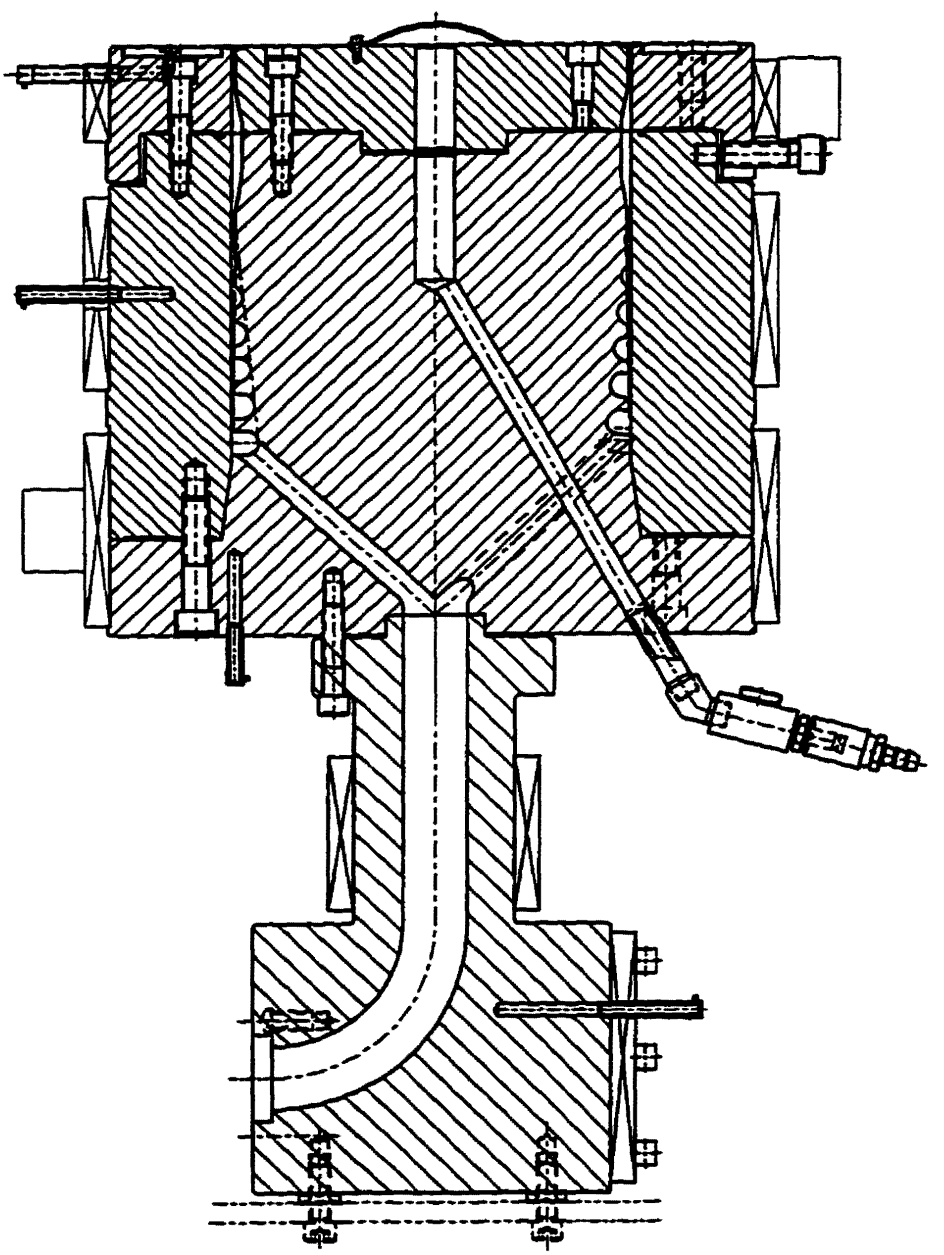


Figure 1.2.3 A spiral mandrel die (Brampton Engineering)

cross sectional area of the film that is produced. The BUR and DDR are used to control the mechanical properties of the film in both the transverse and machine directions.

1.3 Multi-layer Blown Film

High barrier flexible packaging is a rapidly growing area of polymer processing. The September, 1996 issue of *Plastics World* reported that a study by Mastio & Co. estimated the PE film business to account for 5.9 billion kg of resin with 30% of this going into coextrusion applications. Further, it is projected that this will increase to 8.2 billion kg by the year 2000. Technological advances in both machinery and resin design have made blown film coextrusion a viable method of obtaining many different structures. The greatest advantage of coextrusion comes from the ability to combine the significant properties of many materials into one structure. The most practical aspects of this, with no doubt, occur in the food packaging industry. One can begin to understand the importance of developing cost efficient packaging if one considers that approximately 50% of the food in third world countries spoils for lack of proper packaging as opposed to 1% in more industrialized nations (Hinsken, 1987).

A multi-layer barrier structure generally consists of a relatively expensive barrier resin coextruded between a less expensive structural resin. In most cases, the barrier resin restricts the transmission of oxygen into the package to prevent the food from spoiling. The barrier resin may also prevent flavours and odours from leaving the package. The structural resin is generally a polyolefin and is primarily used to add strength to the package and protect the barrier layer. For barrier polymers such as ethylene vinyl alcohol (EVOH) and

many polyamides, the barrier properties diminish in the presence of moisture. Polyolefins are generally good moisture barriers and as such have an additional function in protecting the barrier layer from moisture. In cases where the barrier resin does not adhere to the structural resin, an additional adhesive layer is employed. The choice of materials for the structural layers depends on the package requirements and may be different on either side of the package. In addition to protecting the food from oxygen, the package must also handle properly through the packaging equipment for efficient production.

Up to now most of this discussion has been directed to gas barrier in the food industry; however, significant markets exist elsewhere. Milk packaging, for instance, requires a dark UV barrier which could be sandwiched between layers of white film for a more aesthetically pleasing container. Agricultural film, which reduces produce growing time by as much as 6 weeks and increases yield by 30%, is a growing area in coextrusion. Silage bags, which are portable and provide the proper environment for grain fermentation, is another present day market.

Other coextrusion benefits come from combining commodity resins to obtain high strength and barrier properties without giving up the required surface properties and printability. It has been reported (Gates ,1989) that a coextruded film (all layers containing the same material) is about 10% stronger than a mono-layer film of the same material. This implies that one can down gauge to produce more of a thinner product with the same properties as the mono-layer product. Others have found that a three layer structure consisting of one layer of linear low density polyethylene (LLDPE) and two layers of high molecular weight high density polyethylene (HMW-HDPE) can be made to the same

thickness as a mono-layer HMW-HDPE keeping the same strength but adding the gloss and print appeal of LLDPE (Sneller, 1987). Another example of the benefits of coextrusion involves 50 lb (23 kg) sacks for dry powder pharmaceuticals. One company was able to replace the standard 3 mil (76 micron) LLDPE film with a 1.4 mil (36 micron) coextruded structure (HMW-HDPE/LLDPE/HMW-HDPE). This is a significant reduction in raw material usage.

The coextrusion blown film process is very similar to the single layer process with the added requirement that the die combines the layers from different extruders. A three layer spiral mandrel blown film die is shown in Figure 1.3.1. Of course the design of the die becomes more complicated but up until the point where the layers combine, each layer can be considered as a single layer die. The additional equipment requirements in coextrusion is related to the number of different polymers that are coextruded (each polymer requires its own extruder). All of the equipment past the die is virtually identical to that in a single layer process.

1.4 Current Problems

Although synthetic polymers have been around for many years, there still exist many processing problems. Even today, the processing of some polymers is considered more of an art than a science. The reason for this is that most industrial problems are solved by the processors themselves (sometimes the equipment operators) through trial-and-error and no scientific reasoning. Once a solution has been found, the competitive nature of the business inhibits the transfer of this information from industry to research institutes. In fact,

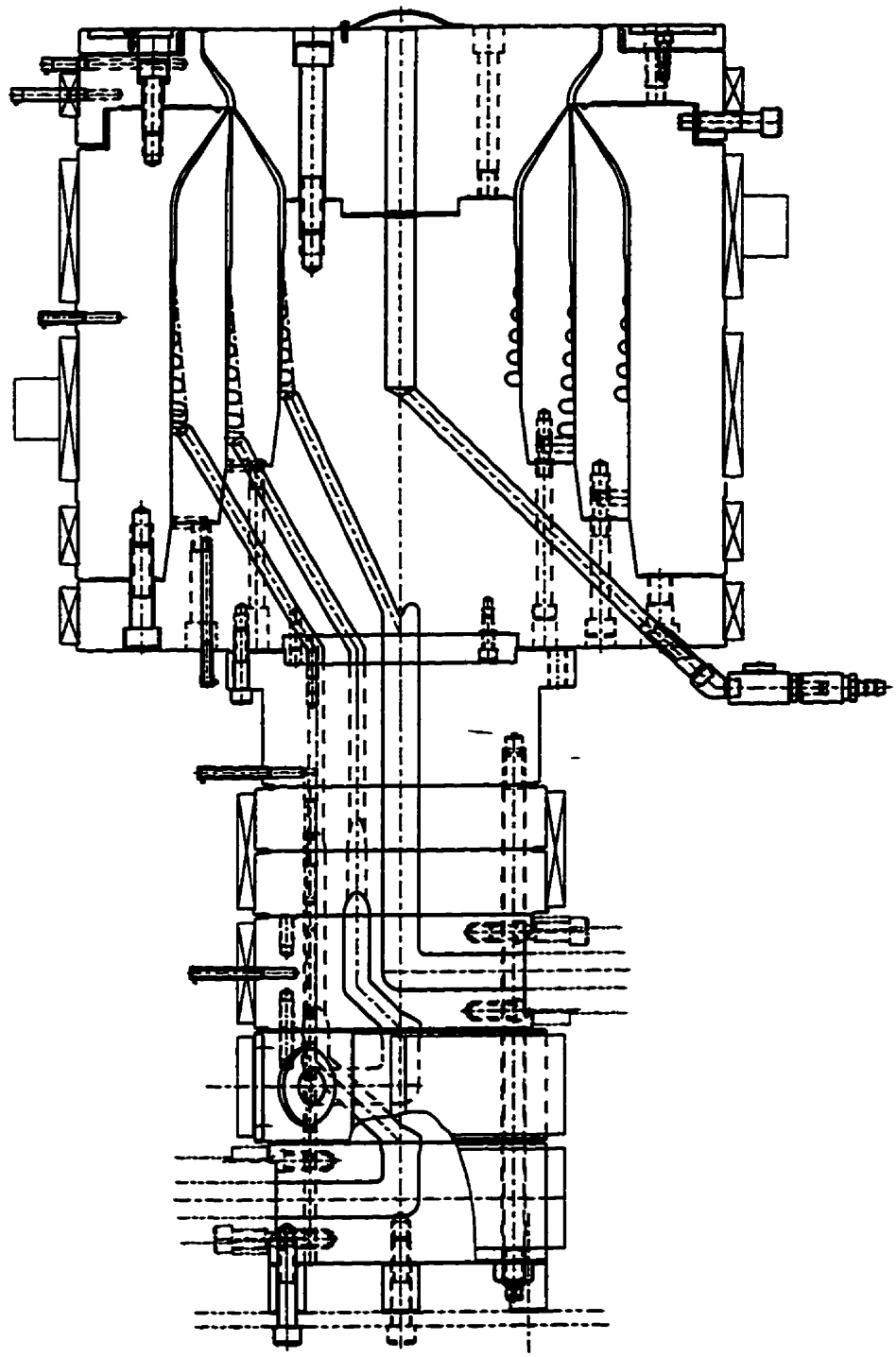


Figure 1.3.1 A three layer spiral mandrel die (Brampton Engineering)

polymer processors commonly prevent the manufacturers of the equipment from observing their production techniques or monitoring the equipment performance after the initial installation. This limits the amount of feedback that the machinery manufacturer receives and severely impedes the learning process. The rapid introduction of new polymers also makes it impossible to study all of them and understand their particular processing behaviour. This is why mathematical modelling and process simulation have been readily accepted by industry.

In the past, all polymer processing machinery was designed by trial-and-error (experience) using 'steel safe' designs. This means that the designer considered the possibility that modifications may be required and left enough excess steel on the die for these modifications. It was not uncommon for a typical die to be modified 8-10 times before an adequate product could be produced. As people became more and more experienced with the behaviour and processing requirements of a particular polymer, the equipment design process became more efficient. Unfortunately, when a new polymer was developed the complete design process had to start again from the trial-and-error stage. This is where a mathematical model offers definite advantages. An accurate mathematical model can replace a large portion of difficult and expensive experiments. It is much easier, and cheaper, to change a dimension in a data file than to physically alter it on the die. The savings in cost, and time, allow the design engineer to explore many more designs in order to find an optimum design rather than a satisfactory design. However, one of the biggest problems associated with the mathematical modelling of extrusion dies is the lack of experimental data to verify these models.

The new resins that are constantly being developed have brought with them even more processing problems. Although having much improved physical properties, they also require more stringent equipment design and processing conditions. Previously unused design criteria, such as the residence time distribution, are becoming more and more important. Mathematical modelling of these processes has to keep up with the requirements of the polymers. In the past, low and high density polyethylene were basically the only types of polymers to flow through spiral mandrel dies. The system pressures were high (35-50 MPa) and the outputs were low (0.4 - 0.5 kg per mm of die diameter), by today's standards, as were the physical properties of the plastic film produced. Also, the blown film dies were more dedicated to one or two materials. Today's typical blown film dies operate at much lower pressures (15-30 MPa) and higher outputs (.8 - 1.2 kg per mm of die diameter) producing better quality film. The improved physical properties of the film is primarily due to the new polymers being developed. However, the new polymers need better die design. An additional requirement of new dies is the ability to process a variety of polymers with a minimum residence time so that colour and resin changes may be performed with a minimum of waste. This is especially important in coextrusion processes where the design of the die is much more complicated and the demands placed on the die's performance more stringent. The coextrusion process also brings with it some additional processing problems such as the requirement for much better thickness uniformity, interfacial instabilities and materials that are more difficult to process due to their low thermal stability and small processing windows.

1.5 Objectives and Thesis Outline

The main objective of this thesis was to obtain a detailed understanding of the fundamental requirements of a blown film extrusion die and apply this knowledge towards the creation of an improved design. Special emphasis was placed on the applicability of this research towards improving the coextrusion processes since it is somewhat more complex and it has attracted limited fundamental study.

A systematic approach towards fulfilling the objectives is presented in the following chapters. Chapter 2 will review the development of die designs over the years and outline the various modelling techniques that have been developed. Chapter 3 contains a more detailed analysis of coextrusion dies with respect to their fundamental purpose and current design deficiencies. In Chapter 4, a new die design that is better suited to the needs of coextrusion applications is proposed which minimizes the deficiencies determined in Chapter 3. A Control Volume Method (CVM) simulation of the new distribution system is developed to assist with the design procedure. The mathematical model is used to design a prototype system which is consequently manufactured and tested. In addition, this chapter presents the results of a set of visualization experiments that were performed in order to better understand the flow field. Chapter 5 presents the results from a Finite Element Analysis (FEM) of the distribution system used in the visualization experiments of Chapter 4. In addition, the FEM results are compared to the CVM results in this chapter. Chapter 6 presents some fundamental coextrusion experiments which have provided valuable new insight into the interfacial instability phenomena. Finally, Chapter 7 presents a list of conclusions and recommendations for future study.

CHAPTER 2

LITERATURE REVIEW

2.1 Blown Film Dies

The die is considered to be the heart of the extrusion process so it is important to understand its design and to have a detailed understanding of the flow behaviour of the polymer melt within it. The purpose of the blown film die is to take the polymer melt from the extruder and form a uniform annular flow stream. It is also very important that this is done with a minimum residence time in the die. Today, virtually all blown film dies employ the spiral mandrel concept and so its development and design will be discussed in detail. The reader is referred to a very good text book by Michaeli (1984) for more details about extrusion die design in general.

2.1.1 Die Development

The purpose of the spiral mandrel die is to form an annular polymer flow stream. To understand the function of the spiral mandrel design, it will be helpful to consider the initial methods used to produce an annular flow. An annular flow path is formed with two concentric circular pieces of steel. The outer piece is called the body and the inner piece is often referred to as the mandrel. The mandrel must be physically supported to the body to remain concentric. There are several ways to do this, the most common of which are shown in Figure 2.1.1. Several variations of the mandrel support die are shown in Figure 2.1.2.

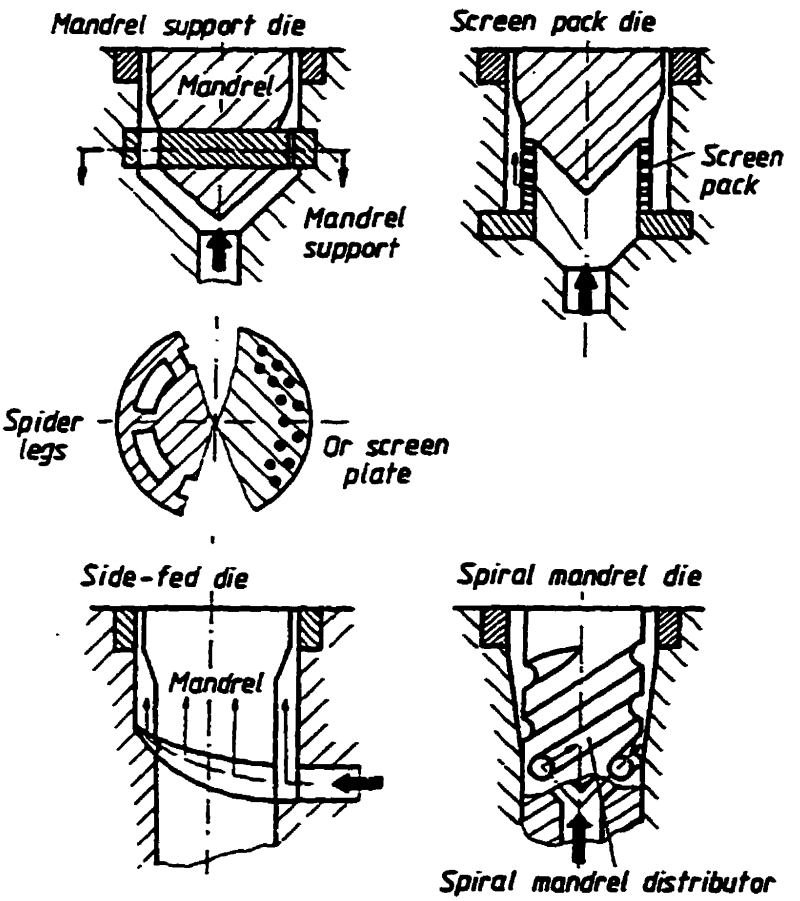


Figure 2.1.1 Some common annular dies (Michaeli, 1984)

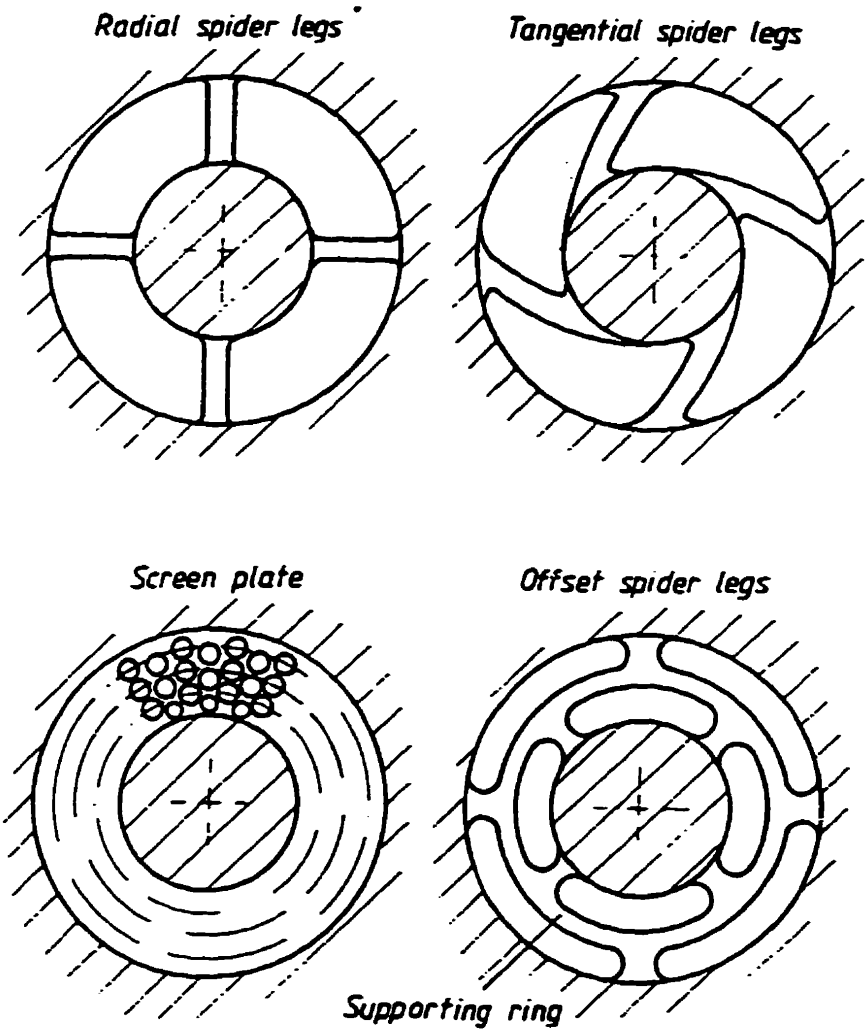
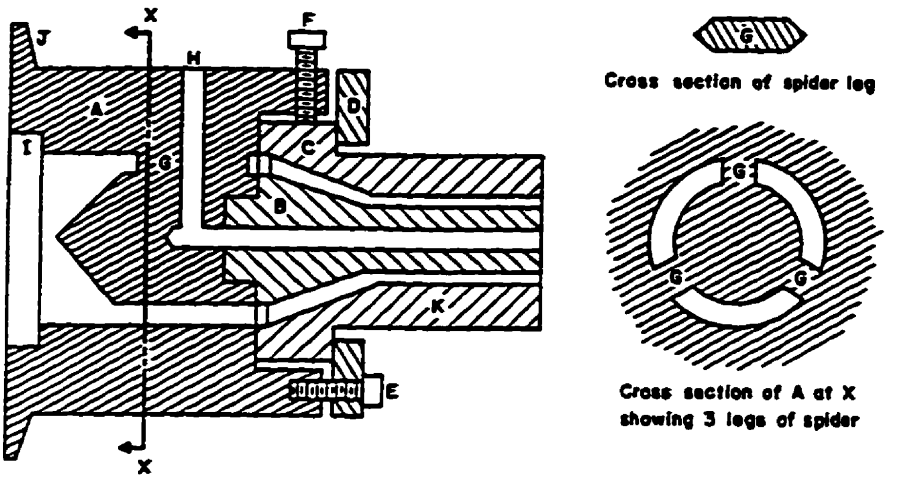


Figure 2.1.2 Several mandrel support systems (Michaeli,1984)

In the pipe and tubing industry, the most common method is to use the radial spider legs to support the mandrel from the body. Two typical spider type dies are shown in Figure 2.1.3 The disadvantage of this die is that the polymer melt must flow around the spiders and then recombine, thus forming of a weld line. For the relatively thick walled pipe, the weld lines are sometimes tolerated but they severely detract from the mechanical properties of the film. The various mandrel support systems shown in Figure 2.1.2 are attempts to reduce the effect of the weld line. In the case of side fed dies, shown in Figure 2.1.4, the mandrel is supported by the body at a point before the annulus. Now, the polymer melt must flow around the mandrel eliminating all the weld lines except the one that occurs on the opposite side from where the melt enters the die. The concept of supporting the mandrel before the annulus was used in the 'star feed' die shown in Figure 2.1.5. The radial tubes or ports direct the melt to the annulus from an inlet tube at the centre of the die. This method is no better than the previous two since a weld line is created wherever flow fronts combine. Helical grooves or spirals, as they are commonly called, were cut into the mandrel in an effort to smear the polymer and reduce the effect of the weld lines. A typical spiral mandrel distribution system is shown in Figure 2.1.6. The polymer melt travels through radial ports to the spirals where it flows in a helical path while it simultaneously leaks out of the spirals and into the annular path between the mandrel and the body. Actually, the weld lines are still present but with a different orientation as depicted in Figure 2.1.7. With spider, sidefed and star type dies, the weld lines are in a plane, through the melt, that goes radially through the die axis. In a spiral die the weld lines travel from the outer surface of the annulus to the inner surface in a circular fashion. This is caused by the layering effect which assists in



A. Die body
B. Mandrel, pin, male die part
C. Die, die bushing, female die part
D. Die retaining ring
E. Die retaining bolt
F. Die centering bolt
G. Spider leg
H. Air hole
I. Seat for breaker plate
J. Ring for attachment to extruder
K. Die land

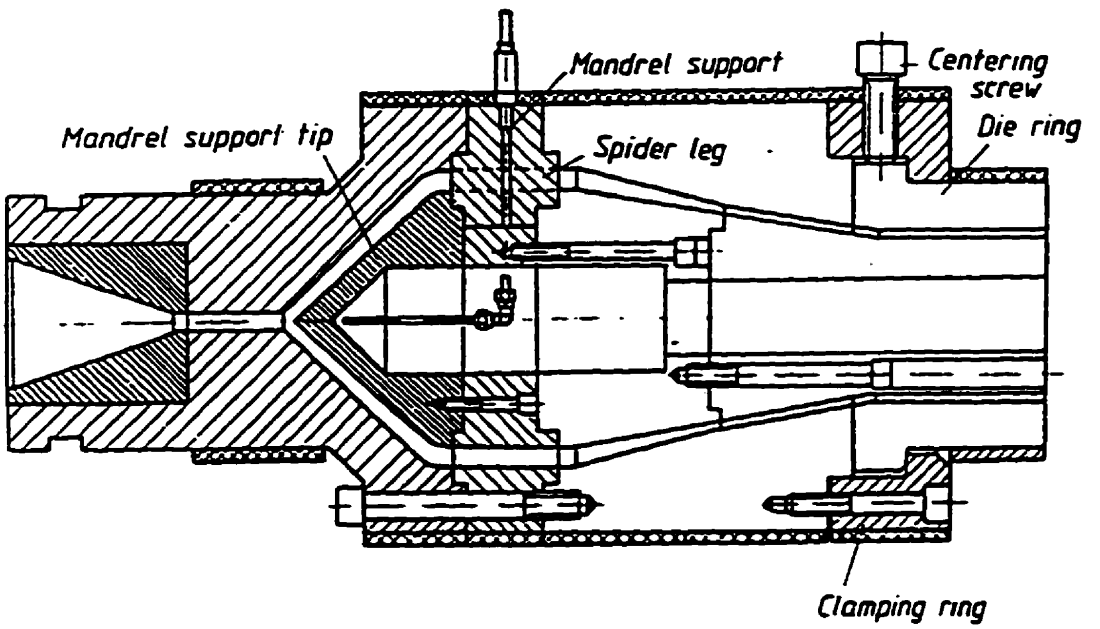
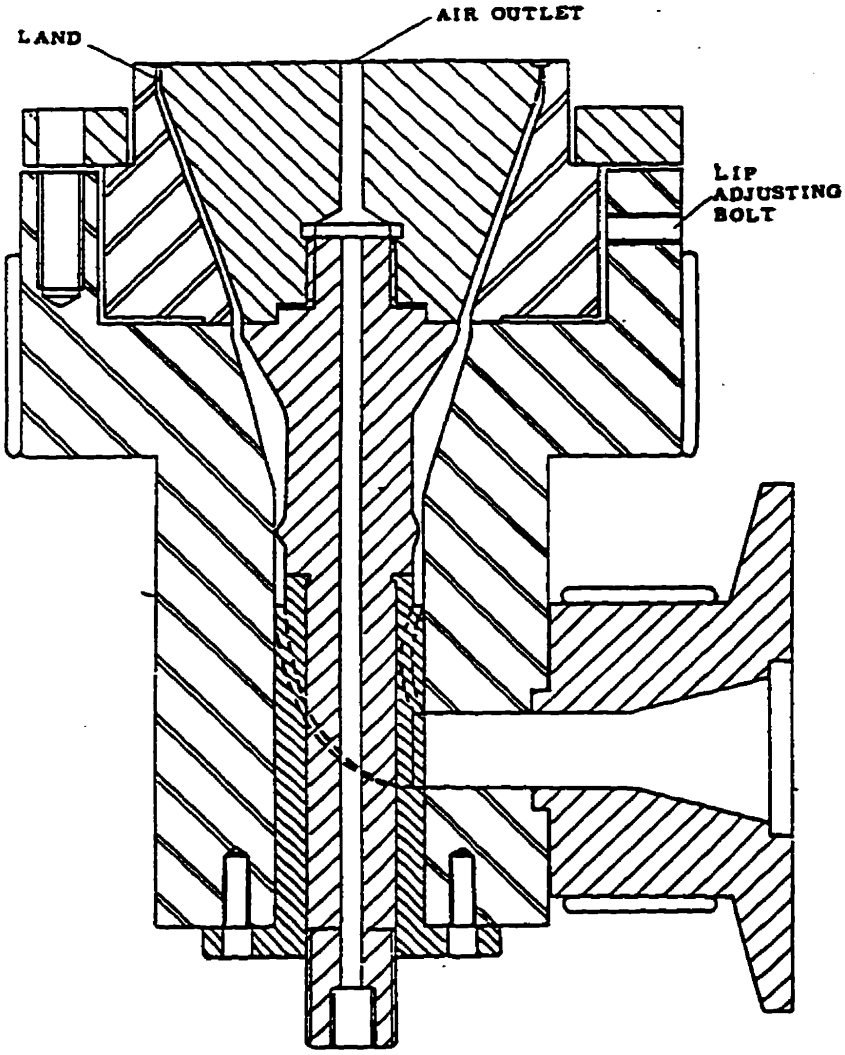
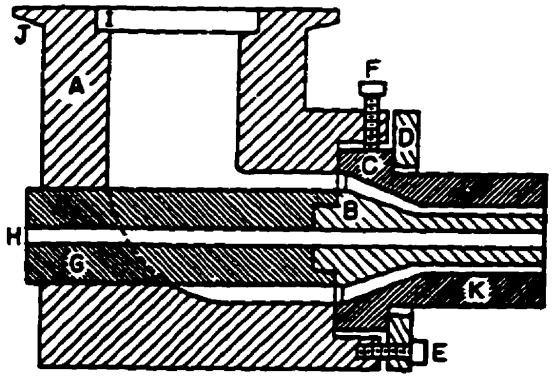


Figure 2.1.4 Two radial spider dies used for pipe production (Top - Richardson, 1974 Bottom - Michaeli, 1984)





A. Die body, crosshead
B. Mandrel, pin, male die part
C. Die, die bushing, female die part
D. Die retaining ring
E. Die retaining bolt
F. Die centering bolt
G. Mandrel holder
H. Air hole
I. Seat for breaker plate
J. Ring for attachment to extruder
K. Die land

Figure 2.1.4 Side fed dies used for film (top) and pipe (bottom) production (top - Michaeli,1984; bottom - Whelan,1982)

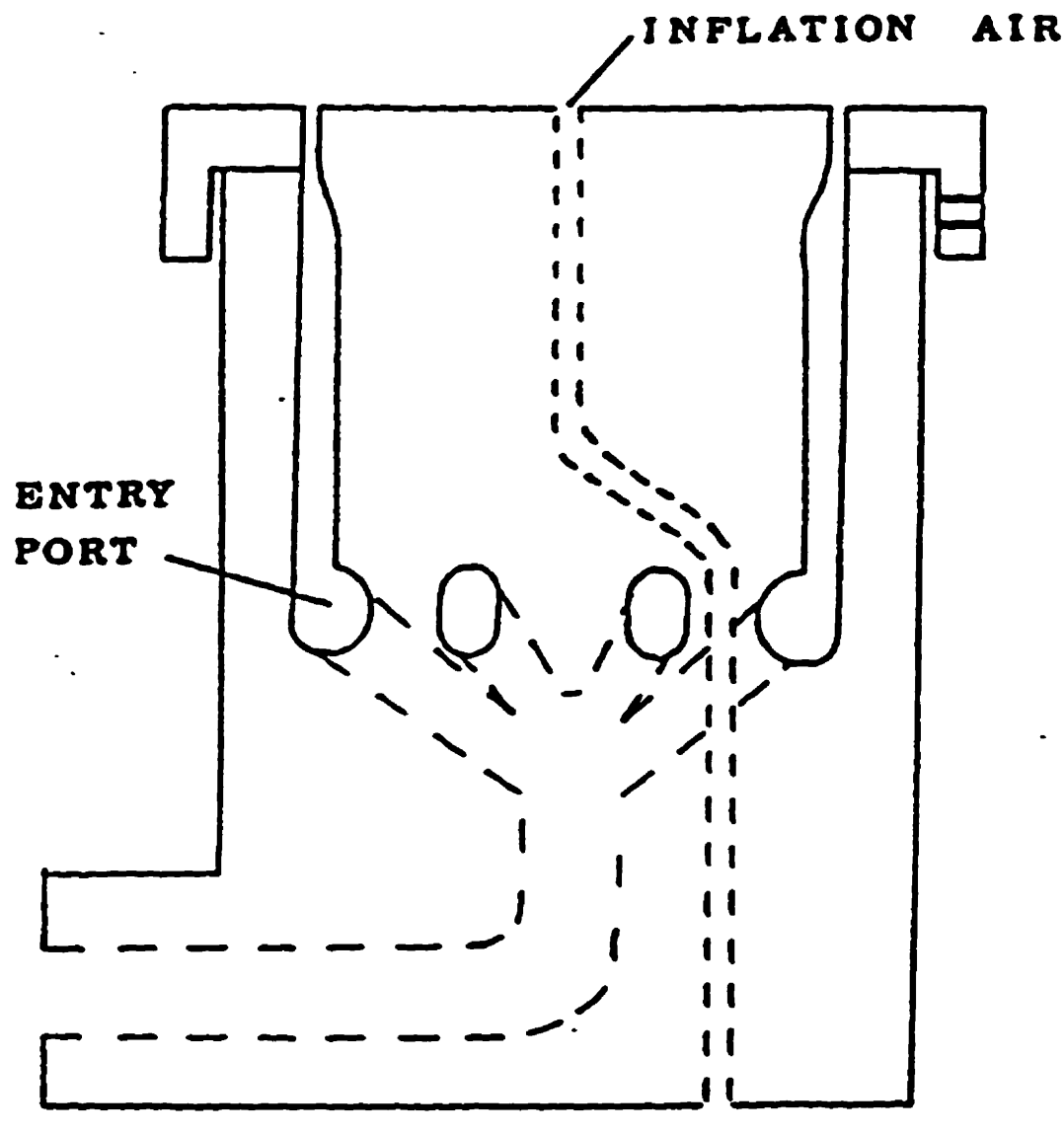


Figure 2.1.5 A star fed die (Whelan,1982)

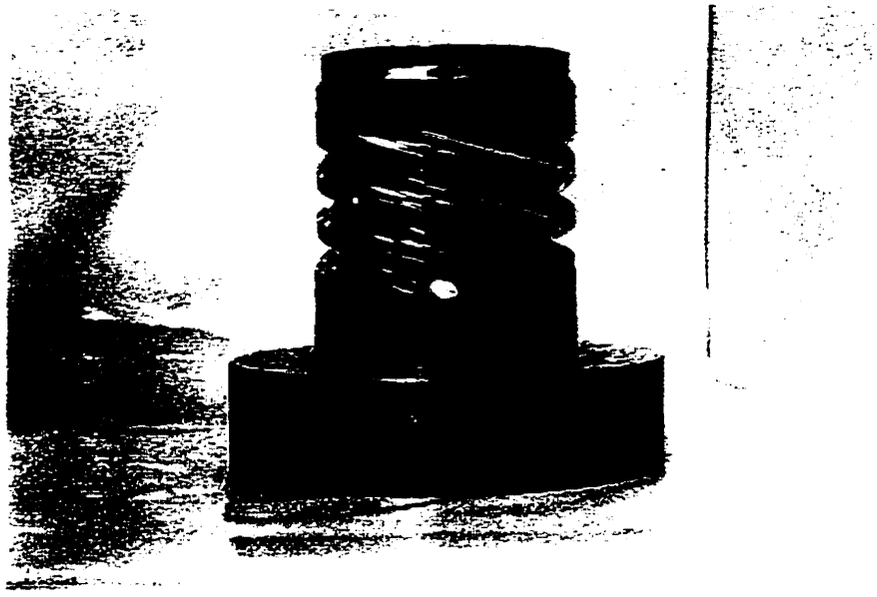


Figure 2.1.6 A photograph of a spiral mandrel distribution system.

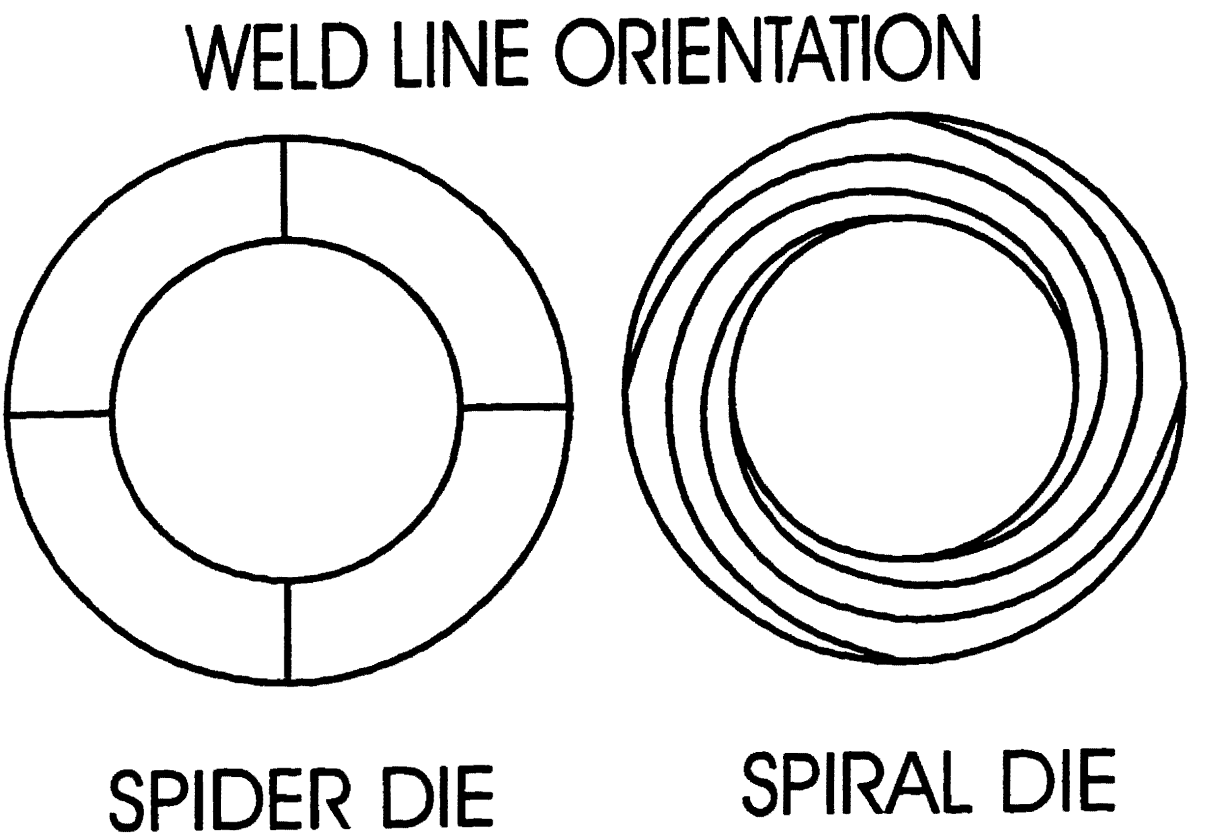


Figure 2.1.7 The orientation of weld lines in a plastic pipe produced from a radial spider die and a spiral mandrel die.

'knitting' the material from different ports. This type of die has been very successful and it is now considered to be the standard in the blown film industry.

There is a limit to the number of spirals that can be cut into a mandrel which depends on the size of the mandrel, the size of the spirals and helix angle of the spirals. Current designs commonly range from 0.4 to 1.2 spirals per centimetre of mandrel diameter. To facilitate easier machining, the spiral depth generally varies linearly with its length. The introduction of numerically controlled multi-axis milling machines has allowed some manufacturers to explore new designs where the spiral channel depth is decreased in a non-linear fashion.

Multi-layer die construction is more complicated than a single layer die because of the requirement for multiple distribution systems (see Figure 1.3.1). Apart from the more complicated mechanical engineering aspects of designing and manufacturing the die, the individual layer flow passages are designed as they would be in a single layer die. Each layer is formed into a uniform annular flow and then they are combined prior to exiting the die. Of course, as the number of layers increases so does the complexity of the die. The difficulty is in equally distributing the polymer melt among the many spirals. This will be discussed in more detail in Chapter 3.

2.1.2 Mathematical Models

This section will briefly overview the mathematical modelling of spiral mandrel flow field. The purpose of any model is to mathematically describe the physics of the process. The advantages of an accurate mathematical model, especially for designers of

spiral mandrel dies, are immense. Mathematical models can provide detailed information about certain aspects of a process that may be difficult or even impossible to witness experimentally. With an accurate model, a process engineer can test new operating strategies or the performance of a new polymer without interfering with production. The simulation can help the process engineer predict if a new polymer or operating point will increase the system pressures to an unsafe level. The largest benefit of an accurate model, to the spiral mandrel die manufacturer, is that it will vastly reduce the 'guess work' involved when designing spiral mandrel dies. Also depending on the accuracy of the model, the amount of overdesign can be reduced to make the die more efficient. The following sections will provide a quick review of the limited amount of work done in the past on modelling spiral mandrel dies. The general procedure used by most models will be outlined and a detailed description of the models compared in this work will be provided.

The first published attempt at modelling the flow through spiral mandrel dies is credited to Proctor (1972). Making several simplifying assumptions, he outlined a method of predicting the flow distribution through a spiral mandrel. The flow field is represented by the arrows in the cutaway view of a spiral mandrel distribution system in Figure 2.1.8. Several simplifying assumptions need to be made about this flow field before modelling can begin. The first assumption is to neglect the effect of curvature. This is a common and quite valid assumption considering that the width of the gap between the mandrel and the body is much smaller than the diameter of the mandrel. The mandrel can now be "unwrapped" and studied in the co-ordinate system shown in Figure 2.1.9.

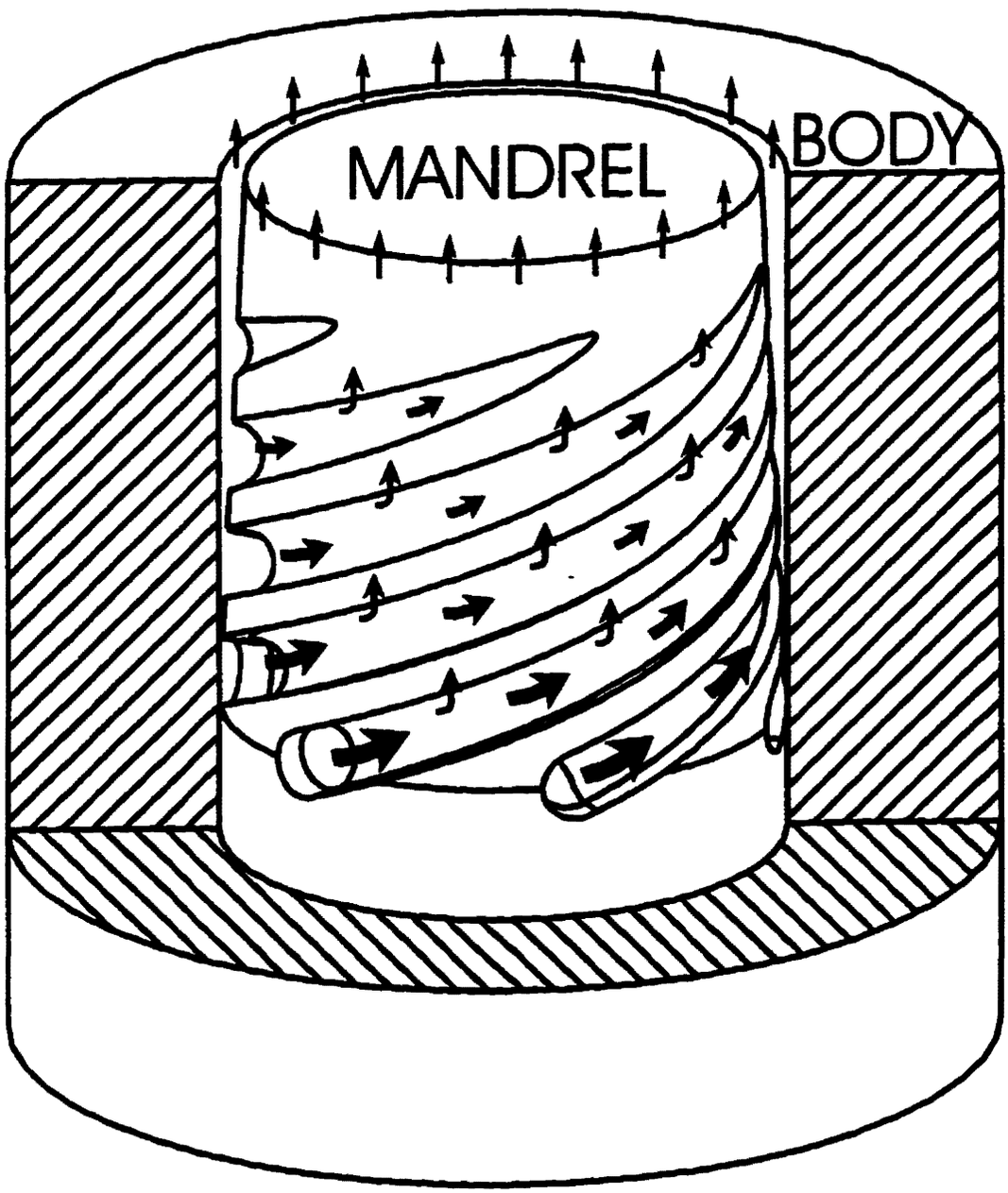


Figure 2.1.8 A spiral mandrel die with half the body cut away. The arrows give the direction of melt flow.

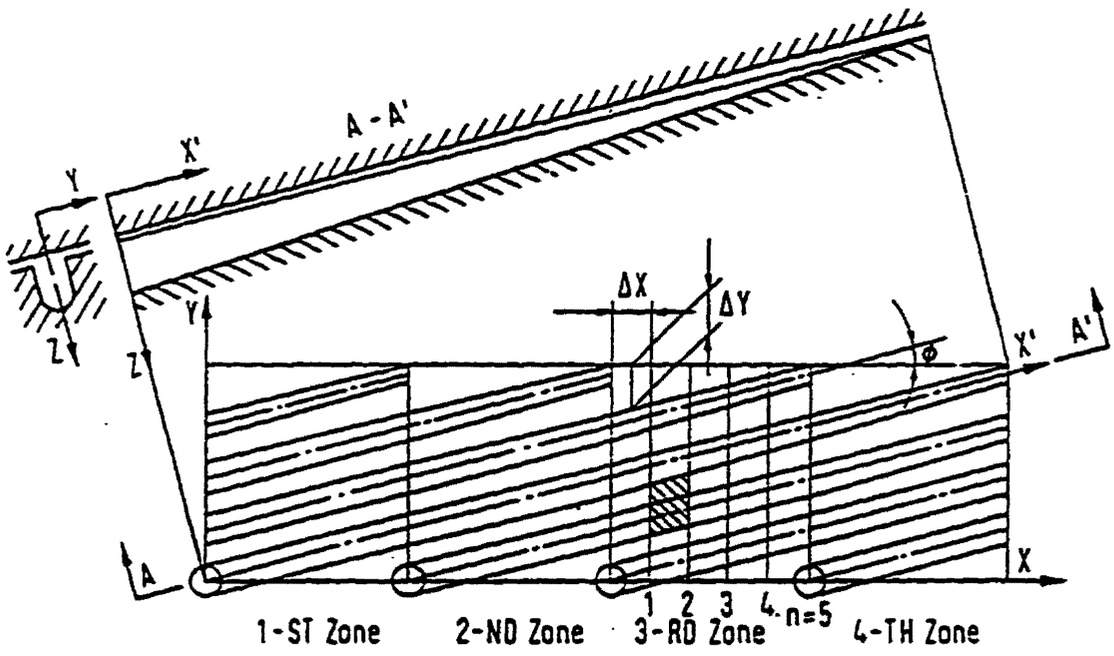


Figure 2.1.9 An unwrapped view of a spiral mandrel surface with 4 zones. The longitudinal and transverse section of a spiral channel is also shown.

Figure 2.1.9 represents a die with 4 spirals each of which travels a full 360 degrees. Also, included in this figure are views of the initial cross section of a channel and the variation in channel depth and annular gap along a spiral. A **zone** is defined as the area between two ports and due to the similarity of all the zones, the problem is further simplified by studying only one zone. A **section** is defined as a channel and its associated land. All of the spirals are machined identically, so it makes no difference which one is modelled. Modelling one zone or one spiral is one and the same thing.

Consider zone 3 in Figure 2.1.9. The first section in this zone is identical to the first section in zone 1. The second section in zone 3 is identical to the second section in zone 2. The third section in zone three is one and the same and the fourth section in zone three is identical to the fourth section in zone 4. Therefore, one complete spiral and its associated land is identical to one zone. It follows that the amount of material flowing out of the first section of zone 3 into the second section of zone 4 would be identical to the material flowing into the second section of zone 3 from the first section of zone 2. This is what is known as the periodicity of the problem and it is applied when performing the flow balances.

The flow field is further subdivided into control volumes or elements, also shown in Figure 2.1.9. In the Y direction, each section provides a division and so four (4) are shown. The number of divisions in the X direction is arbitrarily chosen to be five (5) making the total number of elements equal to 20. A typical element is cross hatched in Figure 2.1.9. More divisions can be used in the X direction depending on the required accuracy but this will increase the time required for the calculations.

Figure 2.1.10a is a section of the actual spiral distribution system while 2.1.10b

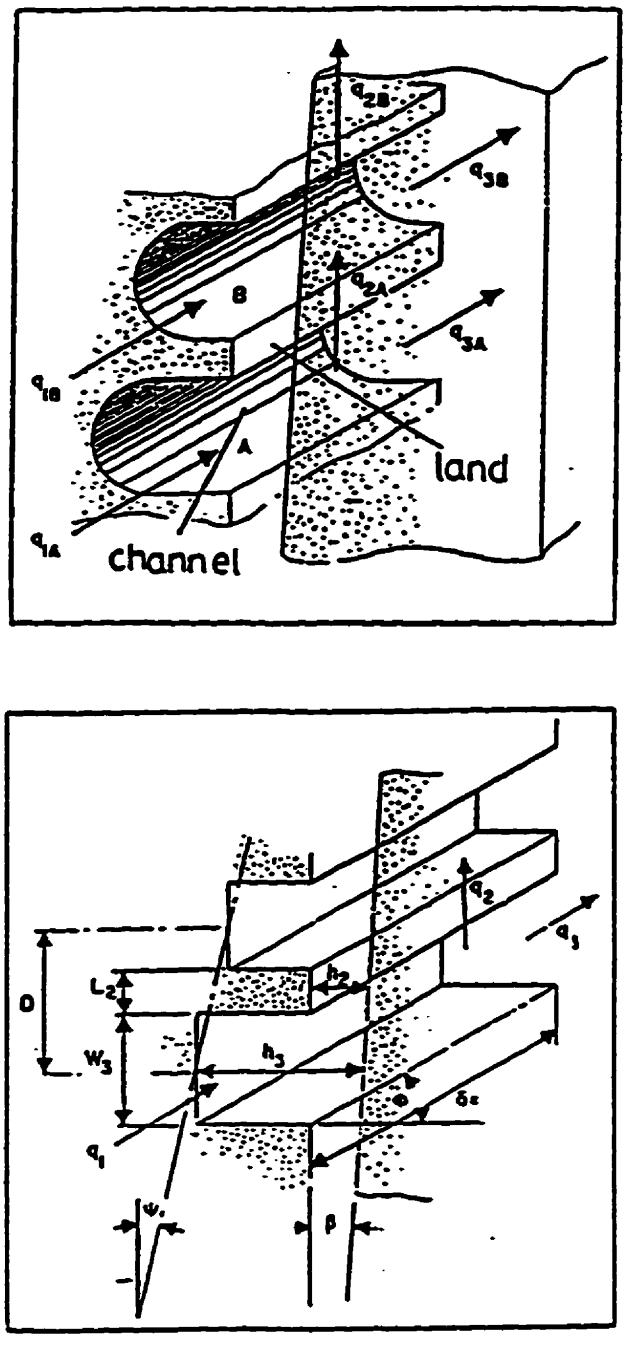


Figure 2.1.10 A perspective view of: (a) the actual flow geometry and (b) the approximate geometry used by Proctor (1972).

is the approximate geometry used by Proctor in his analysis. Figure 2.1.10a consists of two elements (A and B) stacked one upon the other. As shown, the flow rate entering the second element in channel A is labelled q_{1A} while the flow leaving the second element and entering the third is labelled q_{3A}. The material that flows axially over the land from the second element of channel A to the second element of channel B is labelled q_{2A}. Since the depth of the spiral decreases, Proctor made the assumption that the pressure drop in the channel decreases linearly. He further assumed that the flow could be approximated as flow through a rectangular channel of equal cross sectional area. It was also assumed that the flow in the annular gap could be approximated as flow through a slit the width of the element (dx) and the length of the land (L2). It was further assumed that the flow over the land and the flow in the channel had no influence on each other. The assumption of a linear pressure drop makes the problem linear. One simply specifies the pressure drop through the system and determines the flow rates in each element in a step-wise progression from the start of the spiral. What is of primary importance, is the volumetric flow in each of the land elements in the last section of the die. The volumetric flow variation at this point is what determines the variations in the dimensions of the final product.

Subsequent efforts have attempted to develop improved models by relaxing some assumptions and introducing new ones. Wortberg et al (1982) using a similar model, made allowances for the dimensions of the flow field to be described by higher order functions. Kurzbuch (1974), Helmy et al (1980) and Cheng (1981) relaxed the assumption of a constant pressure drop along the spiral channel and made the assumption that the pressure was uniform in the circumferential direction. This means that any path from the start of the spiral

to any level would have an equal pressure drop. An initial guess of the pressure drop was made and then through an iterative process, the pressures were updated until convergence. Saillard et al (1984) developed a model that relied upon the solution of a set of non-linear difference-differential equations for the unknown pressure. In addition, this model appears to be the first to include thermal effects by incorporating a bulk temperature in each element. Vlcek et al (1984) also used a set of non-linear difference-differential equations, to describe the system, however, this model appears to be the first to allow two dimensional flow in each control volume. Fahy et al (1986) developed a set of ordinary difference-differential equations to describe the pressure distribution and solved them using a one dimensional finite element approximation. Menges et al (1984), took a different approach to die design in that they made the assumption that the flow out of the spiral channel was uniform and determined the dimensions of the annular gap. The main problem of this method is that the geometry that gives you a good distribution is generally too difficult and expensive to machine accurately. Rauwendaal (1987) presented a simple model that related the pressure drop through the channel to the pressure drop over the land through the helix angle of the spiral. This made the problem linear, allowing a stepwise solution. Vlcek et al (1987) developed a new model which is an improvement of the previous model presented by Vlcek et al (1984) which also includes temperature effects. Benkhoucha and Sebastian (1989) have presented a 2-D model based on the flow analysis network (FAN) method which allows the use of more general rheological models for the viscosity. A comprehensive study of spiral mandrel dies including a comparison of several models with experimental data was performed by Perdikoulias (1988).

Due to the complexity of the flow field and the fully three dimensional nature of the flow, many simplifying assumptions must be (and are) made by all of the models mentioned above. All of these models basically use a 'lumped parameter' or 'control volume' approach in which the flow field is divided into many small control volumes and assume a fully developed flow profile in each control volume.

Many of the assumptions presently made can be eliminated by using a three dimensional finite element numerical analysis. However, this is currently impractical for design purposes. Some work by Coyle and Perdikoulias (1991a), indicated that although the FEM can provide for a very detailed analysis of the flow system, the major flow characteristics predicted by FEM are very similar to those predicted by a control volume method analysis. The major drawback of using the FEM is the demanding computational requirements. Fine mesh solutions may require up to 2800 Megabytes of memory and 1 hour of CPU time (using 3500 brick elements, 34,000 grid points, and 83,000 degrees of freedom) for 1 iteration. A non-Newtonian material with a moderate shear thinning behaviour such as LDPE may require up to 6 iterations for adequate convergence. An experienced FEM user can obtain adequate results for average flow and pressure drop using a courser grid (2150 elements, 15,000 grid points and 30,000 degrees of freedom). Advanced solution techniques can also reduce the memory requirements for such a problem down to 12 Megabytes so that these calculations can be performed on a powerful workstation (such as a Convex C-340) in about 15 minutes for one iteration. This may be an acceptable amount of time for a single simulation but during the design process, an experienced designer may simulate over 50 geometries to obtain a proper spiral design. For typical non-Newtonian material requiring

6 iterations, this still amounts to over 75 hours of CPU time. These staggering computer demands, even if possible, would be extremely expensive for the average die designer/manufacturer to afford. Of course, the rapid developments in the area of computers and computational fluid dynamics will no doubt make this the way of the future.

At present, the lumped parameter or control volume approach still appears to be the most practical method of analysing and designing spiral mandrel dies. In fact, a number of commercially available computer software packages have been developed based on this method. A good description of these packages is given by O'Brien (1992).

2.2 Coextrusion

Coextrusion is the extrusion of two or more layers of polymers through the same die. It has been used since the early 1950's to improve product quality, functionality and process efficiency. However, under certain conditions, the coextrusion process exhibits some flow phenomenon which are not well understood. The following paragraphs will provide some background information on this topic.

Consider the two streams combining as shown in Figure 2.2.1. This flow field can be found in many extrusion processes. The velocity profile of the individual streams will be different from that in the combined flow area depending on the viscosity and/or velocity differences of the two materials. Figure 2.2.2 is a FEM grid representing two flow streams merging. Figures 2.2.3 are the streamlines that occur under various flow conditions for a A:B viscosity ratio of 2:1 as presented in a study by Perdikoulias at al (1991). As can be

seen, the interface position will depend on the viscosity and flow rate ratios and, since the geometry is fixed, the interface development path will vary.

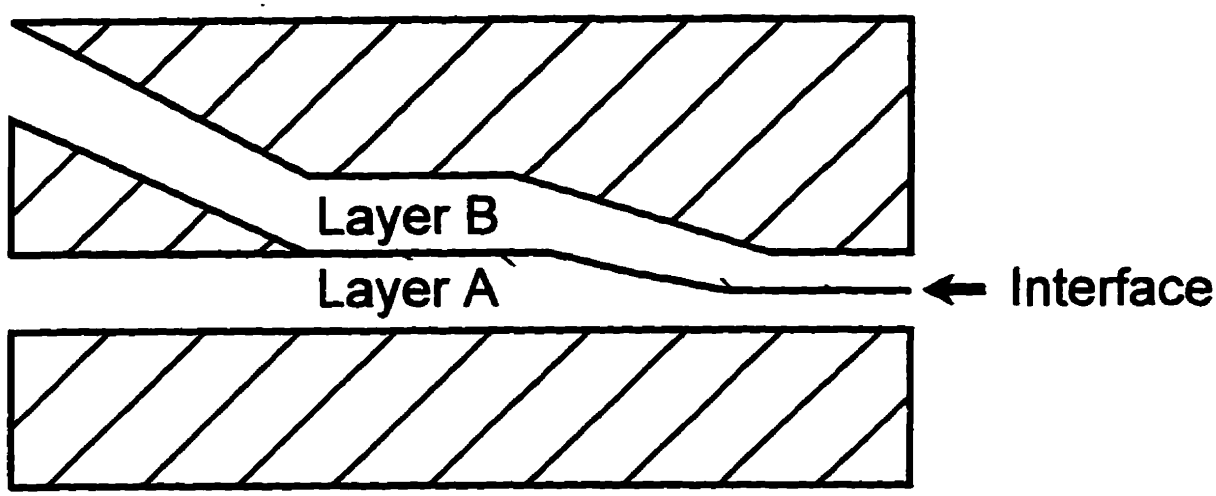


Figure 2.2.1 A typical coextrusion flow field.

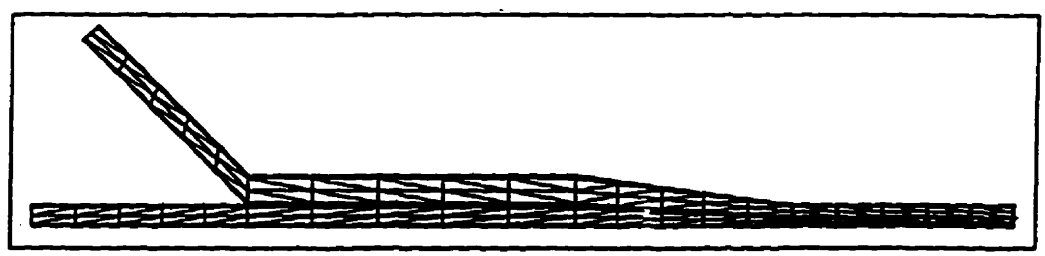


Figure 2.2.2 A FEM grid of a coextrusion flow field.

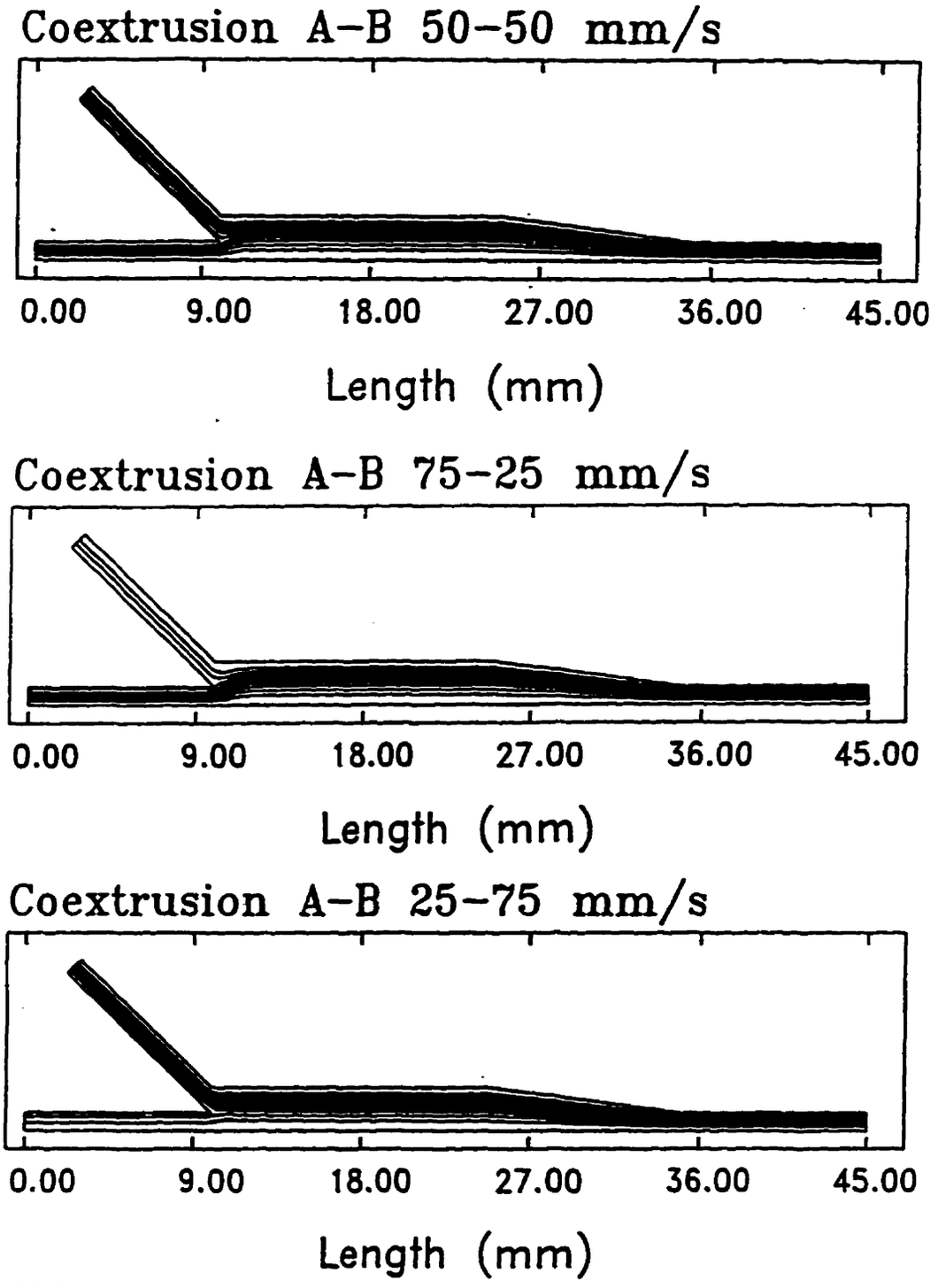


Figure 2.2.3 Streamlines for a 50/50 ratio (top), 75/25 ratio(middle) and a 25/75 ratio (bottom)

This topic has been dealt with in detail in a book by Han (1981). Others (Nordberg and Winter,1988; Mavridis and Shroff, 1994; Mitsoulis and Hannachi, 1990) have suggested additional numerical techniques for interface determination. A review of modelling of coextrusion flow fields has been presented in a dissertation by Karagiannis (1989) who has also presented some 3-D FEM modelling results. Torres et al (1995) have also studied the effect of various processing conditions on the development of the interface. The problem however, is that under certain conditions the interface becomes unstable which results in undesirable product properties. This transient behaviour is of particular interest because it limits the processor in what materials and layer ratios that can be produced.

Gross instabilities are readily apparent whereas finer instabilities affect film properties such as clarity. This was nicely demonstrated by Mavridis and Shroff (1994) as shown in Figures 2.2.4 and 2.2.5. Figure 2.2.4 is a photograph of a couple of coextruded film samples, which have been placed on a sheet of paper with some writing that is clearly visible. Figure 2.2.5 is a photograph of the same film samples but they have been placed some distance above the writing. The interfacial instability in the sample on the left diffuses the light to the point that the writing is illegible. Figure 2.2.6 contains photographs of magnified cross sections of these film samples. The smooth interface is shown during run # 6 (bottom) of Figure 2.2.6 while the interfacial instability is readily apparent as an irregular interface during run # 1 (top) in Figure 2.2.6.

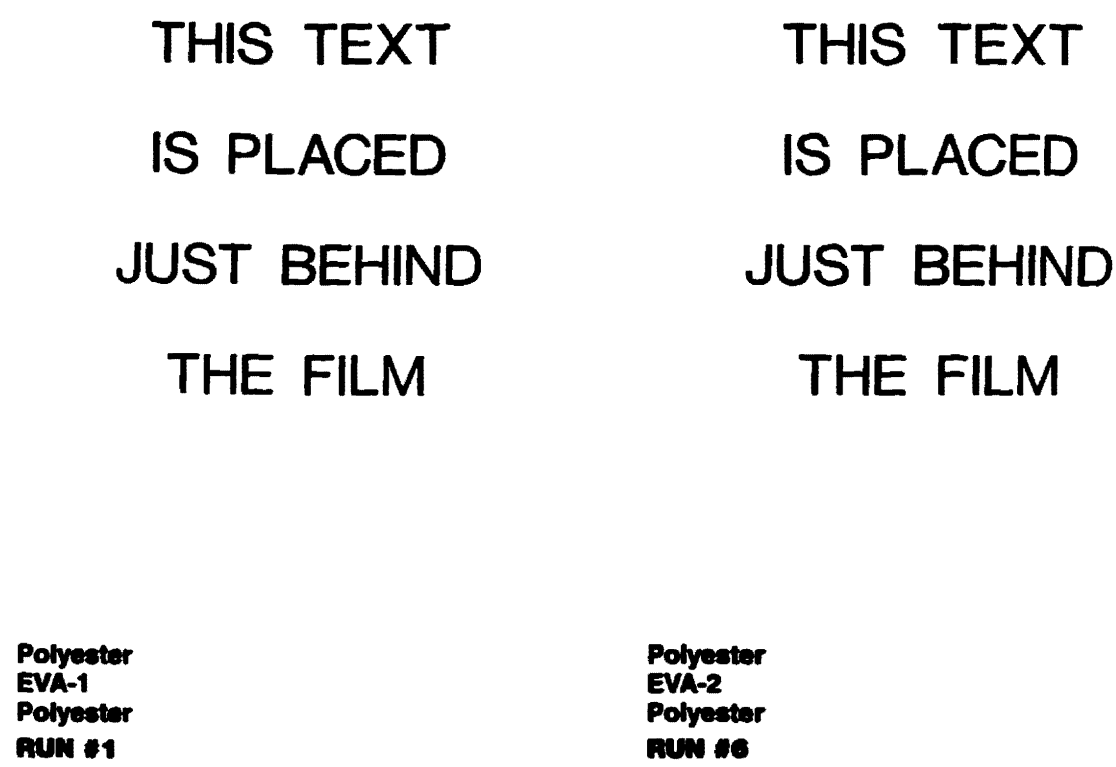


Figure 2.2.4 Photograph of two coextrusion film samples on pages with writing.

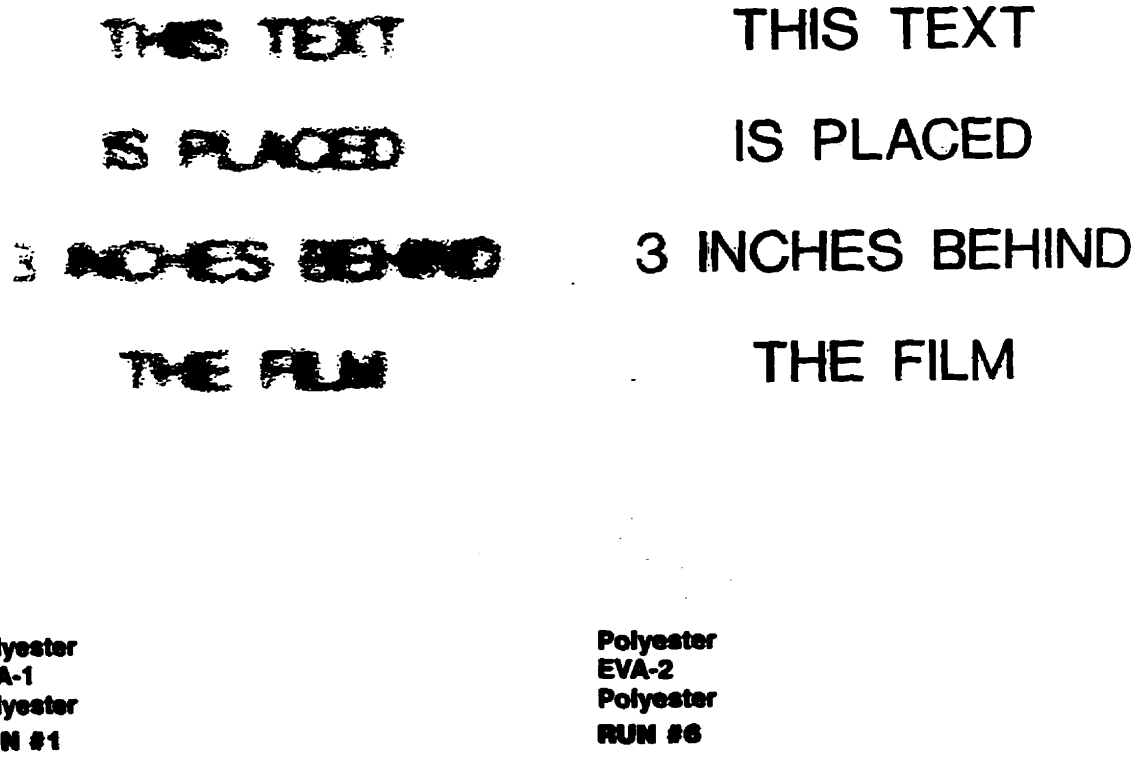
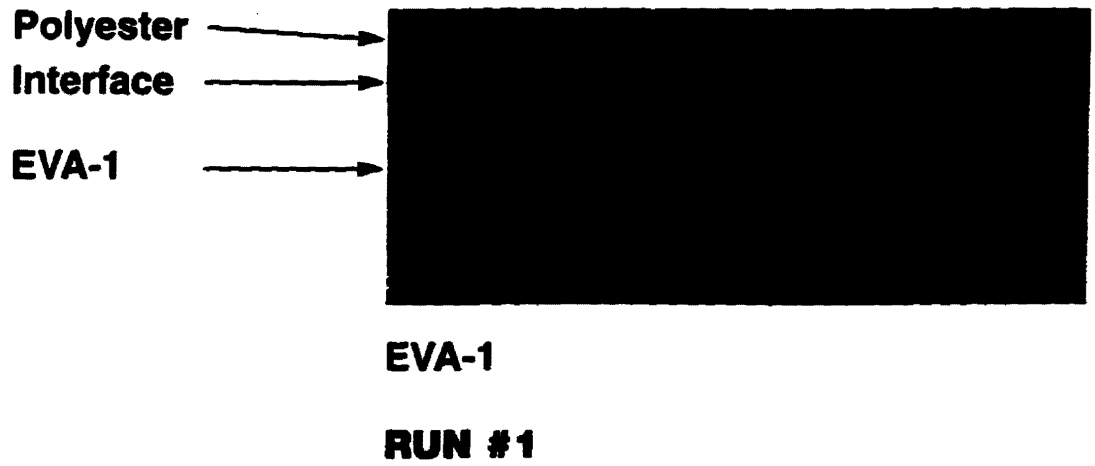


Figure 2.2.5 Photograph of two coextrusion film samples 80 mm above pages with writing



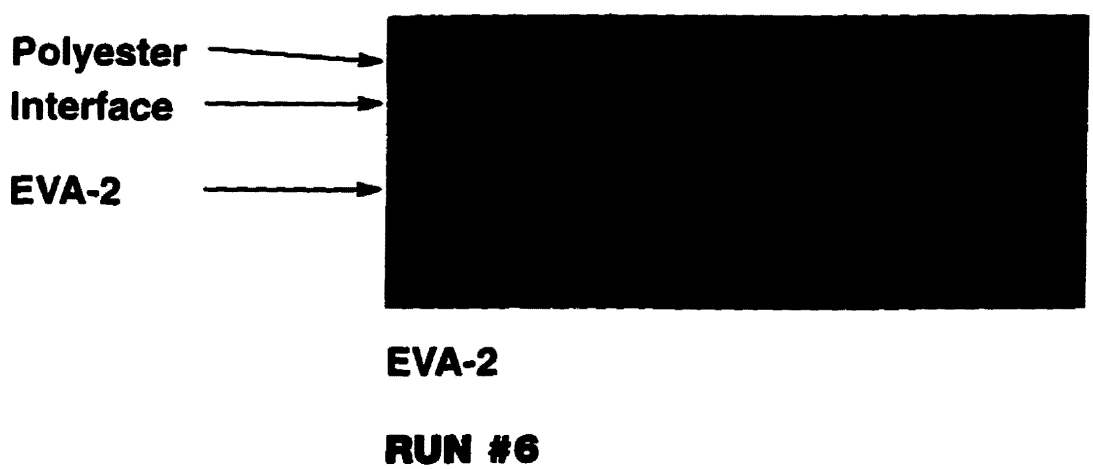


Figure 2.2.6 Photograph of a magnified cross-section showing a smooth interface (bottom - run # 6) and an unstable interface (top - run # 1).

This topic appears to have been initially investigated by Schrenk et al. (1978). They concluded that the interfacial instability sets in when the interfacial shear stress exceeds a critical value. Han (1978) and his co-workers have shown that although the critical shear stress theory is valid for a particular system, the critical shear stress value is affected by factors such as layer arrangement and thickness.

Wilson and Khomami (1993) have published several papers about their experiments, with several polymer systems, where they studied the effect of introducing a regular wave disturbance. They suggested that interfacial instabilities are due to waves present in the flow field (possibly from the extruder), and the polymer characteristics and flow conditions are such that these waves are either dampened out or amplified to form an observable instability. Rincon (1995) has also developed a transient numerical analysis of the interfacial instability phenomenon based on a periodic flow input. A great deal of work on coextrusion has been performed by researchers at the Dow Chemical Company, Midland, Michigan.. Dooley and Hilton (1993) and Ramanathan et al (1992,1993,1996) and Shanker et al (1995) have presented several papers on coextrusion. Ramanathan and Schrenk (1993) have established the idea that there are essentially two types of interfacial instability which they have termed 'wave' and 'zig-zag'. They attribute the 'zig-zag' instability to be due to excessive shear stress at the interface while the 'wave' instability has a much more elusive source.

Perdikoulias et al. (1991), Vlcek et al (1993) and Mavridis and Shroff (1994) have also investigated the effect of material properties and processing conditions on interfacial shear stress and shown how viscosity selection, layer ratios and die design can affect the

shear stress and consequently the instability due to stress. Some preliminary investigations by Perdikoulias et al (1993) have shown that interfacial instabilities can occur in multi-layer flow of the same polymer melt. This observation had not been found in any of the previously published literature.

One of the reason why progress in this area has been relatively slow is believed to be due to the lack of good experimental data. There have been many observations and a great deal of happenstance data published but most of these publications omit material properties and confound the effects with their choice of systems. There have been very few good fundamental studies of this phenomenon. One of the objectives in this work is to perform a systematic study of the effects of material properties and flow geometry on the appearance of interfacial instability and generate a set of data that can be used to evaluate present and future theories.

CHAPTER 3

RESIDENCE TIME ANALYSIS

3.1 Residence Time Distribution

In the production of plastic film by the blown (tubular) film process there have been observed some problems which appear to be related to the residence time of the polymer melt in the extrusion system. These problems include, long colour or material change-over times, polymer degradation, and the appearance of haze bands. These problems are particularly common to coextrusion dies. The qualitative effect of residence time is known and it has been discussed in papers by Butler (1989) and Gates (1990). It is the general consensus of these papers that most of the problems experienced with coextrusion are related to the residence time of the polymer in the system. However, the industry has advanced to the point that it is necessary to quantify the residence time distribution of an extrusion system. The first step in doing this, however, requires that the residence time of the individual components that make up the system be known.

The concept of residence time distribution (RTD) is slowly beginning to gain the respect it deserves in polymer processing. It is the key to solving many extrusion problems and it should be well understood by anyone involved in polymer processing. Fluid elements, passing through a system, have different velocities because of their relative position with respect to the solid boundaries (where the velocity is zero), and they follow different paths

travelling from the entrance to the exit. This gives rise to a distribution of times.

The residence time distribution (RTD) or the exit age distribution function of the exit stream from a system are two different names for the same function, E(t), which gives the probability of a fluid element having a residence time between t and t+dt. The fraction of the exit stream of age between t and t+dt is given by E(t)dt (Levenspiel, 1972; Himmelblau and Bischoff, 1968). Understanding the influence of the various processing, rheological and geometrical conditions on the RTD of a polymer flowing through several pieces of equipment can lead to the establishment of design criteria that minimize polymer degradation due to prolonged exposures of the polymer to high temperatures and also to the clarification of purging and mixing concerns.

An interesting study by Halle(1989) deals with the stability of various ethylene copolymers and how it is affected by multiple passes through an extruder. In other words, how these materials stand up to prolonged exposure to high temperatures. Halle's study found that EVA copolymers are particularly prone to degradation (chemical reactions causing molecular changes) and this agrees with the experience of the author of this work. A similar study was performed by Butler (1989) dealing mostly with the extruder but also presenting some RTDs for a complete film line. In fact, most of the RTD studies on polymer processing performed in the past have focused on the extruder (Pinto and Tadmor, 1970; Wolf and White, 1976; Schott and Saleh, 1978; Kemblowski and Sek, 1981; Stamato and Weiss, 1985) but the flow channels from the extruder to the exit of the die also impart a RTD on the fluid. Some published experimental work by Perdikoulias and Tzoganakis(1987) explains how the RTD of the adapters, block and die can explain a

phenomenon known as haze lines.

3.1.1 Theory

Most of the polymer flow paths in coextrusion film dies can be approximated as tubes or annulii as shown in Figure 3.1.1. The RTD for isothermal, laminar flow of a non-Newtonian fluid through a tube can be derived and it has been given by Nauman and Buffham (1983) as shown below.

$$E(\theta)=\frac{2n}{(3n+1)\theta^3}\left(1-\frac{n+1}{(3n+1)\theta}\right)^{\frac{n-1}{n+1}} \tag{3.1}$$

where $E(\theta)$ is the exit age distribution based on the dimensionless time θ, and n is the power-law index. The dimensionless time, θ, is defined as:

$$\theta=\frac{t}{t_{avg}}$$

where t is greater than the minimum time it takes for the fastest element of fluid to exit the system. The relationship to a non-dimensionless exit age distribution, E(t), is given by equation 3.2.

$$E(t)=\frac{E(\theta)}{t_{avg}} \tag{3.2}$$

where t_{avg} is the average time the material takes to flow through the system.

There is no exact analytical solution for the corresponding equation for flow through an annulus. However, Lin (1980) has proposed the following solution (equation 3.3) based on an approximation made by Mirshra and Mirshra (1976) for determining the position of the maximum velocity (λ) within 4%.

$$E(\theta)=\frac{2nA}{(1+k)(n+1)\theta^3}\left(1-\frac{A}{\theta}\right)^{-\frac{1}{(n+1)}}\left(\lambda+(1+k-2\lambda)\left(1-\frac{A}{\theta}\right)^{\frac{n}{(n+1)}}\right) \tag{3.3}$$

where

$$A=\left(\frac{n+1}{1+k}\right)\frac{(2n+1)(1+k)+2n\lambda}{(3n+1)(2n+1)} \tag{3.4}$$

where n is again the power-law index and k and λ are shown in Figure 3.1.1.

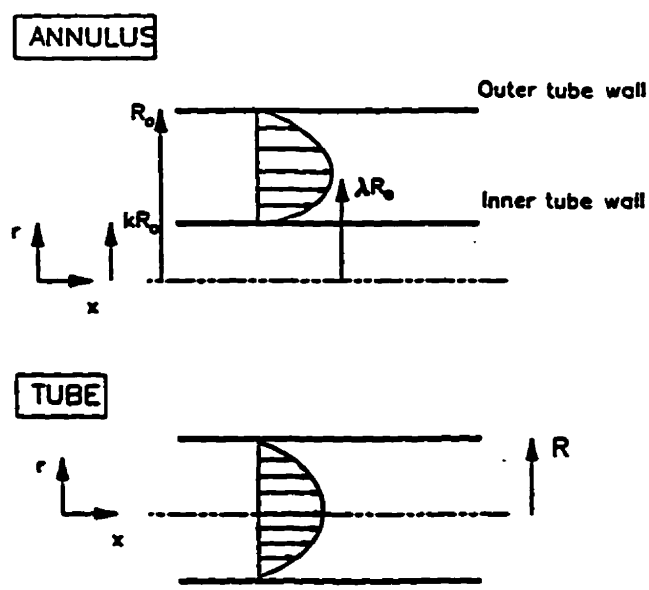


Figure 3.1.1 Geometry of a tube and an annulus

3.2 RTD and Pressure Drop In The Block

The relationship between residence time and pressure drop is qualitatively simple. To decrease the residence time, one must increase the velocity of the fluid and hence increase the pressure drop across the passage. Conversely, the pressure drop can be lowered by increasing the flow area of a system which decreases the velocity and increases the residence time. The relationship is slightly more complicated when comparing different systems.

One particular fundamental design problem associated with blown film coextrusion dies is the efficient conveying and even distribution of the polymer among the many spirals. This is generally done in a device called the **block**. There are basically two types of block designs currently being used in the industry and they will be referred to here as ***port*** and ***annular***. This section presents an analysis used to determine which fundamental design would be best.

3.2.1 Port Design

Consider the port block design for a two layer die shown in Figure 3.2.1. The inner layer flow path is relatively simple. The melt is fed into the centre and up the axis of the block in a single channel. At the base of the die, the polymer is radially fed to the spirals through ports. The outer layer flow path is a little more complex. The polymer is again fed to the centre of the block (below the previous layer) where it is symmetrically split into a number of smaller channels. These channels run parallel to the axis of the block and feed directly into the radial ports which feed the outer layer spirals. The section A-A in Figure 3.2.1 shows the inner layer channel and the 4 channels which transport the material for the

outer layer. These 4 channels may be fed directly into 4 spirals or each of these may be split once again to feed 8 spirals on perhaps a larger die. This splitting can continue in a binary fashion (2^n, where n = number of splits) until the required number of channels is achieved. Additional layers would be introduced in a similar fashion entering the block below the previous layer and splitting into a number of ports. The quantity and positioning of the ports is determined by the flow rate and the positioning of the bolts required to keep the system together.

3.2.2 Annular Design

The annular block design is shown in Figure 3.2.2. The inner layer is virtually identical to the port block design in that the polymer is conveyed to the centre axis of the die and then flows along the axis to where the ports connect it to the spirals. The subsequent layers, however, use concentric cylinders to create a flow path to transport the polymer from the extruder adaptor to the spiral ports. The polymer for the subsequent layers enters the block above the entry for the inner layer and is forced to flow into an annular passage. Usually the polymer is passed through a 'side-feed' distribution system to create a uniform annular flow. The 'side-feed' system is comparable to a flat die distribution system which has been wrapped around a cylinder so that the edges connect. The polymer then flows through the annulus to the base of the die where the ports split the flow into as many paths as there are spirals. The number of annuli (or concentric cylinders) required depends on the number of layers in the die.

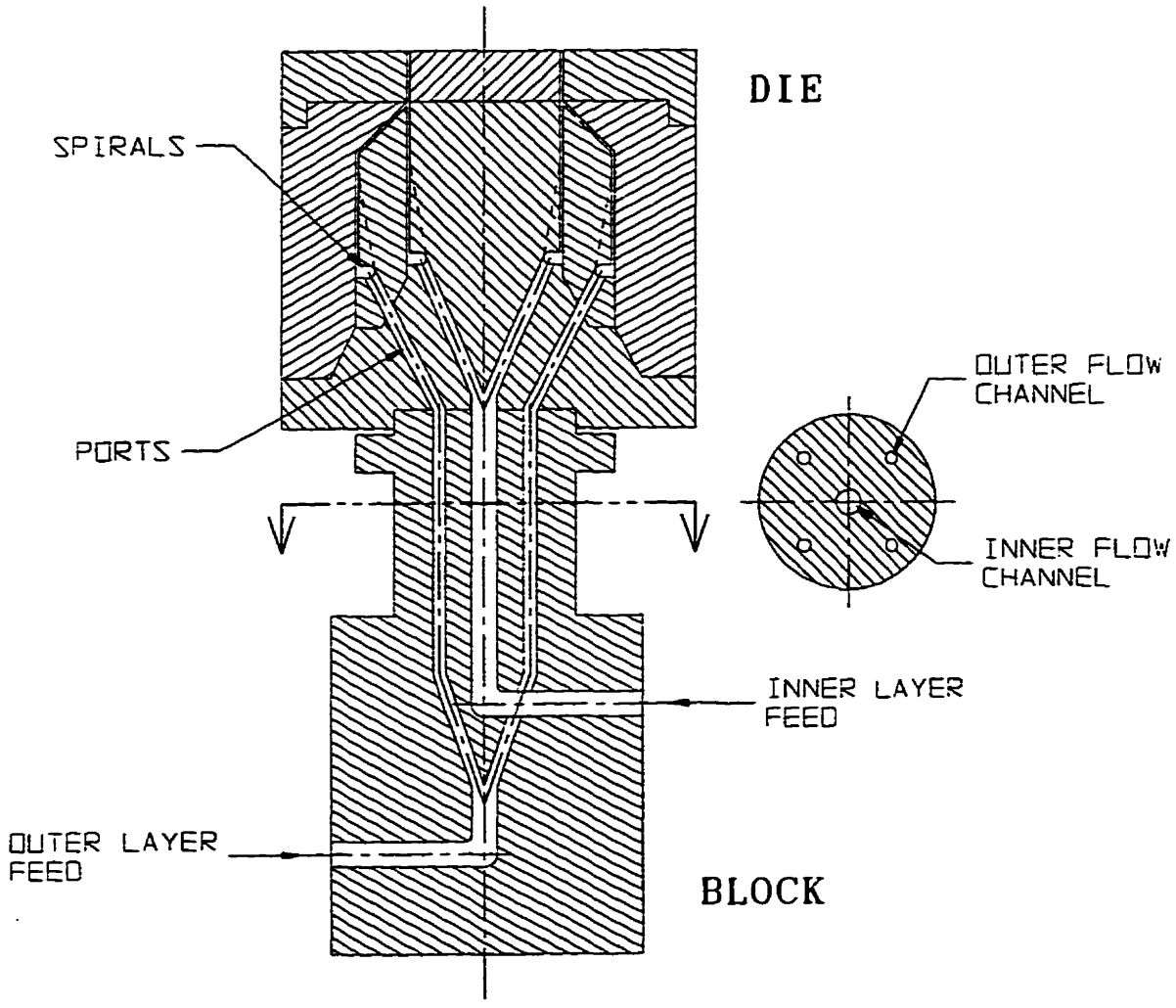


Figure 3.2.1 A drawing of a 2 layer die with a port block design

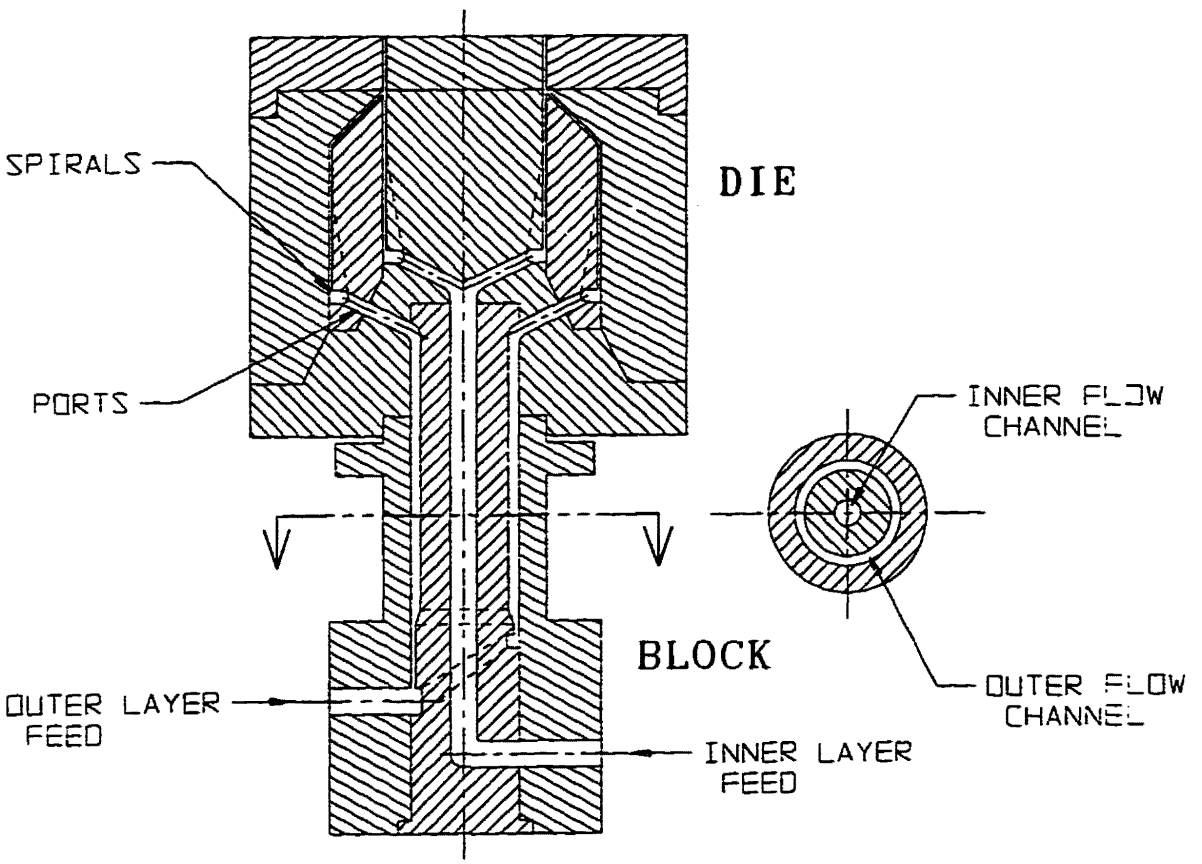


Figure 3.2.2 A drawing of a 2 layer die with an annular block design.

3.2.3 Comparative Analysis

When designing equipment for polymer processing it is preferable to maintain low system pressures while also keeping the residence time of the polymer melt in the system to a minimum. These two design criteria are somewhat conflicting since lower residence times (higher velocities) generate higher system pressures. This is why careful attention must be paid to the interaction of these design criteria with respect to the design of the block. Since there is no analytical solution describing the flow of a non-Newtonian fluid through an annulus, a numerical approach example will be used to demonstrate these relationships. Consider the fundamental goal of conveying a polymer over a certain distance. The basic conditions and material properties can be found in Table 3.2.1.

Table 3.2.1 Basic Conditions and Material Properties

Flow Rate	180 Kg/hr
Melt Density	760 kg/m^3
Power Law Index	0.45
Consistency Coefficient	13790 $Pa*s^n$
Distance	25.4 cm

The most obvious method would be to use a single tube (or port) which, based on the author's experience, would typically be about 5.08 cm in diameter. The pressure drop through this tube would be about 0.65 MPa. The corresponding average velocity and shear rate are about 3.23 cm/s and 6.6 s^{-1} respectively. Now consider the same flow rate being delivered through 4 tubes (or ports), each of the same length as before (25.4 cm) but sized to maintain the same average velocity as the single tube. This is depicted in Figure 3.2.3.

TUBULAR FLOW

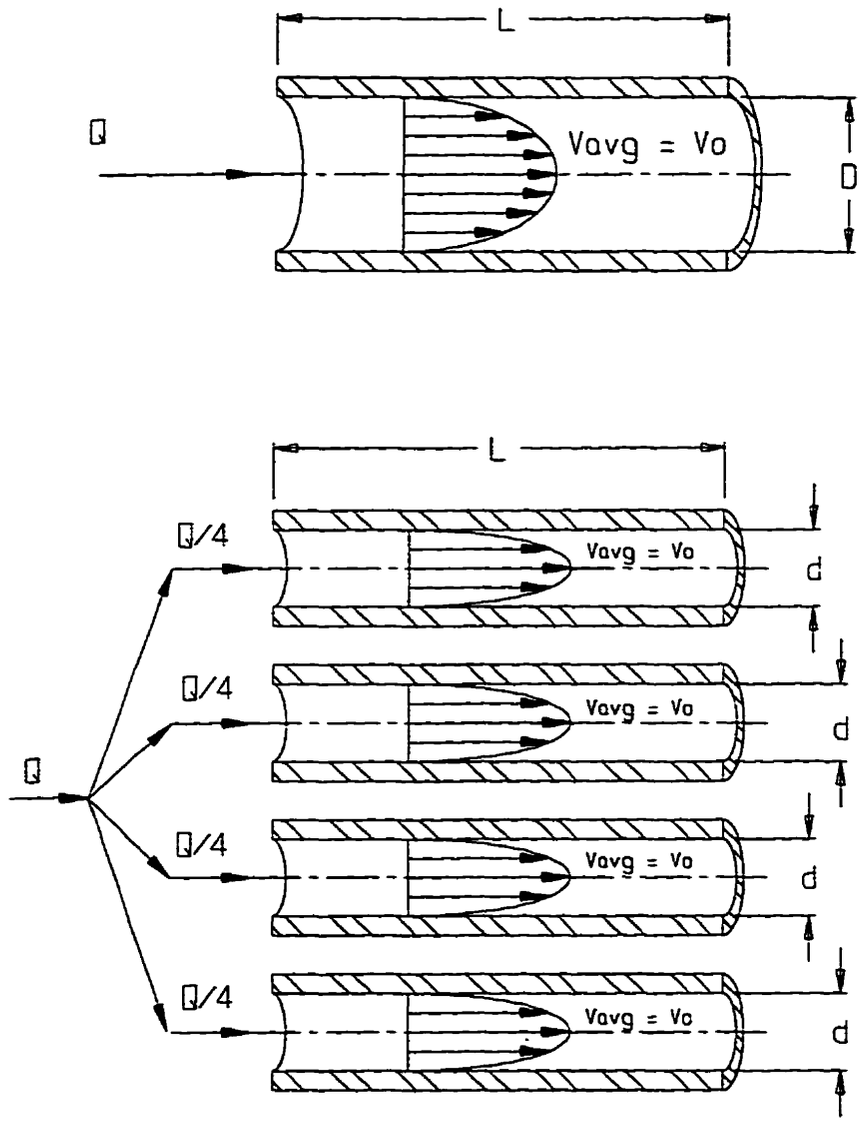


Figure 3.2.3 A representation of 1 tube and 4 tubes with the same average velocity.

In doing so, the residence time of the polymer melt remains the same in both systems. However, the pressure drop across this system will increase to 1.76 MPa and the shear rate will increase to 13 s^{-1}. The analysis was extended to 8 and 16 ports and the results are plotted in Figure 3.2.4.

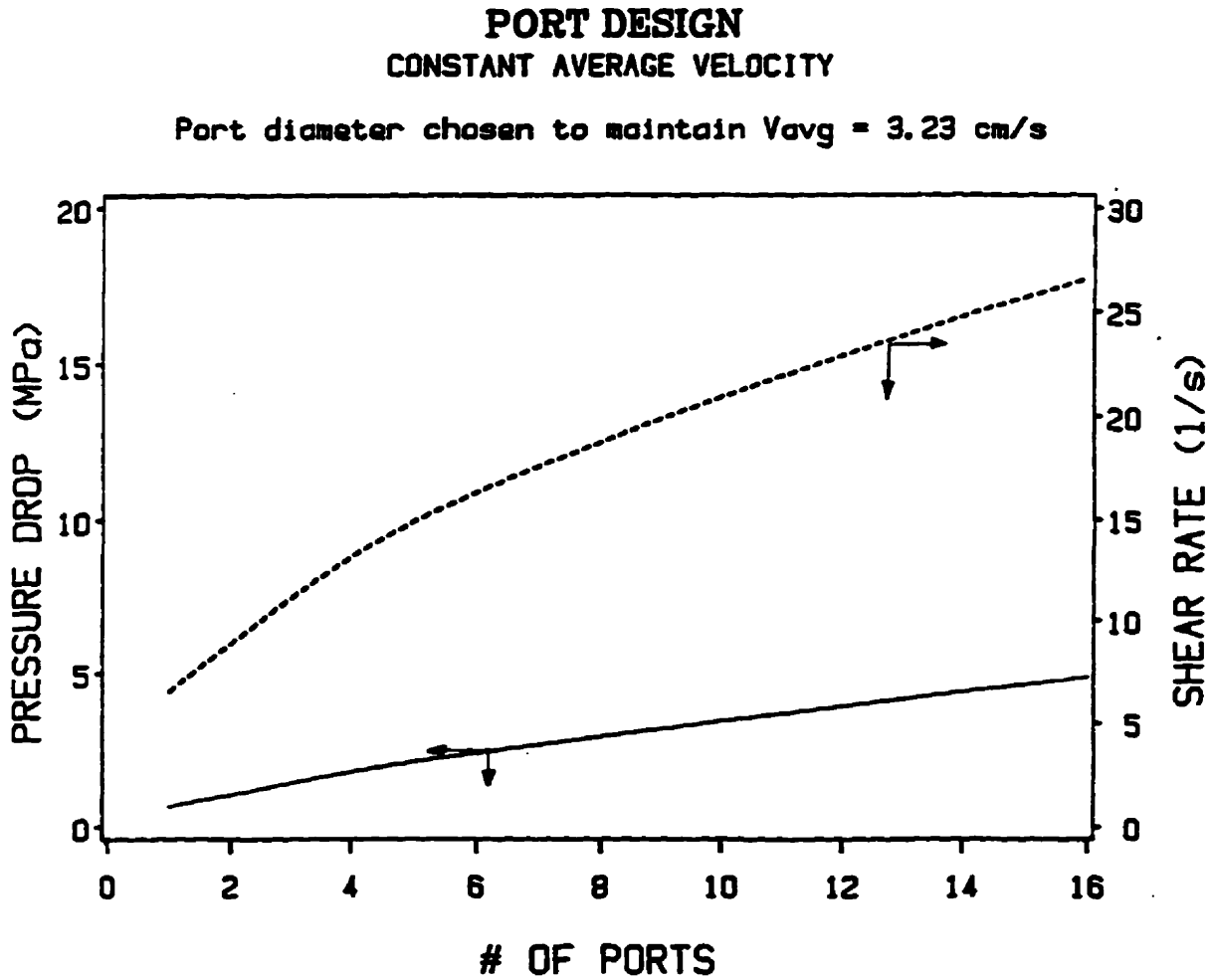


Figure 3.2.4 Pressure drop versus the number of tubes used to convey the polymer.

A similar analysis is performed on the annular design. In this case, the I.D. of the annulus is increased and the gap is adjusted to maintain a constant average velocity. As seen in Figure 3.2.5 the gap between the two cylinders decreases as the diameters increase in order to maintain the same flow area (and average velocity) . Figure 3.2.6 shows the effect of the above on the pressure drop. An annulus with an I.D. of 2.54 cm (O.D. of 5.7 cm) will have a pressure drop of about 1.6 MPa and a shear rate of 17 s^{-1}. Increasing the I.D. to 10.0 cm (O.D. now becomes 11.4 cm) will cause the pressure requirements to increase to 6.5 MPa and the shear rate to increase to 45 s^{-1}. Keep in mind that the average velocity is maintained at 3.23 cm/s. In a typical multi-layer die the average diameter of an annular channel can be from 10 to 25 cm. It is readily apparent that the annular system has a higher pressure consumption. The above differences between the port and annular system are basically due to the fact that for equal average velocities, the annulus has a larger surface area than the tubes. The surface area of the 8 ports is about 1150 cm^2. The surface area of an annulus with a 10 cm I.D. is about 1600 cm^2 (40 % larger). The actual RTD for the systems described by Figures 3.2.4 and 3.2.6 is compared in Figure 3.2.7. The material enters the system at time zero and some time later begins to exit the system with the characteristic curves shown in Figure 3.2.7. In both the port and annular systems, the material to exit first is the material with the highest velocity. Although both systems have the same average velocity, the maximum velocity in a port is about twice the average velocity whereas the maximum velocity in a typical size annulus is about 1.7 times the average velocity. This is why the RTD of the annulus starts after the RTD of the port. For all practical purposes, however, it can be assumed that the RTD of a port system and the RTD of an annular system are the

same for constant volumetric flow rate and average velocity.

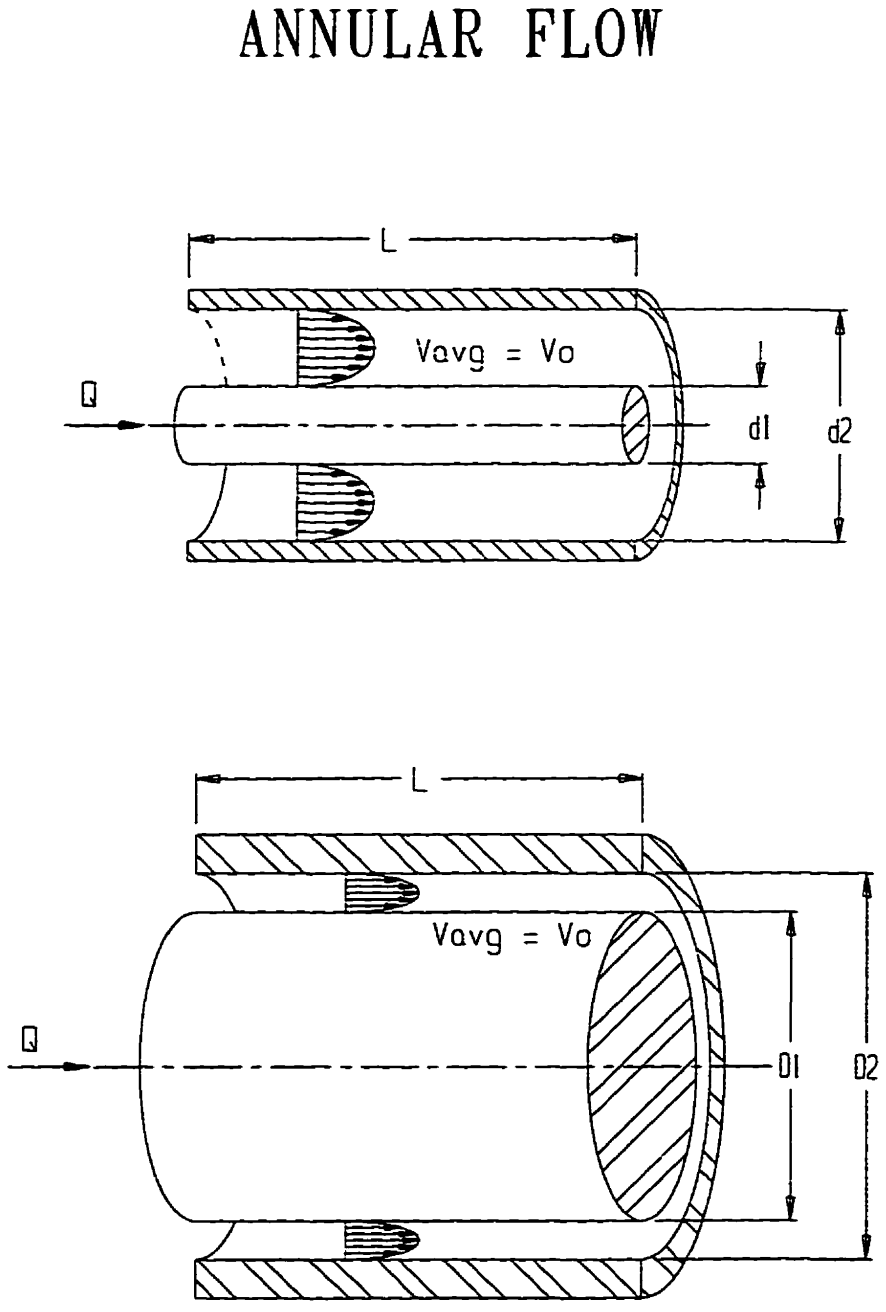


Figure 3.2.5 A representation of a small annulus and a large annulus with the same average velocity.

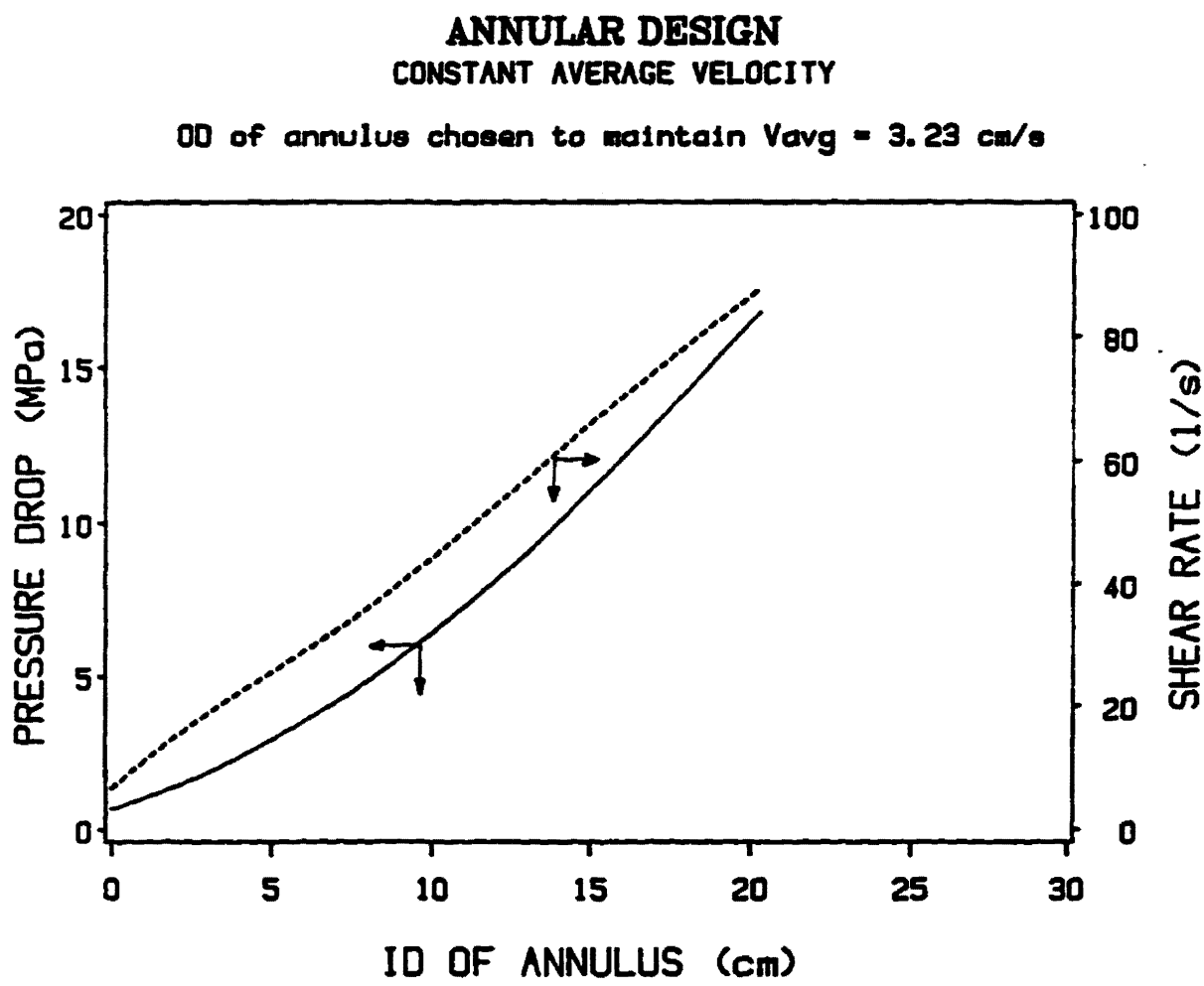


Figure 3.2.6 Pressure drop versus the nominal annulus diameter.

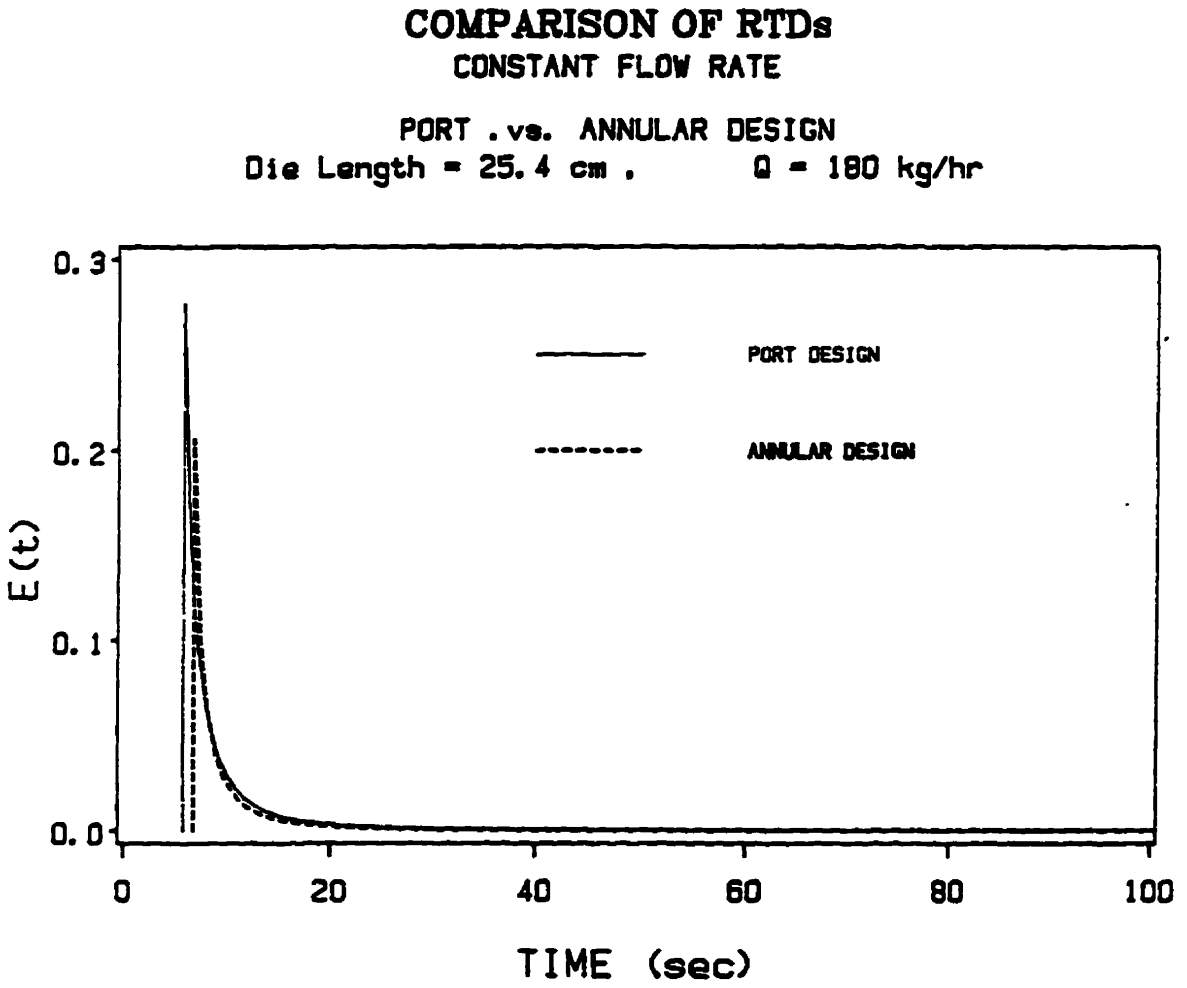


Figure 3.2.7 A comparison of the age distribution for a tube and an annulus.

Comparing Figures 3.2.4 and 3.2.6, it is observed that, unless the I.D. of the annulus is kept small, the port design system (Figure 3.2.4) will have a much lower pressure requirement than the annular system (Figure 3.2.6). A typical port design will have 8 ports and a pressure drop of about 2.93 MPa whereas the annular design with an I.D. of 10 cm and the equivalent average velocity will have a pressure drop of 6.5 MPa. This means that if the annular design is to have the same system operating pressure as the port design, the residence time of the material will be higher. This is represented in Figure 3.2.8 which shows how the average velocity decreases as the diameter of the annulus increases when the system pressure is kept constant. From Figure 3.2.8, it can be seen that an annulus with an I.D. of over 5.0 cm will have a lower average velocity than the 8 port system at equal pressure drops.

Now consider the complete RTD. Figure 3.2.9 shows the effect of increasing the diameter, but maintaining the system pressure constant, on the actual RTD of the system. The annulus dimensions and flow parameters are included in Figure 3.2.9. First, the lower average velocity (reduced to maintain the pressure drop) increases the minimum time required for the fastest moving fluid to exit the system. This shifts the initial peak to the right in Figure 3.2.9. Figure 3.2.9 also shows how the RTD broadens as the diameter of the annulus is increased (average velocity is lowered). In fact, it is this broadening of the distribution and not the minimum or average residence time that causes most of the problems. The broadening of the RTD can be represented by calculating the time it takes for 99% of the material, which entered the system at time zero, to exit. These are included in Figure 3.2.9.

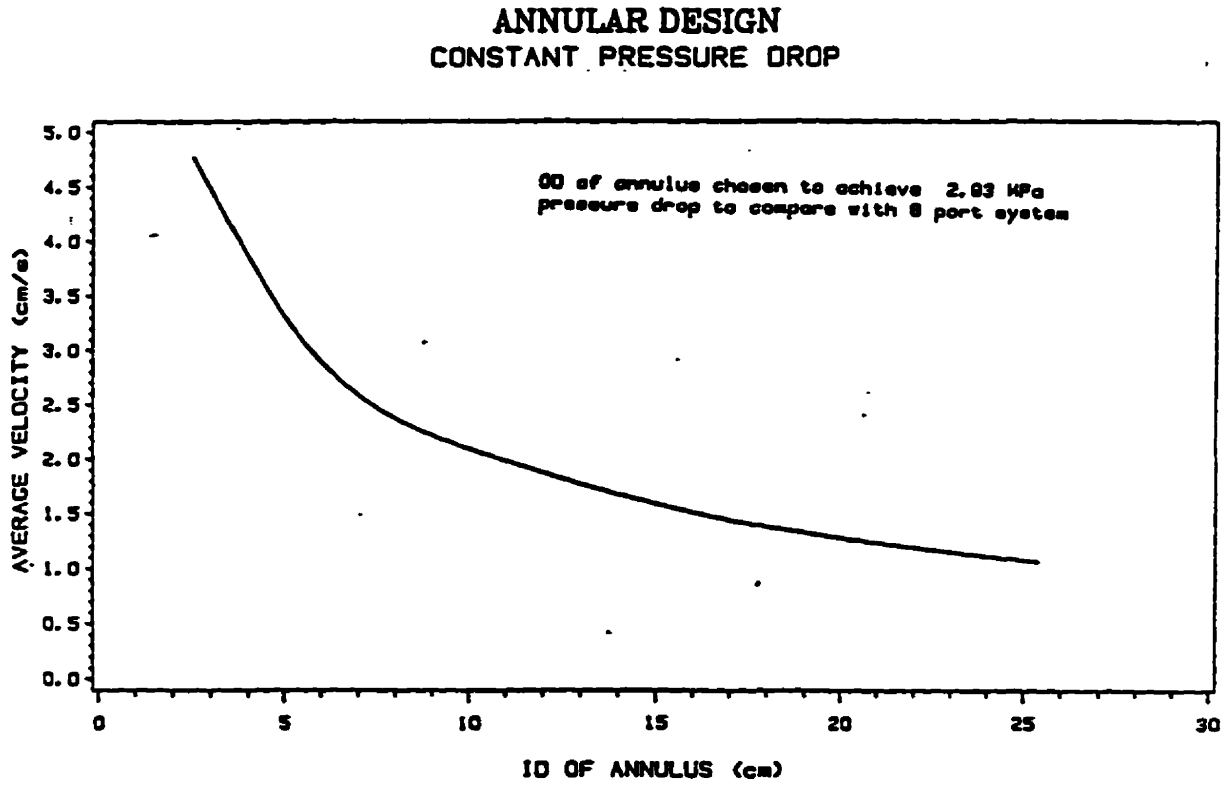


Figure 3.2.8 Pressure drop versus annulus diameter for a constant average velocity

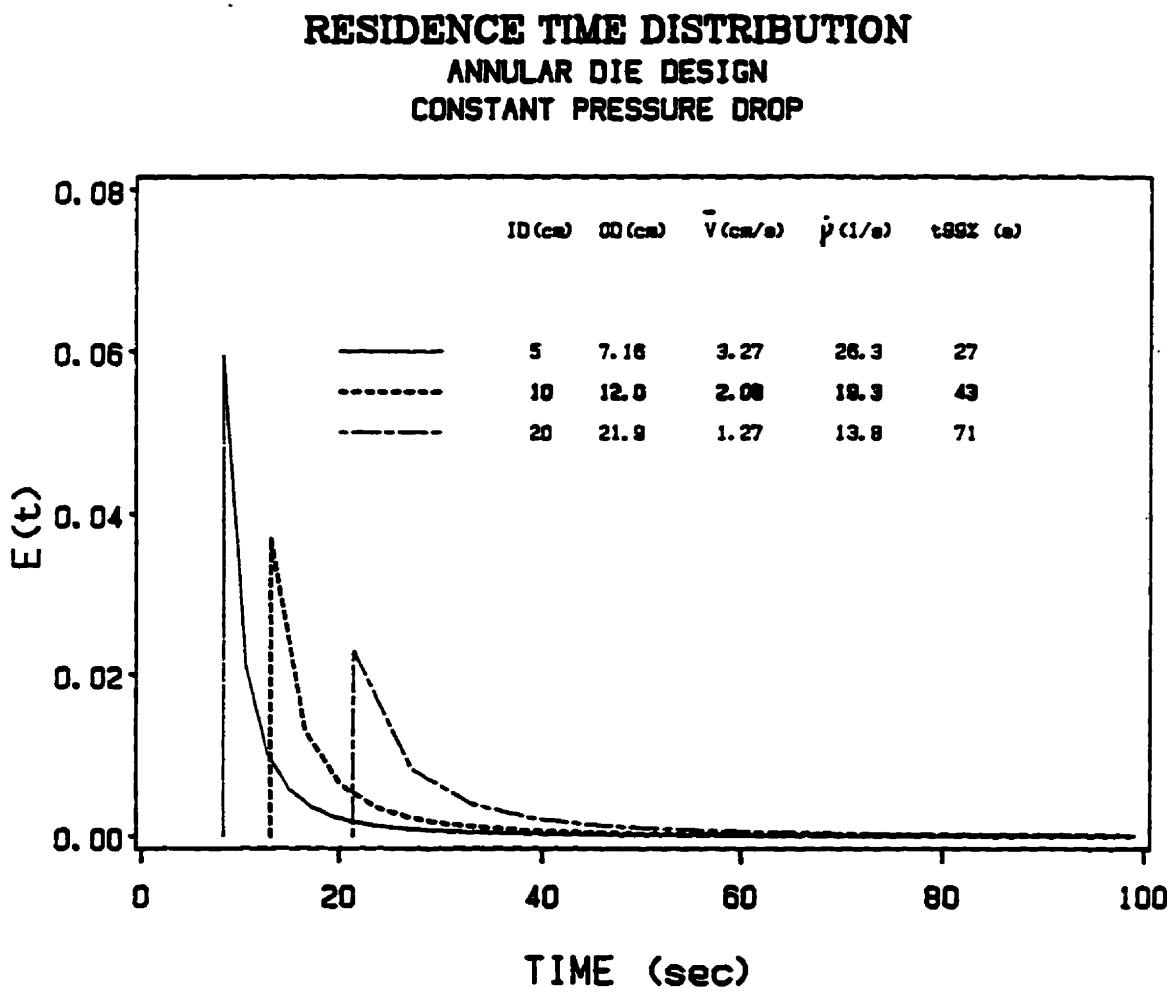


Figure 3.2.9 The age distribution versus nominal annulus diameter for a constant pressure drop.

These 99% times along with the minimum and average times are plotted in Figure 3.2.10 as functions of the diameter of the annulus. Again, the velocity is reduced to maintain the pressure constant for each system. One can see that although the minimum and average times are not changed dramatically, the effect on the time at which 99% of the material, entering the system at a particular time instant, exits from the system is more pronounced. This is very important in terms of answering questions pertaining to purging of the system when switching from one material to another and degradation of the polymer. This increase in residence time may result in excessive polymer degradation and the formation of gels.

This analysis has also assumed that the flow in the annulus is uniform. This is only true if the side feed distribution system is designed properly or if sufficient length is provided for the flow to even out on its own. Of course, this will create additional pressure drop in the annular design which is not required in the port design.

3.2.4 RTD and Flow Rate

Up to now the analysis has focused on the design of the coextrusion system but the operation of the system is just as important if not more so. Consider a three layer coextrusion die designed to produce a film of equal layer ratios (1:1:1). It will be assumed that the maximum production rate, due to cooling limitations, is 540 kg/hr (180 kg/hr/layer) and so each layer is supplied by a 90 mm (3.5") extruder. Even though the flow channels are designed for a 1:1:1 ratio, it is quite likely that the need may arise for the die to produce a film with a layer ratio of 8:1:3 or 360 kg/hr through the inner layer, 45 kg/hr through the middle layer and 135 kg/hr through the outer layer. If the upper limit on the extruder is 270

kg/hr, then in order to maintain the required layer ratios, the output of the other two layers will have to be reduced. The flow rate through the outer layer will be 100 kg/hr and the output through the middle layer will be 34 kg/hr. The flow rate through the middle layer has been reduced to less than 1/4 of what it was designed for. Figure 3.2.11 shows the broadening of the RTD as the flow rate is reduced through a tube with an I.D. of 5 cm and a length of 25 cm. This is only for a portion of the flow path but it shows how the 99% point increases from about 34 s at 180 kg/hr to 136 s at 45 kg/hr.

Performing this analysis for the complete system is much more difficult because the polymer flowing through each section of the die (adapters, ports, spirals, chambers, etc) will have a different velocity profile. Determining the RTD of two or three relatively short flow paths of varying geometry can be done quite easily using a Finite Element Method (FEM) analysis (Vlachopoulos et al, 1989). For large flow systems however, a FEM analysis is prohibitively expensive due to the amount of CPU time and memory required. The following section will present a procedure for quantifying the residence time behaviour of the spiral distribution system.

Most, if not all, polymer degradation takes place on the surfaces that comprise the flow system (screw, adaptor, block, die, etc). Since it is the polymer that is 'sticking' to the surface of the flow channels that has the highest potential for degradation, this surface area must be kept to a minimum. This analysis demonstrates how the port system offers the best design for obtaining lower relative system pressures while maintaining adequate velocities to ensure lower residence times.The analysis presented also shows the dramatic effect that flow rate (velocity) has on the RTD and how this can lead to processing difficulties.

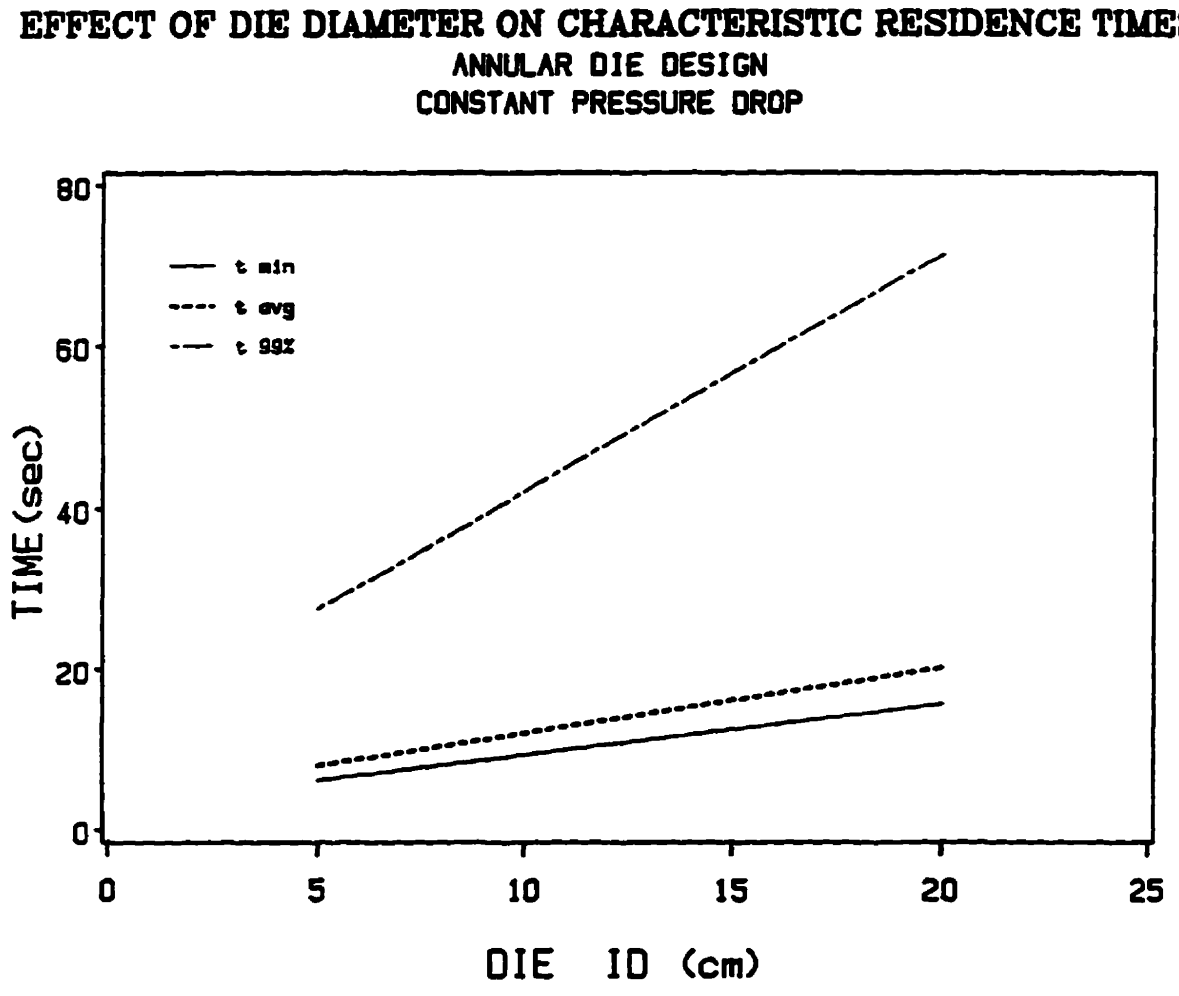


Figure 3.2.10 Various residence times versus nominal annulus diameter.

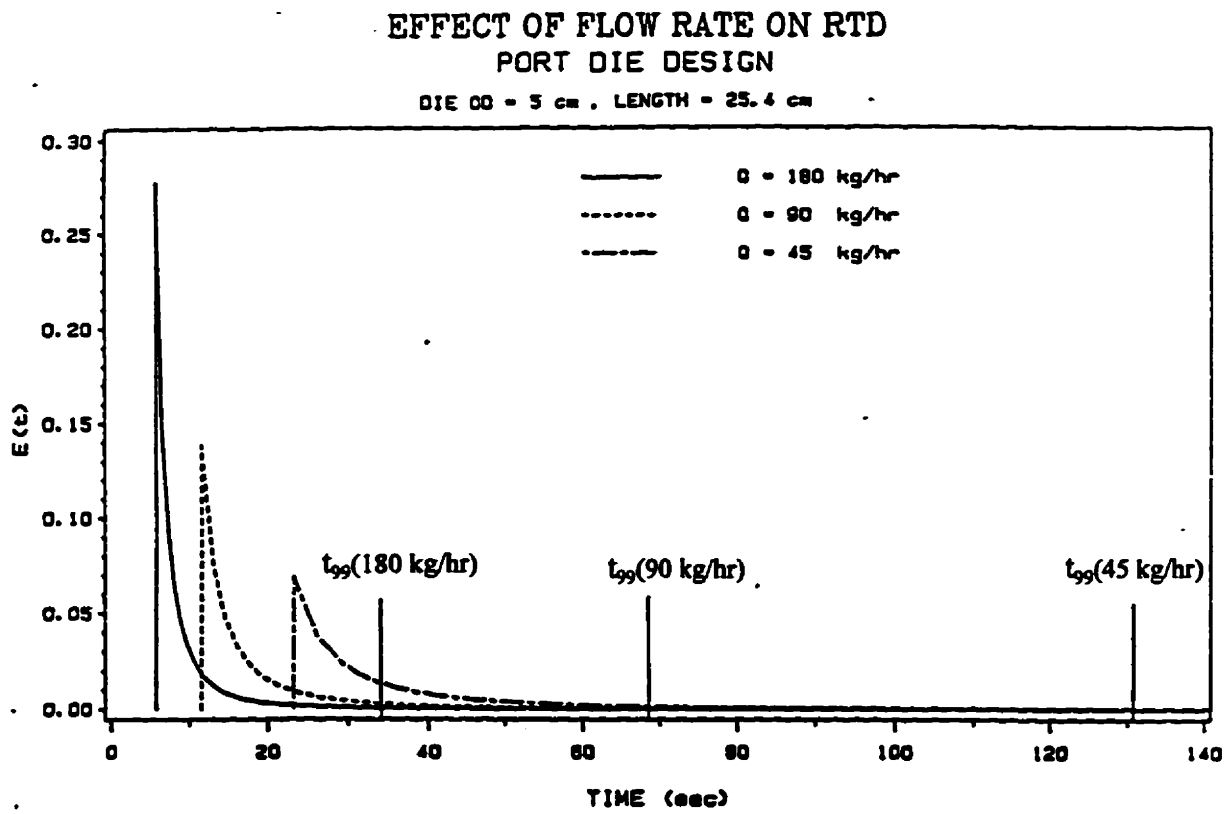


Figure 3.2.11 The RTD versus flow rate for a given system.

3.3 Residence Time Analysis in Spiral Dies

One of the most important components in a tubular film system is the die which distributes the melt into a uniform annular flow. As discussed earlier, this is typically done within a spiral distribution system. The complexity of the flow field, which exists in a spiral distribution system, requires that it be analyzed by numerical techniques. One of the most successful modelling techniques is the **Control Volume Method** (CVM) which approximates the flow system as a set of many smaller flow systems. This approach has been used to develop computer simulations that can accurately predict the flow patterns within spiral distribution systems (Vlcek et al, 1988). However, there has been little or no work to date on incorporating the capability of determining the residence time distribution to this analysis. Some preliminary investigations into the residence time distribution of a spiral mandrel die have been presented in a paper by Perdikoulias and Tzoganakis (1989), which included a very simplified model. It is believed that the approach presented here will provide more accurate and detailed results that can be used for quantitative comparisons.

3.3.1 Description of Method

From the existing computer simulations the average velocities in each of the control volumes, that comprise the spiral distribution system, are known. This implies that each control volume has a residence time associated with it. The total residence time experienced by an element of polymer melt at the exit of the spiral distribution system will

be a function of the time it spends within the control volumes through which it passes during its course through the die. From the flow analysis, it is possible to determine all of the possible flow paths from the entrance of the distribution system to the exit. Further, it is also possible to calculate the volume fraction of polymer melt for each flow of these flow paths. The resulting volume fraction and corresponding residence time data can be used as an indication of the residence time distribution of the polymer melt within the die.

The following example will help to illustrate this method. Consider the flow system in Figure 3.3.1. The system is divided into 6 control volumes. Assume that 100 units of material enter this system from the left of the first control volume and exit from the top of control volumes 4, 5 and 6. Further, the flow distribution in the system is also known to be as shown. For instance, the 100 units that enter control volume 1 are distributed such that 60 units go to control volume 2 and 40 units go to control volume 4. Of course, the sum of the material exiting from control volumes 4, 5 and 6 is equal to the material entering the system. Now consider the flow in control volume 6. The flow analysis has indicated that 30% of the material to enter the system will come out of this control volume. This 30% however, consists of material that has arrived at this point by 3 possible paths:

Path 1: 1 - 4 - 5 - 6

Path 2: 1 - 2 - 5 - 6

Path 3: 1 - 2 - 3 - 6

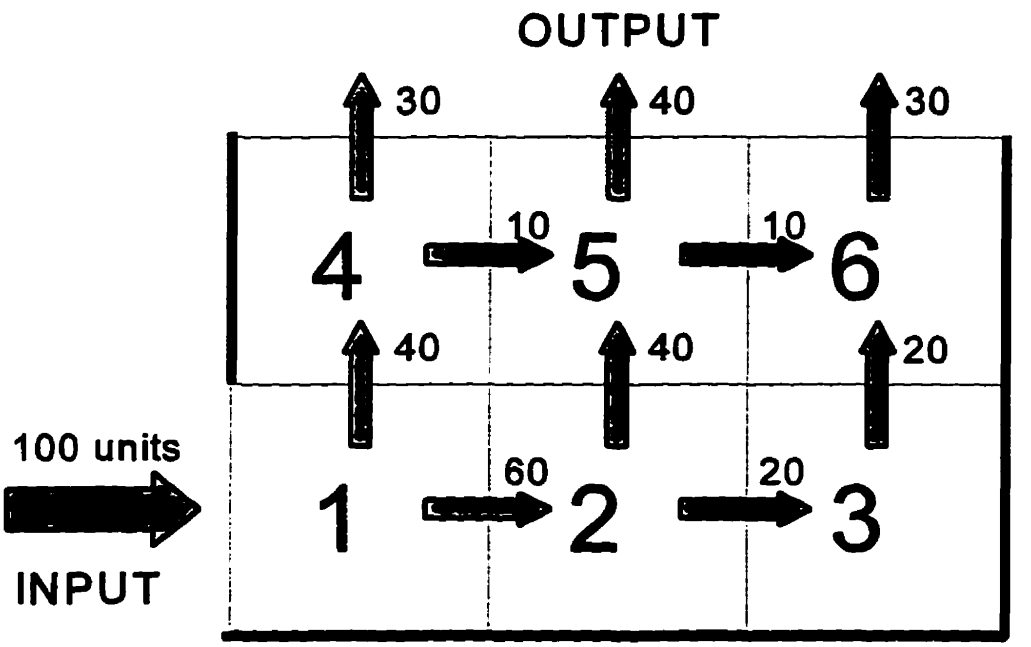


Figure 3.3.1 A simple flow system divided into 6 control volumes.

Since the possible flow paths are known, the amount of material through each path can be determined. Consider path 1:

1 - 4, 40% of material entering 1

4 - 5, 25% of material entering 4

5 - 6, 20% of material entering 5

$0.40 \times 0.25 \times 0.20 = 0.02$

This means that 2% of the original material took path 1. The residence time of this portion of material would therefore be the sum of the residence times in each of the control volumes that it passed through (1,4,5,6). Similarly, 8% of the original material took path 2 (1,2,5,6) and 20% of the original material took path 3 (1,2,3,6). Through this analysis, the composition (volume fraction through each path) of the material in each control volume can be determined along with the corresponding residence time of each volume fraction. These data can then be used to compare designs which exhibit residence time related problems to designs which have been proven more successful.

In this analysis, the residence time is represented by the average residence time of each control volume which is simply the volume divided by the flow rate. Hence, what results is not really a true residence time distribution but a distribution of average residence times. Nevertheless, this data should be better able to quantify the mixing (spreading) effect of the spiral mandrel distribution.

3.3.2 Application to a Spiral Die

The method described above was applied to a spiral mandrel die used in some previously performed visualization experiments by Perdikoulias and Tzoganakis (1989). Figure 3.3.2 is a representation of the flow geometry. Details about the die geometry can be found in the original publication. The residence time analysis was performed for the two flow fields used in the previously published experiments.

The basic difference between the dies was that Die 1 had a constant 1 mm gap between the body and the mandrel while Die 2 had a constant 2 mm gap between the body and the mandrel. This was accomplished by simply changing the die body and thus keeping all other dimension constant. Of course this gap change altered the flow field considerably as can be seen in Figure 3.3.3. This figure is a plot of the predicted volumetric flow in the channel versus channel length for Die 1 and Die 2. For this analysis, the total spiral channel is divided into 60 control volumes or elements. Increasing the die gap allows more of the fluid to leave the channels sooner and increases the total hold-up volume of the system. This will result in a larger average residence time and a different residence time distribution.

The RTD analysis method described above has been used to determine the RTD for both Die 1 and Die 2 in order to determine whether the method could be used to quantify the differences between these two dies. It should be noted that the 3-D flow field in the spiral mandrel distribution system is significantly more complex than the 6 element, 2-D flow field used in the above example. In fact, the 60 elements used in this analysis resulted

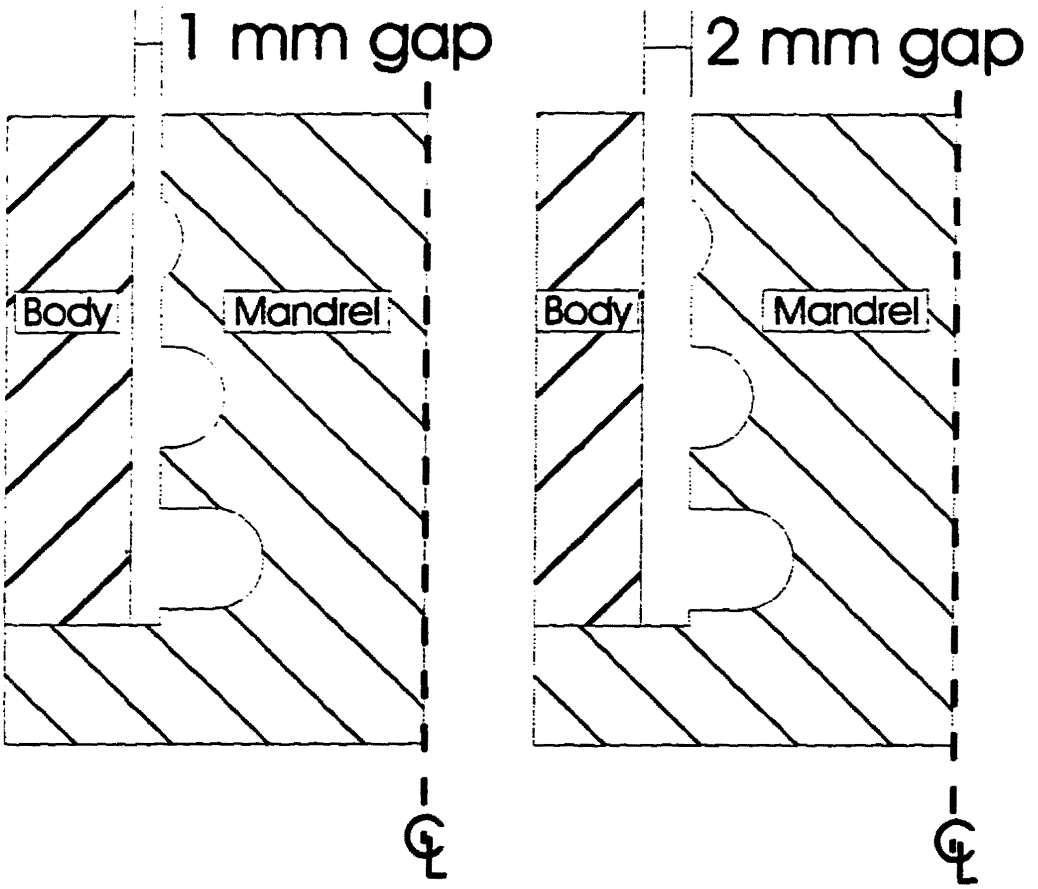


Figure 3.3.2 The flow geometry of the spiral mandrel die.

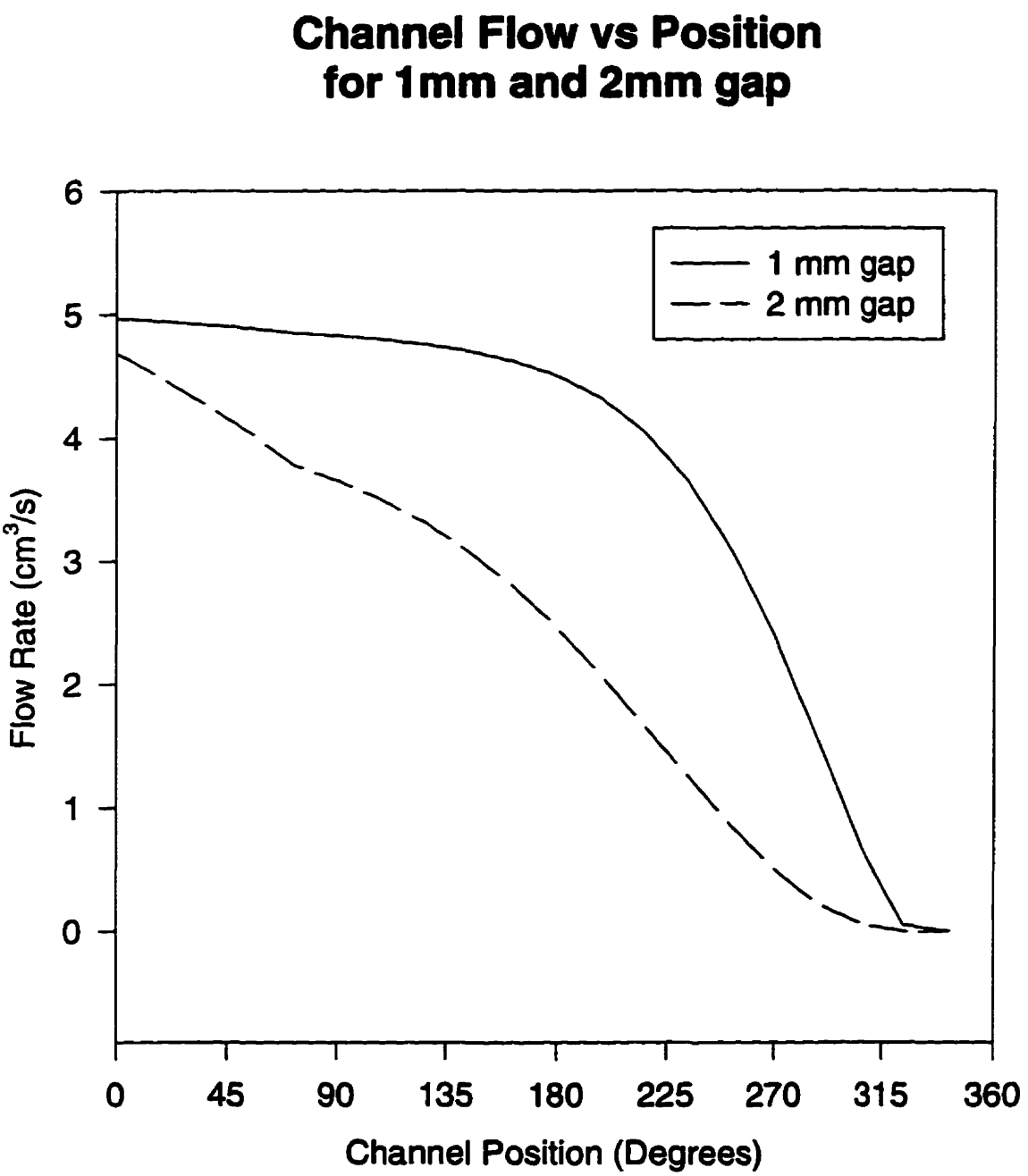


Figure 3.3.3 Channel flow versus channel length for the 1 mm and 2 mm gap geometry.

in over 5000 possible paths the fluid could take from the first to the last element. The volume fractions and corresponding average residence times were calculated for each of the control volumes at the exit of the spiral section. A time step of 0.25 seconds was chosen and volume fractions with average residence times within the same time step were added together. This resulted in a complete average residence time distribution shown in Figures 3.3.4 and 3.3.5 for Die 1 and Die 2, respectively. Figure 3.3.4 shows a relatively narrow distribution with a well defined peak while Figure 3.3.5 shows a substantial broadening of the distribution resulting from the larger gap.

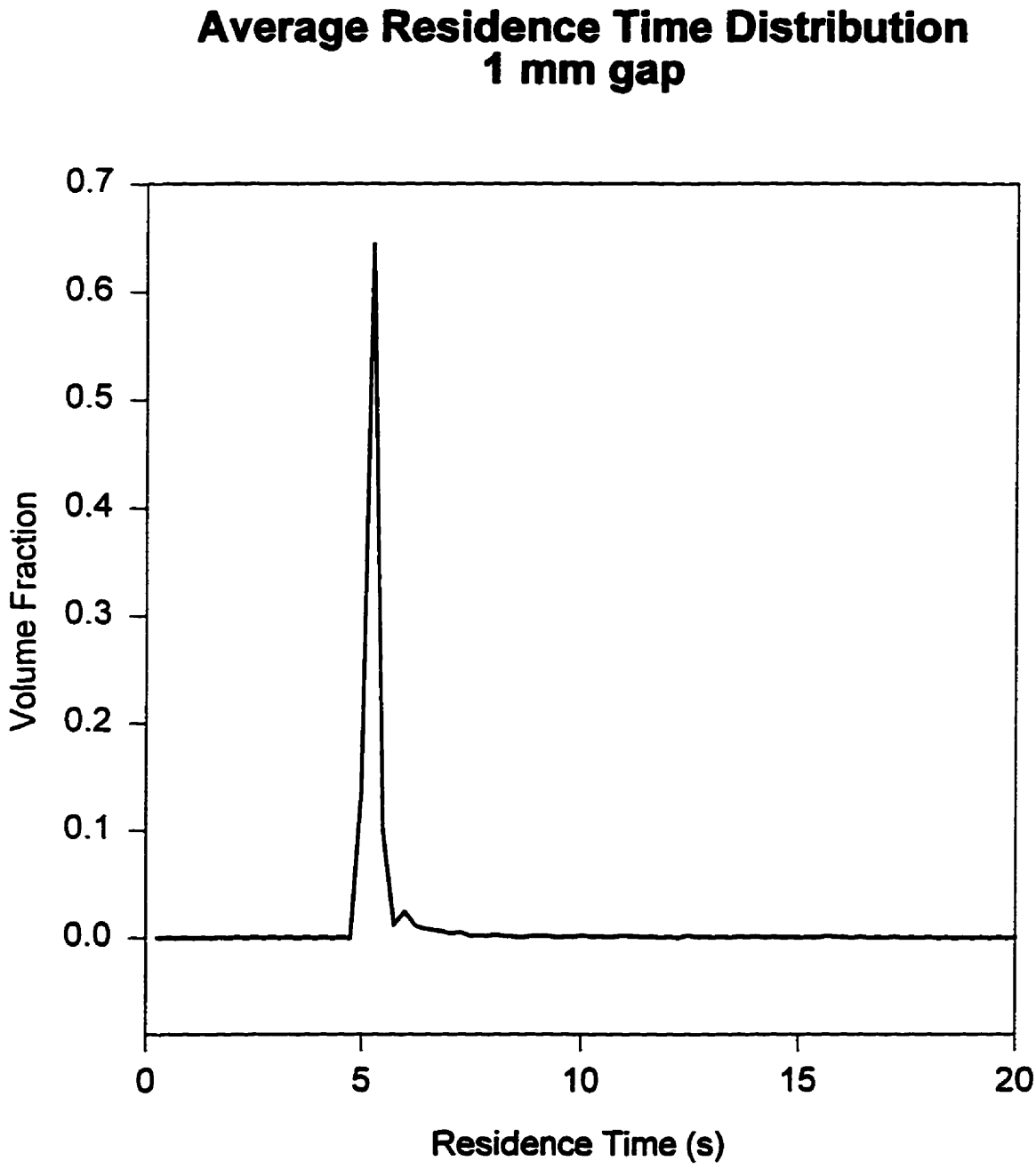


Figure 3.3.4 Average residence time distribution for the 1 mm gap geometry.

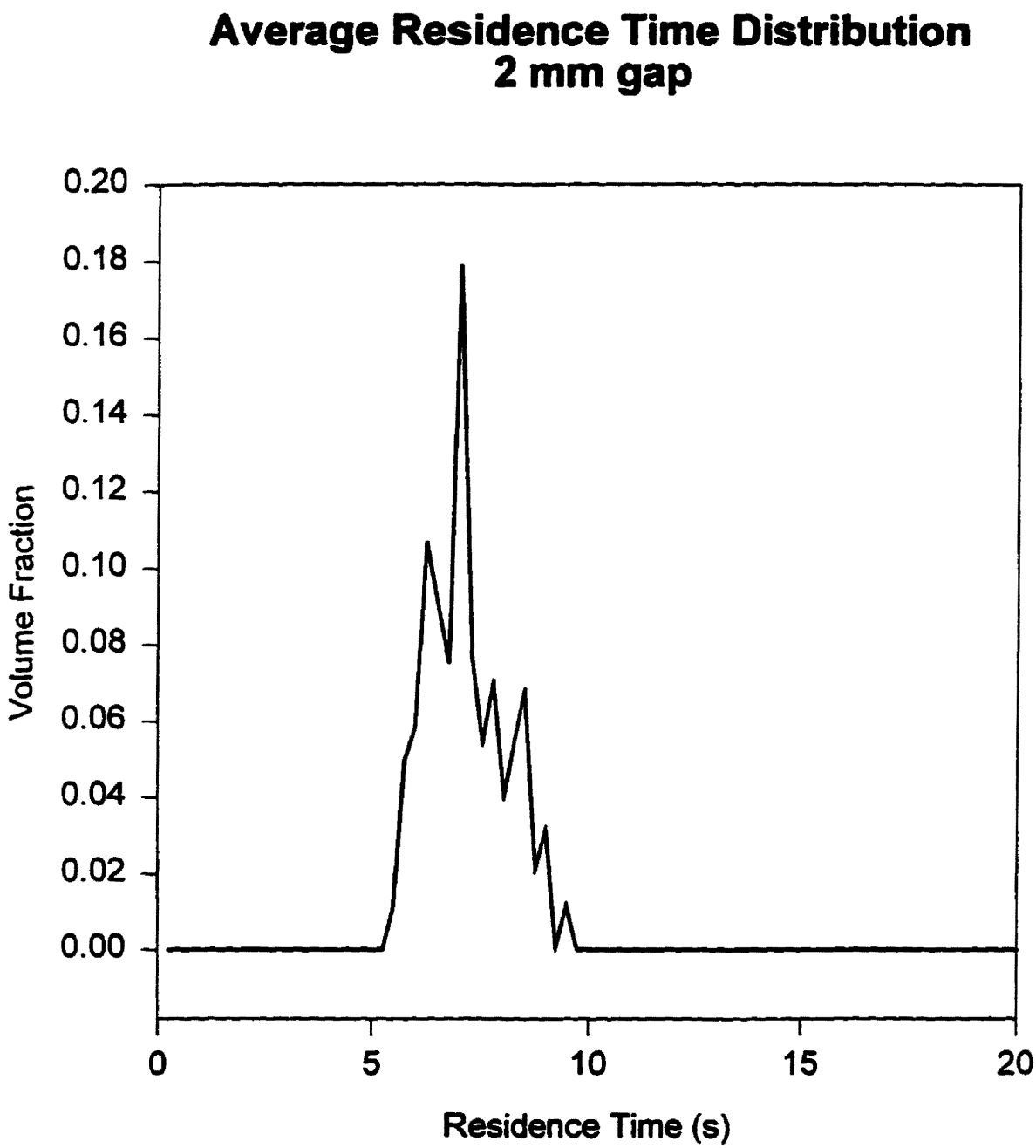


Figure 3.3.5 Average residence time distribution for the 2 mm gap geometry.

3.4 Discussion

Even though the Die 1 geometry resulted in the material having a shorter overall residence time in the system, it does not necessarily mean that it will be the better design. Figure 3.3.3 shows that the channel flow in Die 1 does not really begin to reduce until about the 10th element. This means that only about one half of the total channel length is really being used to distribute the material. Figure 3.3.4 shows that the Die 2 geometry results in an almost linear reduction of channel flow over the total channel length. In other words, more of the spiral channel is being used to distribute the material. The corresponding broader distribution shown in Figure 3.3.6 indicates that the Die 2 geometry results in better mixing characteristics. This would tend to improve material homogeneity around the circumference of the die and ultimately the final product. The above method provides a means of quantifying a characteristic residence time distribution for a spiral mandrel die based on a control volume method analysis. It should be emphasized however, that this characteristic residence time distribution is based on the average velocity of the material within each control volume and therefore does not account for the slow moving material near the surface of the flow field.

CHAPTER 4

NEW FLAT SPIRAL DIE DESIGN

4.1 Introduction of Concept

In Chapter 3 it was determined that an annular flow channel was a relatively inefficient method of conveying a polymer melt and therefore a port block design is preferable. Now consider the single layer blown film die shown in Figure 4.1.1. By removing the spiral channels and other details, this die can be represented as a simple annular channel shown in Figure 4.1.2. Even though we have shown that the annular channel is inefficient at conveying polymer, at some point it is essential to creating a tube. Now consider a similar representation of a typical 5 layer coextrusion die configuration shown in Figure 4.1.3. The layers are nested together with each layer represented by an annulus at the indicated diameters. The centre layer 'C' merges with layers 'B' and 'D' and then these three layers merge with layers 'A' and 'E' prior to exiting the die. Now consider the following. The production rate in the blown film process is typically cooling limited. Since cooling is a function of the surface area, the output becomes a function of the die size. In fact the industry commonly refers to a specific output rate such as (rate)/(circumferential exit length) or (rate)/(die exit diameter). Therefore, if the single layer die shown in Figure 4.1.2 and the 5 layer die shown in Figure 4.1.3 had the same nominal exit diameter and they

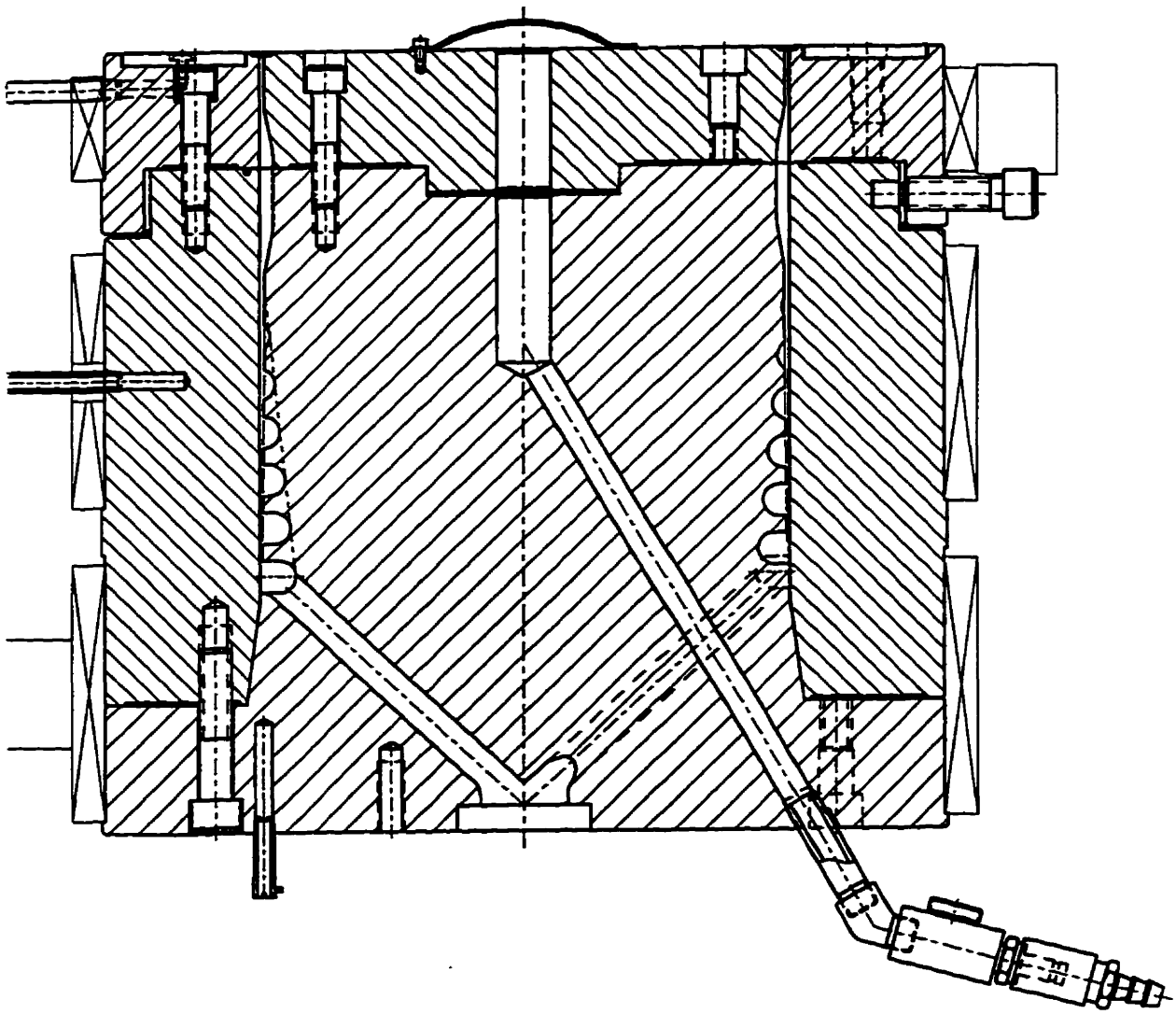


Figure 4.1.1 A single layer spiral mandrel blown film die. (Brampton Engineering)

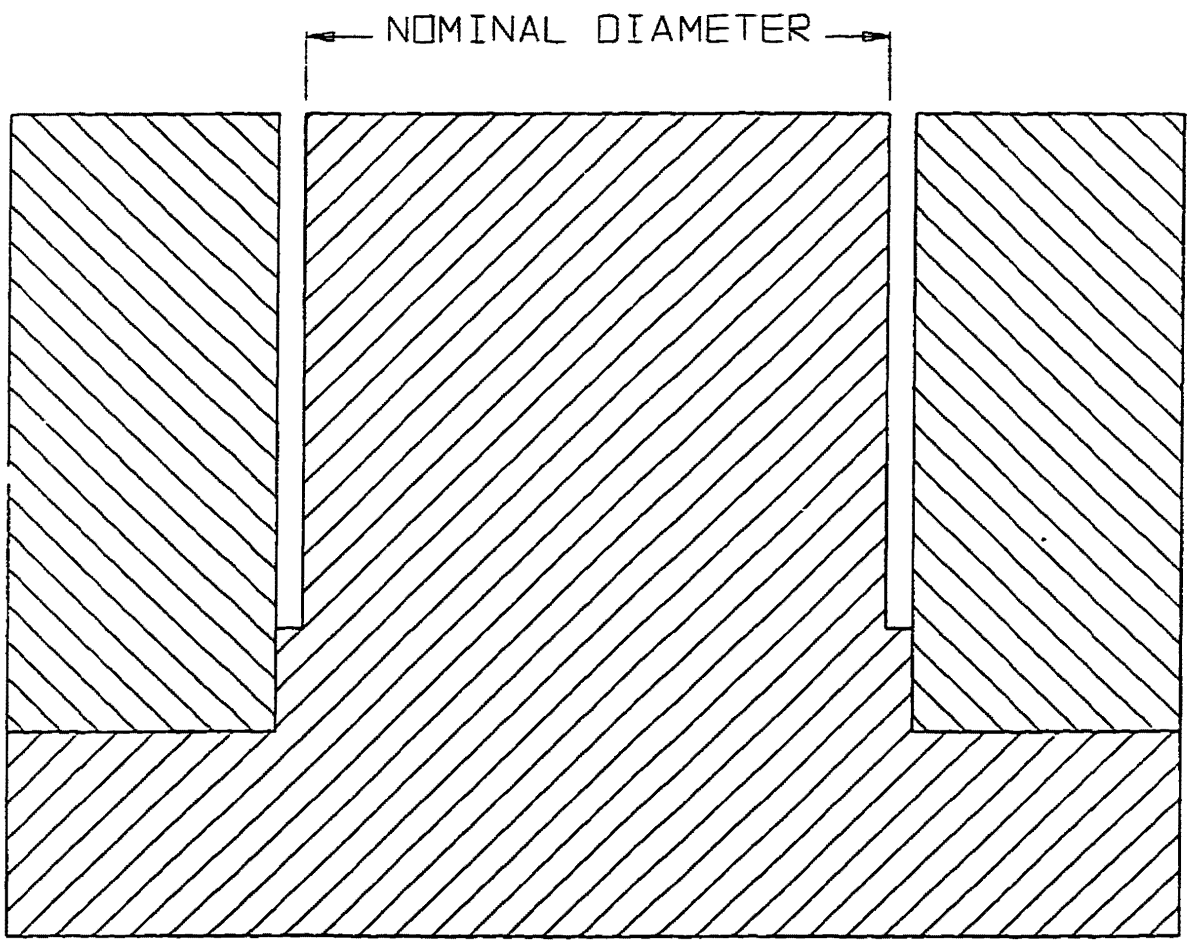


Figure 4.1.2 A simple representation of a single layer annular die.

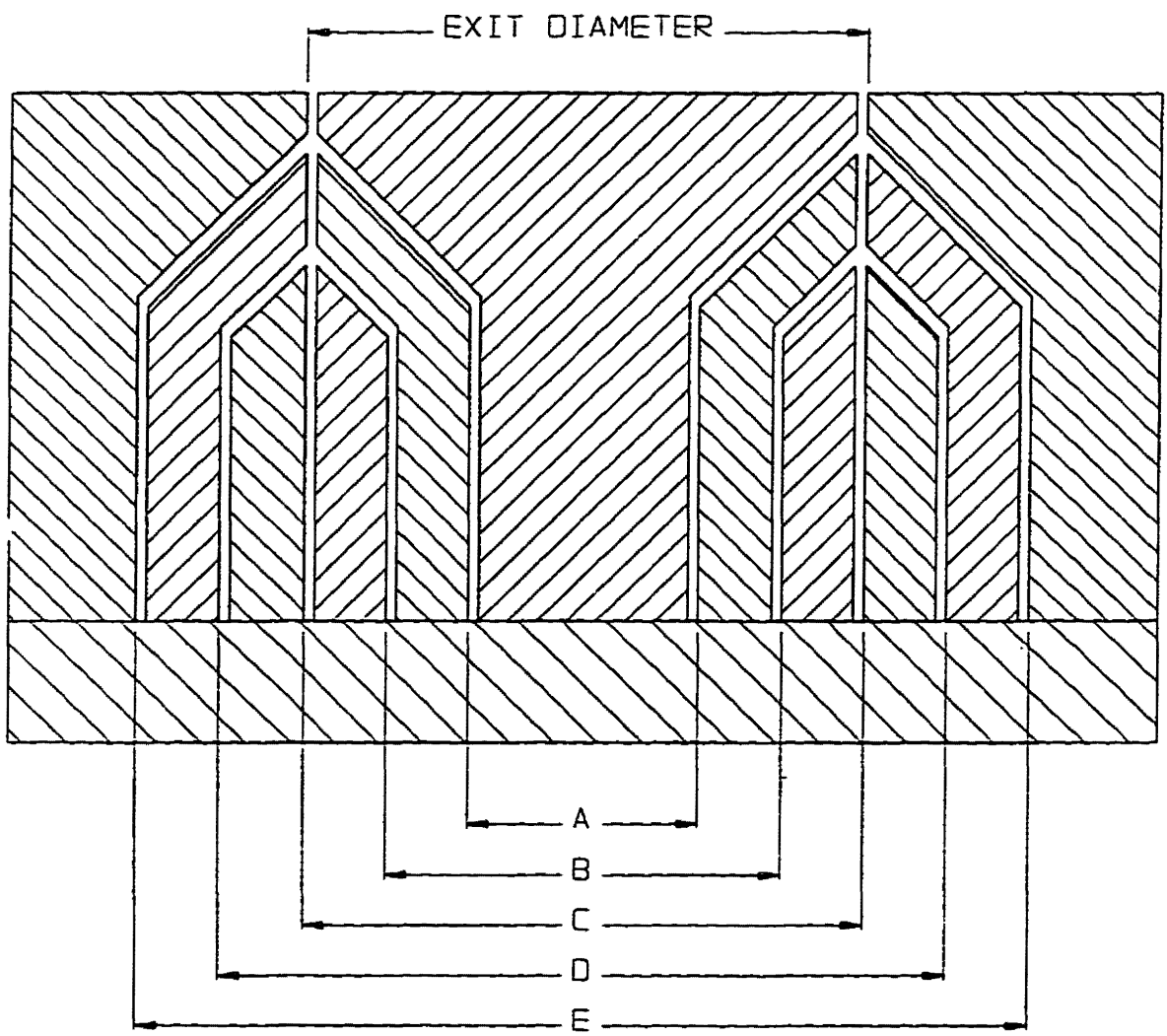


Figure 4.1.3 A simple representation of a five layer annular die.

were processing the same polymer, the production rate of both these dies would be identical. However, the 5 layer die has approximately 5 times more surface area than the single layer die. Furthermore, the surface area is lowest for the inner layer and increases towards the outer layers.

Now consider the design from a fluid mechanics viewpoint. If it is assumed that the flow in the 5 layer die is divided equally among the 5 layers, then, each layer would have 1/5 the amount of material that would be flowing through the single layer die. If the design criterion requires that the polymer flowing through each of the layers has the same average velocity as the polymer flowing through the single layer die, then the cross section area of each layer would have to be reduced accordingly. The analysis in chapter 3 showed how dramatically the pressure drop increased as the flow was reduced but the average velocity remained constant. It was also shown, in chapter 3, how the pressure requirements increase with the nominal diameter of the annulus. These results prompted the development of an improved design which would be more efficient at conveying the polymer while still maintaining the benefits of a spiral mandrel distribution system.

It was deduced that the difference in surface area amongst the layers could be minimized if the layers were stacked on top of each other as represented in Figure 4.1.4 . In this figure each layer would consist of two plates which form a module. It is relatively easy to see that the flow area of all of the modules can be identical if so desired. The only layer which would be exposed to a significantly higher surface area than the rest would be the inside layer which would flow against the surface of the centre mandrel. This is of little

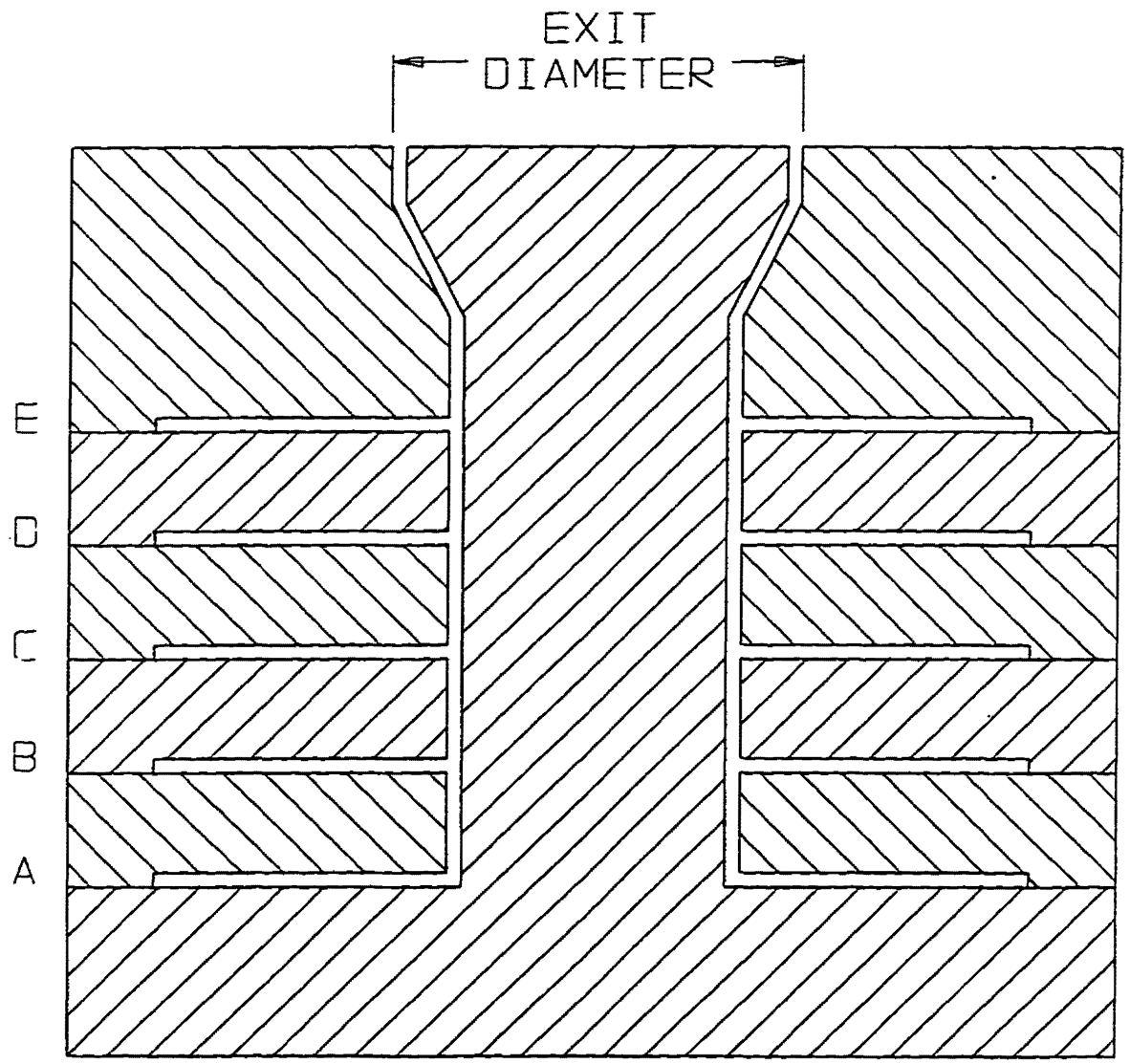


Figure 4.1.4 A simple representation of a five layer 'stacked' annular die.

consequence since this material would generally be a relatively stable polyolefin. The polymer in each of the other layers would only contact the surface of its own module before being encapsulated by the next layer. This is especially significant since the materials in these layers are generally adhesives and barrier resins which are more prone to thermal degradation (Foster, 1989; Volungus, 1991). The increased surface area of the inside layer can be offset by the fact that the mandrel diameter can be kept relatively small. This also helps to reduce the pressure requirements of the system.

It should be pointed out that the idea of 'stacking' the layers is not completely new. In fact, this 'stacked' configuration has been used with blow moulding dies since the late 50's (Colombo, 1958; Shrenk, 1967). However, these designs had some disadvantages which made them unattractive for blown film applications. In general, these designs used a simple side feed distribution system as shown in Figure 4.1.5. The polymer is essentially split into two flow streams which are distributed around the circumference of the die and meet at a point directly opposite to the entrance point. This would resemble a flat die distribution system that has been wrapped around so that the edges would connect. This distribution system, however, suffers from a couple of drawbacks. First, the merging of the streams around the back of the die entrance generally results in a stagnant flow region where the polymer may degrade. Secondly, there is no overlapping of the flow streams as would happen in a conventional spiral mandrel die. This means that the orientation of the weld line would be perpendicular to the axis of the die and possibly result in a weak point or a visual defect in the final product. In addition, the lack of overlapping makes the die more sensitive to any inhomogeneities in the melt stream entering the die. For these reasons, it was

desirable to incorporate a spiral distribution system into the new configuration.

Figure 4.1.6 is a drawing of a flat spiral distribution system with 4 spirals, each of which travels 360 degrees. Figure 4.1.7 is a side view showing how the depth of the spiral decreases from its start to its finish. The polymer entering the die must be divided equally among the spirals. This is done with a binary distribution system prior to the spirals as shown in Figure 4.1.6. In the binary distribution system, the polymer entering the die is first divided into two identical flow streams. Then each of these streams is also divided into two streams resulting in 4 streams of equal flow. The flat spiral distribution system then distributes the flow in a similar manner as would a conventional cylindrical spiral distribution system. The goal is to obtain a circumferentially uniform radial flow stream. This radial stream can then be redirected to flow in the die's axial direction. The following section describes the development of a modelling procedure for ensuring a proper distribution system design.

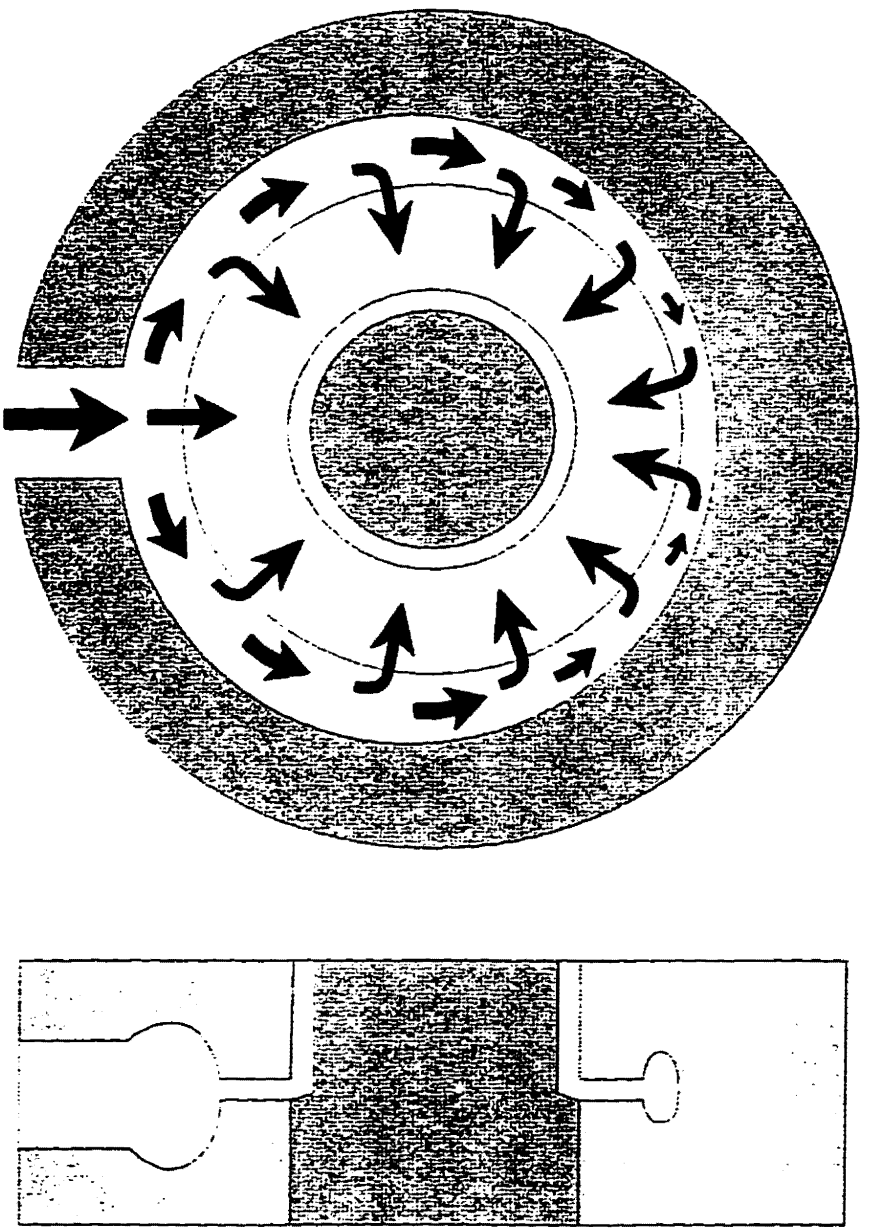


Figure 4.1.5 A typical side feed distribution system.

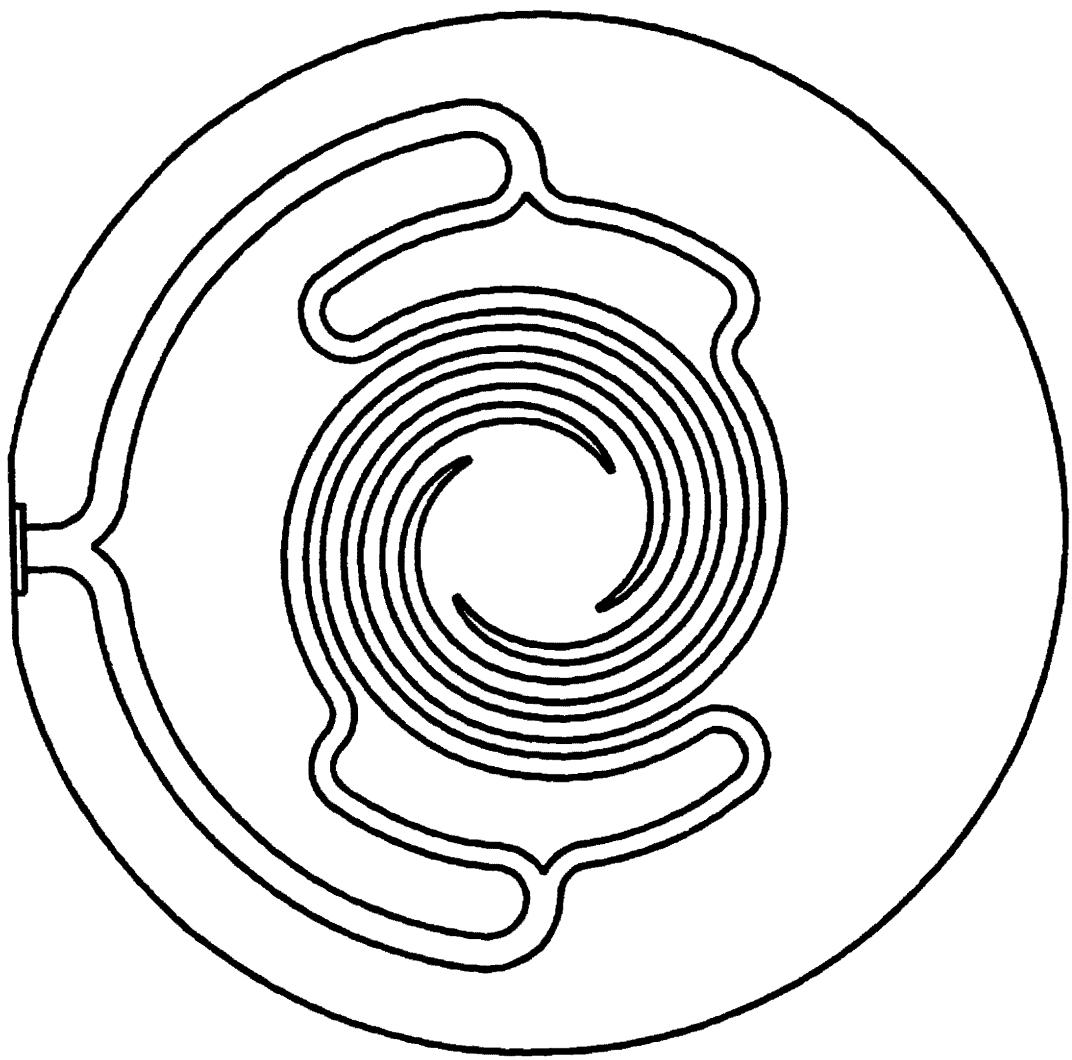


Figure 4.1.6 A flat spiral die distribution system with 4 spirals.

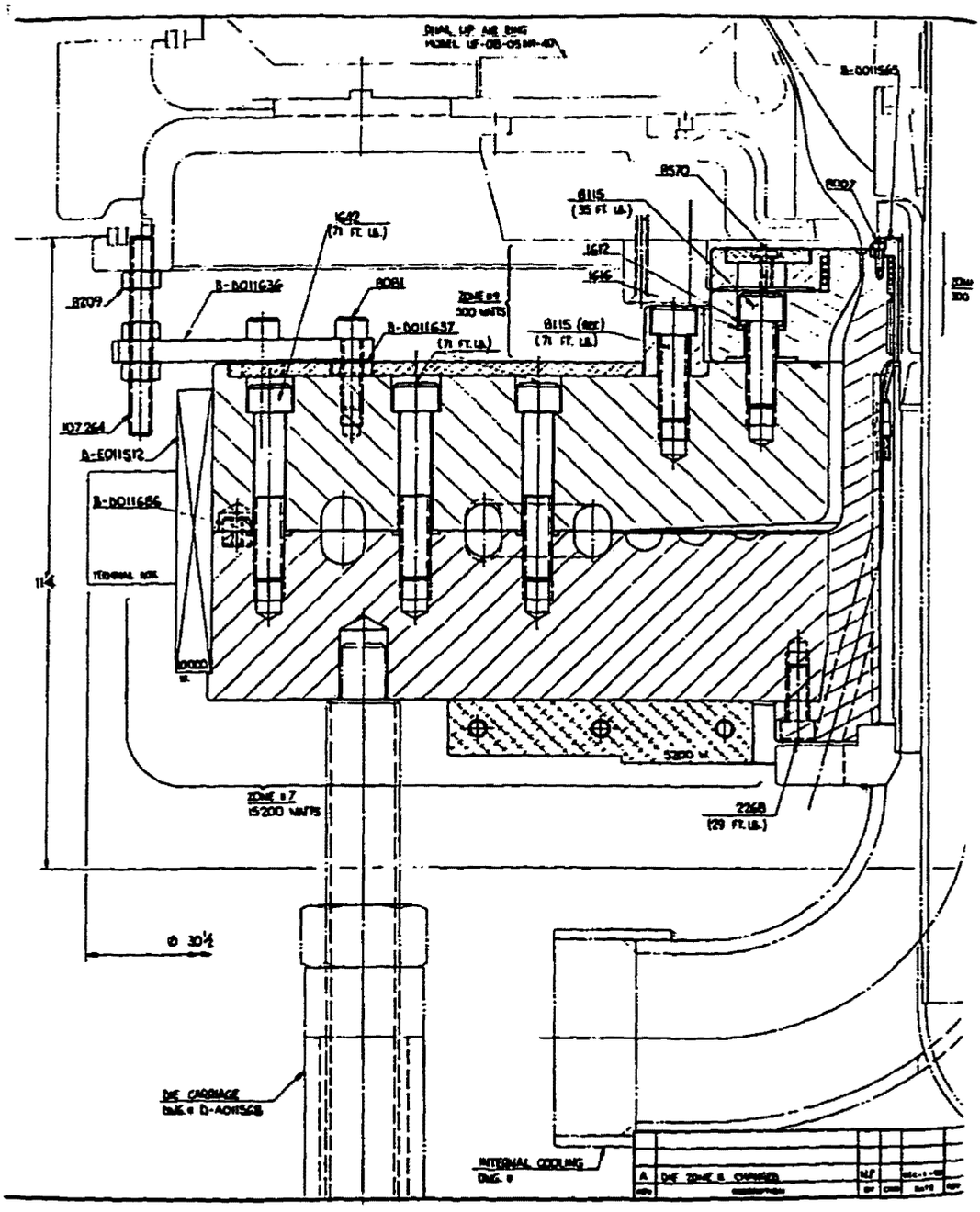


Figure 4.1.7 A cross section of a flat spiral die distribution system.

4.2 Flat Spiral Modelling

The modelling technique that will be used is based on the Control Volume Method which was used by Vlcek et al (1988) for the modelling of conventional spiral mandrel dies. The method begins with the division of the flow field into a set of small control volumes. Consider just the spiral section of the flat spiral distribution system shown in Figure 4.1.6. It is fairly easy to see that there is a periodicity to the geometry such that each quadrant is identical. The analysis can be simplified if this periodicity is used because only one quadrant (or section) will have to be modelled. Figure 4.2.1 represents one section of a spiral flat die which has been divided radially (r-direction) and circumferentially (θ-direction). The radial divisions are a result of the number of overlaps that are used; 4 in this case. The number of circumferential divisions is arbitrarily chosen as 5 for the purpose of this demonstration. For actual design purposes, the number of division depends on the design and the required accuracy. This has a particular influence on the first assumption that is made during this modelling procedure; neglecting the effect of curvature. Figure 4.2.2 represents a perspective view of one major control volume from Figure 4.2.1. Figure 4.2.3 is a side view of a flat spiral section showing the flow directions and the sub-division into smaller control volumes. Each control volume is assumed to have two significant flow directions (Q and q) as represented by the arrows in the Figures. In addition, each control volume also has a pressure node associated with it. Another assumption that is made is that all the flows are of the Poiseuille type. This means that the flow in any direction is a function of the pressure drop.

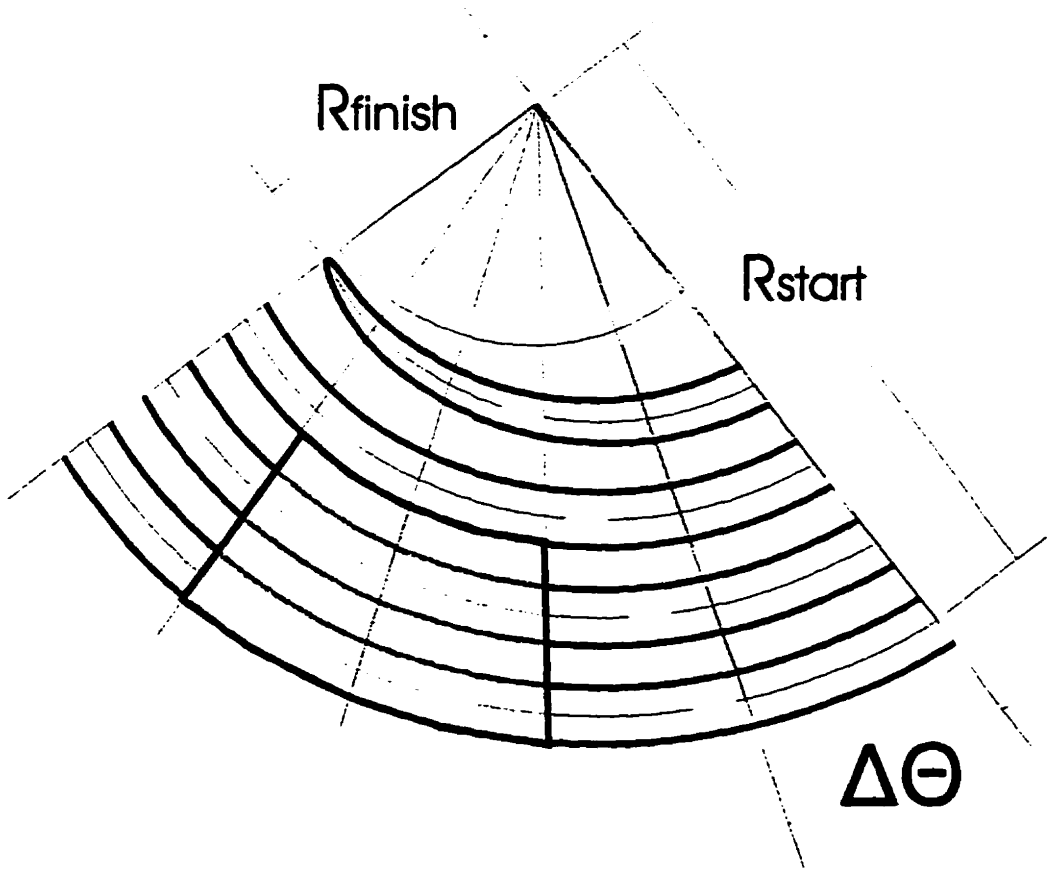


Figure 4.2.1 A representation of one periodic section in flat spiral distribution system

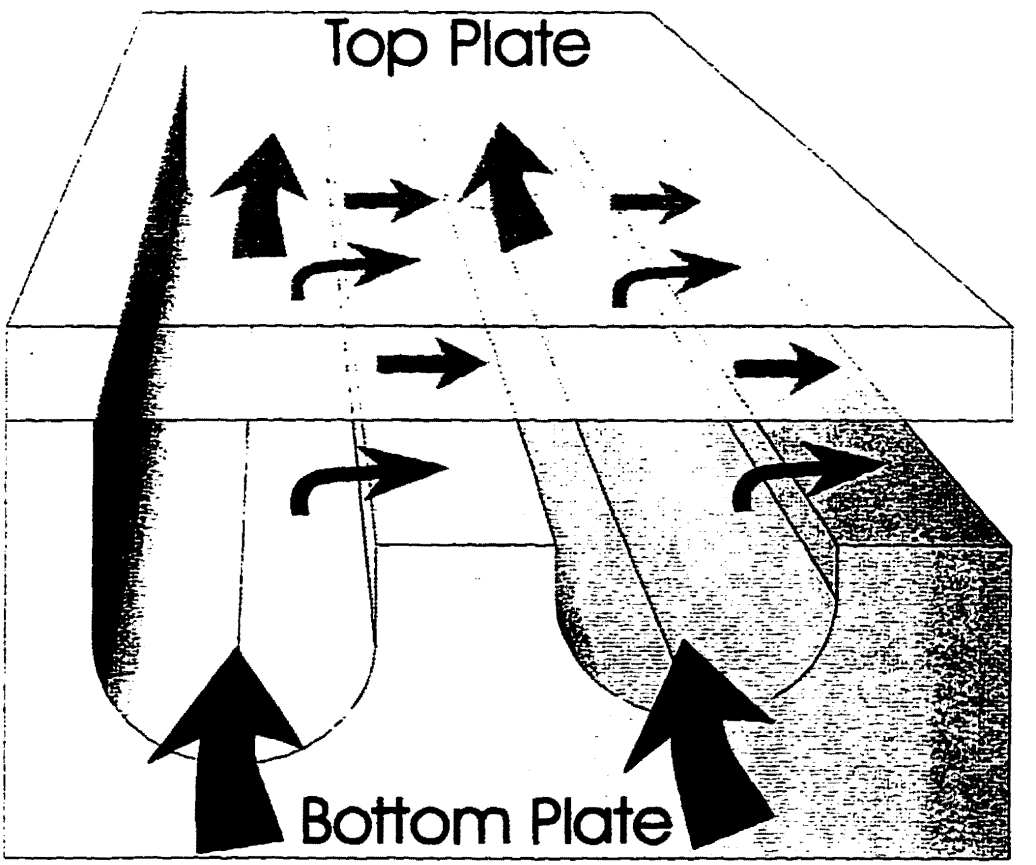


Figure 4.2.2 A perspective view of the geometry showing the flow field.

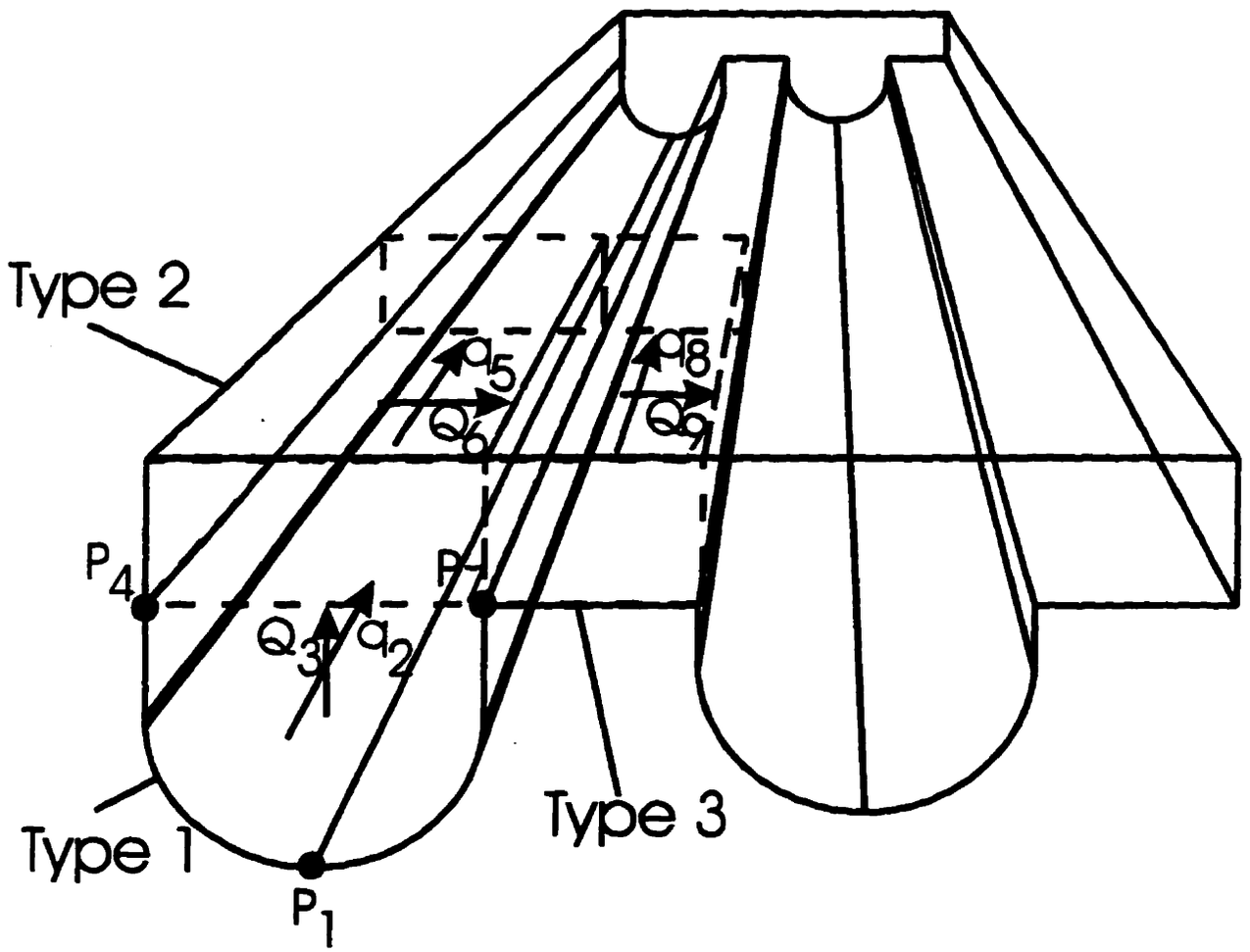


Figure 4.2.3 A perspective view of the flow field showing the three different types of control volumes.

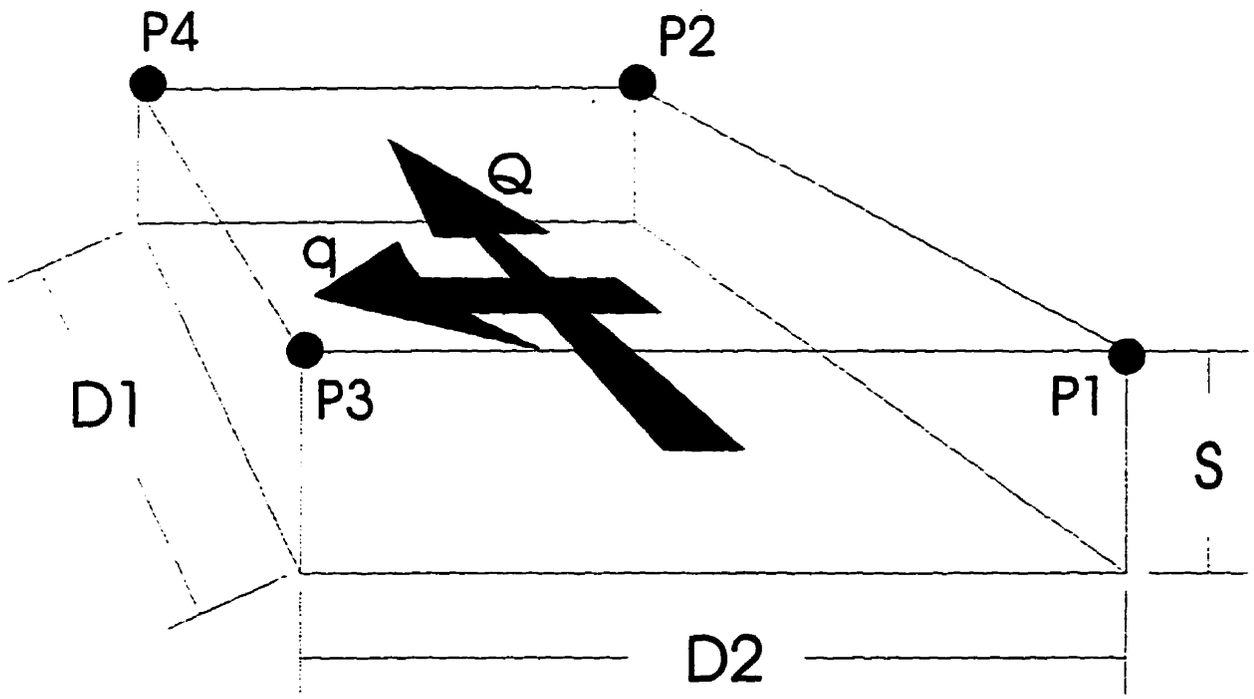


Figure 4.2.4 A representation of the variables associated with a type 3 control volume (flow between flat plates).

Figure 4.2.4 represents a typical control volume which can be modelled as flow between two flat plates. The flow equations take the following form:

$$\frac{dP}{dx}=f(Q,q)Q$$
$$\frac{dP}{dy}=g(Q,q)q \tag{4.1}$$

where f(Q,q) and g(Q,q) represent the resistance functions and Q and q are the volumetric flow rates in the x and y directions, respectively.

For a power-law viscosity model, the resistance functions take on the following form:

$$f(Q,q)=\left(\frac{2mD_1\dot{\gamma}^{(n-1)}}{S}\right)\left(\frac{2(2+\frac{1}{n})}{D_2S^2}\right)$$
$$g(Q,q)=\left(\frac{2mD_2\dot{\gamma}^{(n-1)}}{S}\right)\left(\frac{2(2+\frac{1}{n})}{D_2S^2}\right) \tag{4.2}$$

where D1, D2 and S are the dimensions shown in Figure 4.2.4. The quantity $\dot{\gamma}$ is the total

shear rate given by:

$$\dot{\gamma} = (\dot{\gamma}_1^2 + \dot{\gamma}_2^2)^{\frac{1}{2}}$$
$$\dot{\gamma}_1 = \frac{2(2+\frac{1}{n})Q}{D_2 S^2} \qquad (4.3)$$
$$\dot{\gamma}_2 = \frac{2(2+\frac{1}{n})q}{D_1 S^2}$$

A third independent equation comes from continuity of flow:

$$Q + q = Q^* + q^* \qquad (4.4)$$

where Q* and q* are the volumetric flows in adjacent control volumes. The remaining equations can be found in the literature (Vlcek et al, 1988).

There are essentially two boundary conditions in this problem. First, the flow entering the distribution system is assumed to be known or specified. Second, the pressure at the exit of the distribution system is also assumed to be known. It is generally assumed to be zero gauge. Since there is a periodicity to this flow field, it is advantageous to use a periodic boundary condition. This simply states that the flow that exits from one side of the flow field is equal to the flow entering from the other side. Since the equations are derived for a non-Newtonian fluid, an iterative approach is used to obtain a solution. The initial

condition assumes that there is a constant rate of flow out of the channel to the exit. A Fortran computer program was written to perform the above analysis and the following section presents a verification of the results.

4.3 Experimental Verification

In order to check the simulations and confirm the accuracy of the model, a prototype die was designed and manufactured. It was determined that the die would be designed for an LLDPE and tested with 3 materials. These are 2 LLDPEs (Dow 2045 and Dow 2071) and 1 LDPE (Dow 607). The material properties used in the simulations are shown in Table 4.3.1.

Table 4.3.1 Material Properties for Experimental Evaluation

	DOW 2045	DOW 2071	DOW 607
Consistency Index	8100	6600	3545
Power-law Coefficient	.565	.726	.625
Density (kg/m^3)	760	760	760
Temperature (°C)	210	210	190

The die manufactured had 4 spirals, each of which travelled 360°. The input parameters for the simulation are shown in Table 4.3.2. The number of divisions per section is 10 and the solution tolerance for convergence requires that the norm of the residuals is less than 0.01 .

Table 4.3.2 Input Parameters for the Simulation

Parameter	Value	Parameter	Value
Starting Diameter (mm)	330.2	Ending Diameter (mm)	152.4
Starting Gap (mm)	0.5	Ending Gap (mm)	4.0
Starting Channel Depth (mm)	22	Ending Channel Depth (mm)	0
Initial Channel Width (mm)	12.7		
Number of Channels	4	Number of Overlaps	4
Flow Rate (kg/hr)	110	Density (kg/m^3)	760
Consistency Coefficient ($Pa \cdot s^n$)	8100	Power-Law Index	.565
Number of divisions	10	Solution Tolerance	.01

Figures 4.3.1 to 4.3.3 show the predicted flow characteristics of the die using the parameters in Table 4.3.2. Figures 4.3.1 is a plot of the channel flow along the channel showing a smooth decline. Figure 4.3.2 is a plot of the pressure drop along the channel which also shows a relatively constant rate of pressure drop. Figure 4.3.3 is a plot of the predicted final flow variation for all three models. These flow characteristics were obtained through an iterative process. The criteria for the desired shape of the flow channel flow curve and the magnitude of the thickness variation were based on current design experience with successful conventional spiral designs. Figure 4.3.4 to 4.3.6 show the flow characteristics of the 2071 and 607 material through the die. The model predicts that both of these materials will perform in a similar fashion to the design material.

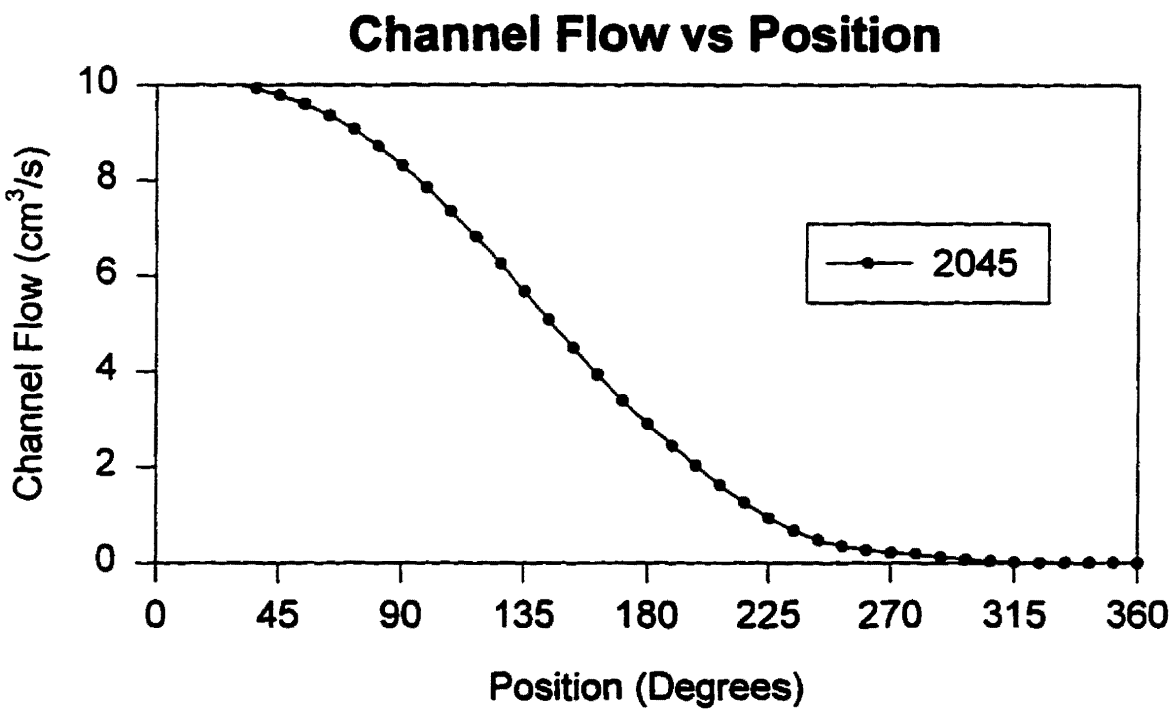


Figure 4.3.1 The predicted flow rate along the channel of the prototype flat spiral die (Material, Dow 2045).

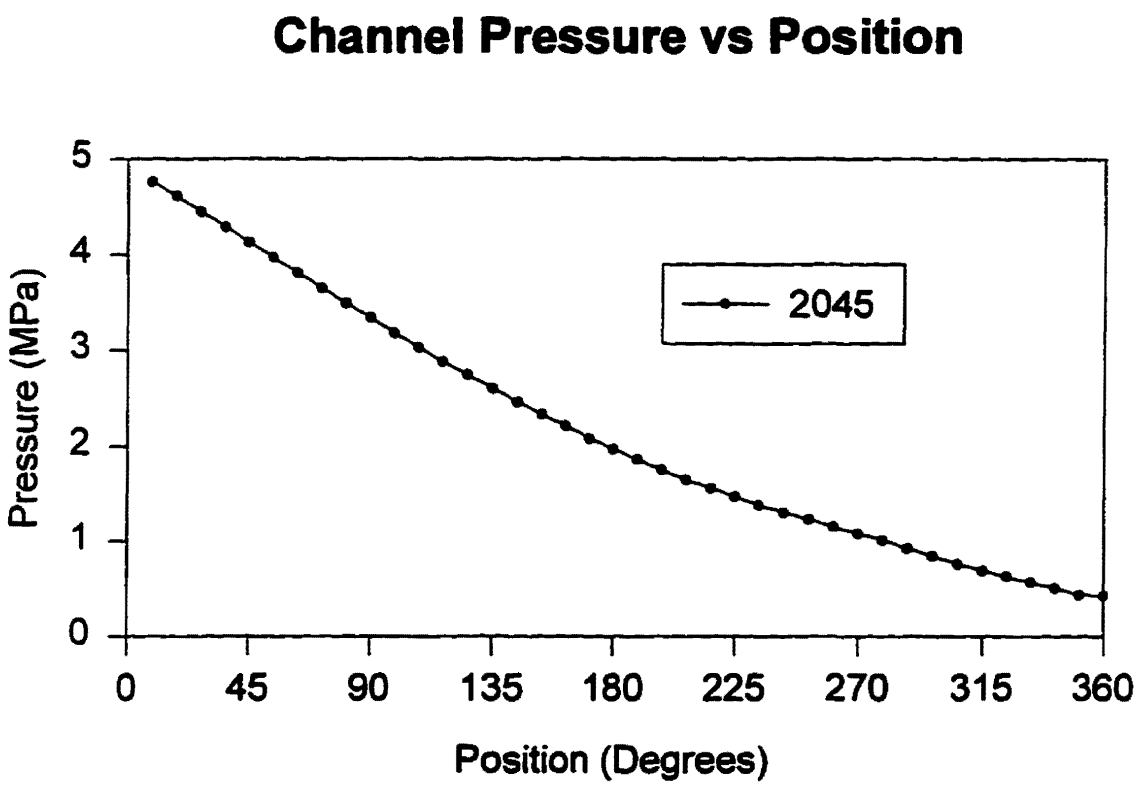


Figure 4.3.2 The predicted pressure along the channel of the prototype flat spiral die (Material, Dow 2045).

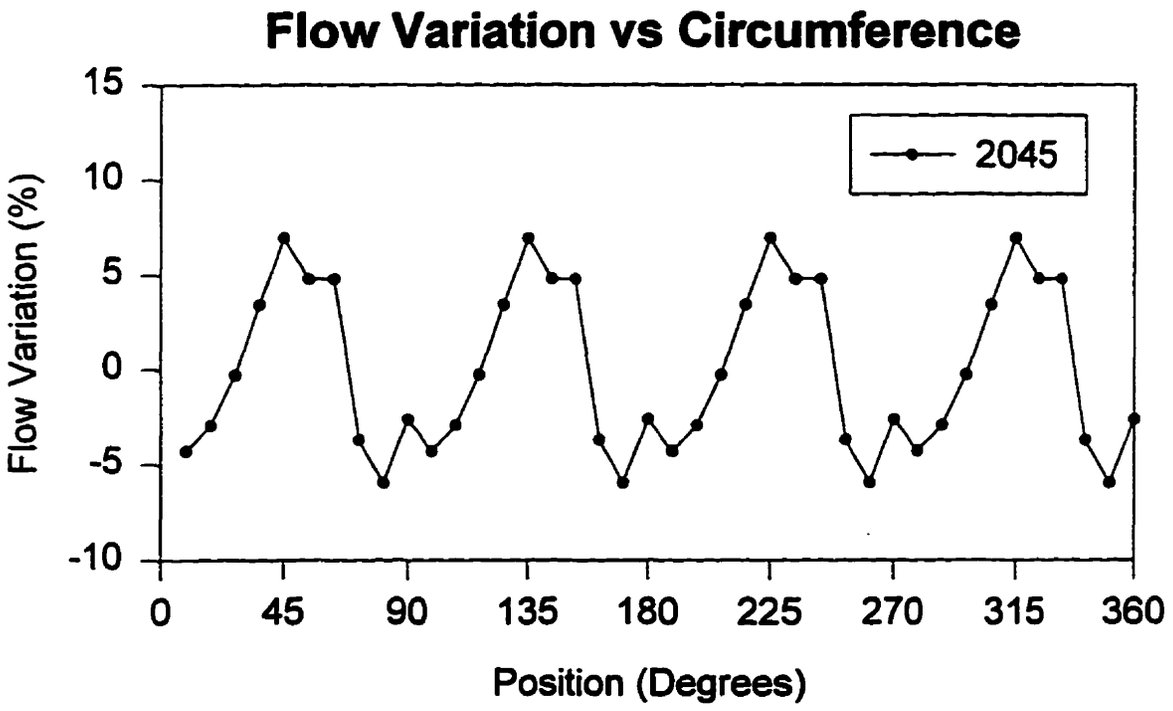


Figure 4.3.3 The predicted flow variation at the end of the flat spiral distribution system (Material, Dow 2045).

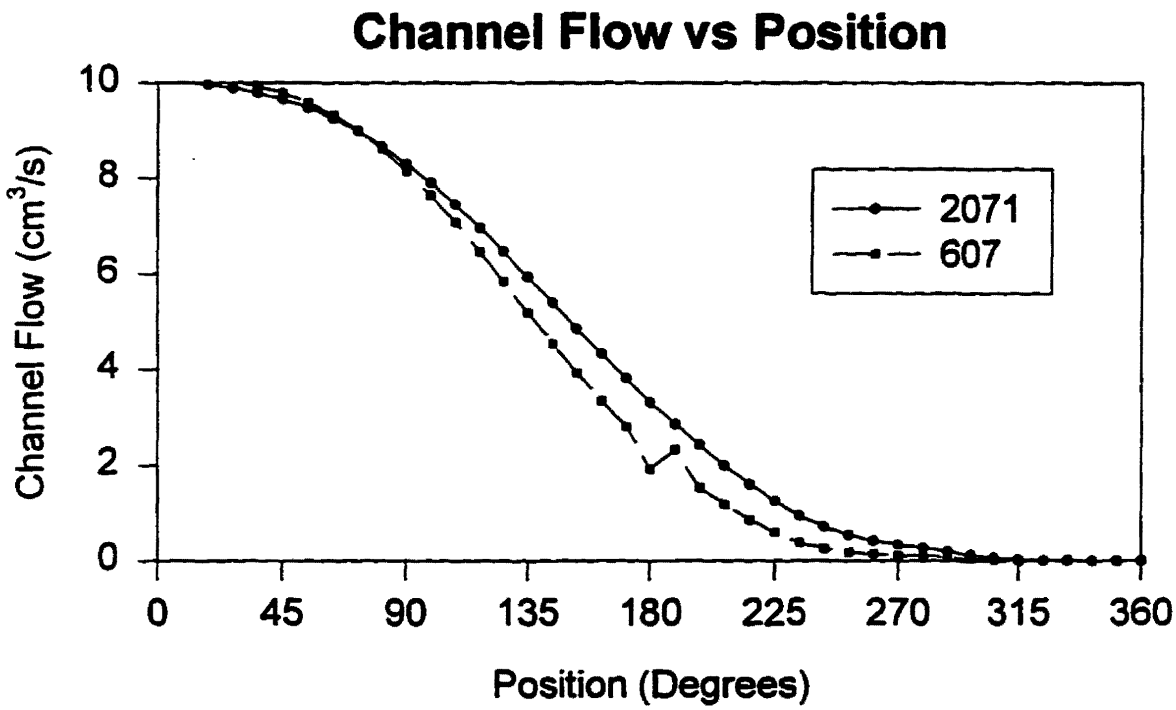


Figure 4.3.4 The predicted flow rate along the channel of the prototype flat spiral die for the Dow 2071 and the Dow 607 materials.

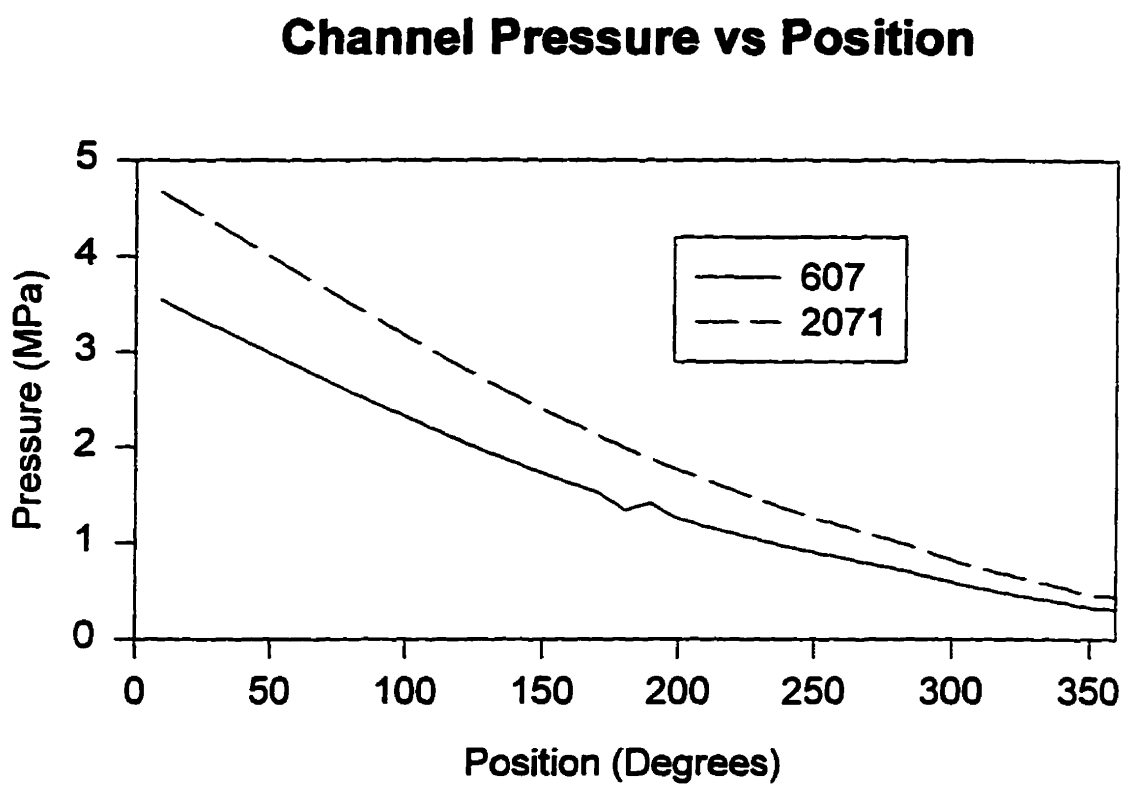


Figure 4.3.5 The predicted pressure along the channel of the prototype flat spiral die for the Dow 2071 and the Dow 607 materials.

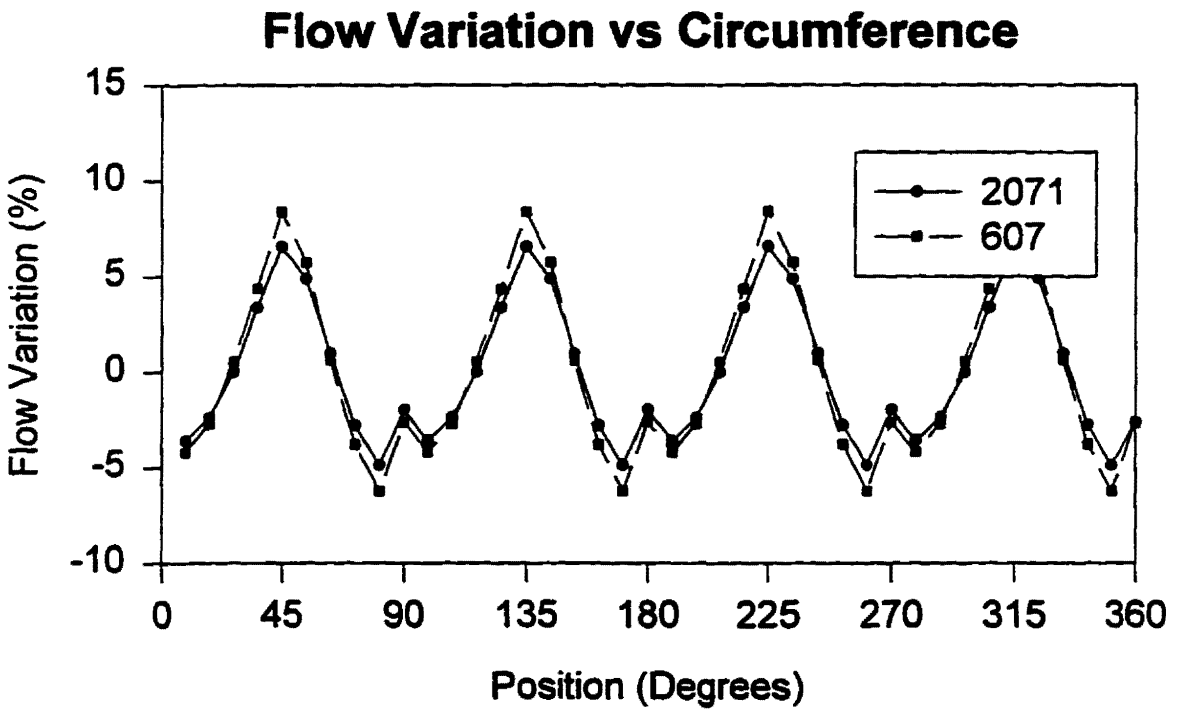


Figure 4.3.6 The predicted flow variation at the end of the flat spiral distribution for the Dow 2071 and the Dow 607 materials.

The die was manufactured by Brampton Engineering and connected to a 63 mm lab line extruder. Since the purpose of this test was to obtain information about the distribution of the polymer in the new flat spiral distribution system, the die lip restrictions were not incorporated in the design. The effects of air cooling and stretching were eliminated by extruding the melt downward into a cold water bath immediately as it exited the die.. This essentially produced a pipe with the same diameter as the exit of the die (approximately 100 mm) and a wall thickness of about 6 - 7 mm. The wall thickness of the pipe samples was measured at 40 points around the circumference. The variation of the thickness is plotted in Figure 4.3.7 and this provides an indication of the distribution uniformity. The thickness variation appeared to be below the predicted variations of the model of about +/- 6 %. Furthermore, there does not appear to be a periodic variation as predicted by the model. Figure 4.3.8 shows the measured thickness variation for materials 2071 and 607. Again, the actual thickness variation is lower than the predicted variation indicating that the simulation tends to overpredict the flow variation. This provides the designer with some confidence that the actual thickness variation will be lower than predicted.

Having established that the flat spiral distribution system was capable of distributing the polymer, the die was outfitted with a proper set of die lips, an air ring and it was installed on the blown film line to produce film as shown in Figure 4.3.9. Figure 4.3.10 show the measured thickness variation from film samples produced on the die using 2071 and 607. In both cases there is no apparent indication of a periodic thickness variation indicating that the flat spiral distribution system is performing in a satisfactory way.

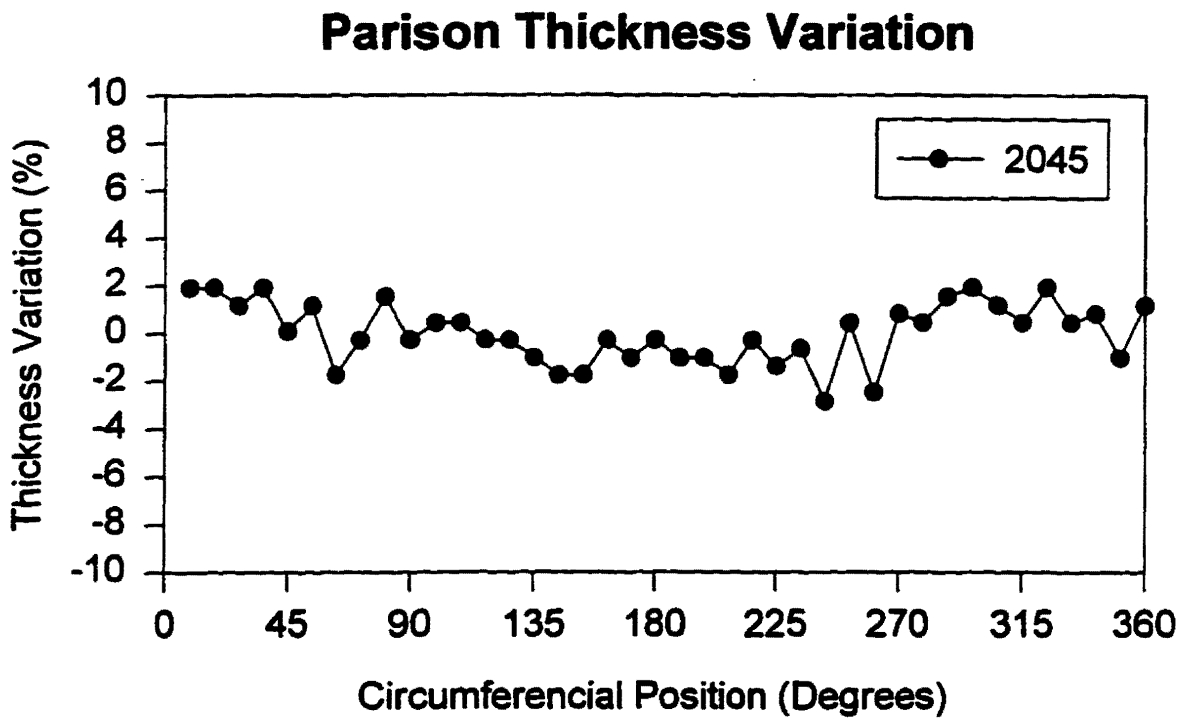


Figure 4.3.7 Thickness variation of the parison produced with 2045.

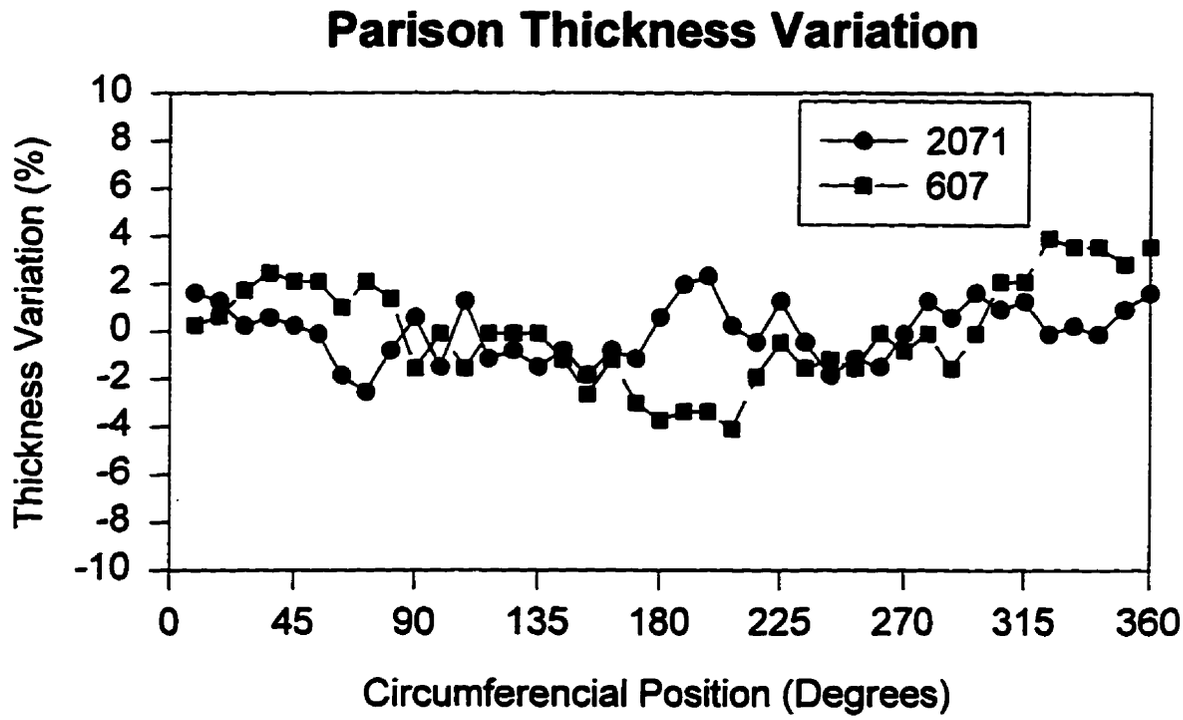


Figure 4.3.8 Thickness variation of the parison produced with 2071 and 607.

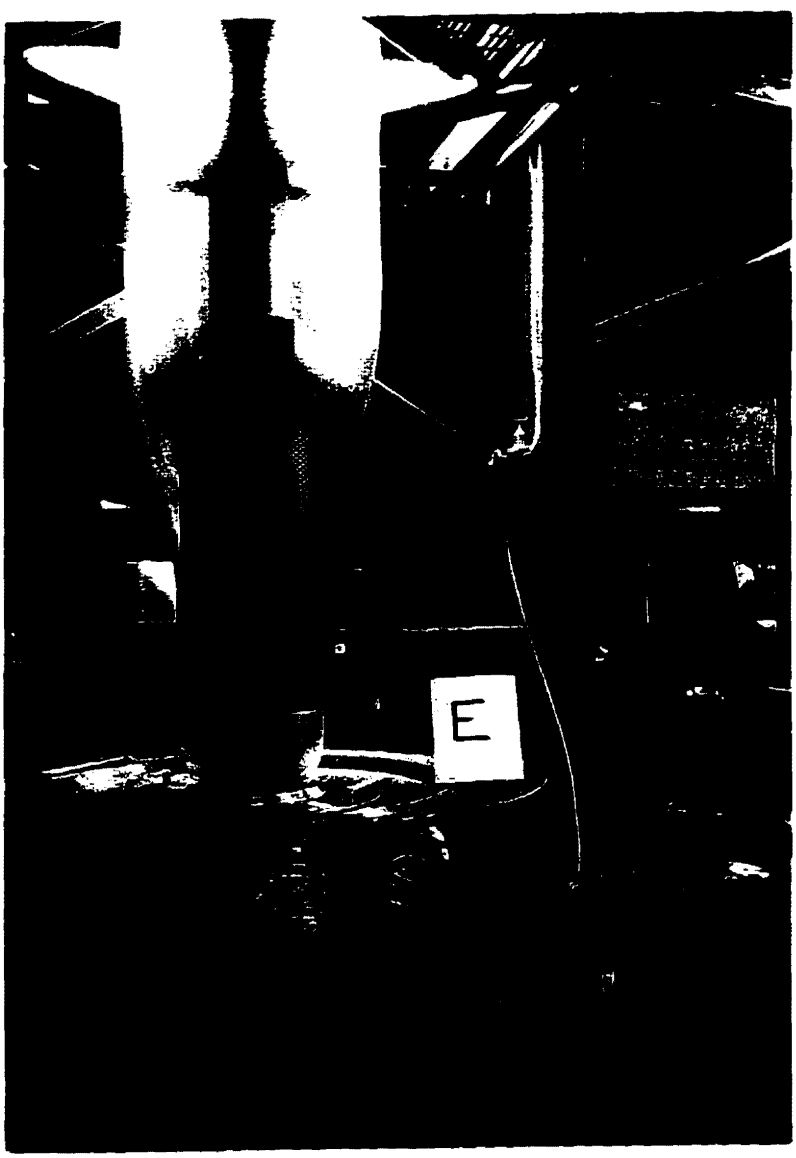


Figure 4.3.9 A photograph of the die with an air ring producing film.

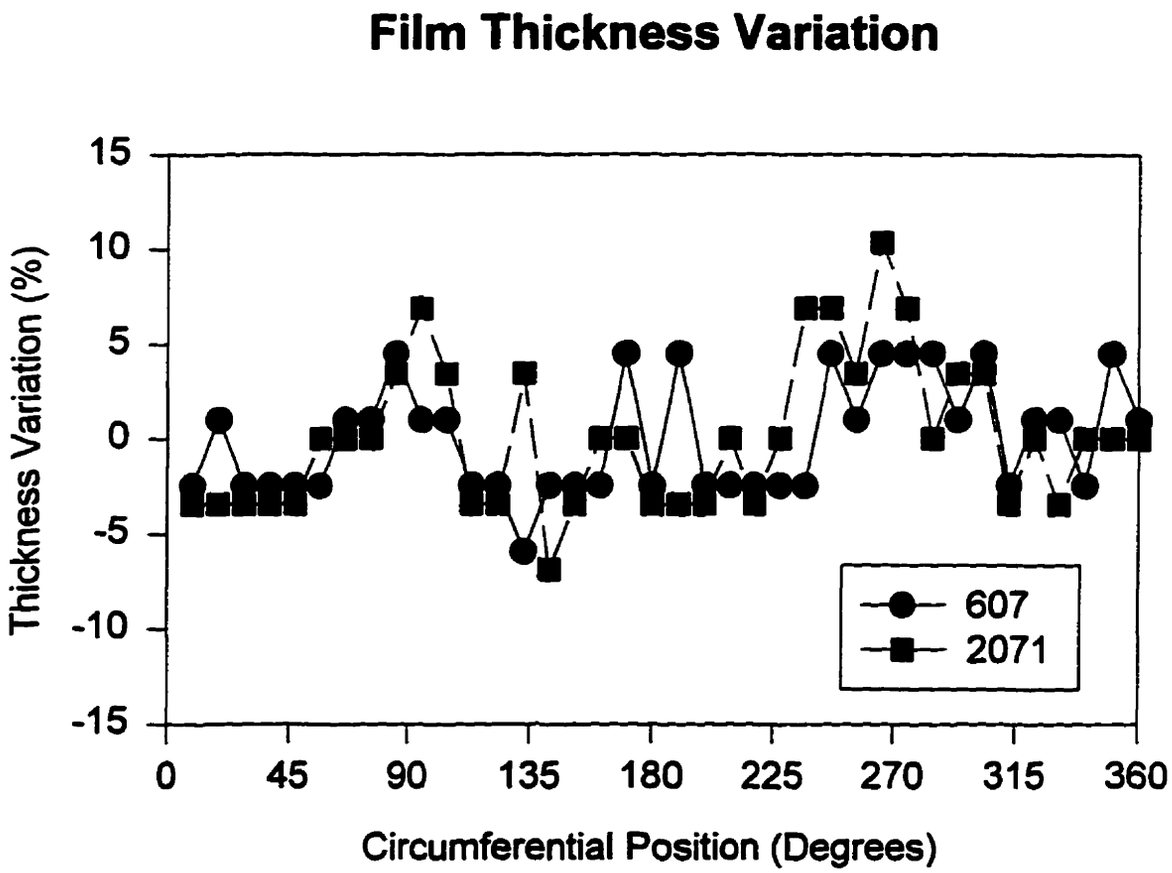


Figure 4.3.10 Percent thickness variation of the 40 micron film produced with 2071 and 607.

4.4 Small Die Experiments

This portion of the chapter focuses on an experimental and theoretical analysis of a smaller die. This die had 2 spirals and an exit lip diameter of 50 mm.

4.4.1 Thickness variation and CVM comparison

Figure 4.4.1 is a photo of the small flat spiral die that was used in these experiments. Figure 4.4.2 contains a perspective view of the small flat spiral system along with a cut-away view showing the cross section of the flow field. Figure 4.4.3 is a close up of one side of the cross section. The die was designed based on the Control Volume Method described above and manufactured by Brampton Engineering. Table 4.4.1 contains the design parameters of this die.

Table 4.4.1 The small flat spiral design parameters.

Parameter	Value	Parameter	Value
Starting Diameter (mm)	140	Ending Diameter (mm)	70
Starting Gap (mm)	0.35	Ending Gap (mm)	1.5
Starting Channel Depth (mm)	17	Ending Channel Depth (mm)	0
Channel Width (mm)	6.45		
Number of Channels	2	Number of Overlaps	3
Flow Rate (kg/hr)	24	Density (kg/m^3)	760
Consistency Coefficient ($Pa \cdot s^n$)	20818	Power-Law Index	.49
Number of divisions	10	Solution Tolerance	.01

Figures 4.4.4 to 4.4.6 show the flow characteristics of this die using the parameters in Table 4.4.1. Figure 4.4.4 is a plot of the channel flow again showing a relative smooth decline along the length of the channel. Figure 4.4.5 is a plot of the pressure drop indicating



Figure 4.4.1 A photograph of a small flat spiral die.

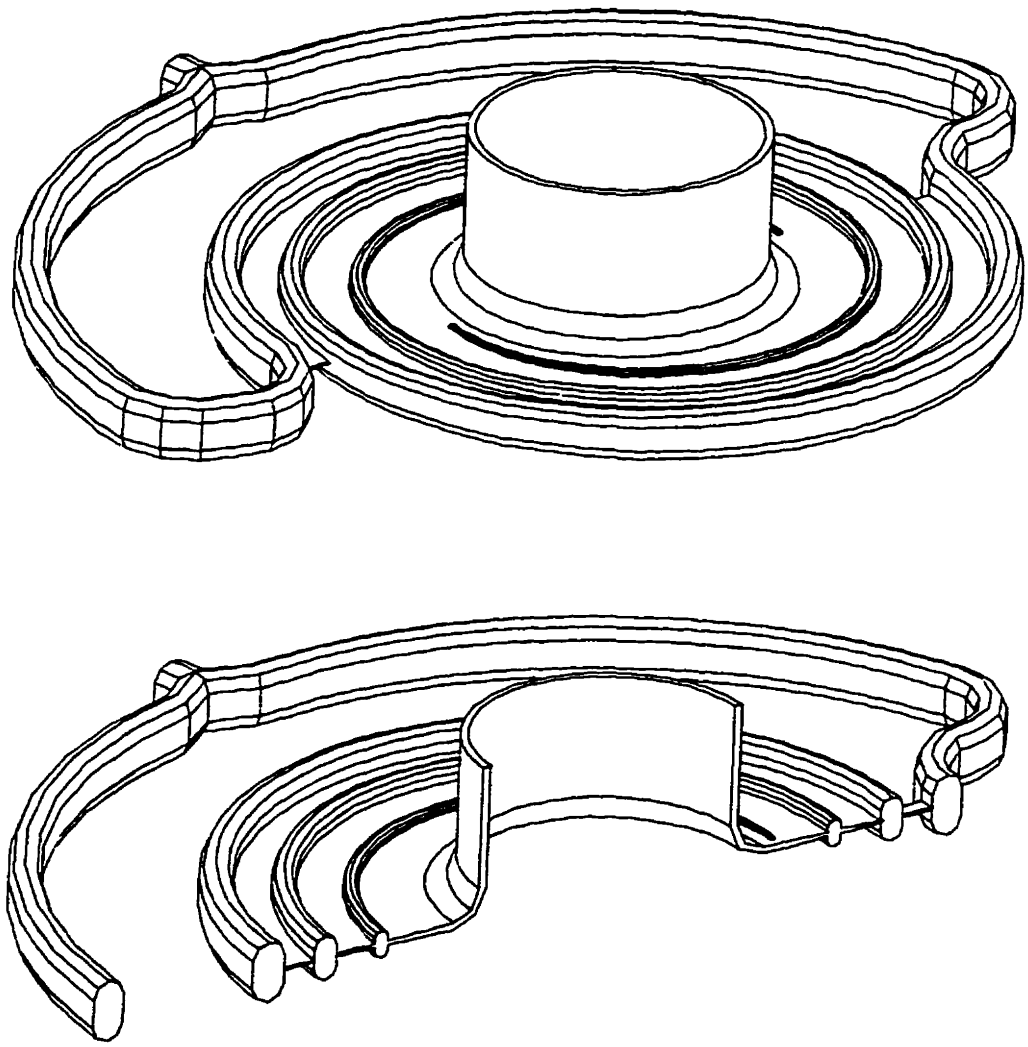


Figure 4.4.2 A perspective view of the small die flat spiral distribution system (above) and a cut-away view (below).

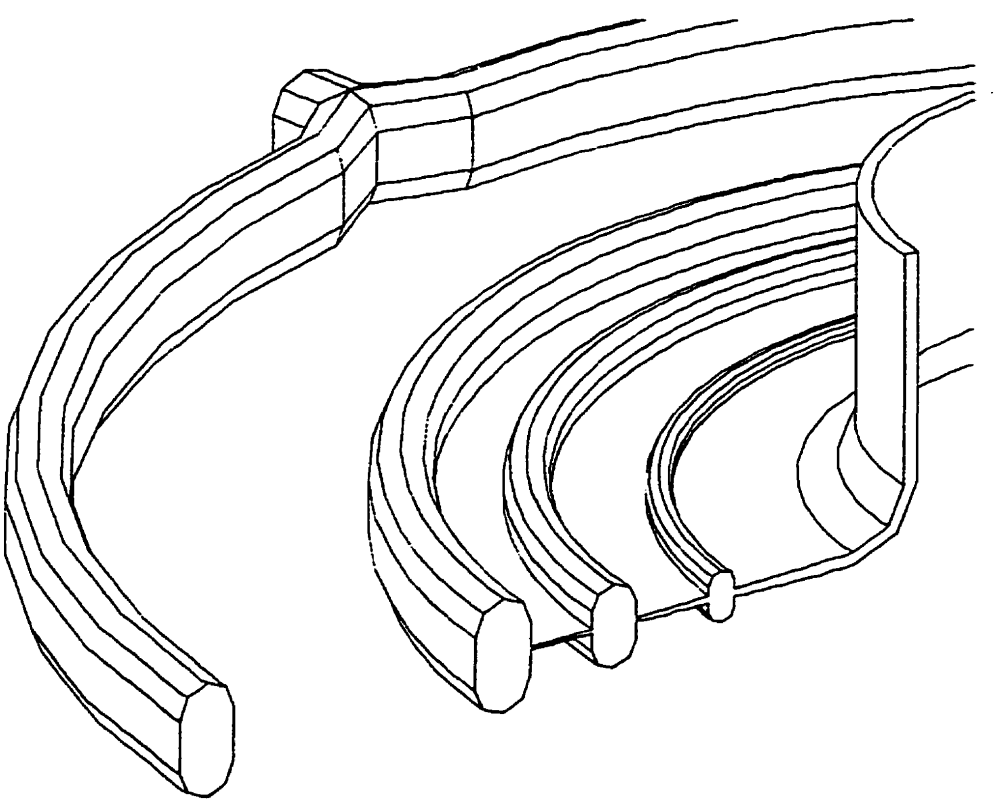


Figure 4.4.3 A close up view of half the cross section of the small flat spiral die.

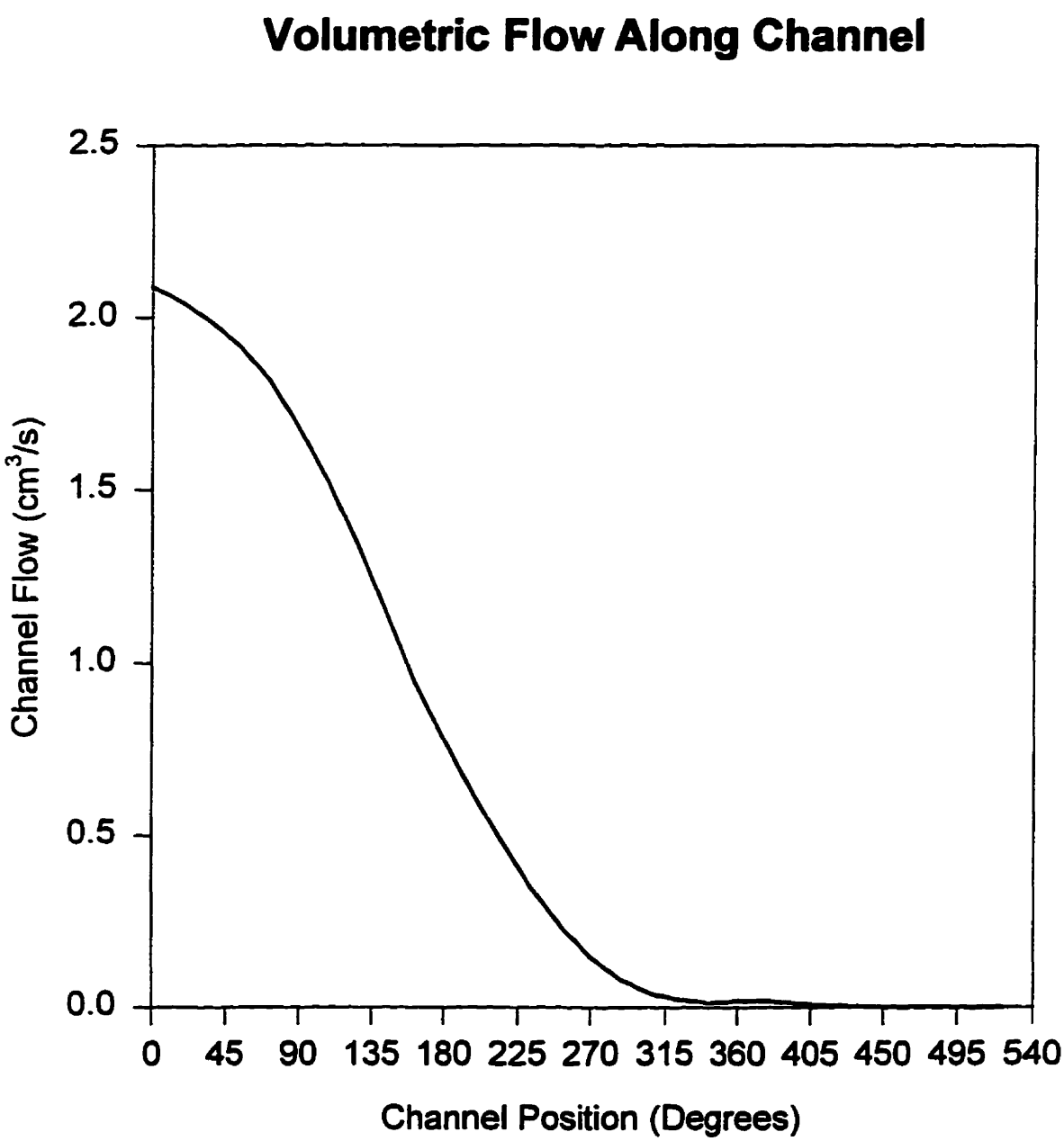


Figure 4.4.4 The predicted flow rate along the channel.

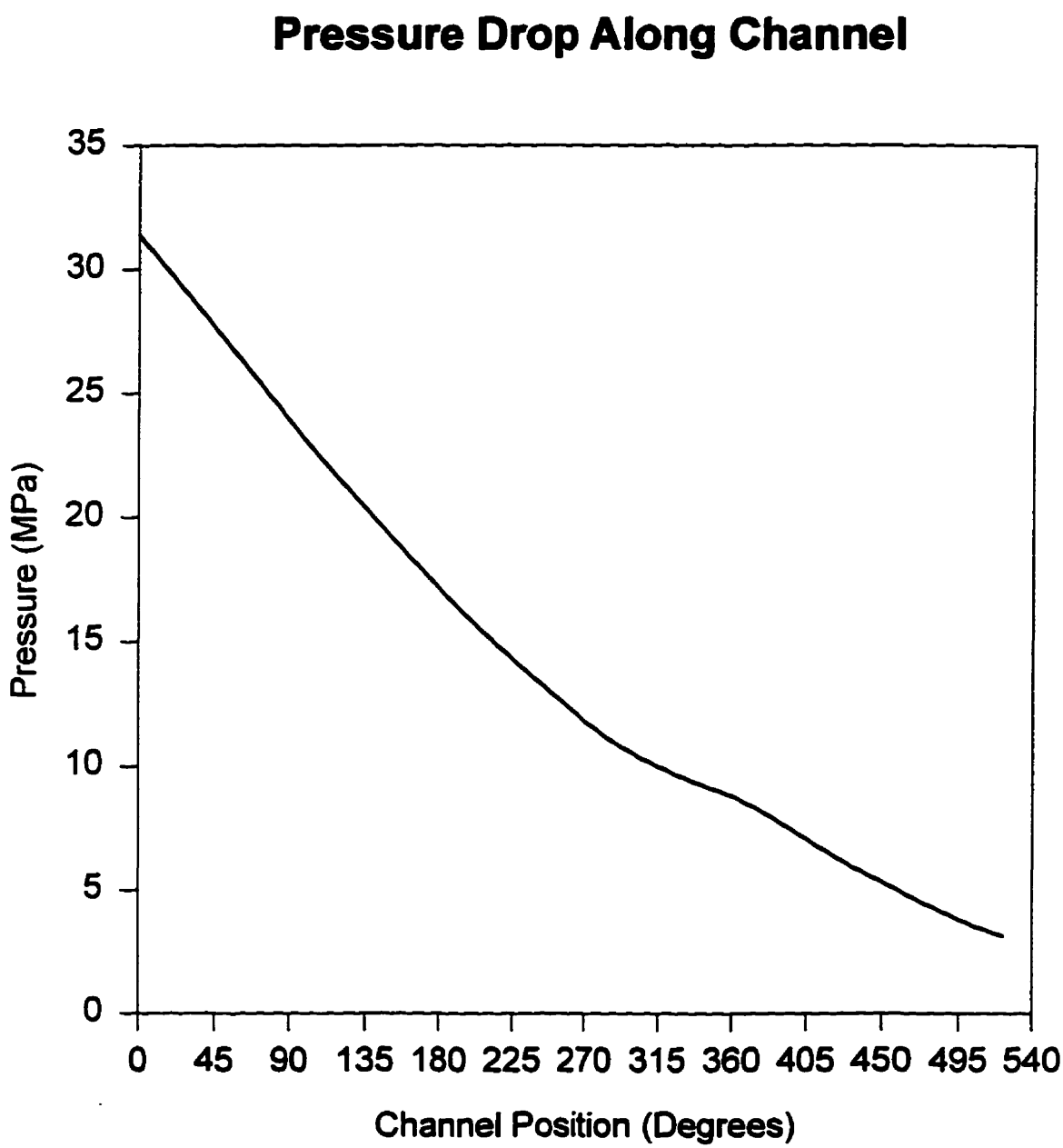


Figure 4.4.5 The predicted pressure along the channel.

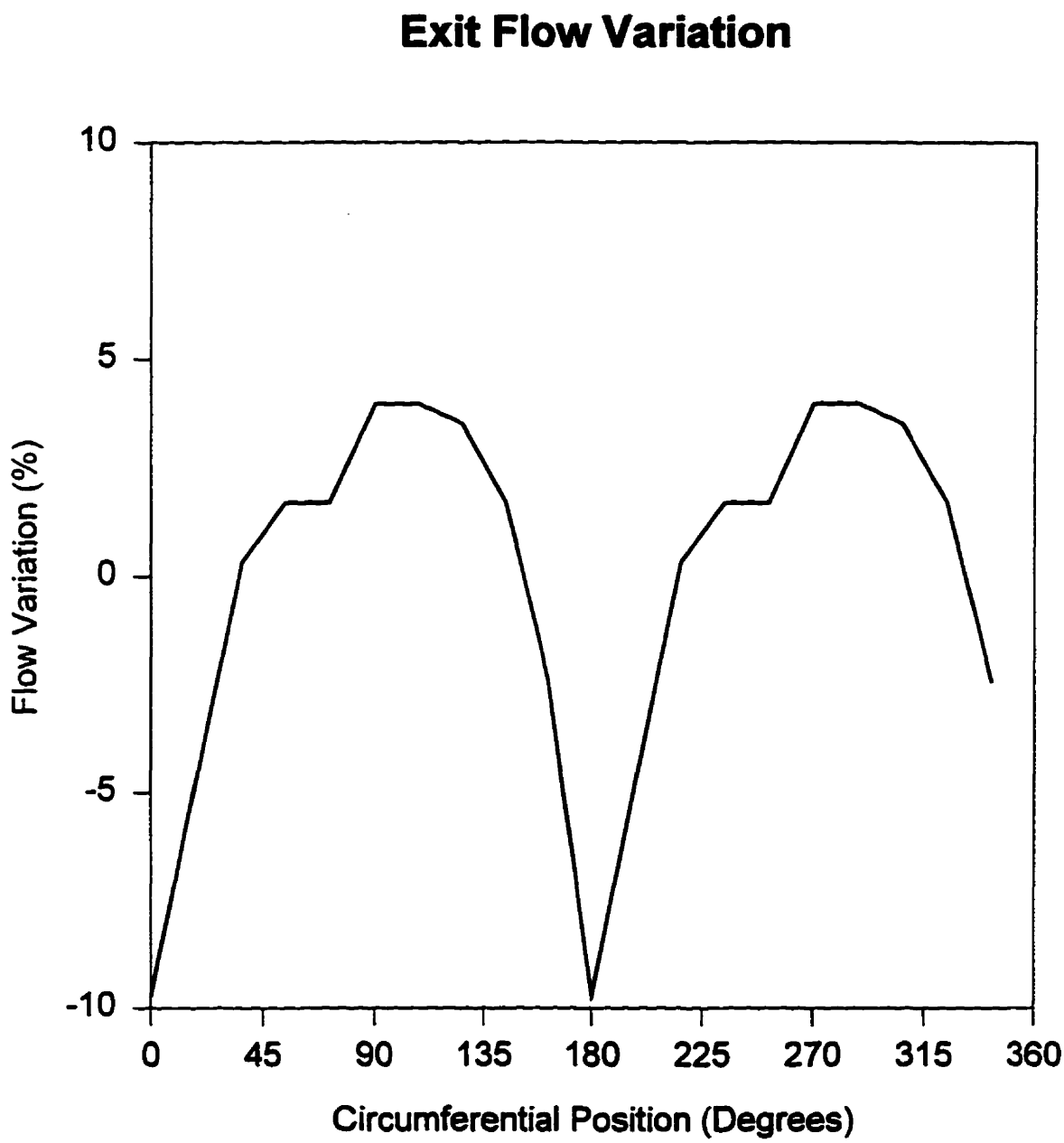


Figure 4.4.6 The predicted final flow variation.

a gradual decline from the initial 33 Mpa to zero. Figure 4.4.6 is a plot of the predicted final thickness variation around the circumference at the exit. In this design the material is predicted to have a thickness variation of about -9 to +4 %

As in the previous experiment, the die was connected to an extruder and the polymer was extruded downward into a water bath. Figure 4.4.7 shows the percentage thickness variation of two samples having an average thickness of 650 microns. The line is a 6^{th} order least squares fit of the data showing the trend. Figure 4.4.8 shows the percent thickness variation on actual film samples produced with the same die and material. The average thickness of the film samples was 45 microns. It appears that the measured thickness variation is about -7% to +10% which is in the same order of magnitude with the model predictions.

4.4.2 Visualization Experiments

Visualization experiments have been found to be very helpful in terms of improving one's understanding of the flow field and what is happening within the die. In some instances, visualization experiments can also help verify the accuracy of mathematical models and computer simulations. Figure 4.4.9 shows a duplicate of the metal die that is manufactured from a clear acrylic polymer. This allowed for the direct observation (and video recording) of the flow field. Figure 4.4.10 contains a photograph and a schematic of the experimental setup. A 340 cst. silicone fluid was circulated through the die using a centrifugal pump. The die was constructed such that, upon exiting the die, the silicone fluid would flow back into the reservoir. A metering valve was used to control the flow rate.

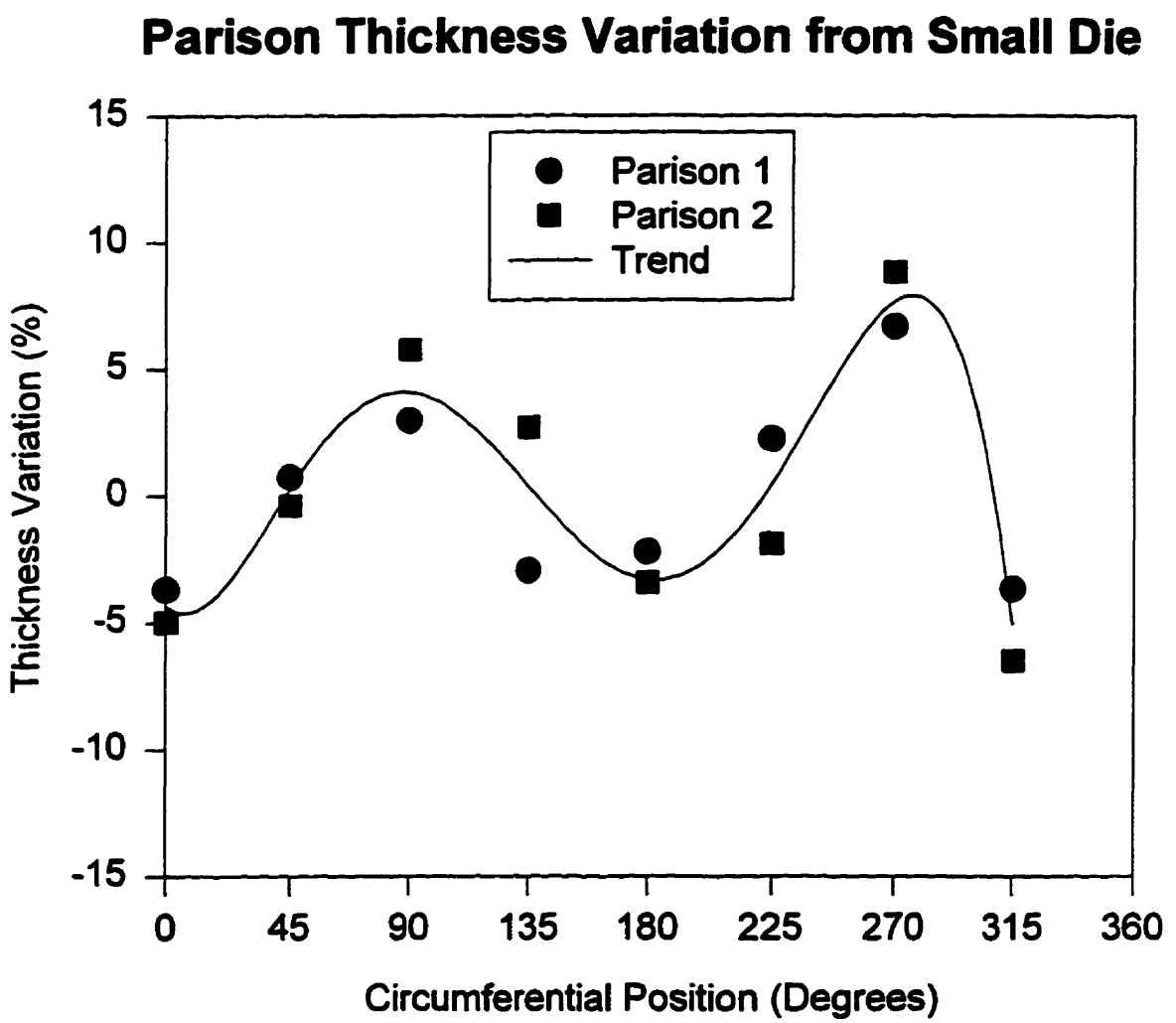


Figure 4.4.7 Measured thickness variation of two parisons.

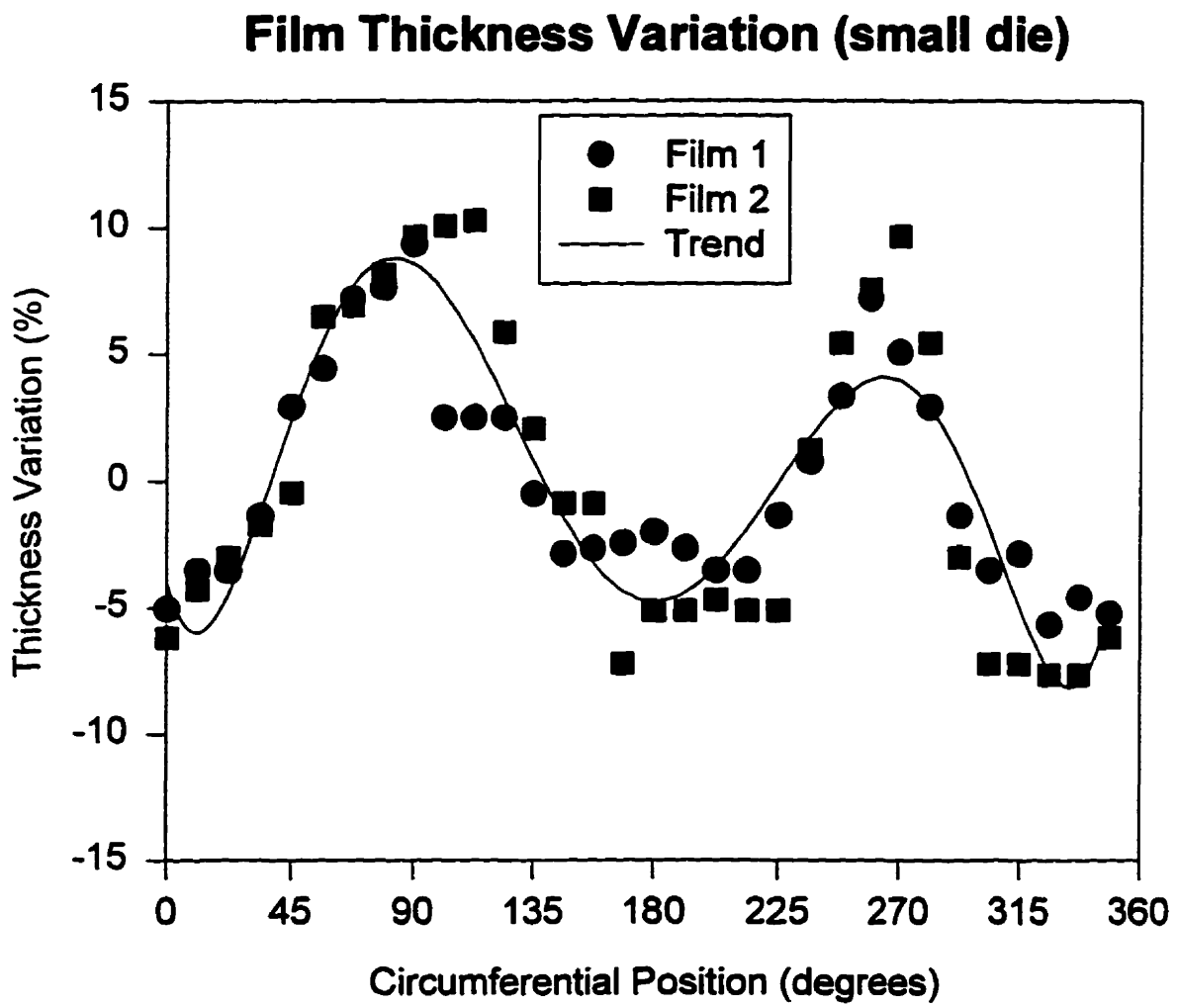


Figure 4.4.8 Measured thickness variation of two film samples.

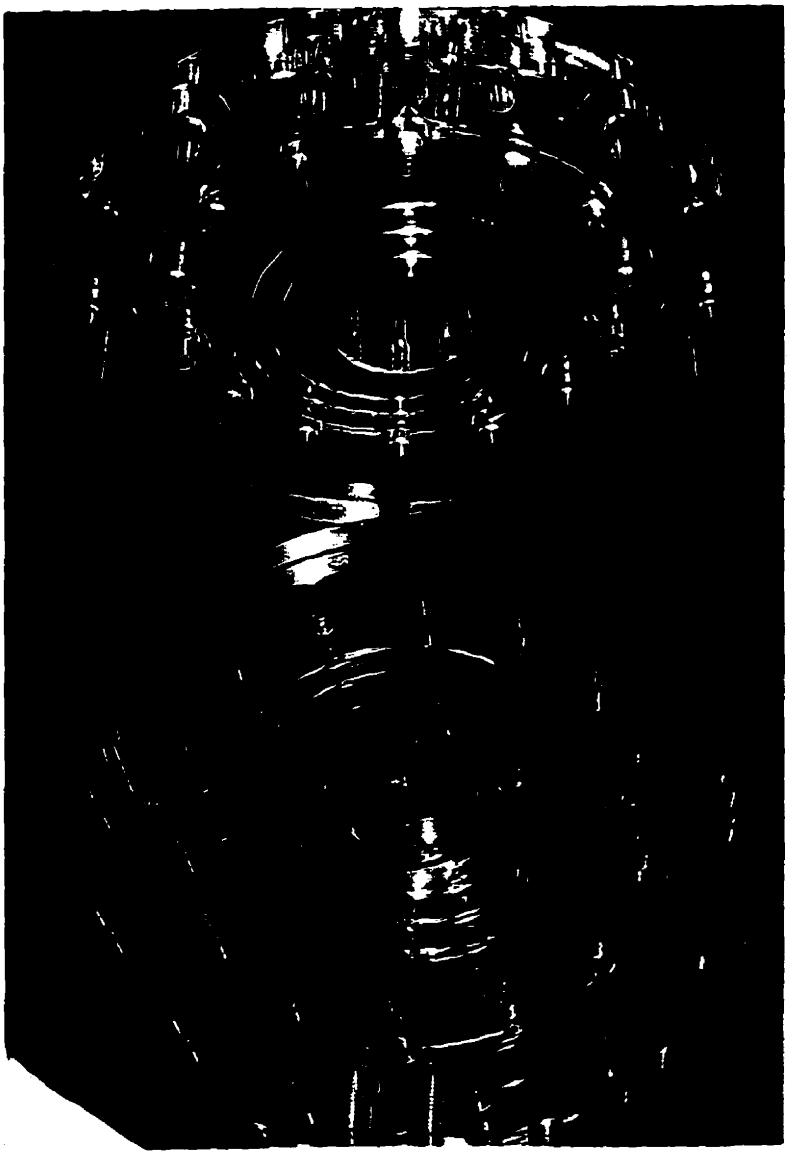


Figure 4.4.9 A photograph of the small die manufacture from clear acrylic.



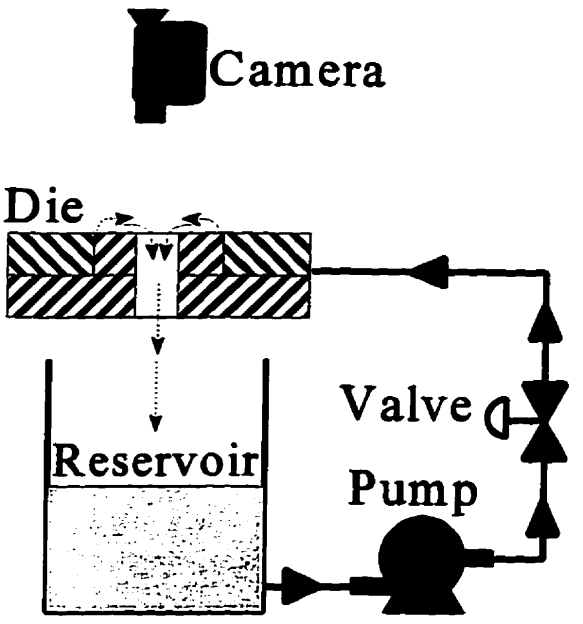


Figure 4.4.10 A schematic of the experimental setup.

Injection ports were drilled at 4 locations for the purpose of injecting a coloured (black) tracer into the flow field. Figure 4.4.11 shows the location of the injection ports which will be referred to as 1 through 4 as shown. In addition, the tip of the injection needle could be placed at any point across the flow field as shown in the inset in Figure 4.4.11. The tracer consisted of some carbon black powder mixed into the silicone fluid and injected with a manually operated syringe. A needle valve was used to control the flow at about 400 ml/min. This would represent a flow rate of about 24 kg/hr which would be typical of a die with a 50 mm exit diameter. A video camera was placed above the die to record all of the observations.

4.4.3 Visualization Results

Although the results are best viewed in the video tape, the highlights will be presented here. Figure 4.4.12 is a photograph showing the path of the tracer from injection points 1a and 1b. It can be seen that the material from point 1a exits the channel immediately, flows over the land and is swept clockwise for about 90° before it begins to flow radially to the exit. Figure 4.4.12b shows a photograph of the tracer path from injection point 1b, the inside centre surface of the right inlet channel. In this case, the tracer can be observed to continue along the surface of the channels for about 270° before it begins to flow radially and exits from the die.

Figures 4.4.13 shows the tracer paths for outside and inside, respectively, centre surface injection points for the left inlet channel. It is interesting to note that although the

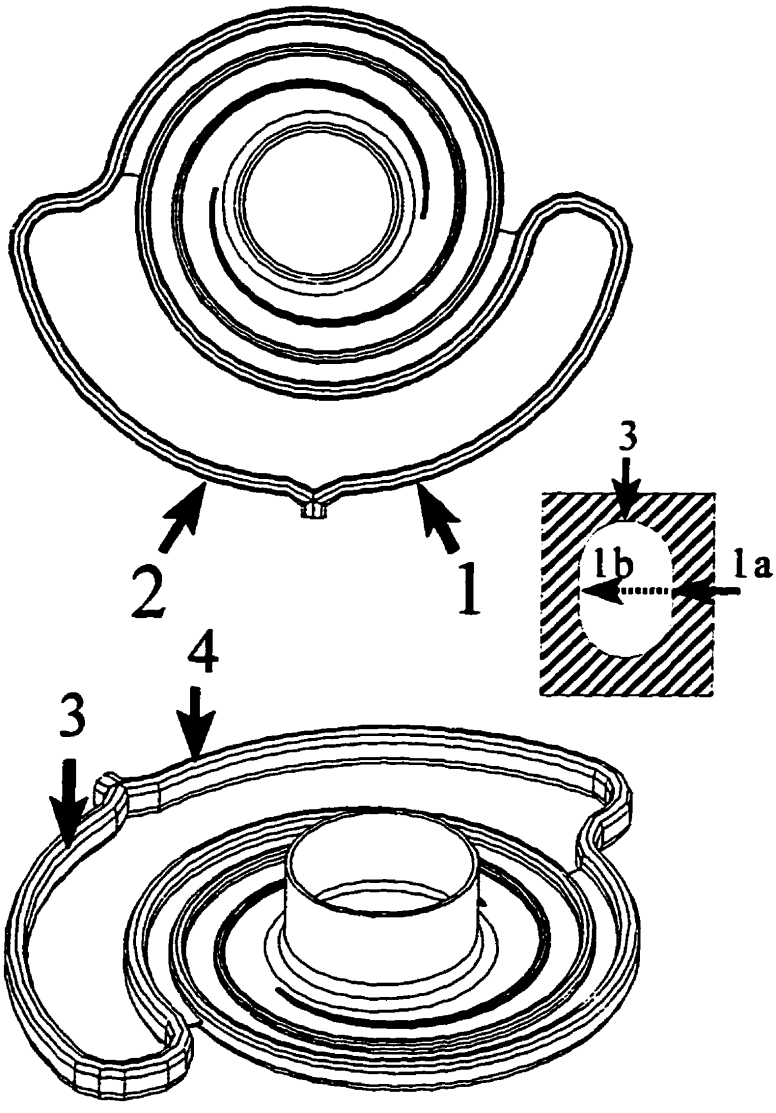


Figure 4.4.11 The location of the injection points used in this experiments.

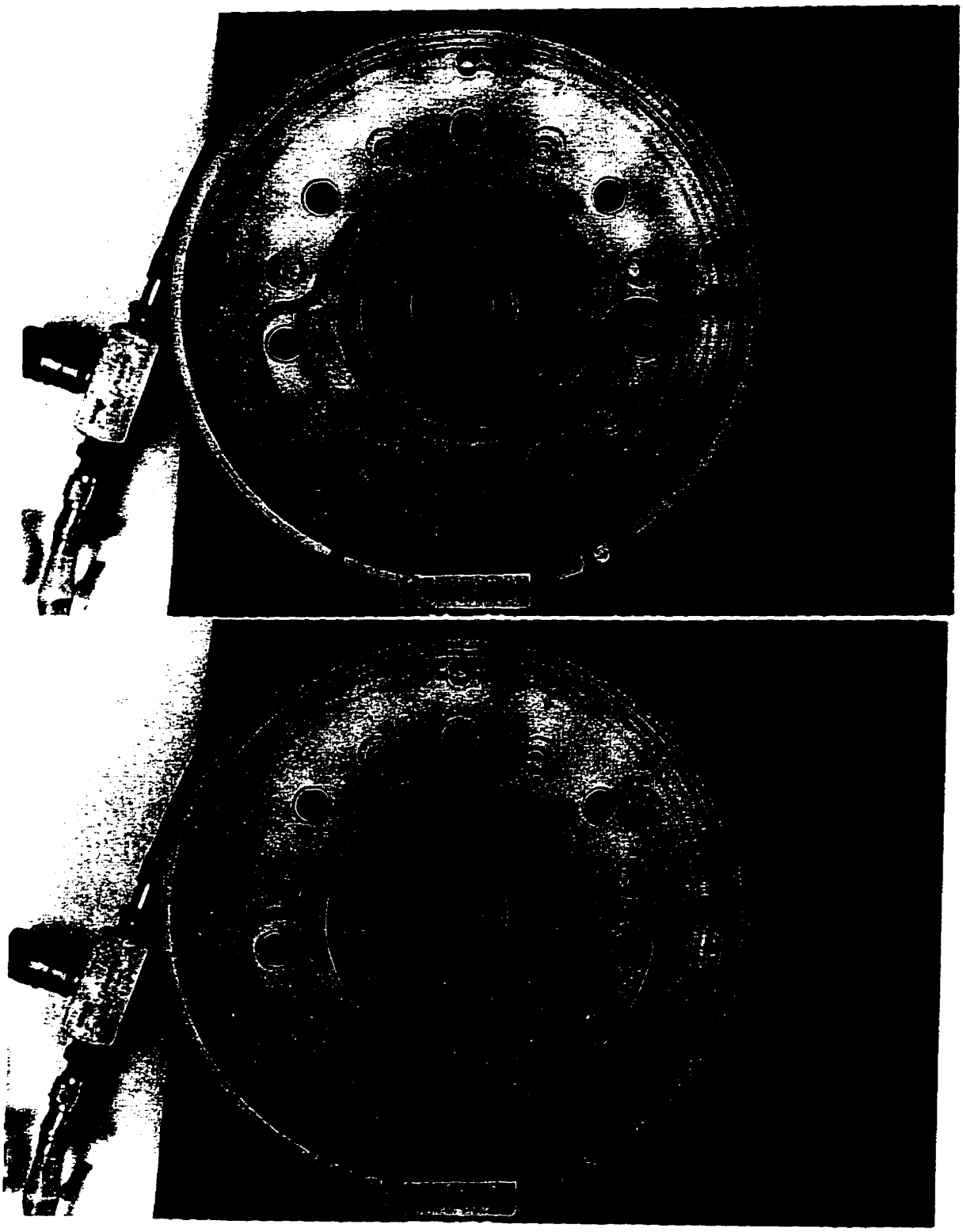


Figure 4.4.12 Photographs of the tracer path from injection points 1a(4.4.12a-top) and 1b(4.4.12b-bottom)



Figure 4.4.13 Photographs of the tracer path from injection points 2a(4.4.13a-top) and 2b(4.4.13b-bottom)

design of the die appears to be symmetric and both paths from the die entrance to the spirals are of equal length, the distribution of the material is different in each spiral. Of particular importance is the flow at the outer sides of each of the two inlet channels (Figures 4.4.12a and 4.4.13a). This flow represents the slow moving material that has been flowing against the wall of the adaptor that connects the extruder to the die. Upon entering the die, this material from the adaptor is split into the two flow paths leading to each of the two spirals. At this point, the material in each of the channels consists of high residence time material in the outer portion of the channel and low residence time material in the inner portion. The distribution of this material within the die now depends on which side is considered. In the right channel, the high residence time material will exit the die as shown in Figure 4.4.12a but in the left channel, the high residence time material will exit the die as shown in Figure 4.4.13a. Of course, if the adaptor is very short relative to the length of the flow channels in the die, the effect of this asymmetry will be only dependent on the die and the length of the left and right channels. This discussion of course neglects any residence time distribution patterns that are created within the extruder.

Figures 4.4.14a and 4.4.14b are photographs showing the path of the tracer for injections at the top centre surfaces of the right and left inlet channels, respectively (injection points 3 and 4). In this case, both flow paths are similar with the material travelling about 300° from the initial gap. It was observed that this material took the longest time to emerge from the die indicating that the path was one of relatively low shear rate (or shear stress).



Figure 4.4.14 Photographs of the tracer path from injection points 3(4.4.14a-top) and 4(4.4.14b-bottom)

During the visualization experiment, it was observed that the flow field appeared to achieve steady state within a few seconds of starting the pump. This made it possible to fill a portion of the channel in the region of the injection port and then start the pump and observe the distribution of material from that channel. Figures 4.4.15(1-9) are a series of photographs showing the distribution of the 'plug' of tracer from the right channel. It appears as though the material from the right channel distributes itself primarily in the left half of the die despite the fact that the channel wraps around 540°.

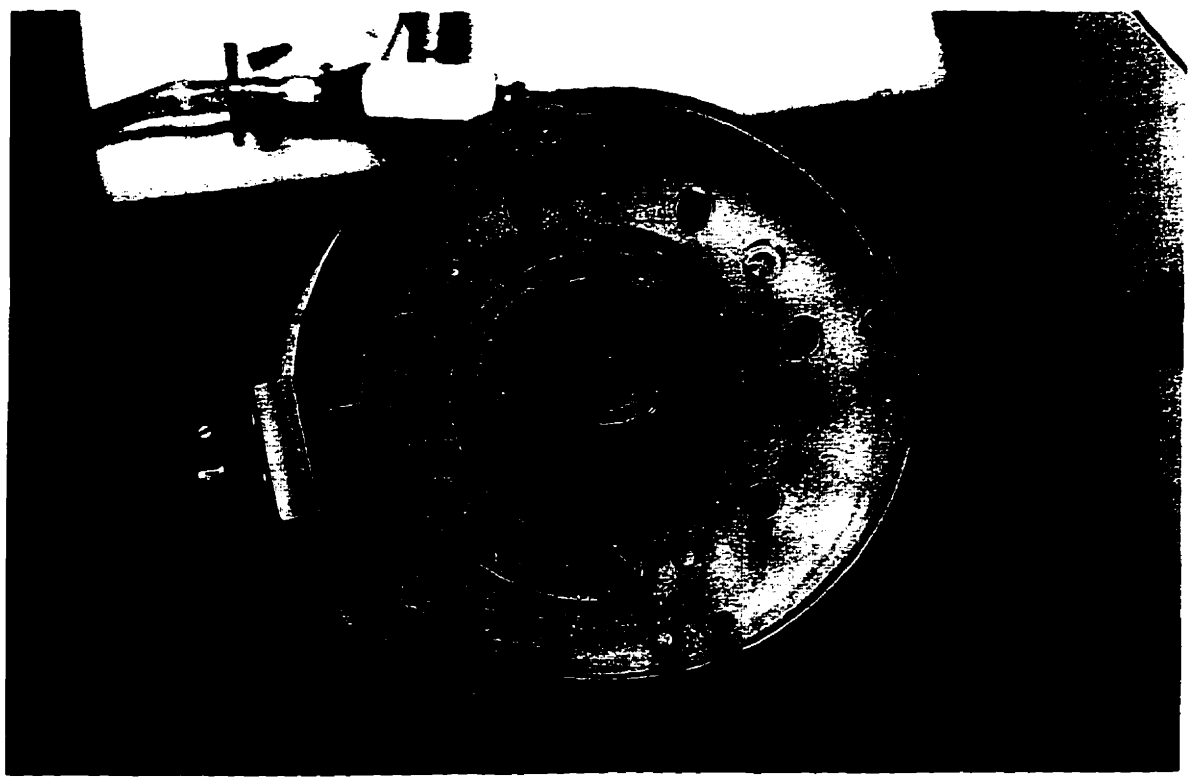


Figure 4.4.15 A sequence of photographs showing the distribution of a 'plug' of tracer injected in the right channel (1).

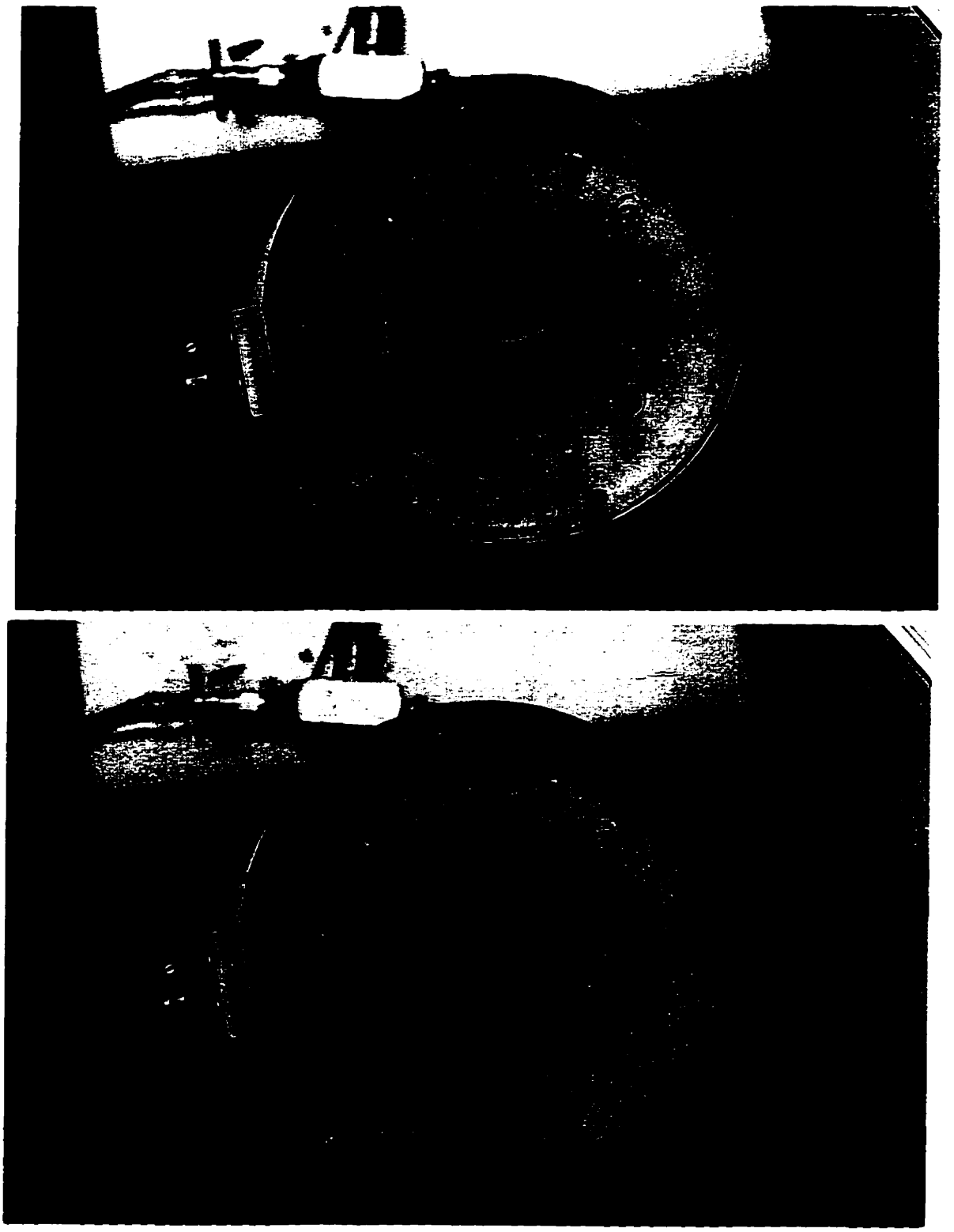


Figure 4.4.15 Continued sequence of photographs showing the distribution of a 'plug' of tracer injected in the right channel (2 top, 3 bottom).

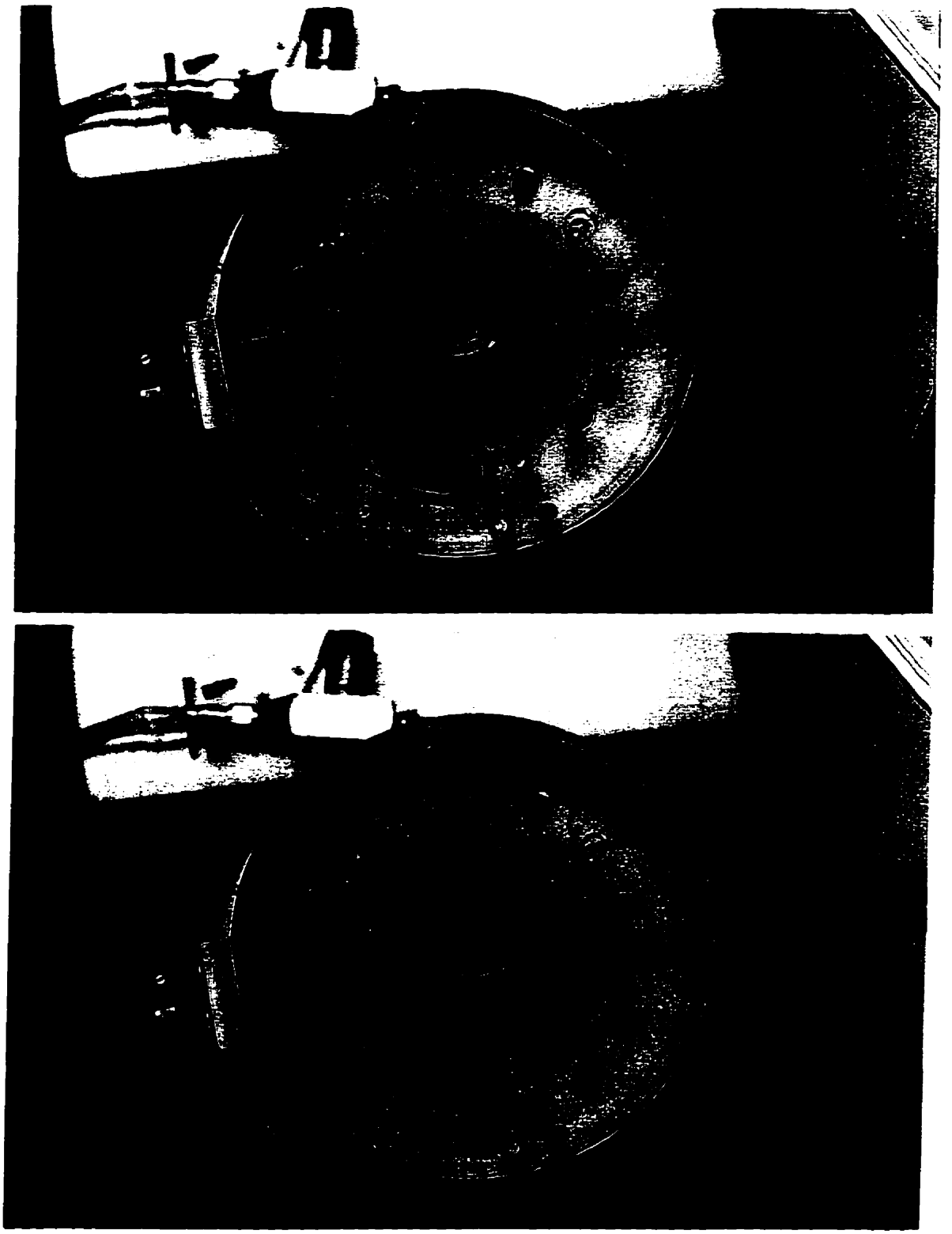


Figure 4.4.15 Continued sequence of photographs showing the distribution of a 'plug' of tracer injected in the right channel (4 top, 5 bottom).

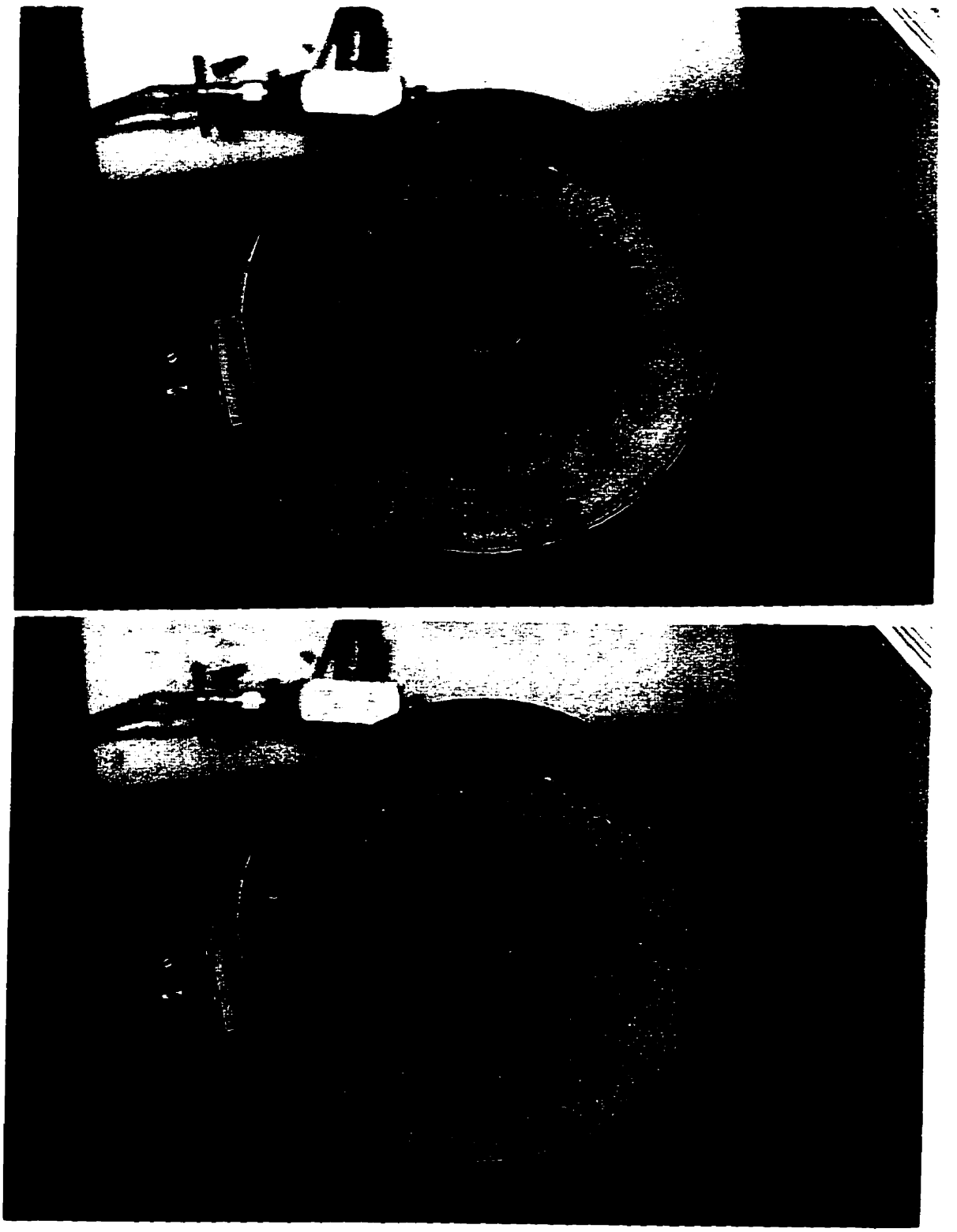


Figure 4.4.15 Continued sequence of photographs showing the distribution of a 'plug' of tracer injected in the right channel (6 top, 7 bottom).

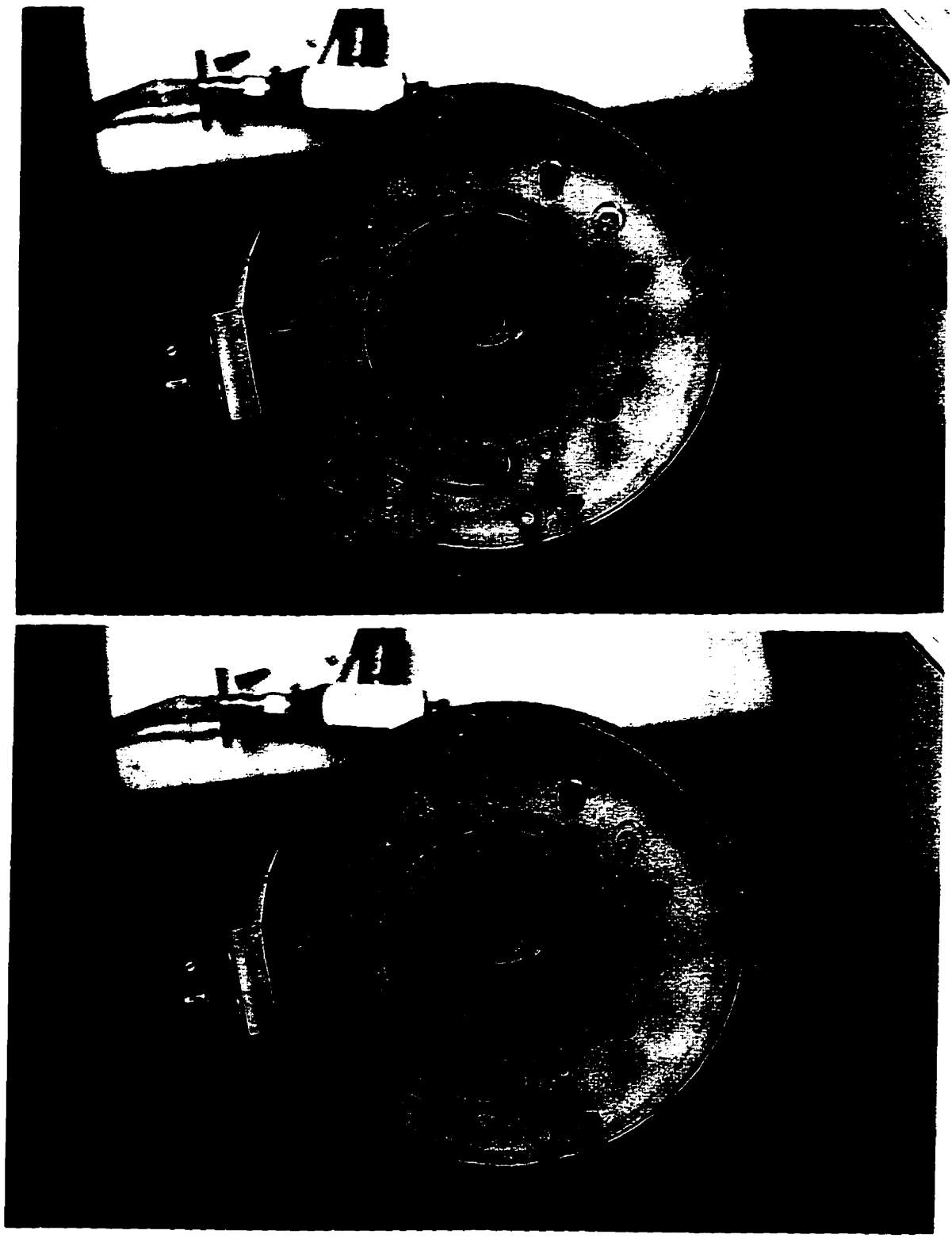


Figure 4.4.15 Continued sequence of photographs showing the distribution of a 'plug' of tracer injected in the right channel. (8 top, 9 bottom)

4.5 Benefits to Coextrusion

The driving force for the development of the new die was the improvement of the coextrusion process. In order to somewhat quantify the differences between the new system and the conventional system, a comparison will be made between two coextrusion dies designed to produce the same product. Figure 4.5.1 is a drawing of a conventional style 5 layer coextrusion die using the concentric mandrel principle and lower distribution block. Figure 4.5.2 is a drawing of the new 5 layer die with the stacked spiral configuration. In order to minimize the variables and simplify the comparison, it was assumed that all layers had the same flow rate and the same material. The same techniques were used to calculate the residence time and pressure drop through both systems.

Table 4.5.1 contains the predicted pressure drop and residence time for each layer ("A"-inner to "E"-outer) of a conventional five layer die. Table 4.5.2 contains the same information for the new die design.

Table 4.5.1 Pressure Drop and Average Residence Time through a Conventional 5 Layer die

Layer	Pressure (MPa)	Avg. Residence Time (seconds)
A-inner	37.0	62
B	42.4	87
C	45.5	110
D	45.0	130
E	44.7	162

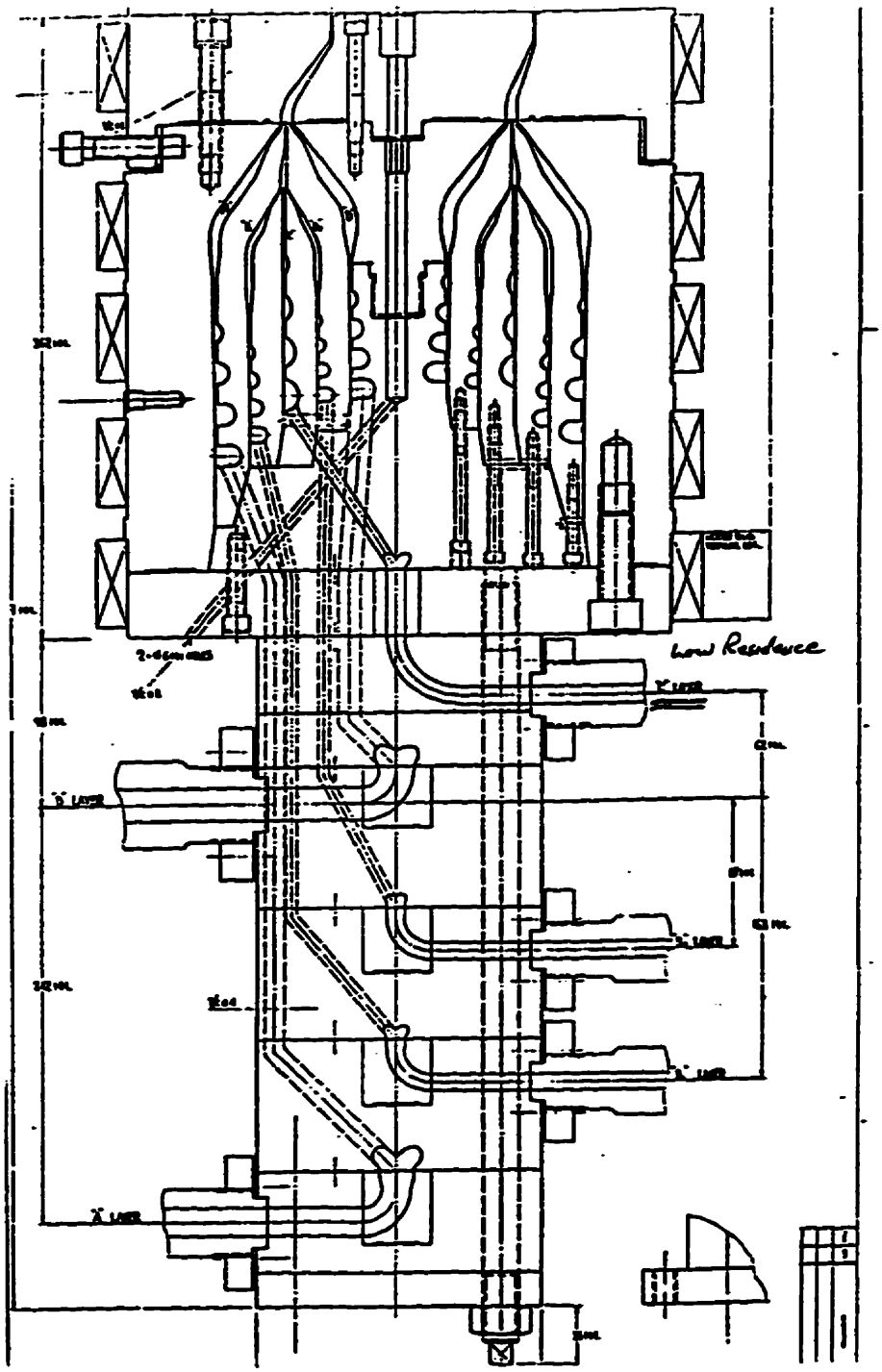


Figure 4.5.1 A conventional 5 layer spiral mandrel die.

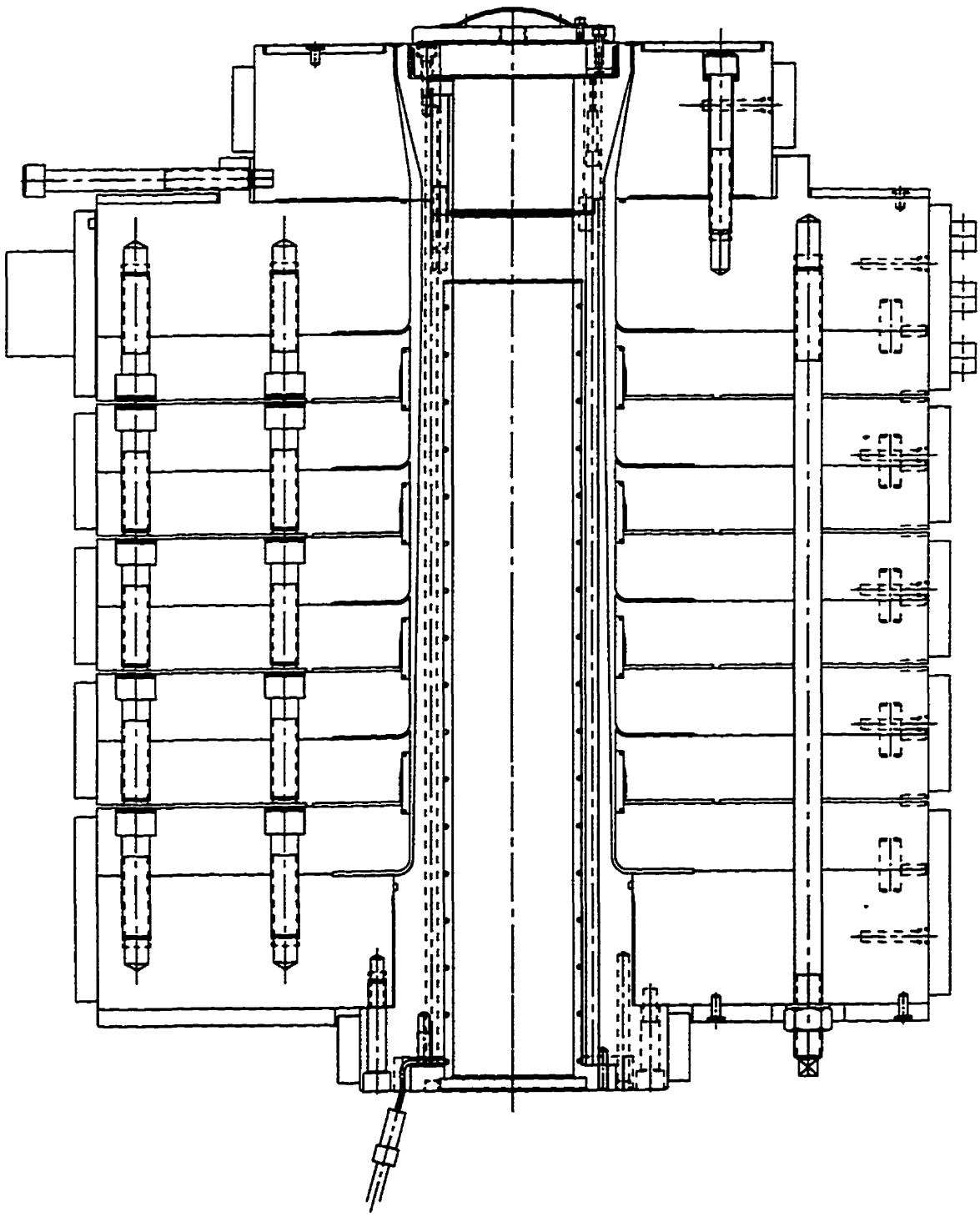


Figure 4.5.2 A new stacked 5 layer flat spiral die

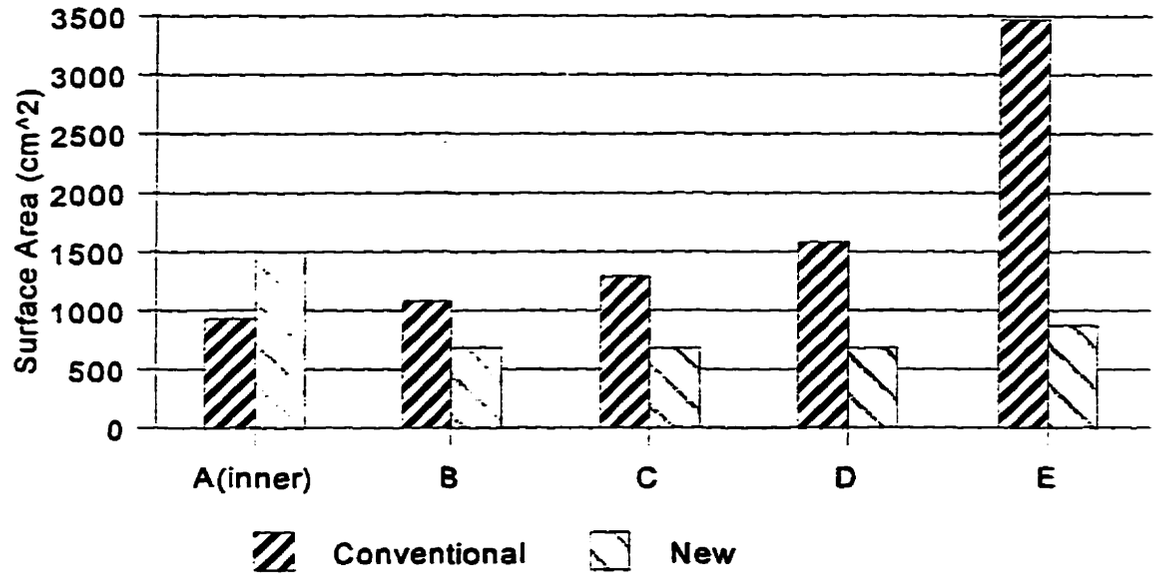
Table 4.5.2 Pressure Drop and Average Residence Time through New 5 Layer die

LAYER	PRESSURE (MPa)	Avg. Residence Time (seconds)
A-inner	31.0	110
B	29.7	93
C	28.4	84
D	26.8	79
E	26.2	75

From Tables 4.5.1 and 4.5.2, it can be seen that the new die system has both a lower residence time and pressure drop for layers 'C', 'D' and 'E'. Layer 'B' of the new design has a slightly higher residence time but a much lower pressure drop. For the 'A' or inner layer, however, the new die design had a lower pressure drop but a higher residence time than the conventional design. Of course the relationship between pressure drop and residence time creates an infinite number of design possibilities making an exact comparison very difficult. Perhaps a better way of comparing the two systems is to compare the wetted surface area or the amount of steel that the polymer is exposed to. This is believed to be a better comparison because, whereas the residence time and pressure drop are interdependent, the surface area is more dependent on the construction of the die. Figure 4.5.3 compares the total wetted surface area of each layer in the conventional system with the total wetted surface area of each layer in the new system.

From this comparison, the difference between the two systems now becomes more

apparent. With the exception of the inner layer, which must flow along the centre stem, the wetted surface area of the new system is much less than the conventional system. Again, the differences are more pronounced for the outer layers. Herein is the fundamental benefit of the new construction. Reducing the surface area over which the polymer must be spread out is basically the same as reducing the length of the flow passages. This reduces the pressure



Conventional	930	1080	1290	1580	3470
New	1500	680	680	680	870

Figure 4.5.3 Comparison of wetted surface area in a conventional die with the new die.

requirements of the system as well as the potential for degradation because less polymer is exposed to the metal surfaces of the die.

In practice, both the operating pressure and the residence time are used to design the coextrusion system. The design of a particular layer may be biased by the designer towards lower pressure or lower residence time depending on the requirements of the polymer that is to be processed in that particular layer. As mentioned earlier, the inner ('A')

and outer ('E') layers are commonly very stable polyolefin materials which are very 'forgiving' to the design. Of greater importance are the inner layers which constitute a small portion of the flow and are generally more heat sensitive. These are materials such as adhesive resins and barrier resins such as EVOH which are more prone to degradation and gel formation.

This new type of system also lends itself to a modular die construction in which each layer can be thought of as a separate module. A significant benefit realized from this type of die construction is that it makes temperature isolation more feasible. This is done by minimizing the contact area between modules, as shown in Figure 4.5.2, and leaving a small air gap. This minimizes the heat transfer between the modules making it possible to run adjacent layers at different temperatures. This helps to reduce the amount of time that a particular layer must be exposed to the processing temperature of another layer which, in turn, reduces the risk of polymer degradation. Figure 4.5.4 is a drawing of the first commercially available 8 layer blown film die that is currently in operation and figure 4.5.5 is an actual photograph of this die[1].

[1] As a result of this research, Brampton Engineering has manufactured over 50 flat spiral coextrusion dies which are currently producing 3 to 8 layer films worldwide.

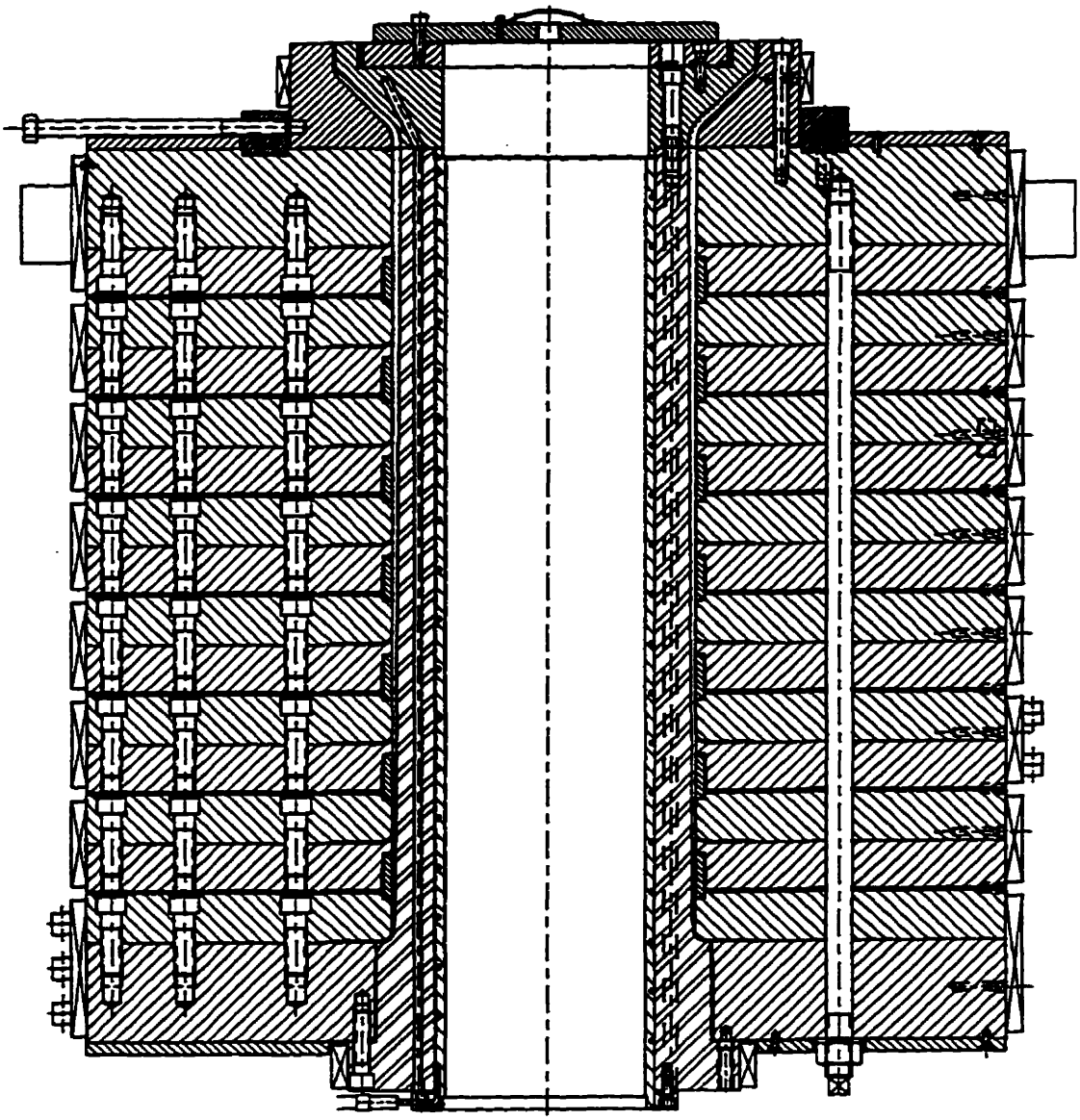


Figure 4.5.4 A drawing of an 8 layer flat spiral die.



Figure 4.5.5 A photograph of an 8 layer flat spiral die.

CHAPTER 5

FINITE ELEMENT METHOD ANALYSIS

5.1 FIDAP Overview

The die that was presented in section 4.4 was of sufficiently small size to allow for numerical simlation using a Finite Element Method (FEM) analysis. The analysis was performed using a commercially available FEM package called FIDAP. The biggest benefit of the FEM is its ability to provide a much more detailed description of the flow field. This, in turn, provides the capability to perform particle traces which help to greatly enhance our understanding of the flow behaviour. This also allows for the numerical verification of the observations made during the visualization experiments that were performed on the acrylic die.

FIDAP is a general purpose computational fluid dynamics code, developed by Fluid Dynamics International, that uses the Finite Element Method (FEM) to simulate many classes of fluid flows. In the FEM, the flow region is subdivided into a number of small regions, called elements. The unknown variables (pressure, velocities and temperature) are approximated by certain 'shape functions' over each element. Then, the Navier-Stokes equations of fluid mechanics are replaced by ordinary differential, for transient analysis, or algebraic equations, for steady state analysis in each element. The system of these equations

is then solved by sophisticated numerical techniques to determine the velocities, pressures, temperatures, species concentrations and other unknowns throughout the region. Although FIDAP is a general purpose computational fluid dynamics (CFD) package capable of being applied to almost any flow field, this overview will focus on the requirements for polymer processing simulations. The reader is referred to the FIDAP reference manuals for detailed information about the software.

FIDAP essentially consists of seven program modules, each of which will be briefly described in the following paragraphs.

FI-GEN: This is the interactive mesh generation module which allows the user to create a grid through a Graphical User Interface (GUI). This module essentially uses a point-and-click approach to place points, and then connect them to form lines, curves, surfaces and solids. Although it is relatively easy to learn and use, it does not allow for easy changes to the flow field making it difficult to use for everyday design purposes.

FIMESH: This is the non-interactive mesh generation module which gives the user a little more flexibility with respect to data input. Although the data can be input via the keyboard, it is more common to have it 'read' in from a text file. Advanced users can create programs that will generate properly formatted FIMESH input files from a minimum number of parameters making complex grid generation much easier.

FI-BC: This is the initial and boundary condition processor module which allows the interactive graphical specification of the initial and boundary conditions.

FIPREP: This is the module which allows the user to input material properties and control information for the problem. The user can interactively specify such parameters as the types of flows (2D, 3D, non-Newtonian, etc.) and the terms or equations that should be included in the solution. The solution procedures or methods are also specified within this module.

FISOLVE: This module transforms the governing partial differential equations in algebraic equations and solves them via various numerical techniques.

FIPOST: This is the module that is used for post-processing of the results. It provides graphical display of the results.

The use of FIDAP (or any CFD software for that matter) requires a general understanding of fluid mechanics, rheology, and numerical methods. The user must be able to correctly describe the flow field and choose the appropriate solution technique. Furthermore, the user should also be able to scrutinize the results and distinguish between actual flow behaviour and numerical artifacts. These skills will help reduce the time and effort involved in order to obtain a valid solution.

The procedure should begin with a well defined flow domain or geometry. This

would preferably be a detailed CAD drawing from which the user can read all of the necessary dimensions. The material property data must also be available for an accurate simulation and the initial and boundary conditions must also be known. Finally, the user must be able to select the equations that are to be solved and the appropriate solution approach.

There are basically two ways to enter and mesh the geometry in FIDAP; the FI-GEN module or the FIMESH module. The FI-GEN module is easier to use initially because it provides an interactive graphical user interface (GUI). The user 'builds' the flow field by designating points and connecting them with lines and arcs. FI-GEN also allows for the easy development of 3-D geometries by allowing the user to project 2-D surfaces along arbitrary paths in three dimensions. The FIMESH module provides the same features as the FI-GEN module except that FIMESH generates the grid from a series of command lines. These command lines can be read from a file which makes it somewhat easier to make small changes in the geometry and re-generate the grid. Furthermore, the user may wish to make an external program that creates the FIMESH input file from some simple parameters. Once the geometry has been defined, it must be meshed. The user has a choice of several elements depending on requirements of the problem. For 3-D situations, the user can choose either 8 or 27 node brick elements, 6 or 18 node wedge elements and 4 or 10 node tetrahedral elements.

The main pre-processor module is FIPREP and it is the module that is used to define the problem and solution strategy. FIPREP can also be used to enter the boundary and initial conditions of the problem. In the FIPREP module the user can define the problem

characteristics so the program can use the appropriate terms in the equations. This includes specifying 2-D or 3-D, steady or transient, compressible or incompressible, laminar or turbulent, linear or non-linear, Newtonian or non-Newtonian, isothermal or non-isothermal, momentum or no momentum and a few more conditions. This is where a good knowledge of fluid mechanics can help because it will allow the user to estimate which terms are important and which terms can be eliminated and thus reduce the solution time.

FIDAP also allows the user to select several solution strategies in order to solve the systems of equations. These include Successive Substitution, Newton Raphson and a Segregated Solver. Each of these has its own merits and should be used according to the demands of the problem. The Segregated Solver is particularly suited for large 3-D systems because it reduces the amount of memory required by essentially solving for one component variable at a time. This may require many iterations but they are much faster than solving the complete system. The segregated solver is preferred for 3-D problems. There are three different approaches with the segregated solver: Projection, Update and Correction. The projection and update methods both solve directly for the pressure at each iteration; the only difference between the two methods is that the projection method performs a mass adjustment of the velocity held at the end of each iteration. This ensures that the velocity field satisfies the continuity equation at each iteration rather than only when convergence is achieved. The correction method differs from the projection and update methods in that at each iteration a pressure correction (increment) is solved for rather than the pressure directly.

FIDAP also allows for the application of a relaxation method. A relaxation method is used to improve convergence by controlling or modifying the size of the steps

during the iteration proceedure. The ACCF parameter on the solution command sets the relaxation factor to the same constant value for all the degrees of freedom. The relaxation data record allows different factors to be set for each degree of freedom, which is useful with the segregated solvers.

The Conjugate Gradient Squared method (CGS) or the Generalized Minimal RESidual method (GMRES) are used to solve non-symmetric linear equation systems. To solve symmetric linear equation systems, the user can choose the Conjugate Residual method (CR) or the standard Conjugate Gradient method (CG). The maximum number of iterations should be specified for each method.

FIPOST is FIDAP's graphics post-processor module. The finite element analysis of any fluid flow problem of realistic size produces an abundance of numerical data that in itself is very difficult to analyse and interpret. FIPOST is a graphical interface that allows the user to visualize simulation results. The solution file processed by FIPOST is the results database file, FDPOST, produced by the FIDAP solver module FISOLV. FIPOST has extensive capabilities for displaying and manipulating the solution data. Some of the most useful graphical results include vector and contour plots of pressure, velocity and temperature. In addition, FIPOST can produce these plots through any plane that the user wishes to define. Other useful plotting features include line graphs of all the variables along any predefined path and particle tracing. Particle tracing is particularly useful in helping to visualize flow paths in complex flow fields. This information can help determine system characteristics such as residence time distributions and mixing. In addition, particle traces can be performed backwards in time. This is a very useful troubleshooting tool in that it can

lead to the source of a problem upstream (within the equipment or flow field) from where it is observed (after exiting the equipment or flow field).

For polymer processing, the general form of the Navier-Stokes equations reduces to:

$$\nabla \cdot \tau - \nabla P = 0 \tag{5.1}$$

which assume a steady-state condition with no significant buoyancy or body forces. It is also assumed that the convective terms can be neglected due to the fact that polymer flows are typically dominated by viscous forces resulting in very low Reynolds number flows. P is the pressure and τ is the extra stress tensor. The form of the extra stress tensor depends on the constitutive equation that is used for the viscosity. For the case of a Newtonian fluid the extra stress tensor is defined as:

$$\tau_{ij} = \mu\left(\frac{\partial v_i}{\partial x_j} + \frac{\partial v_j}{\partial x_i}\right) \tag{5.2}$$

where μ is the viscosity.

Polymer fluids are also considered to be essentially incompressible resulting in the continuity equation taking the form:

$$\nabla \cdot \boldsymbol{u} = o \qquad (5.3)$$

where **u** represents the velocity vector.

The boundary conditions are the following. The inlet velocity is known (or specified) and all the velocity components at a surface defined as a wall are zero (no slip hypothesis). The reader is referred to the FIDAP manuals for more details on the FEM formulation of the problem.

5.2 FEM Analysis of Small Die Thickness Variation Experiment

The small die described in section 4.4 was analysed using the FEM method described above. Figure 5.2.1 is an isometric view and Figure 5.2.2 is a top view of the FEM grid used to describe the flow field. The FEM grid consisted of 9844 elements with 9545 nodes and 16889 equations for an isothermal analysis. Figure 5.2.3 is a cross section of the grid showing the elements that are used. It was believed that this grid would sufficiently describe the flow field and provide accurate results while also minimizing computational demands.

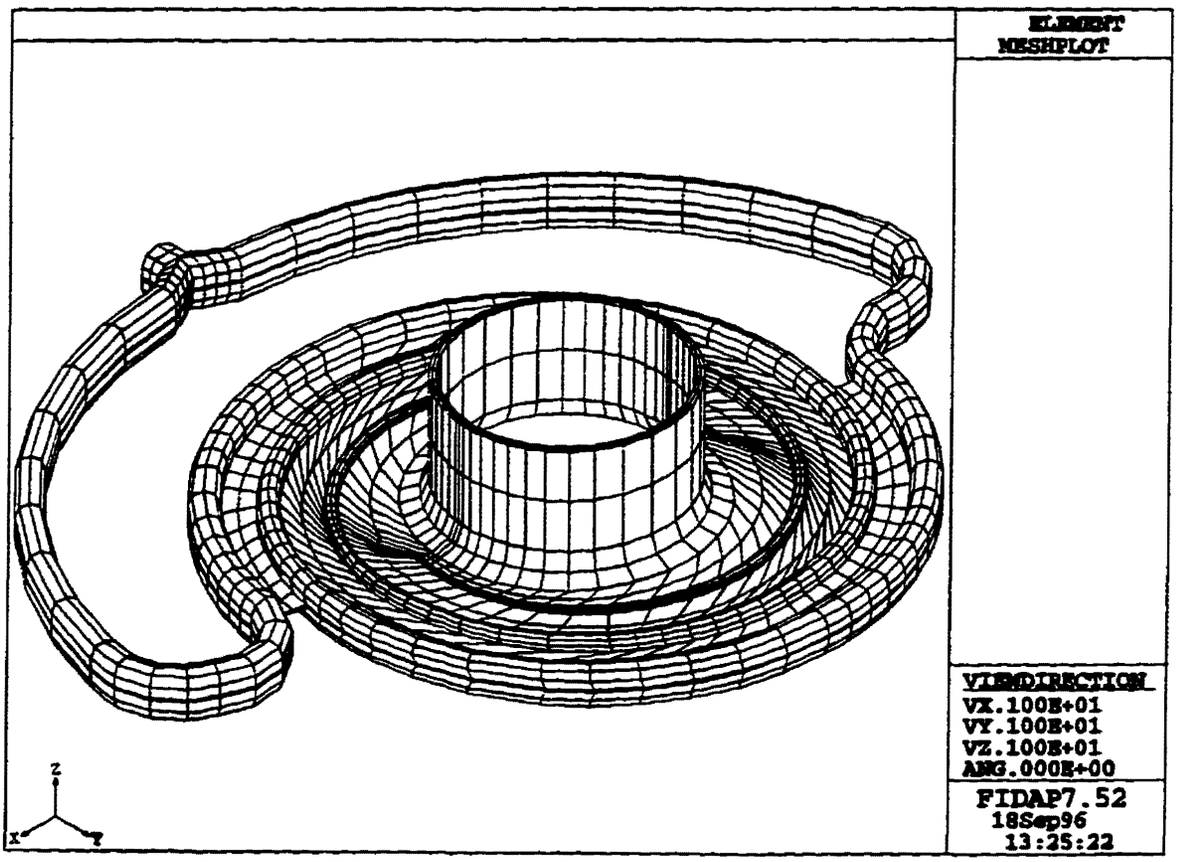


Figure 5.2.1 An isometric view of the FEM grid used for the small die

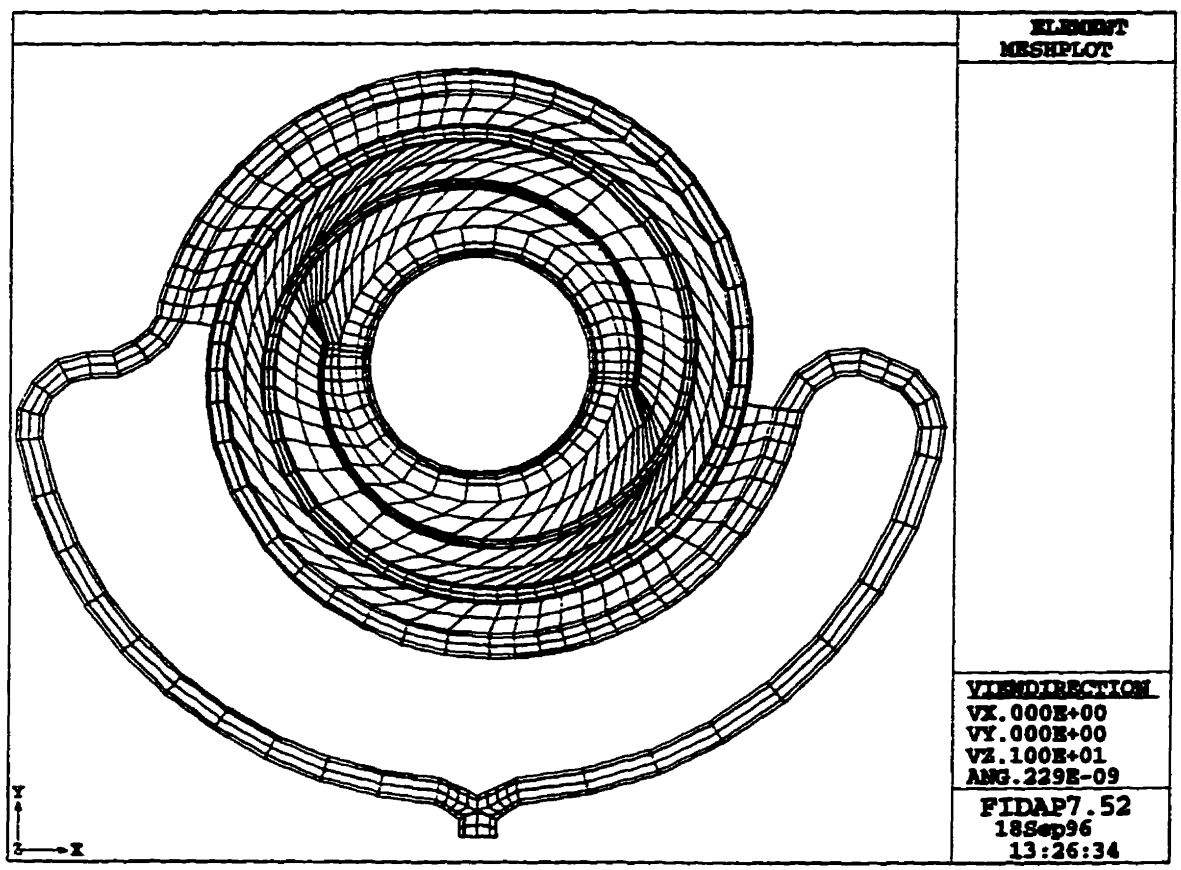


Figure 5.2.2 A top view of the FEM grid used for the small die.

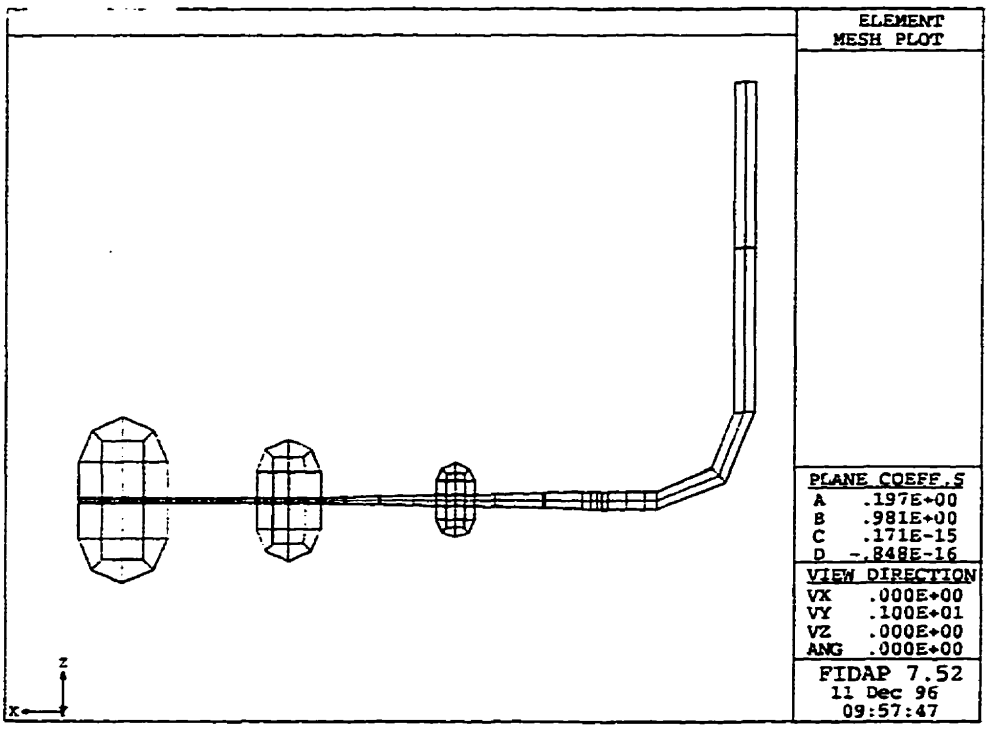


Figure 5.2.3 A cross section view of the FEM grid.

Figure 5.2.4 is an isometric view of the pressure contour plot for an isothermal analysis. This figure shows a gradual reduction in pressure from the entrance to the exit of the die without any exceptionally high pressure drop areas. Figure 5.2.5 is a line graph of the pressure drop along the channel which makes it easier to see that there indeed is a fairly linear pressure drop from the start to the end of the channel. The FEM analysis predicts about a 50% higher pressure drop along the channel in comparison to the CVM results shown in Figure 4.4.5. This difference is likely due to certain deficiencies in both methods. The somewhat crude grid that was used, to minimize the computational demands, will have some affect on the accuracy of the pressure predictions but the analytical expressions used in the development of the CVM also contribute to this difference. Figure 5.2.6 is a line graph of the speed variation around the circumference at the die exit. This represents a variation of about +/- 2% which is lower than the actual measured range of about -6% to +9%. This difference must also be due to the inherent differences and assumptions between the two modelling methods.

A non-isothermal analysis was also performed in order to determine the effect of viscous dissipation on the distribution. The isothermal analysis was performed at a flow rate of 400 ml/min. Unfortunately, it was determined that the FEM grid was not fine enough to allow the non-isothermal solution to converge at the same flow rates as the isothermal analysis. Consequently, the non-isothermal analysis was done at lower flow rates. These were approximately 1/10th (low), 1/5th (medium) and 1/3rd (high) of the flow rate used in the isothermal analysis. Figure 5.2.7 is the resulting temperature contour plot for an analysis using 1/10th the isothermal flow rate and an adiabatic boundary condition on all of the walls.

The temperature rise due to viscous dissipation is about 18 C° which is rather significant at such a low flow rate but also appears to be gradual and evenly distributed. Figure 5.2.8 is plot of the centerline temperature along the channel for the three flow rates used. The temperature increases along the channel but the amount depends on the flow rate. However, the fluctuations also increase with increasing flow rate. It is believed that these fluctuations are due to the coarseness of the grid. The adiabatic boundary condition would cause the predicted temperature rise to be artificially high since, in reality, some of this heat will go into the die but there is no doubt that this would have a significant effect on the local viscosity of the material and consequently the flow distribution. Figure 5.2.9 is the line graph of the centerline speed variation around the circumference of the die exit for all three non-isothermal flow rates. For the low and medium flow rates, the variation increases with increasing flow rate but maintains a similar pattern to what was observed experimentally. At the high flow rate, the variation increases further but appears to be more random. These fluctuations in flow and temperature at the high flow rates would suggest that these results are questionable.

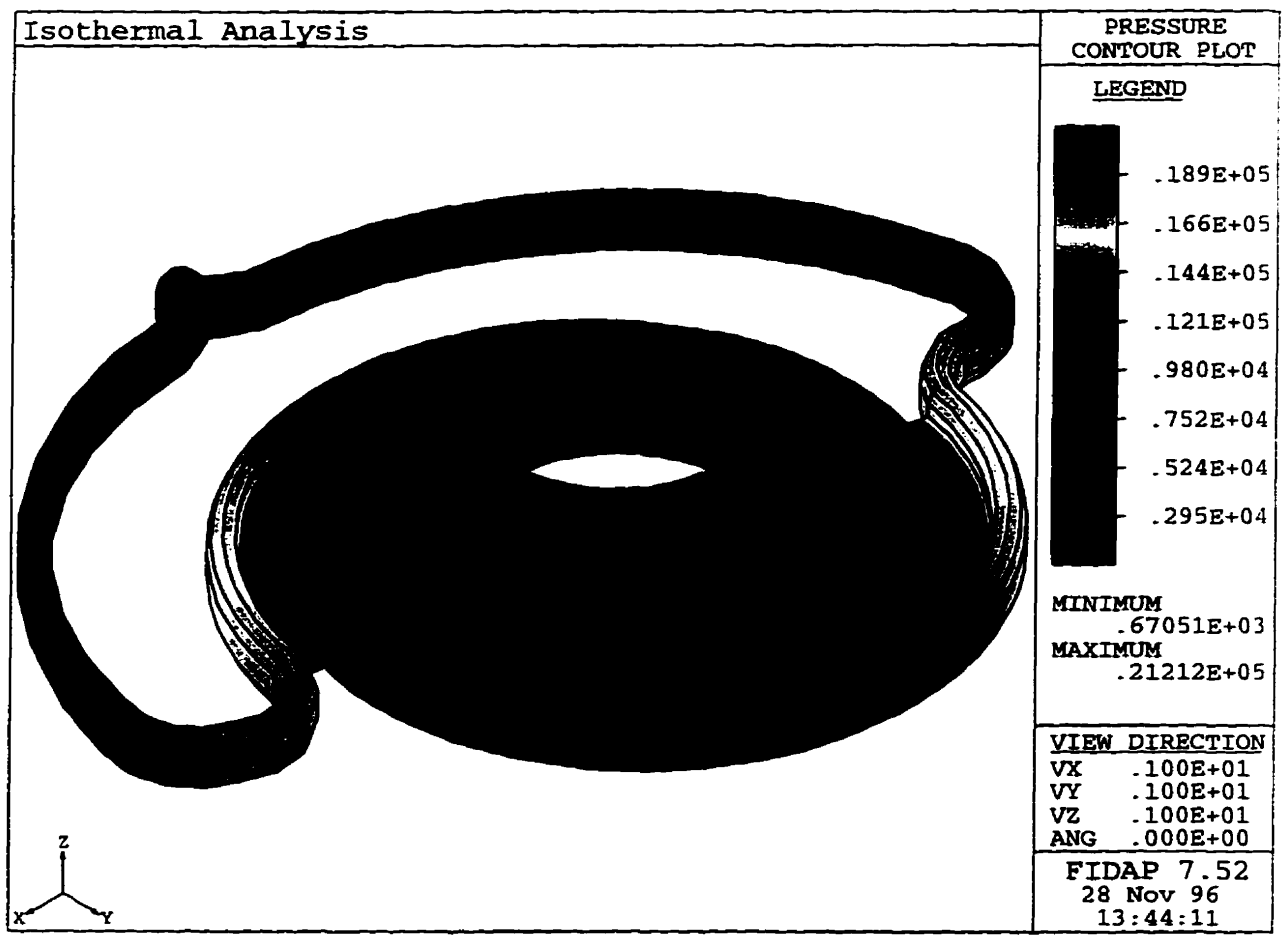


Figure 5.2.4 FEM pressure contour plot of the small die (Isothermal analysis).

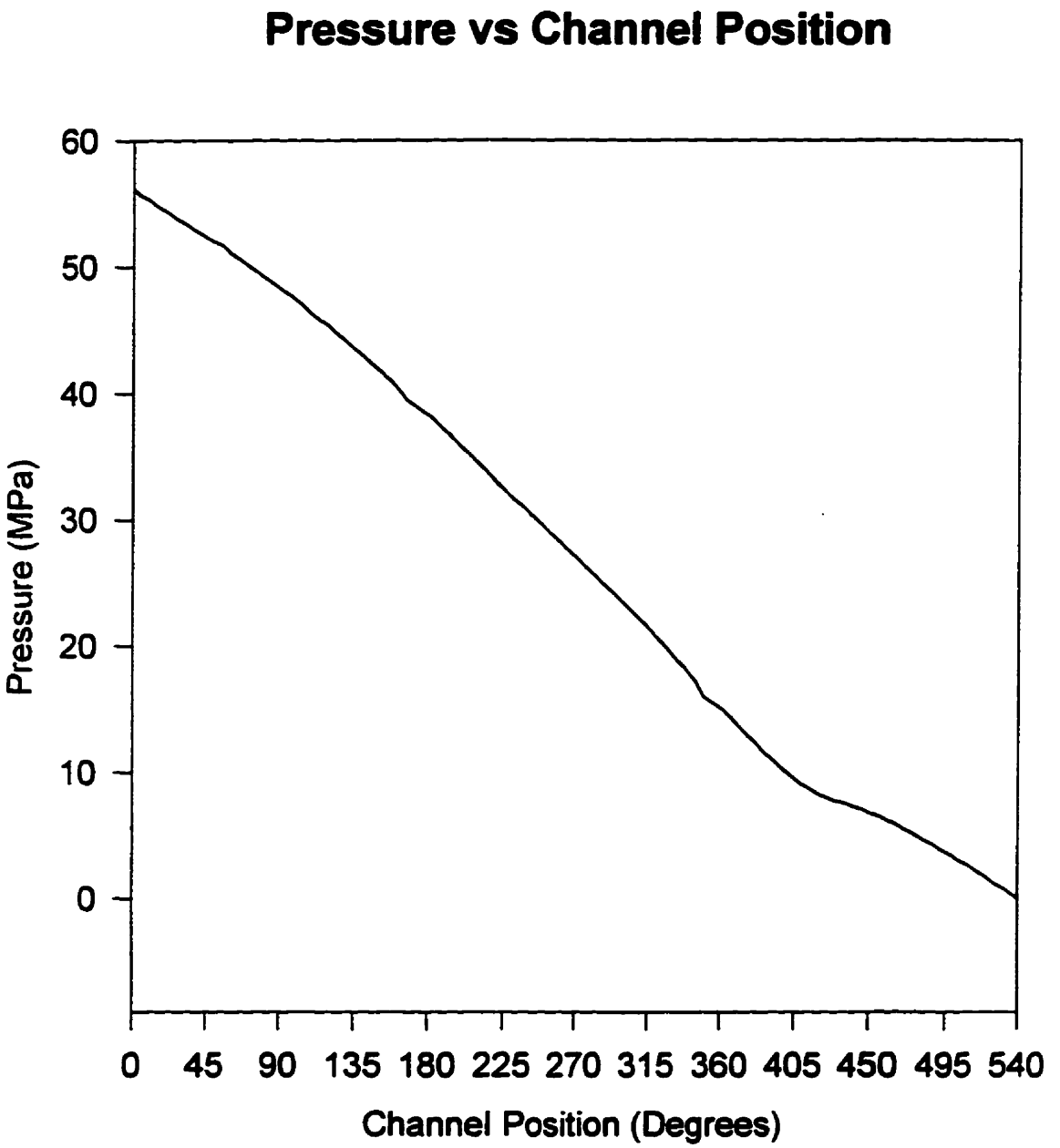


Figure 5.2.5 FEM pressure drop along the channel in the small die.

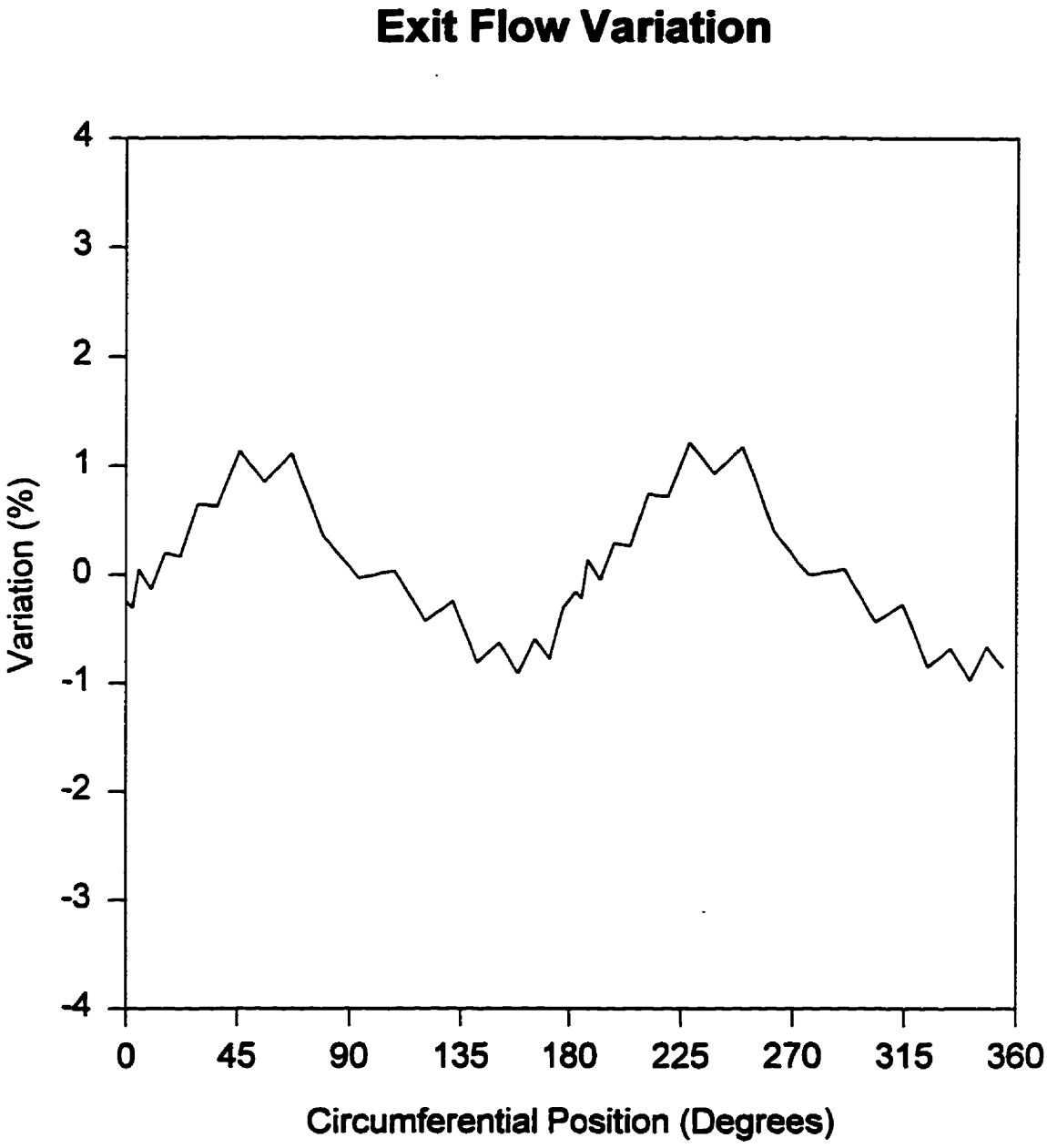


Figure 5.2.6 FEM speed variation at the exit of the small die.

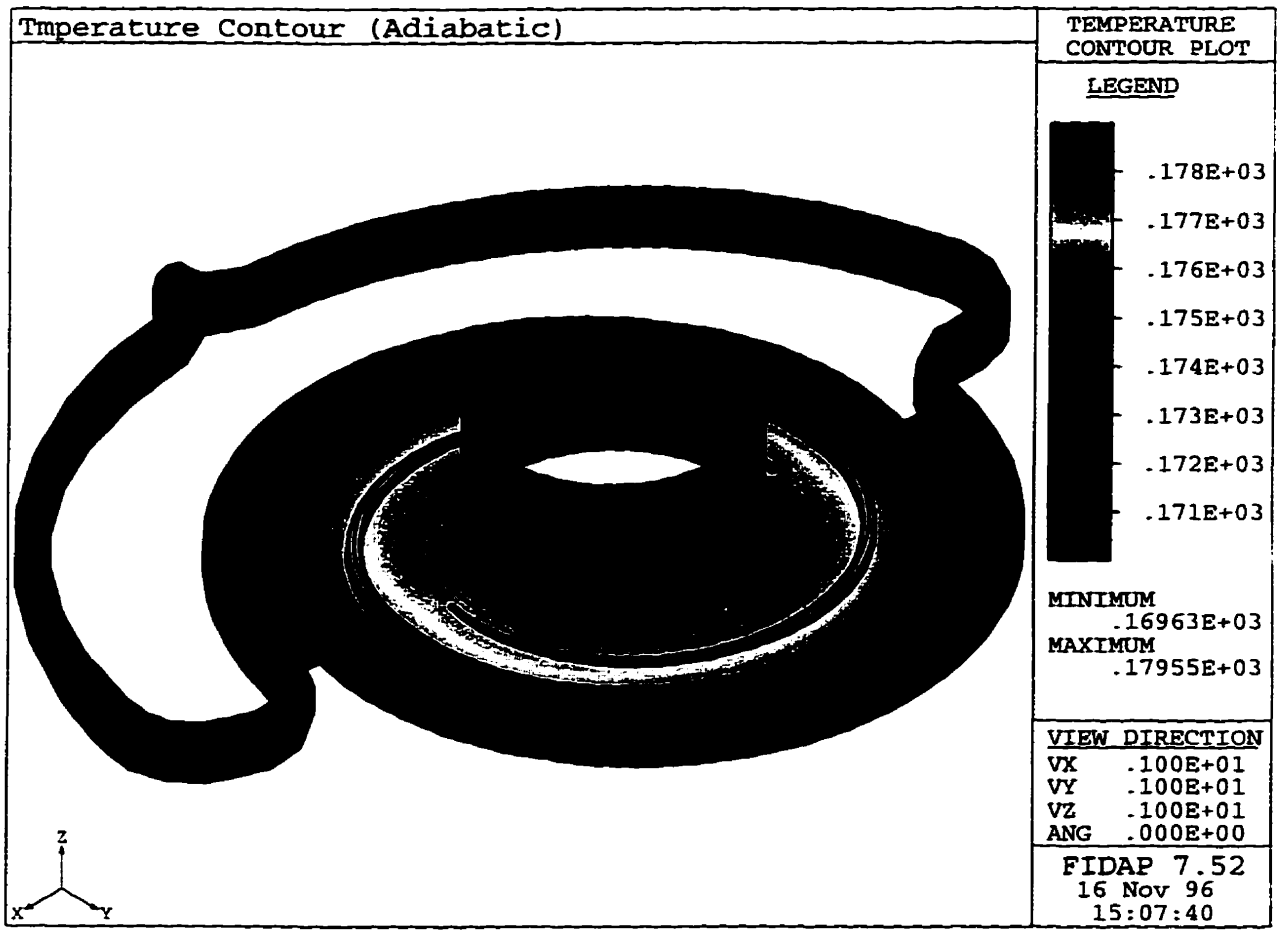


Figure 5.2.7 FEM temperature contour plot for the small die.

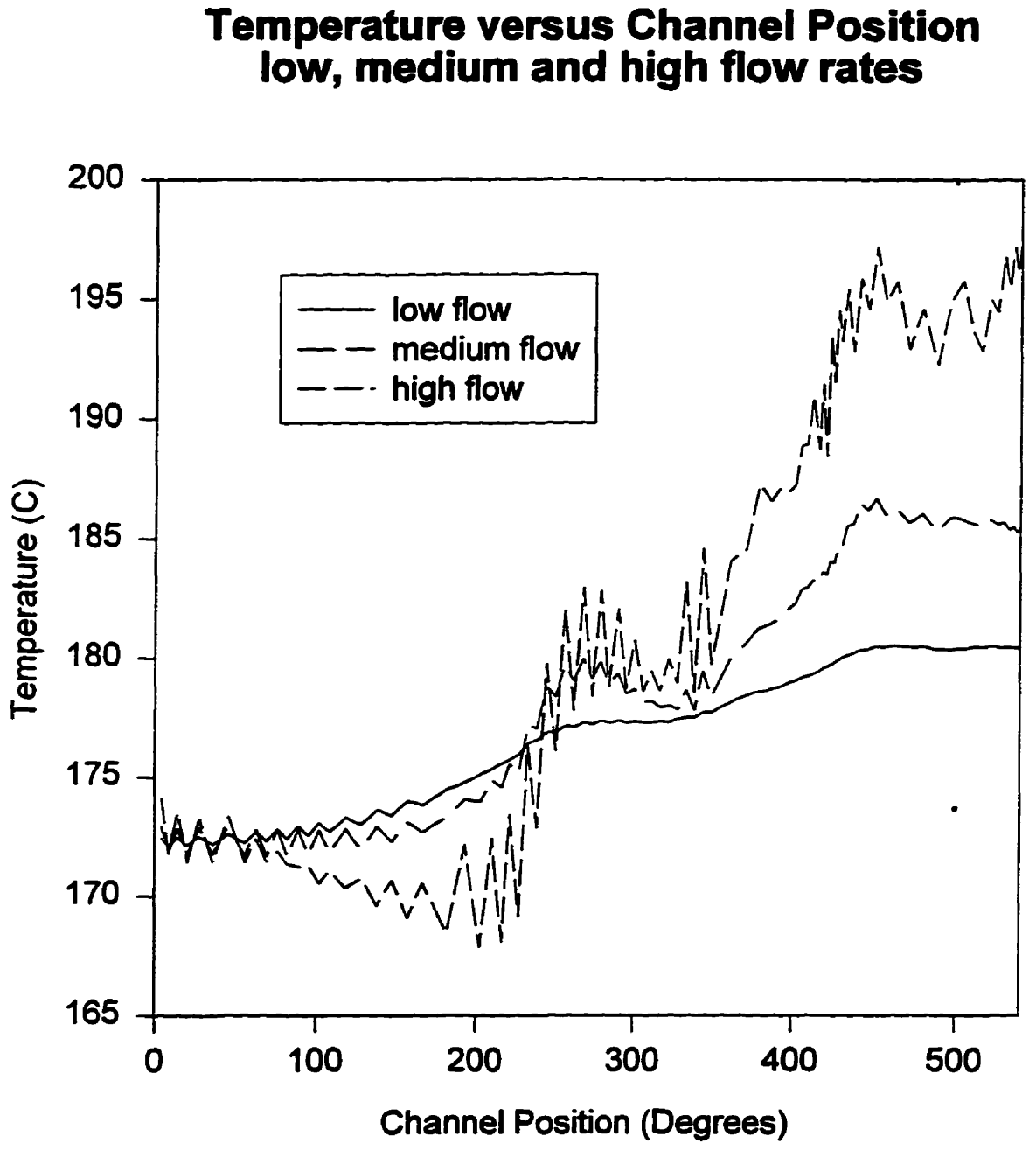


Figure 5.2.8 FEM temperature along the channel for low, medium and high flow rates.

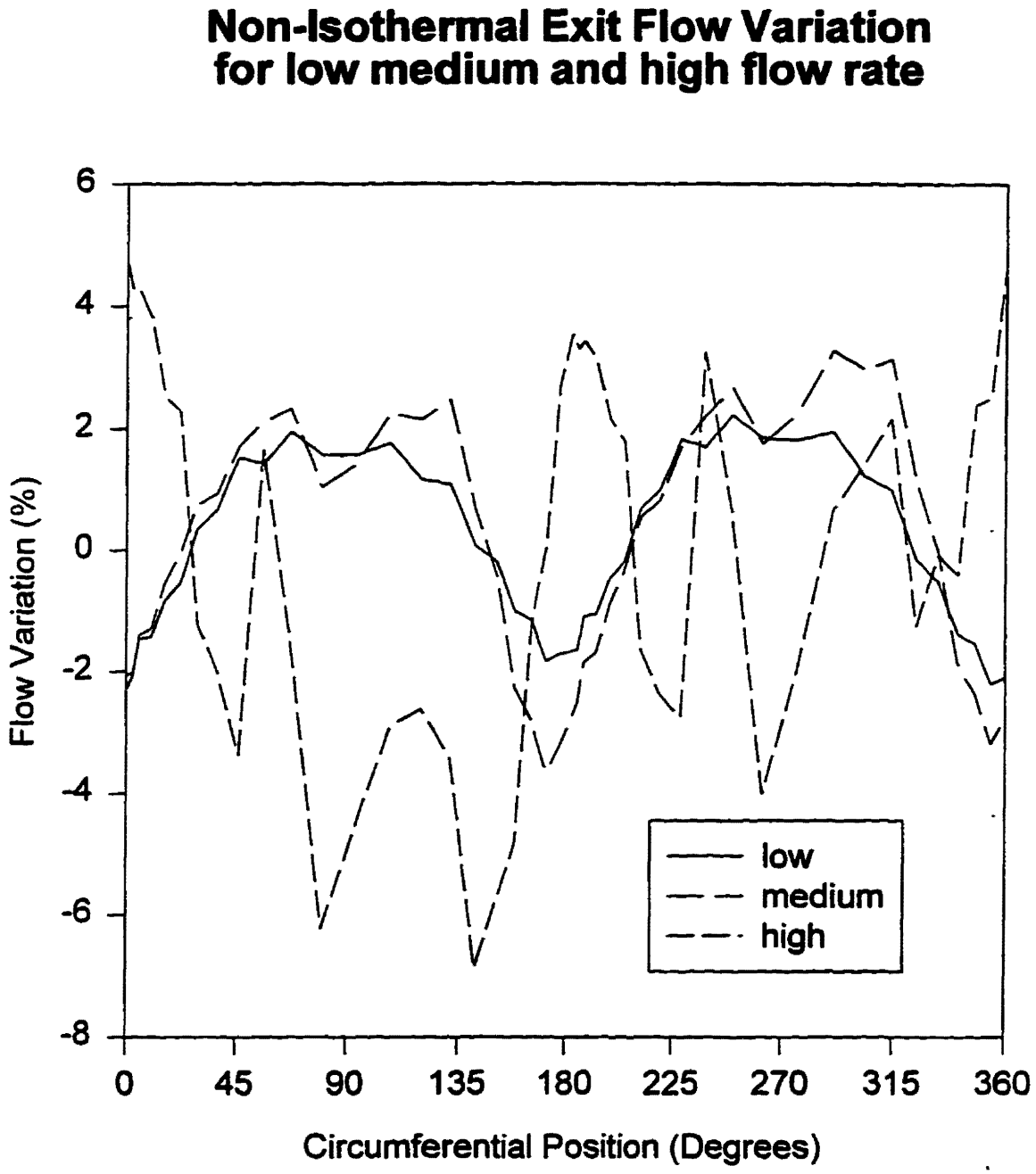


Figure 5.2.9 FEM Speed variation at the exit of the small die. (Non-isothermal analysis for low, medium and high flowrates).

Nevertheless, the medium and low flow rate results suggest that including the non-isothermal effects can bring the predictions closer to the experimental data.

Figure 5.2.10 is a line graph of the speed at the centerline of the channel along its length for an isothermal analysis. The FEM analysis predicts a decrease in speed with an abrupt change in speed at about one third the length of the channel and a minimum at about 420° along the channel position. The speed change at the one third point represents the effect of the point where the material that exits from the other channel enters this channel. Of more concern would be the minimum velocity area at about 80% of the channel length. This represents a region of very low velocity resulting in a high residence time of the material passing through this location. The occurrence of this local minimum can be explained as follows. The material that leaks out of the channel begins to flow in the radial direction towards the centre of the die. At the start of the channel the majority of the flow is in the spiral direction within the channel. At the end of the spiral, all of the flow is radial, inwards. This can be seen in Figure 5.2.11 which contains two views of a velocity vector plot through a cross section of the die. Figure 5.2.12 is a closeup view of the velocity vector plot through a cross section of half the die. These plots show that the channel velocity vectors are large at the start of the spiral section and reduce towards the center of the die. It can be assumed that the low velocity point occurs where most of the material is flowing radially but the depth of the channel is still large enough to slow down the material as it passes this area. This may be a potential problem for certain polymers that are sensitive to prolong exposure to processing temperatures. It would no doubt be beneficial if the design could be altered to eliminate this minimum velocity area.

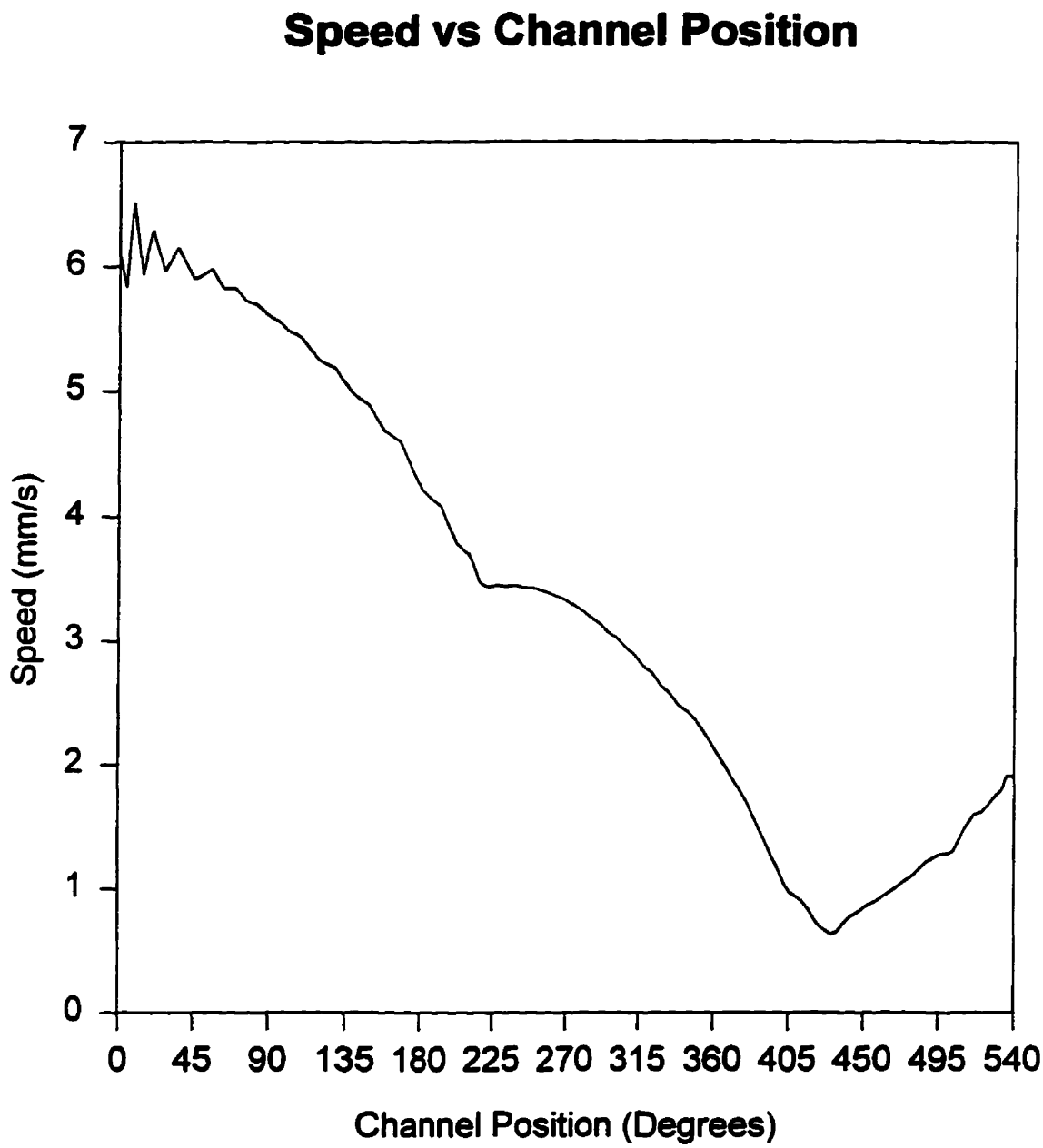
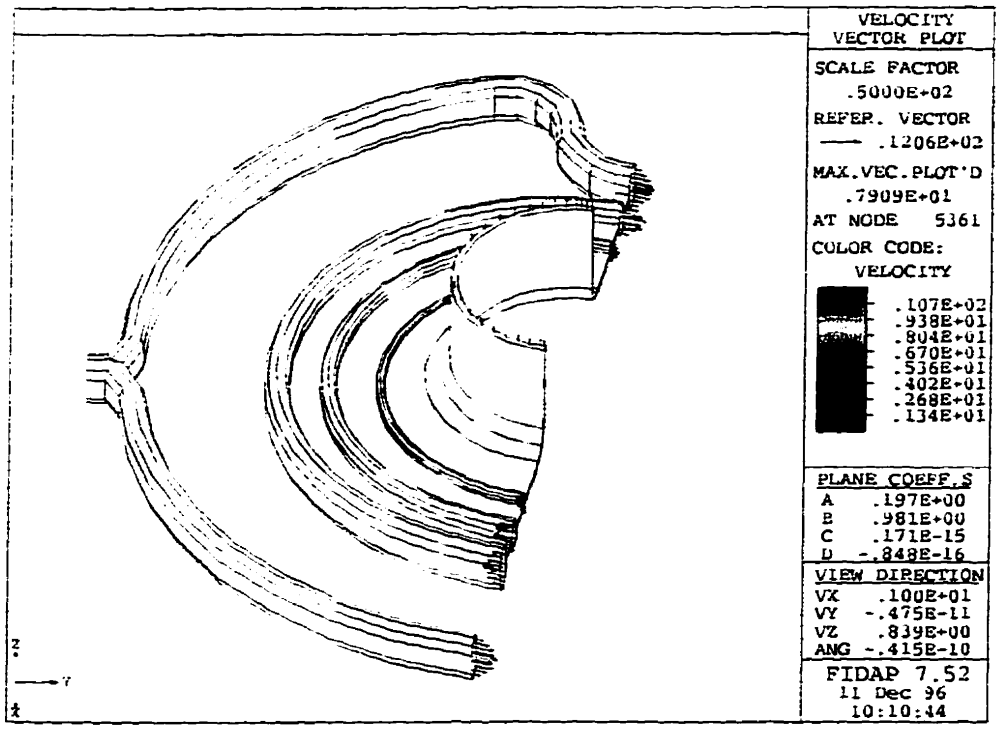


Figure 5.2.10 FEM speed along the spiral channel centerline (Isothermal conditions).



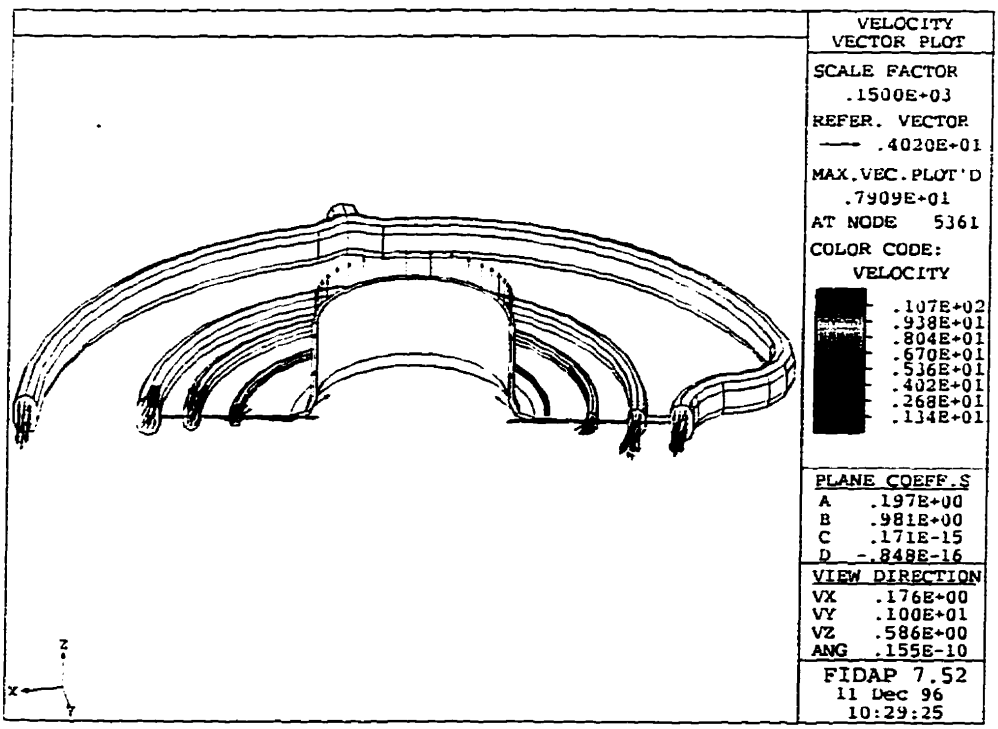


Figure 5.2.11 Velocity vector plots through a cross section of the die.

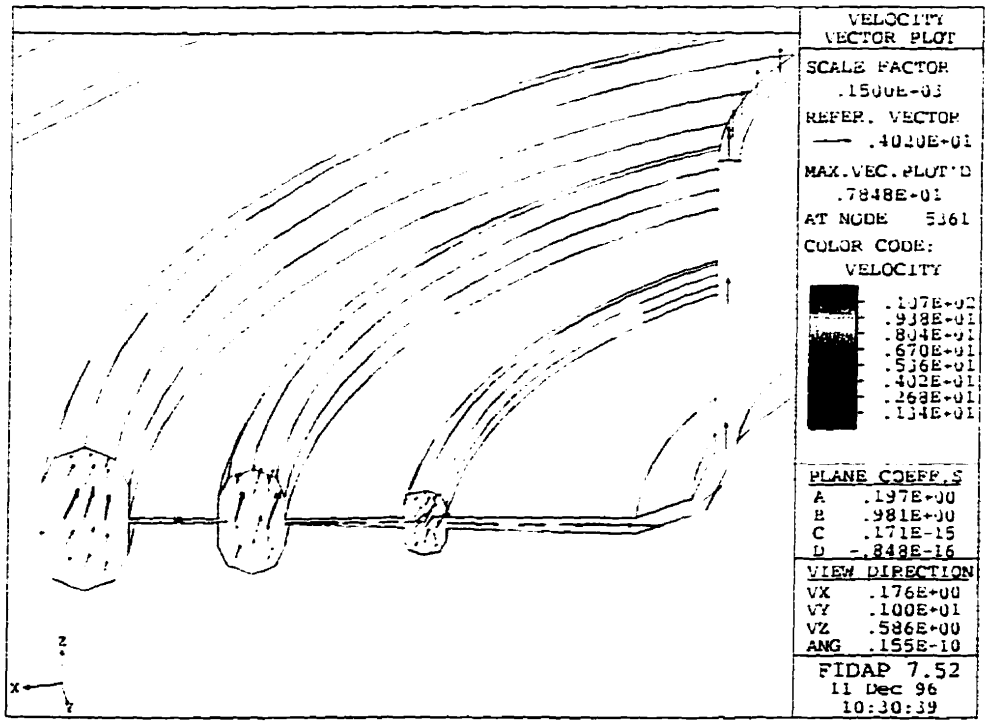


Figure 5.2.12 Closeup view of a velocity vector plot through a cross section of half the die.

5.3 FEM Analysis of the Visualization Experiment

As previously mentioned, the FEM analysis provides sufficient detail to perform particle traces throughout the flow field. This essentially mimics the tracer injection that was performed in the visualization experiments. This has been demonstrated for a conventional spiral die by Coyle and Perdikoulias (1991b). A set of particles were defined at the location corresponding to the injection points of the visualization experiment. Figure 5.3.1 is an isometric view showing the particle paths of a set of particles that were introduced on a line connecting injection points 1a to 1b and tracked. In order to facilitate the comparison to the visualization experiment the subsequent particle plots will be shown from the same orientation as the experiment (top view, entrance at bottom).

Figures 5.3.2 to 5.3.4 are particle traces corresponding to the photographs of the experiment in Figures 4.4.8 to 4.4.10. Comparing the FEM results with the visualization experiments, it appears that the FEM results are quite good considering the rather crude grid that was used.

Another particle plot was used to mimic the introduction of a plug of material as represented by Figures 4.4.11 to 4.4.15. Many particles were placed throughout the cross section at the injection points and traced through the die. Figure 5.3.5 is a top view of the particle paths. These results are very similar to the observations that the majority of the material from the right channel is distributed along the left half of the die. A similar response was observed for the left channel. It is somewhat surprising to see that despite the fact that the spiral channels travel 540 ° around the circumference, the material from each

channel is only distributed over one half of the die. This means that there is very little overlapping of the materials from each channel. This is not what would be expected based on Figure 5.2.10 which indicates that the flow from one channel leaks out over 400 ° of channel length but it must be kept in mind that the results in Figure 5.2.10 are for a non-Newtonian while the visualization experiments are performed with a Newtonian fluid. The effect of the non-Newtonian behaviour will be discussed in the following section.

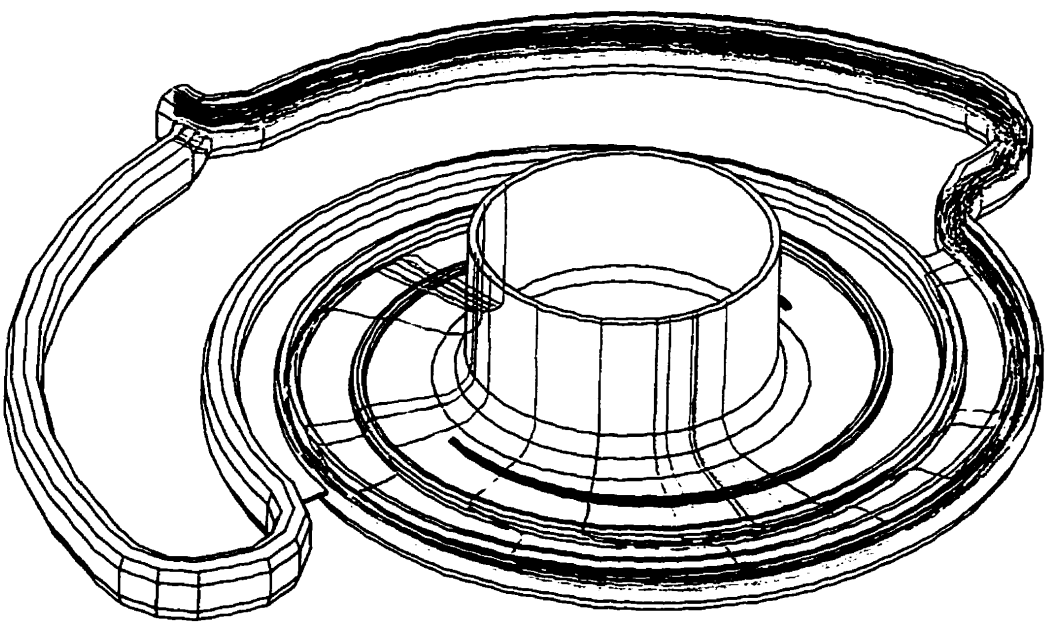


Figure 5.3.1 An isometric view a particle plot for the small die.

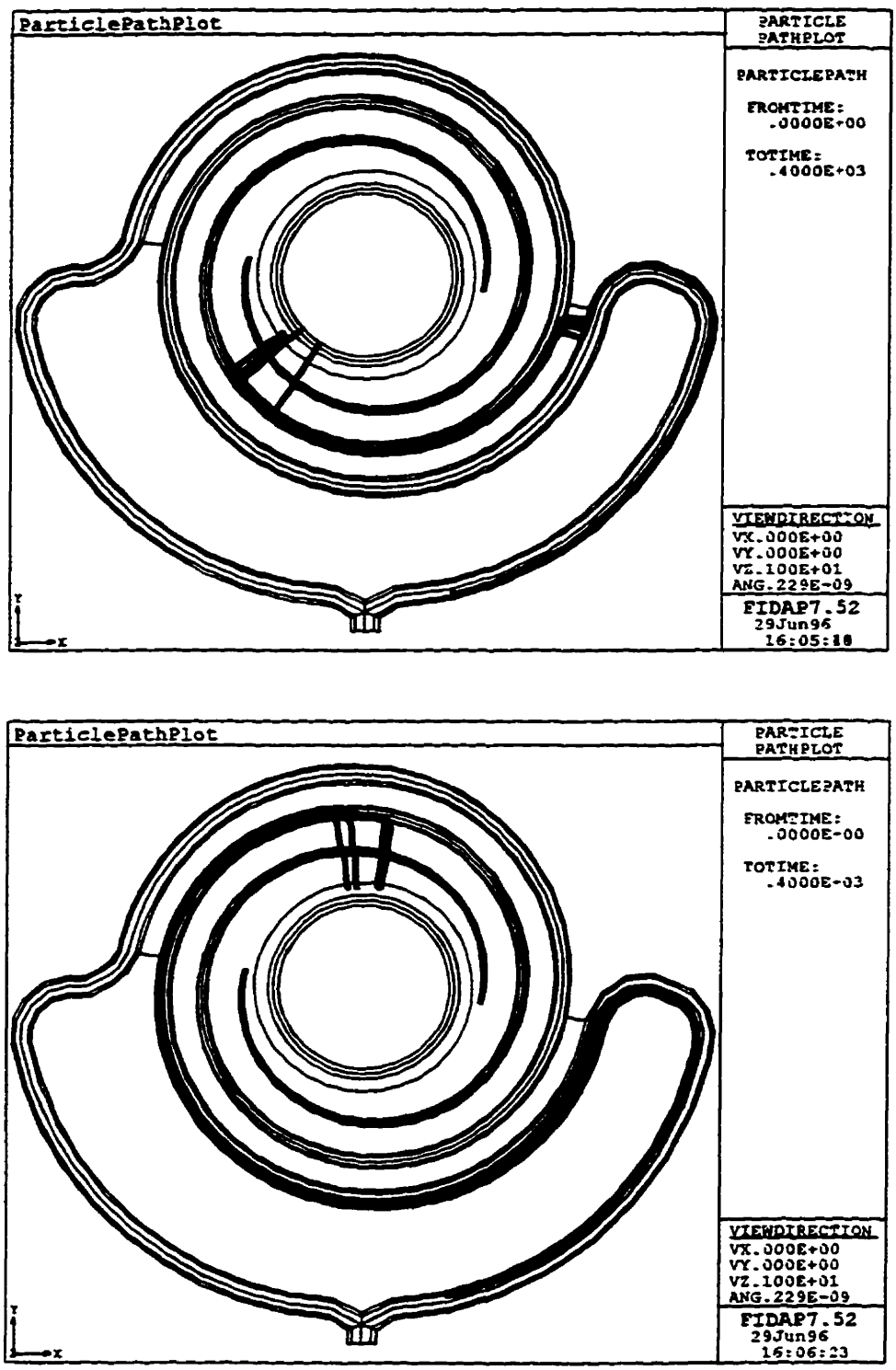


Figure 5.3.2 FEM particle traces from injection points 1a (top) and 1b (bottom).

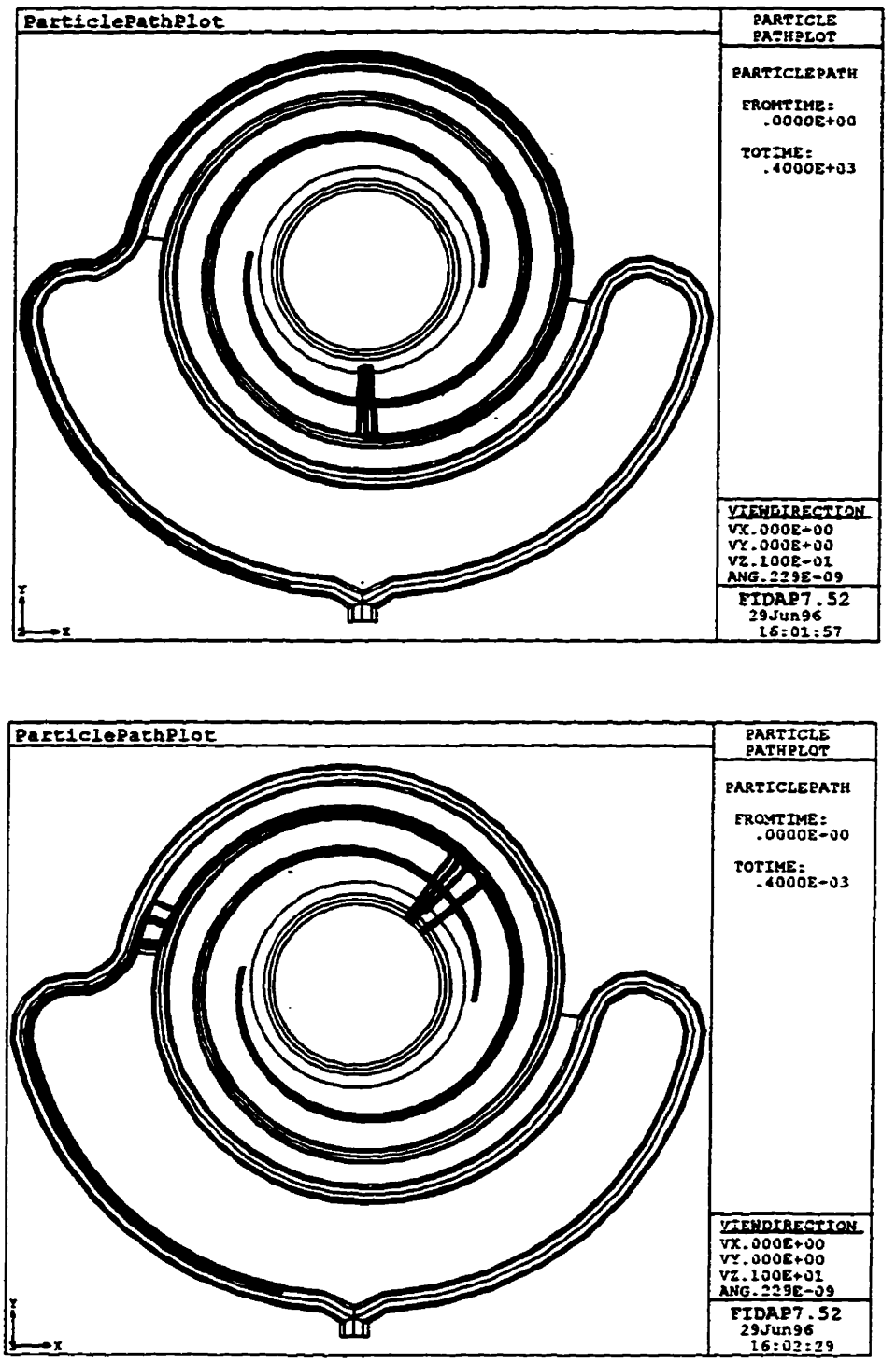


Figure 5.3.3 FEM particle traces from injection points 2a (top) and 2b (bottom).

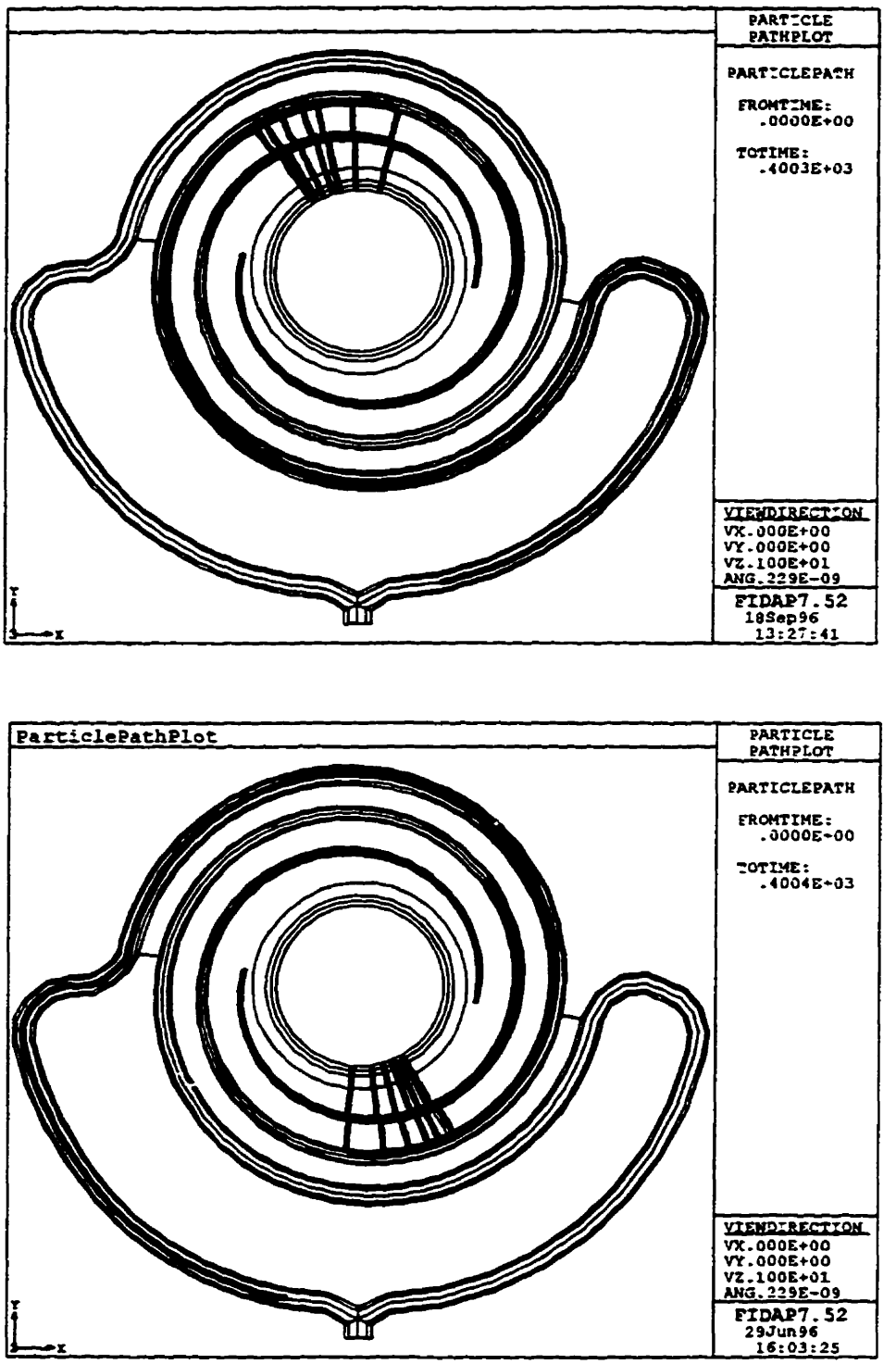


Figure 5.3.4 FEM particle traces from injection points 3a (top) and 4b (bottom).

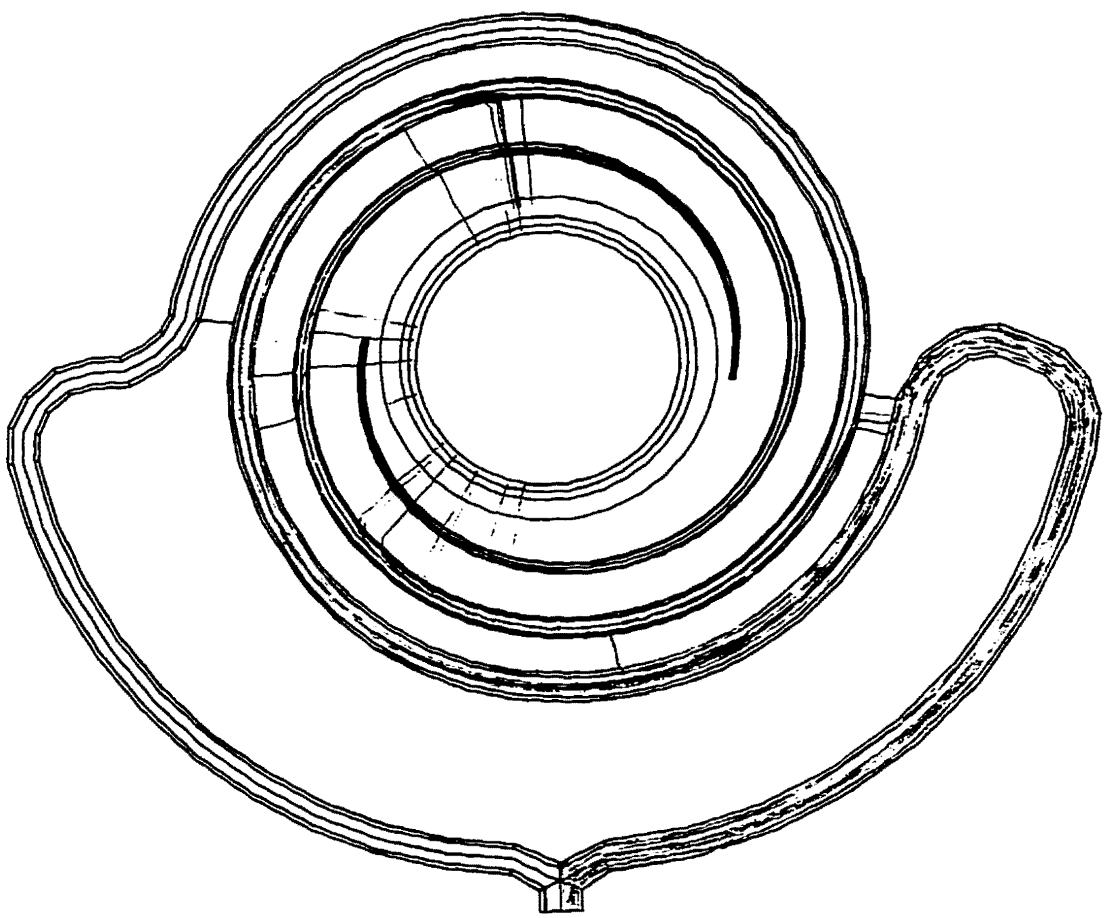


Figure 5.3.5 FEM particle path of the flow in the right channel.

5.4 FEM and CVM Comparison.

In this section, the Finite Element Method (FEM) results and the Control Volume Method (CVM) results are compared with respect to the shear thinning behaviour of non-Newtonian fluids. Figure 5.4.1 is a graph showing the effect of the power-law index on the speed along the centerline of the spiral channel, from the start to the finish, as predicted by the FEM analysis. It appears that the more shear thinning the material is, the faster it will leak out of the channel resulting in the rapid speed reduction that is observed in the first part of the graph. There is a very significant difference in the speed plot from n=1 (Newtonian) to n=0.7. For a n=1, there is actually a speed increase over the first 270 ° of the channel indicating that there is little material leaking out of the channel at the start. Then, there is a rapid decrease in speed from 270 ° to about the 420 ° position of the channel indicating that most of the material from this channel would be distributed over a relatively small area. At first, this appears to explains the lack of overlapping that was observed during the visualizations experiment. However, using the leakage or channel flow to determine the spreading of the material can be misleading because of the complexity of the flow field. The material that leaves the channel within the first overlap flows into the next channel where it is forced to again flow radially and ultimately leaves the die at a different circumferential position . This makes it difficult to judge the distributing effect of the spiral from the channel flow curves. All of this, however, appears to have very little effect on the final velocity variation of the material at the die exit as indicated by Figure 5.4.2. The FEM analysis predicts that exit flow variation will increase as the power law index decrease but this does not appear to be a very significant effect.

The corresponding predictions of the CVM are shown in Figures 5.4.3 and 5.4.4. Figure 5.4.3 is a graph of the channel speed versus channel length for the range of power law indexes used in the FEM analysis. The CVM also predicts that the leakage rate of the material out of the channel increases as the power law index decreases but not to the degree predicted by the FEM analysis. This suggests that the CVM model prediction of the resistance in the channel is lower than in the FEM analysis resulting in a slower rate of leakage out of the channel. Figure 5.4.4 is a graph of the final thickness variation as predicted by the CVM analysis. The CVM predicts a larger exit variation than the FEM analysis. However, the CVM also predicts that the distribution gets worse as the power law index decrease but the effect is not very large.

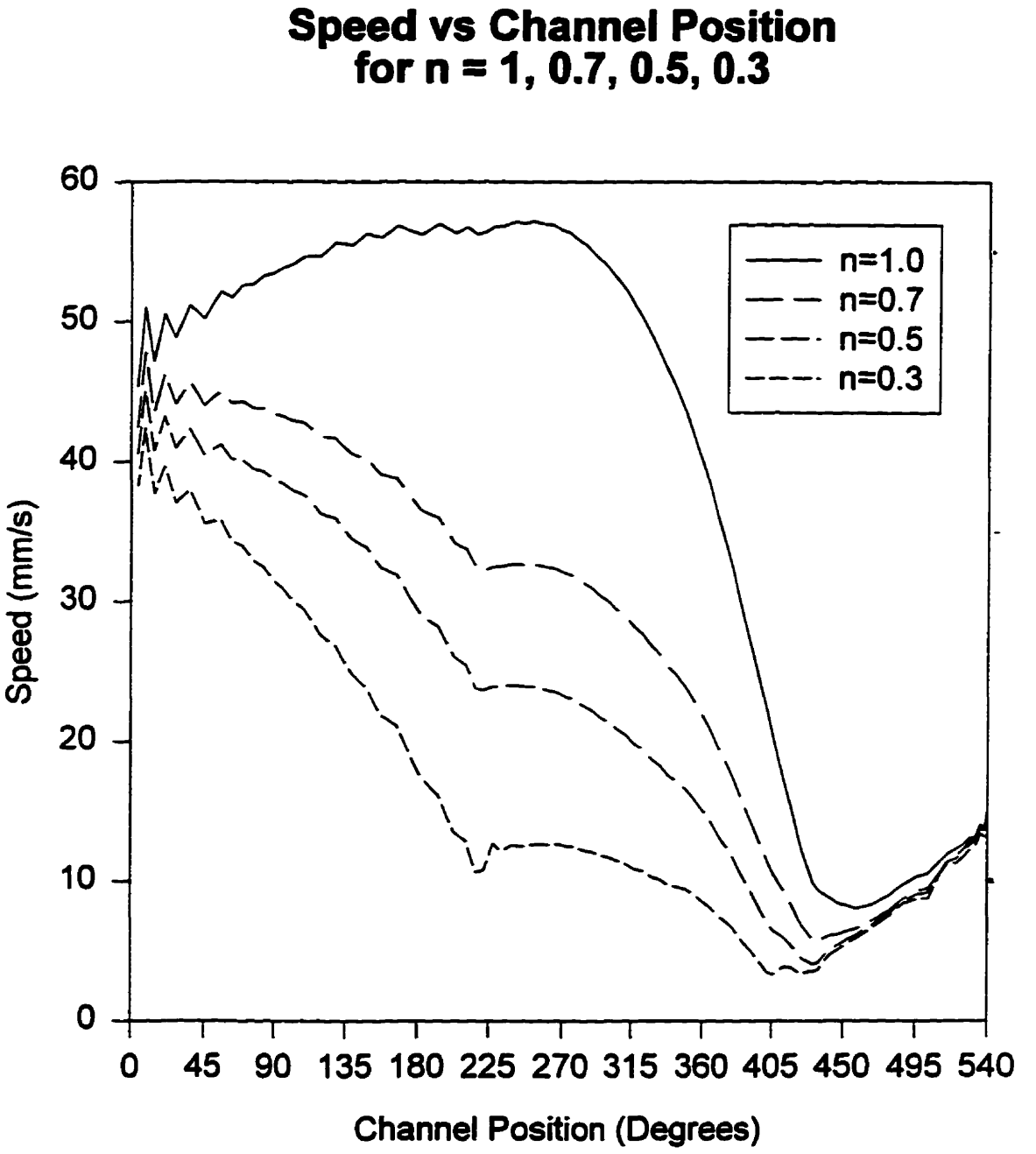


Figure 5.4.1 FEM channel speed for power law index 1.0, 0.7, 0.5 and 0.3.

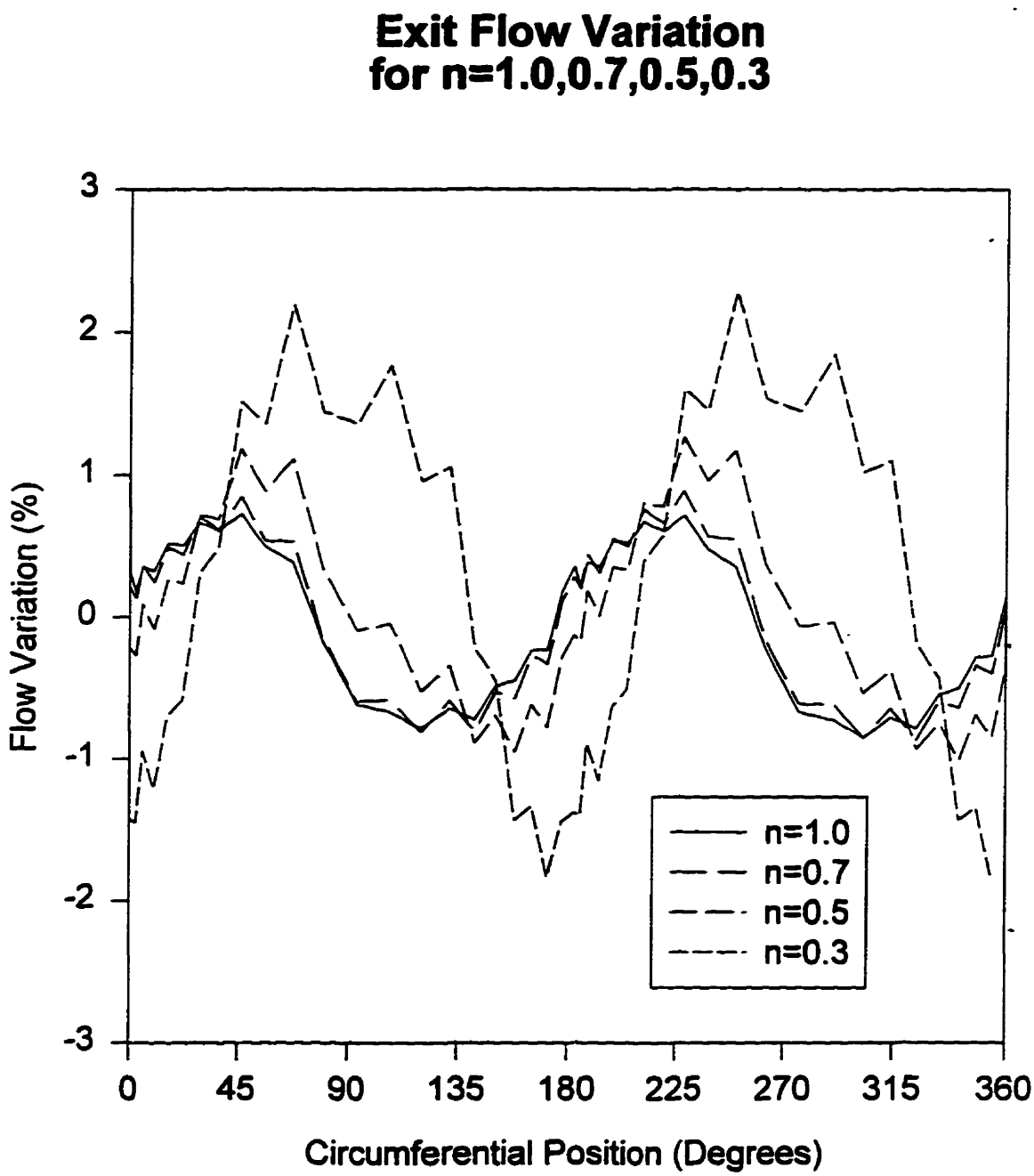


Figure 5.4.2 FEM exit speed variation for power law index 1.0, 0.7, 0.5 and 0.3.

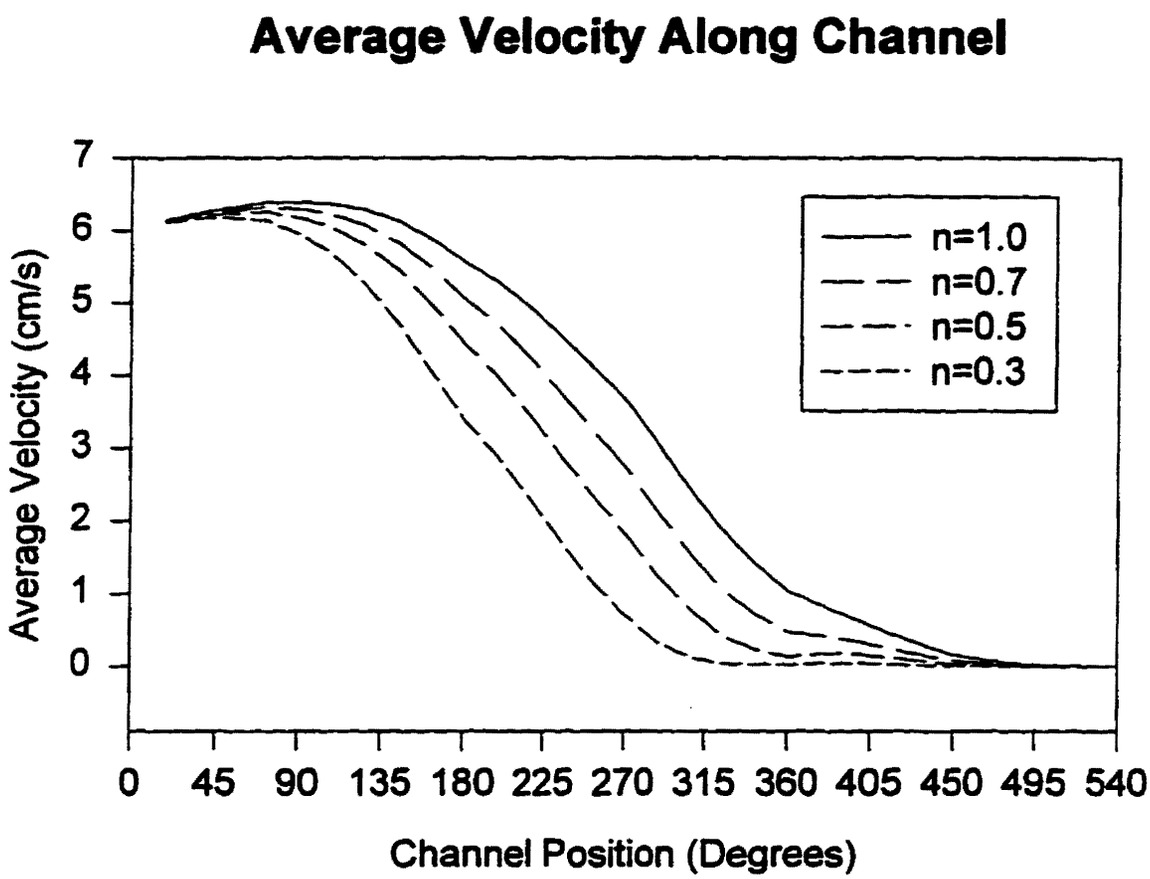


Figure 5.4.3 CVM channel speed for power law index 1.0, 0.7, 0.5 and 0.3.

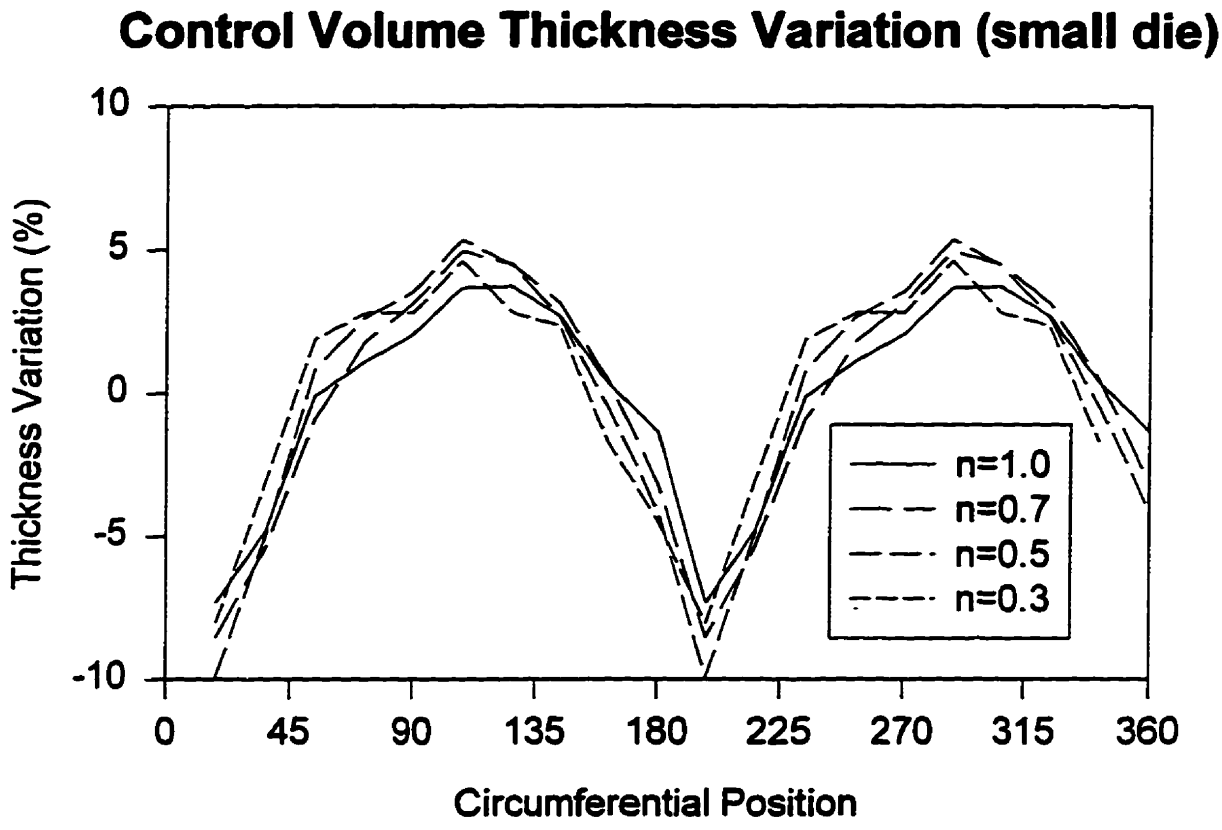


Figure 5.4.4 CVM exit flow variation for power law index 1.0, 0.7, 0.5 and 0.3.

The effect of the power law index on the particle paths was also investigated. Particle paths were traced from the same starting points for power law indexes of 1.0, 0.7, 0.5 and 0.3. The results are shown in Figures 5.4.5 to 5.4.8. It appears that as the power law index decreases, the particles exit the spiral channel sooner and the area over which the majority of the material is distributed is narrower. This supports the point made earlier, about using the channel flow curves to infer overlapping of the material, and further supports the benefit of using a particle path analysis to help understand the flow patterns within these types of dies.

5.5 Discussion

There is no doubt that a FEM analysis can be a very useful tool in terms of providing valuable design information. It also facilitates the conceptualization of complex flow fields such as the one presented in this study. This also makes the FEM analysis a very educational tool for the novice design engineer. The one drawback to this method of analysis is the enormous effort required to apply it correctly and obtain useful results. The generation of a grid for a complex 3-D flow field is quite tedious and time consuming but this is steadily improving. Some software manufacturers are developing grid generation tools that will produce a grid from CAD files. In addition, the computing industry is rapidly developing equipment that can handle the enormous computational demands of a FEM analysis of a flow field. The increasing computing power allows for quicker solutions of larger and larger flow fields.

The FEM analysis indicated that the CVM formulation may under predict

pressure drop through the system and should be re-evaluated. The speed plots indicated that there may be an area of low velocity within the spiral channel which can be a problem if the die was used to process thermally sensitive polymers. The non-isothermal analysis suggested that temperature effects may be significant and that this area of study should be pursued further. The particle path simulations showed good agreement with the observations made during the visualization experiments and it is believed that some further refinement of the FEM grid will enhance this agreement. The particle path analysis also provided a better understanding of the layering effect (or lack thereof) in the spiral channels which can be used to enhance the performance of the die.

From the results presented in this study, it can be concluded that even a crude grid can give dependable and useful results in this very complex flow field and that the use of this numerical technique should be seriously considered for daily design procedures.

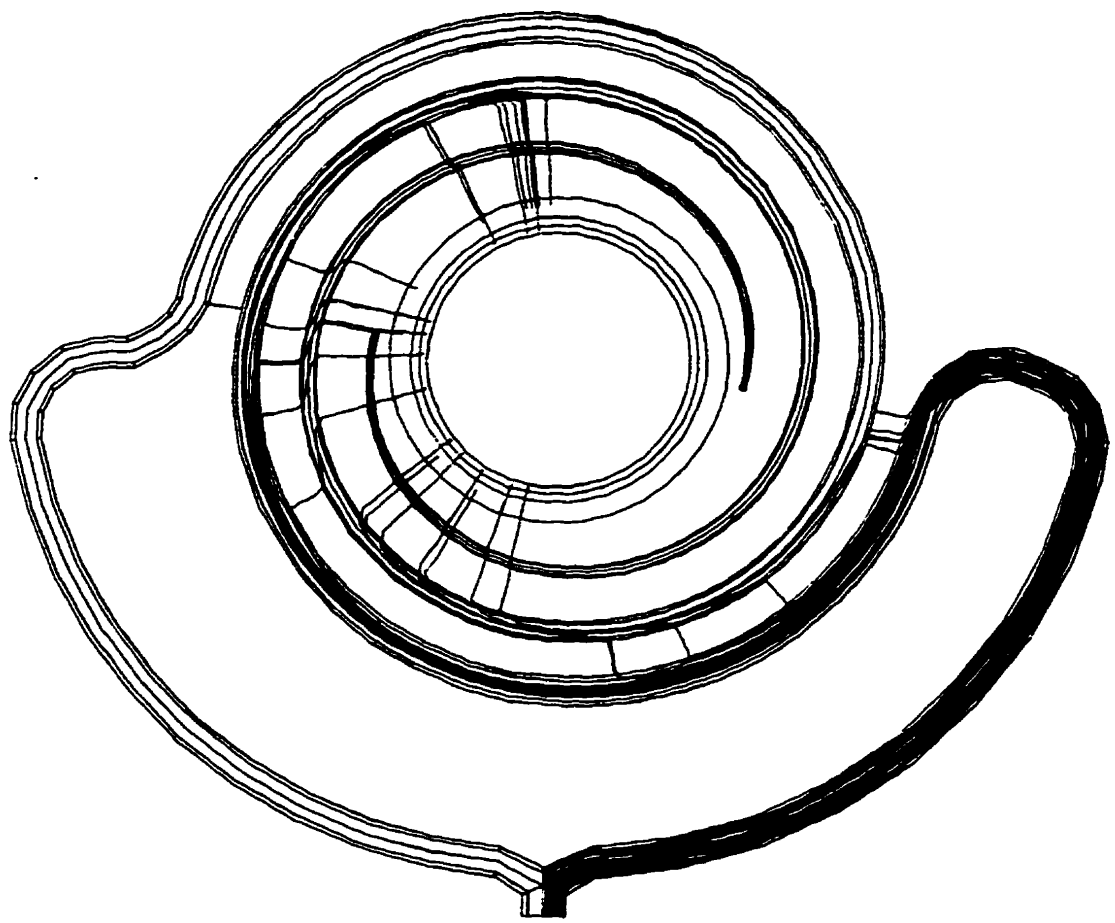


Figure 5.4.5 Particle trace for power law index =1.0.

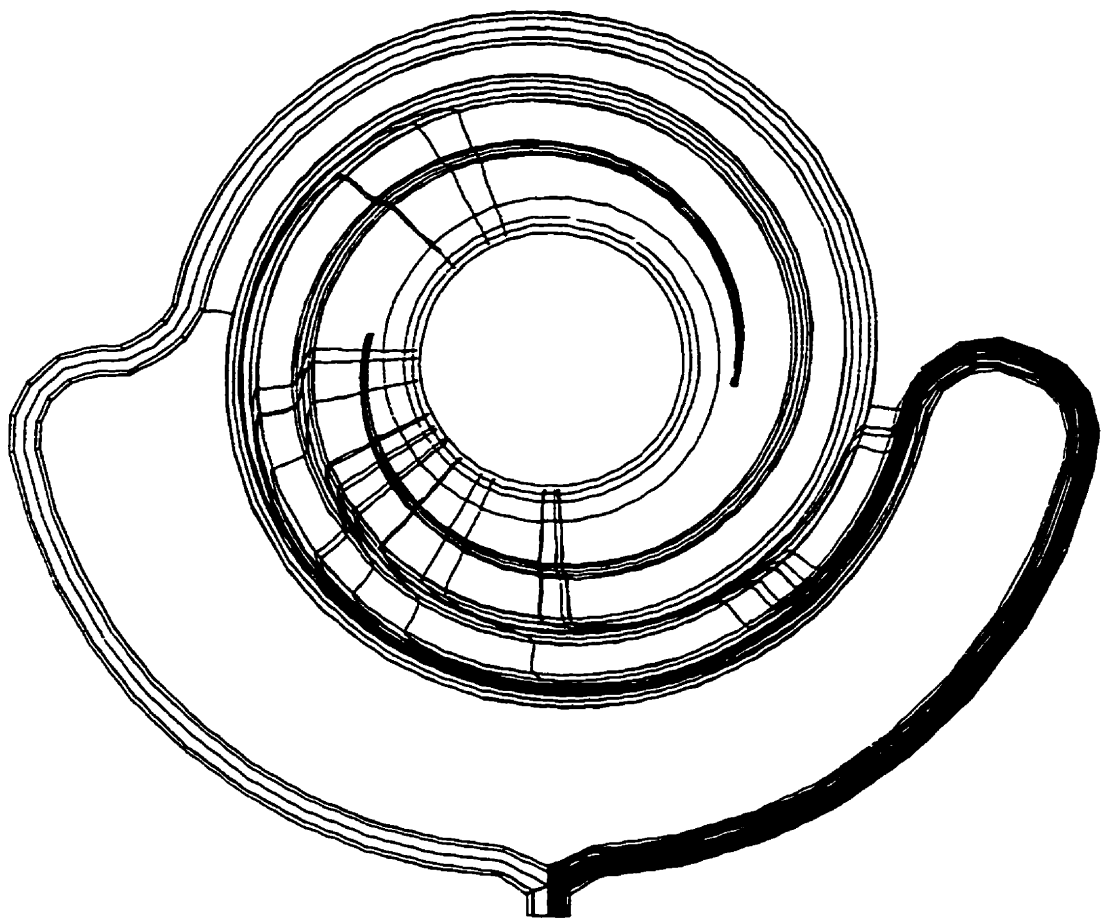


Figure 5.4.6 Particle trace for power law index =0.7.

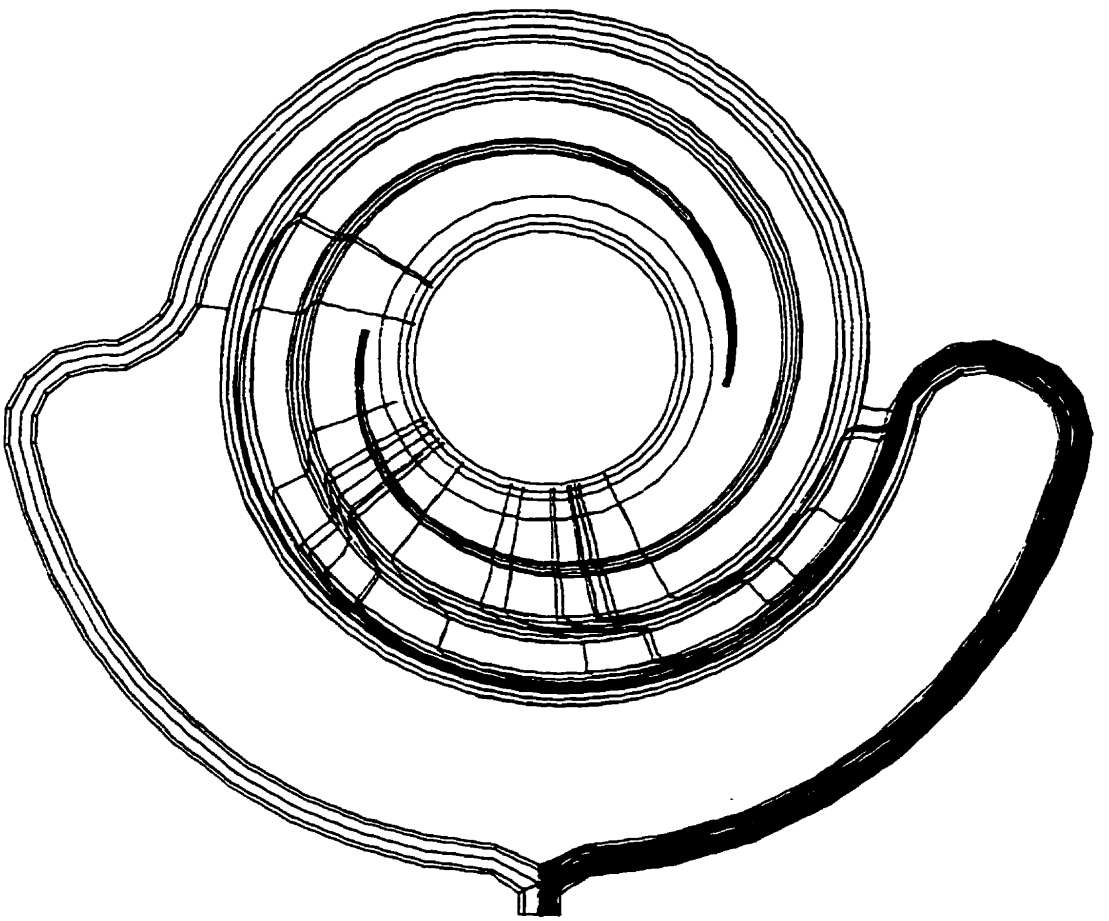


Figure 5.4.7 Particle trace for power law index =0.5.

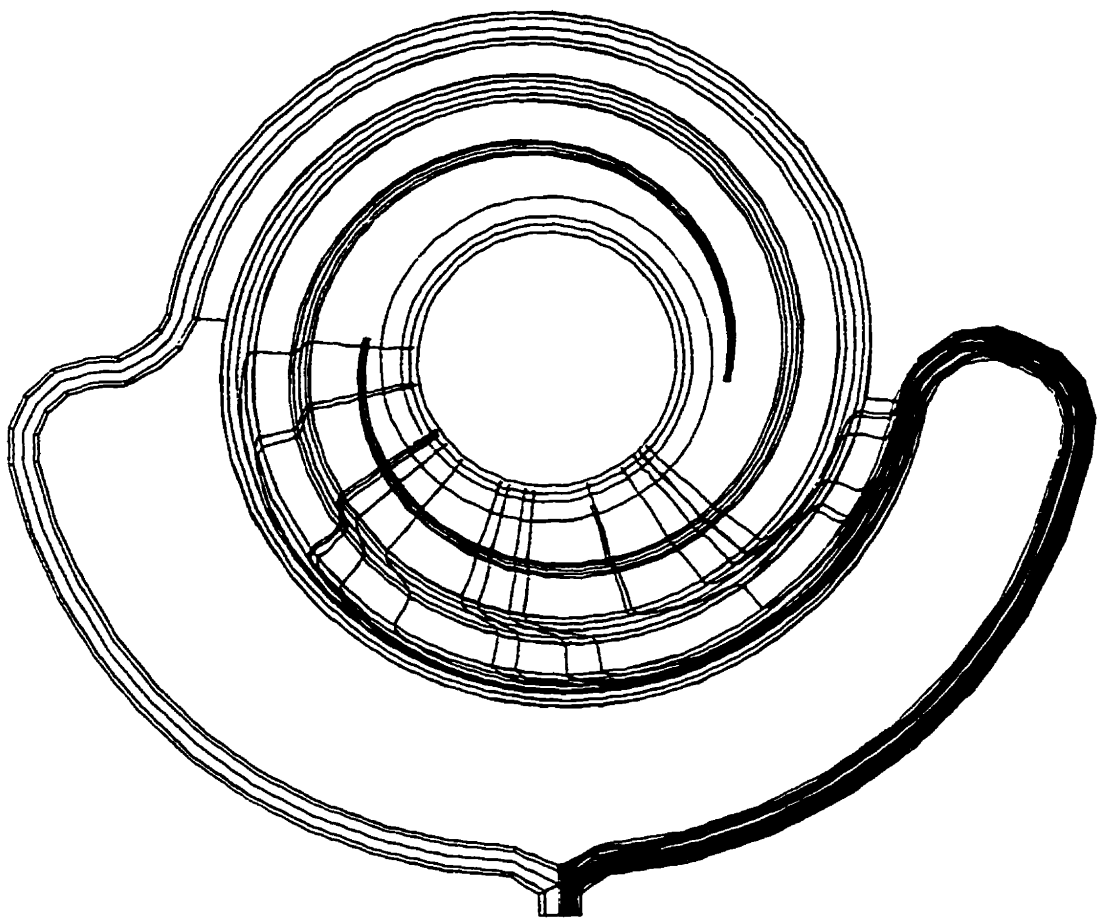


Figure 5.4.8 Particle trace for power law index =0.3.

CHAPTER 6

INTERFACIAL INSTABILITY

6.1 Experimental Investigation

This chapter describes an experimental investigation that was performed in order to obtain a better understanding of the interfacial instability phenomena that may occur during coextrusion. The basic purpose of the experiment was to distinguish between the effects caused by different polymer characteristics and their relationship to the geometry of the flow field.

6.1.1 Equipment.

The experiments were performed on a Brampton Engineering 7 layer coextrusion line that was equipped with two, 45 mm diameter extruders and five, 30 mm diameter extruders. All of the extruders were of the single screw design and had an L:D ratio of 24:1. The screws had a compression ratio of 2.8:1 and were each equipped with a fluted mixing section. Only the two, 45 mm extruders were used in these experiments since only two layers were required. The extruders were equipped with gravimetric feeders which measured the mass flow of material through each layer. The die had a 76 mm exit diameter. A standard air ring, collapsing frame, nip and winder, of the type normally found on a blown film line

used to produce the samples.

The experiments were performed using an annular coextrusion die with essentially two exit configurations; narrow and wide exit gaps. Figure 6.1.1 shows the narrow exit gap configuration in which layer 'A' flows upward to merge with layer B into a coextrusion area with a 6.35 mm gap. The coextrusion flow channel then converges to a 1.52 mm gap for the last 15 mm of the die exit. In the wide die gap configuration, shown in Figure 6.1.2, the coextrusion flow channel gap remains at 6.35 mm right up to the exit of the die.

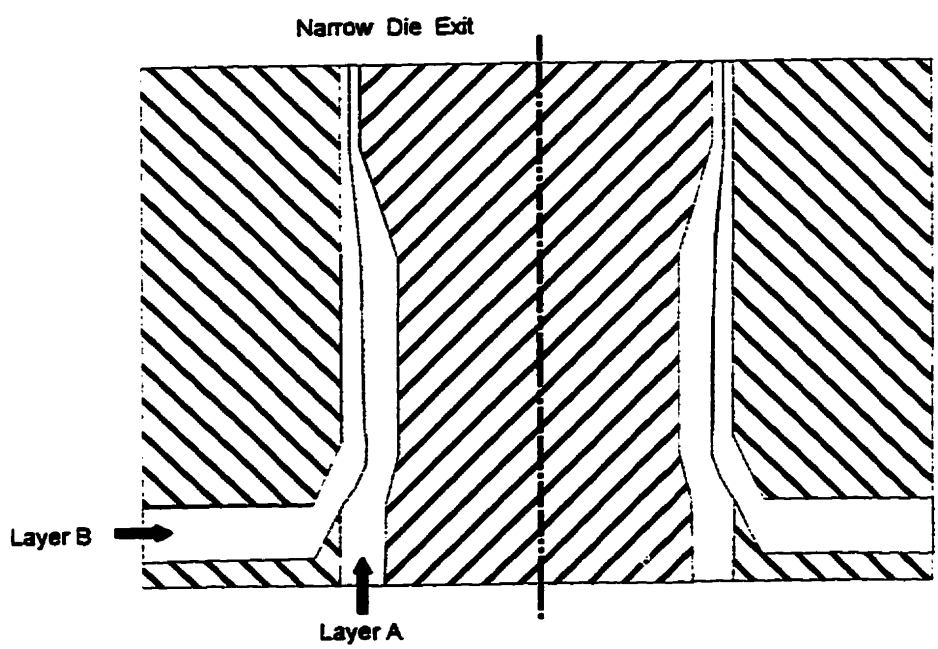


Figure 6.1.1 A representation of the narrow exit gap geometry.

Prior to combining, the polymer is distributed into a uniform annular flow using a distribution system similar to that described in Chapter 4. At the merge point, the minor component of the flow is travelling vertically upwards, while the major component is essentially travelling radially inwards. The annular type die offers one advantage in that there are no edge effects to be concerned with as in a flat die. Detailed dimensions of the die are provided in Appendix A.

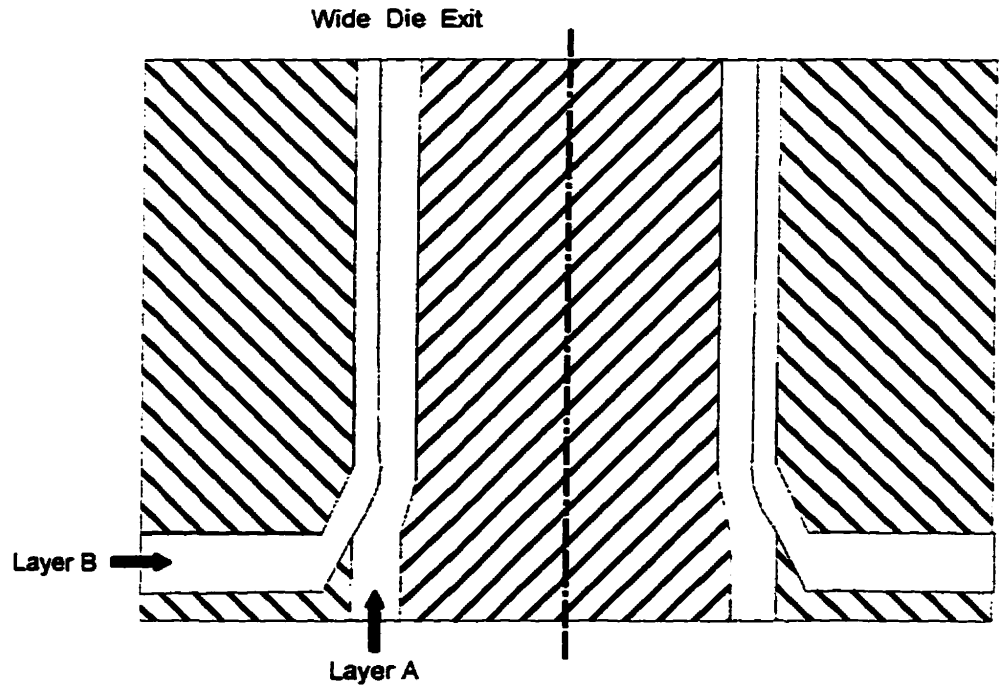


Figure 6.1.2 A representation of the wide exit gap geometry.

6.1.2 Materials

The materials were judiciously chosen in an attempt to distinguish the difference between the effect of the molecular weight (MW) and the molecular weight distribution (MWD) breadth or polydispersity (PDI). Four resins were chosen such that a factorial type of experiment could be set-up. The commercially available materials used in this study were supplied by Quantum and their molecular weight parameter values are summarized in Table 6.1.1. Resins NA957 and NA960 had a relatively broad MWD (as indicated by the Mw/Mn values) while NA345 and NA355 had a relatively narrow MWD. Each resin pair consisted of a relatively high viscosity polymer, NA 960 and NA 355 respectively, and a relative low viscosity polymer, NA 957 and NA 345. The MWD of these polymers are compared in Figure 6.1.3.

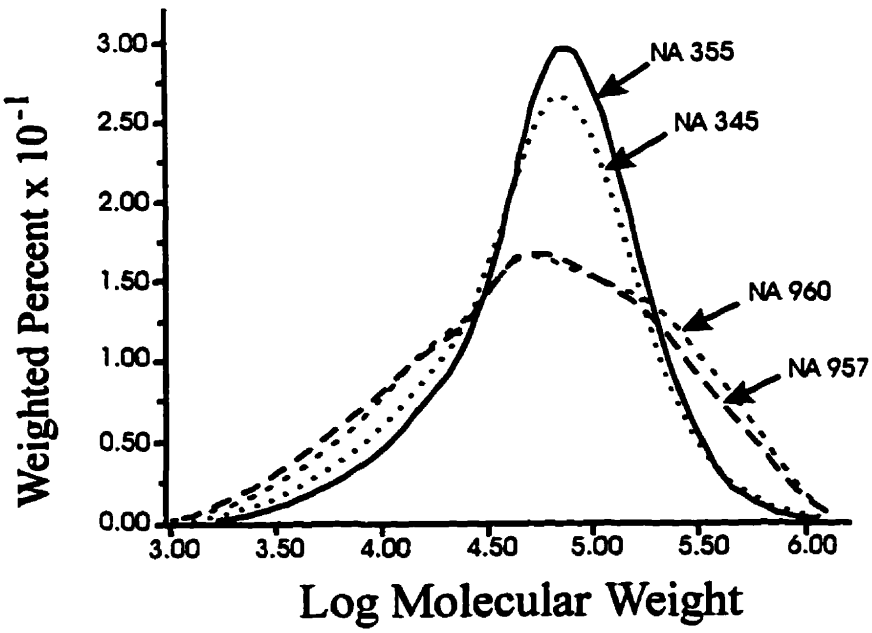


Figure 6.1.3 A comparison of the relative MWD's for the polymers used in this study.

Table 6.1.1 Molecular weight averages and ratios for the materials used in this study.

	NA 957-000	NA 960-000	NA 345-009	NA 355-196
Mn	16304	18139	23475	30710
Mw	111032	121460	85996	90289
Mz	351456	367904	217816	193702
Mw/Mn	6.81	6.70	3.66	2.94
Mz/Mw	3.17	3.03	2.53	2.15
Mz/Mn	21.56	20.28	9.28	6.31

Table 6.1.2 contains viscosity data and the coefficients for a log-log polynomial that was used to describe the effect of shear rate and temperature on the viscosity of the polymer.

Table 6.1.2 Viscosity characteristics of the materials used in this study.

	NA 957-000	NA 960-000	NA 345-009	NA 355-196
Melt Index	2.6	0.9	1.8	0.5
$\eta^*(100)$ poise	4100	5500	6500	10400
$\eta^*(0.1)/\eta^*(100)$	18.2	30.1	9.8	21
Viscosity Function $\ln(\eta) = A1 + A2\ln(\dot{\gamma}) + A3\ln^2(\dot{\gamma}) + A4(T-Tr) + A5(T-Tr)^2 + A6(T-Tr)\ln(\dot{\gamma})$ η in Pa*s				
A1	9.21020	8.61800	9.71720	8.89470
A2	-0.51654	-0.42649	-0.47829	-0.35783
A3	-1.10730e-2	-1.67402e-2	-1.87135e-2	-2.55079e-2
A4	-1.13981e-2	-1.73772e-2	-1.53646e-2	-1.98713e-2
A5	6.17603e-6	9.43233e-7	-6.22502e-6	-1.36558e-5
A6	8.20808e-4	1.24089e-3	1.38712e-3	1.89064e-3
Tr(°C)	180	180	180	180

Figure 6.1.4 compares the viscosity curves of the 4 polymers at 190 °C. Additional rheological data on these materials can be found in Appendix B.

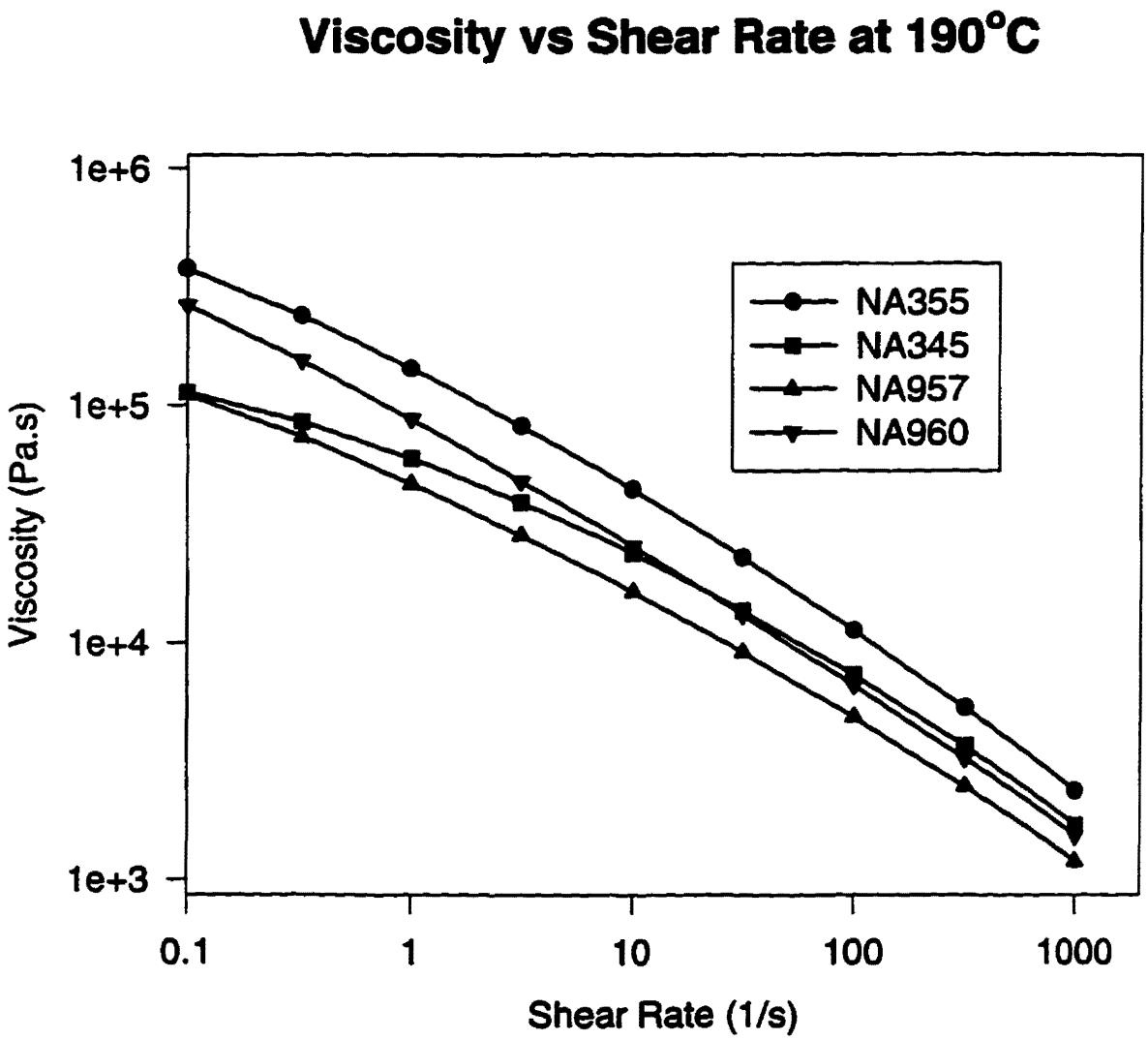


Figure 6.1.4 A comparison of the shear viscosity for the materials used in this study.

6.1.3 Experimental Procedure

Using the narrow die gap geometry, the line was started up and allowed to reach steady-state at a rate of 22.7 kg/hr and an A:B flow ratio of 20:80. The throughput rate was chosen such that the bubble stability could be maintained throughout all runs. The initial flow ratio of 20:80 was used because it showed no signs of interfacial instability. The two layers are designated as layers 'A' and 'B' as shown in Figure 6.1.1. Upon exiting the die, the coextruded annular sample was cooled with the air ring while it was pulled upward by the nips. This process necessitated finding conditions under which a stable 'bubble' could be maintained while making samples which best exhibited instabilities. It was determined that the interfacial instability was more readily observable in relatively thick (250 - 300 micron) film samples.

There were essentially 3 sets of experiments with 2 flow geometries in each set. In the first set of experiments, layer 'A' was the minor flow component while in the second and third set layer 'A' was the major flow component (i.e. A:B of 80:20). In addition, the first and second set of experiments always had the same material in both layers. Only in the third set of experiments, different materials were coextruded together. Once the line reached steady-state, a sample was collected at this flow ratio. The flow ratio was then changed to 18/82 (still maintaining the 22.7 kg/hr output) and a sample was collected. This was repeated down to a layer thickness at which the interfacial instability was clearly visible. The processing temperature was then increased and the experiment was repeated for the same material. The above procedure was repeated for all of the materials. The die gap was then changed to 6.35mm and the experiment was repeated for each material but only at one of the

temperatures used in the narrow die gap experiments.

The procedure for the second set of experiments was essentially identical to the first set but with the flows of the extruders reversed so that the B layer was the minor component. In addition, a small amount (about .5-1%) of carbon black was added to the minor component layer in order to facilitate the viewing of any instability. Finally , a similar procedure was followed for the third set of experiments in which combinations of materials were coextruded.

6.2 Observations

The results of the above experiments are summarized in Tables 6.2.1 to 6.2.6 . In the tables, 'S' is used to represent a stable interface while 'U is used to represent an unstable interface. The 'SU' has been used to denote the indeterminate transition area from stable to unstable. The subscripts 'w' and 'z' indicate that a 'wave' and/or a 'zig-zag' instability is observerved, respectively.

In these experiments, two distinct type of instabilities are observed. These have been termed 'wave' and 'zig-zag' as introduced by some previous and parallel work performed by researchers at DOW Midland on some flat dies (Ramanathan et al, 1996). The 'zig-zag' instability is of relative high frequency (estimated order of magnitude of 5-10 Hz in this experiment) and of low amplitude and has an appearance similar to the melt fracture phenomenon. Figure 6.2.1 is a photograph of a film sample having a 'zig-zag' instability. The film sample consists of a thick clear layer and a thin layer that was mixed with about 2% carbon black in order to make the instability easier to observe.

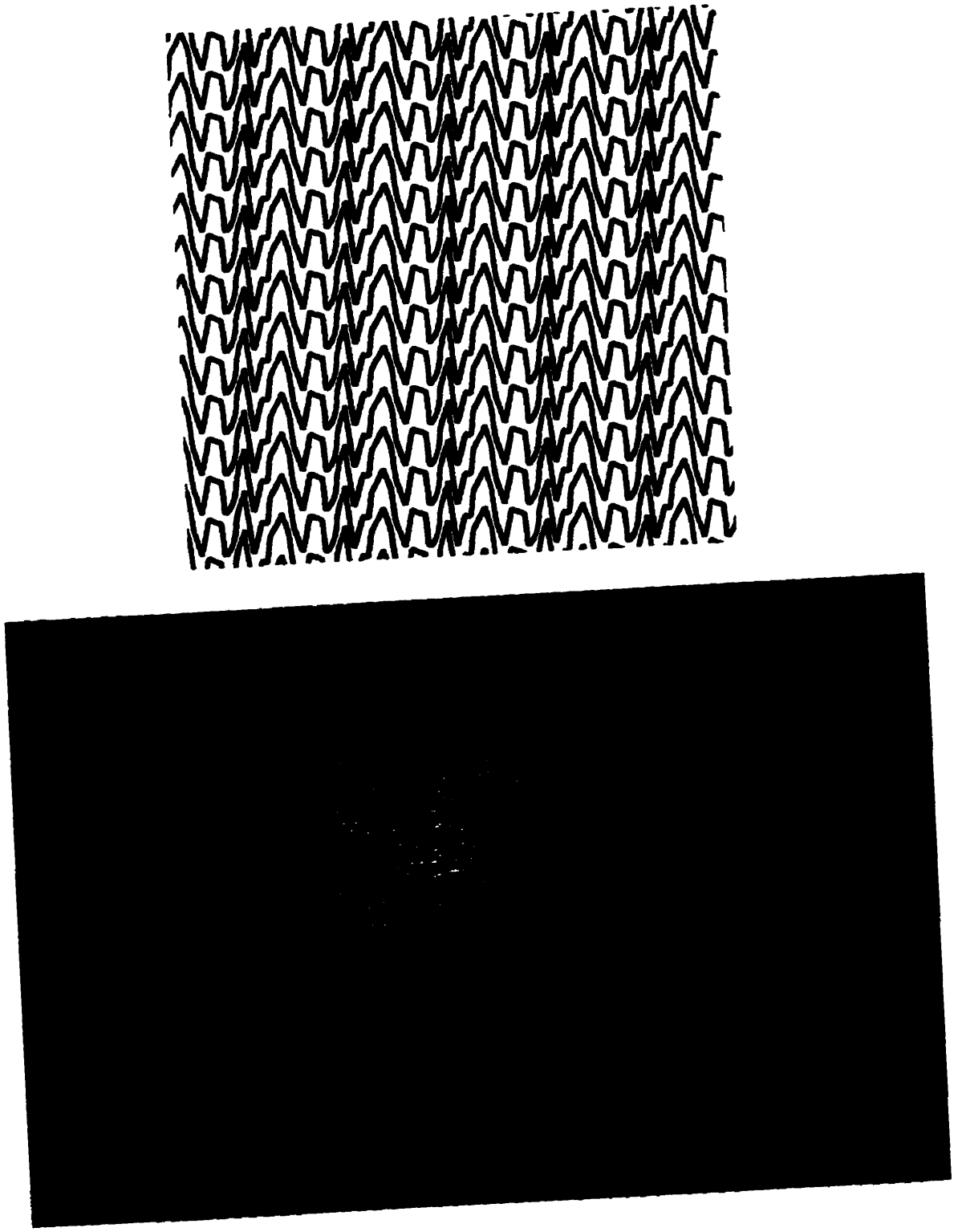


Figure 6.2.1 A photograph showing a 'zig-zag' interfacial instability.

The 'wave' instability has a much lower frequency (less than 0.2 Hz in this experiment) than the 'zig-zag' instability and a higher amplitude. Figure 6.2.2 is a photocopy of a film sample exhibiting a 'wave' instability. This is a photograph of a coextrusion of a clear layer and a layer that has been tinted with carbon black. The wave instability results in an alternating light and dark pattern. In the extreme case, the black layer exits the die as an intermittent narrow ring. Of course both the 'wave' and the 'zig-zag' instability could appear in the same sample.

Consider first the results in Tables 6.2.1 to 6.2.4 in which both layers had the same material. Tables 6.2.1 contains the observations with the 'A' layer as the minor component and the narrow die gap geometry. Table 6.2.2 contains the observations with the 'A' layer as the minor component and the wide die gap geometry. Tables 6.2.3 and 6.2.4 contain the observations with the 'A' layer as the major component and the narrow and wide gaps, respectively. All of the materials showed a 'zig-zag' interfacial instability when using the narrow die gap geometry although not at the same flow rate conditions. When the larger die gap was used, the 'zig-zag' interfacial instability was eliminated for all of the flow ratios used in this experiment. However, the wave instability was now easier to observe in some of the samples.



Figure 6.2.2 A photograph of a film sample exhibiting a 'wave' type instability.

Table 6.2.1 Single material coextrusion experiment with minor flow in 'A' and narrow gap

	Narrow Die Gap (1.52mm)							
Material	NA957 / NA957		NA960 / NA960		NA345 / NA345		NA355 / NA355	
Temp (°C) / Minor Layer %	188	204	198	216	188	198	198	216
2	Uw,z						Uw,z	
4	Uw,z	Uw,z	Uw,z	Uw,z	Uw,z	Uz	Uw,z	Uw,z
6	Uw,z	Uz	Uw,z	Uw,z	Uw,z	SU	Uw,z	Uz
8	SU	SU	Uw,z	Uw,z	SU	S	Uz	SU
10	S	S	SU	SU	S	S	SU	S
12	S	S	S	S	S	S	S	S
14	S	S	S	S	S	S	S	S
16	S	S	S	S	S		S	

Table 6.2.2 Single material coextrusion experiment with minor flow in 'A' and wide gap.

	Wide Die Gap (6.35 mm)			
Material	NA957 / NA957	NA960 / NA960	NA345 / NA345	NA355 / NA355
Temp (°C) / Minor Layer %	188	198	188	216
2		Uw	S	SUw
4	Uw	Uw	S	S
6	SU	Uw	S	S
8	S	SU	S	S
10	S	S	S	S
12	S	S	S	S
14		S	S	S
16			S	

Table 6.2.3 Single material coextrusion experiment with minor flow in 'B' and narrow gap

	Narrow Die Gap (1.52mm)				
Material	NA957 / NA957	NA960 / NA960	NA345 / NA345	NA355 / NA355	
Temp (°C) / Minor Layer %	188	198	188	198	204
2					
4			Uw,z	Uw,z	Uw,z
6	Uw,z	Uw,z	Uw,z	Uw,z	SU
8	Uw,z	Uw,z	SU	Uz	S
10	SU	Uw,z	S	SU	S
12	S	SU	S	S	S
14	S	S	S	S	S
16	S	S	S	S	

Table 6.2.4 Single material coextrusion experiment with minor flow in 'B' and wide gap

	Wide Die Gap (6.35 mm) second experiment			
Material	NA957 / NA957	NA960 / NA960	NA345 / NA345	NA355 / NA355
Temp (° C) / Minor Layer %	188	198	188	210
2				
4	Uw		S	SU
6	SU	Uw	S	S
8	S	Uw	S	S
10	S	SU	S	S
12	S	S	S	S
14		S	S	S
16			S	

Table 6.2.5 Two material coextrusion experiment with minor flow in 'B' and narrow gap

	Narrow Die Gap (1.52 mm)					
Mat1/Mat2/ Temp	NA957 / NA355	NA957 / NA960	NA960 / NA355	NA960 / NA345	NA345 / NA960	NA355 / NA960
Temp (° C) / Minor Layer %	198	198	198	198	188	198
4						S
6		Uw,z		U,z	Uw	S
8		Uw,z	Uw,z	U,z	Uw	S
10	Uw	Uw,z	Uw,z	SU	SU	S
12	SU	SU	Uw,z	S	S	S
14	S	S	Uw	S	S	S
16	S	S	SU		S	

Table 6.2.6 Two material coextrusion experiment with minor flow in 'B' and wide gap

	Wide Die Gap (6.35 mm)			
Material	NA957 / NA960	NA960 / NA355	NA345 / NA960	NA957 / NA355
Temp(° C) / Minor Layer %	198	198	188	198
6			Uw	
8	Uw		Uw	
10	Uw	Uw	SU	Uw
12	Uw	Uw	S	Uw
14	SU	SU	S	SU
16	S	S		S

More specifically, all interfacial instabilities were essentially eliminated for the NA345 and NA355 materials with the exception of the condition when the minor, NA355, layer is very thin. With the NA957 and NA960 materials, increasing the die gap had only a small effect on the layer ratio for which the interfacial instability appeared. Another interesting observation is that the interfacial instabilities (particularly the wave instability) occurred at approximately the same flow ratio in the first and second set of experiments. The geometry of the channels was originally designed for the B layer to be the minor component. In this mode of operation, the velocities of the materials prior to and after combining were assumed to be better matched. It was rather surprising to see that operating the system in the reverse condition affected marginally the layer ratio at which the instability was observed.

Tables 6.2.5 and 6.2.6 contain the observations for the experiments in which different materials were coextruded together with the narrow and wide die gaps, respectively. In these experiments similar results were obtained in that the 'zig-zag' instability was not observed with the wide die gap geometry (Table 6.2.6). The layer ratio at which the interfacial instability was observed was dependent on the materials in each layer. For certain combinations, there was no observable interfacial instability for any flow ratio while other combinations showed flow instabilities at relatively high flows of the minor component when compared with the previous set of experiments. In fact some instabilities were so severe that the bubble could not be properly stabilized.

One of the most interesting observations in this set of experiments was made when the NA960 was coextruded with the NA345 (columns 5 and 6 in Table 6.2.5). When the NA345 was the minor component, it exhibited a 'zig-zag' instability at about 8 - 10 % but

no 'wave'instability. However, when the NA960 was the minor component, only a 'wave' instability was observed starting at about the same flow ratio. This would support the theory that the two instabilities are somewhat independent of each other and should be investigated accordingly.

6.3 Analysis and Simulations

The experiments were simulated using the commercially available software packages LAYERCAD and POLYCAD 2D. This provided an estimate of the position of the interface and also its development. Computer simulations can also provide estimates of other difficult to measure variables such as the interfacial stress which may be correlated to the phenomenon of interfacial instability. Figure 6.3.1 shows the Finite Element Method (FEM) calculation of the shear stress along a stream line using material NA 957 at a temperature of 188°C and a flow ratio of 10/90. The line within the flow field represents a streamline at the interface. As it can be seen, the shear stress at the interface initial drops as the materials combine and then increases to the first plateau at about 10 kPa. The stress increases as the material goes through the converging channel to the narrow die gap and reaches a higher plateau (about 45 kPa) at the exit land. The critical shear stress theory assumes that an interfacial instability will occur if the stress at the interface exceeds a critical value. It is believed that the value of the critical shear stress will depend on the polymers that are being coextruded.

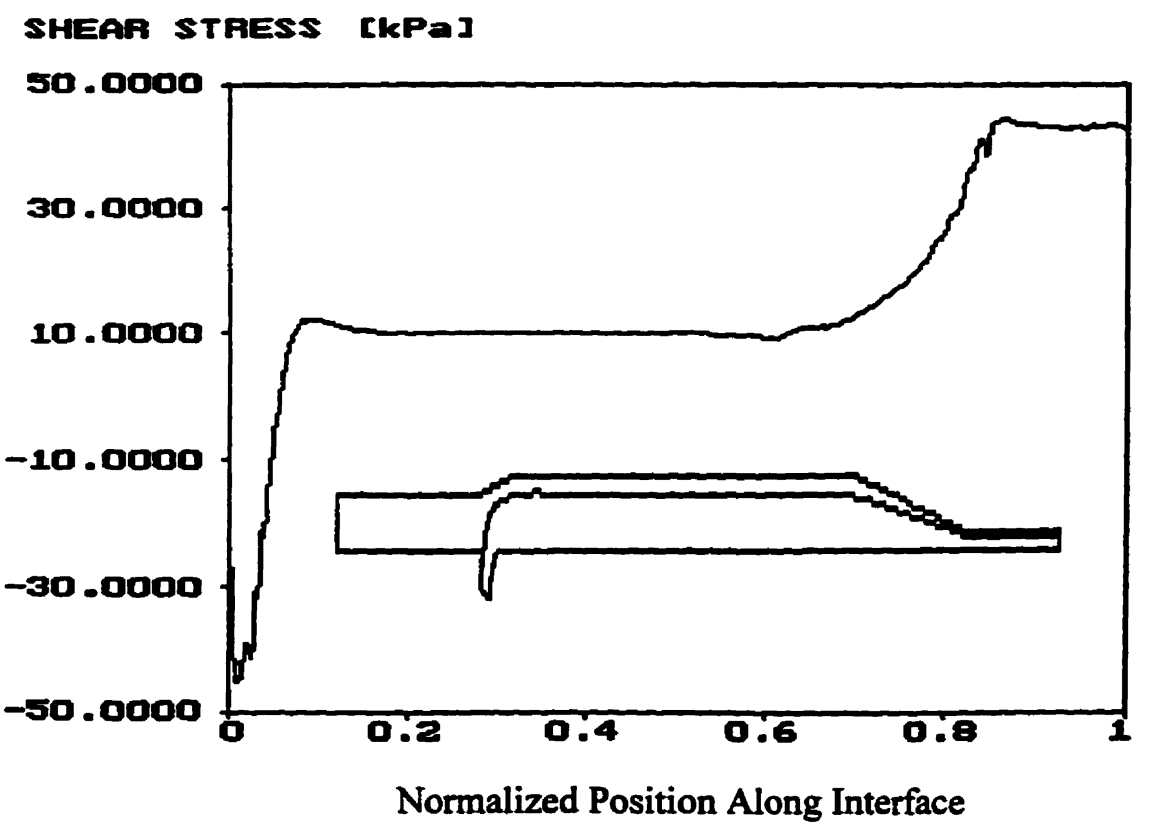


Figure 6.3.1 Shear stress along the interface for a 10/90 ratio of NA957.

Figures 6.3.2 is a plot of the interfacial shear stress versus the layer ratio profile for the broad MWD materials at the flow rates and temperatures of the narrow gap experiment for each polymer. The dashed line indicates the layer ratio range where interfacial instability was observed to form. Figure 6.3.2 indicates that the appearance of an interfacial instability is not a strong function of temperature, and hence shear stress, but is more related to the layer ratio. Figure 6.3.3 is a similar plot for the narrow MWD materials. In contrast to Figure 6.3.2, it shows that the interfacial instability appears at similar shear stress values for each polymer. At both temperatures, the 'zig-zag' instability appeared at about 70 kPa and 80 kPa for the NA345 and NA355 respectively. The relationship between the 'zig-zag' instability and shear stress is further supported by the wide die gap geometry experiment where the high stress area at the exit had been eliminated. Recall from Tables 6.2.1 to 6.2.4 that the broad MWD materials continued to exhibit an interfacial instability at about the same layer ratios while the interfacial instability essentially disappeared for the narrow MWD materials.

The above results would indicate that altering the die geometry (increasing the die gap) or the processing conditions (increasing the melt temperature) would be viable solutions when an interfacial instability is observed with relatively narrow MWD materials. For broad MWD materials, the only viable solution would be to increase the thickness of the thin layer until the interfacial instability disappears or possibly change the material in the thin layer.

The observations made during these experiments would confirm that the 'zig-zag' interfacial instability is in fact due to high interfacial stress. However, the fact that a 'wave' instability is observed once this high stress is removed may indicate that the origin of the

'zig-zag' instability may be related to the 'wave' instability. If a wave instability is present in the flow field, then the interface position is oscillating perpendicular to the flow direction. This means that the stress level at the interface is oscillating as the interface moves towards and away from the wall. This would appear as an intermittent 'zig-zag' instability in the film samples. This was in fact observed in some of the samples.

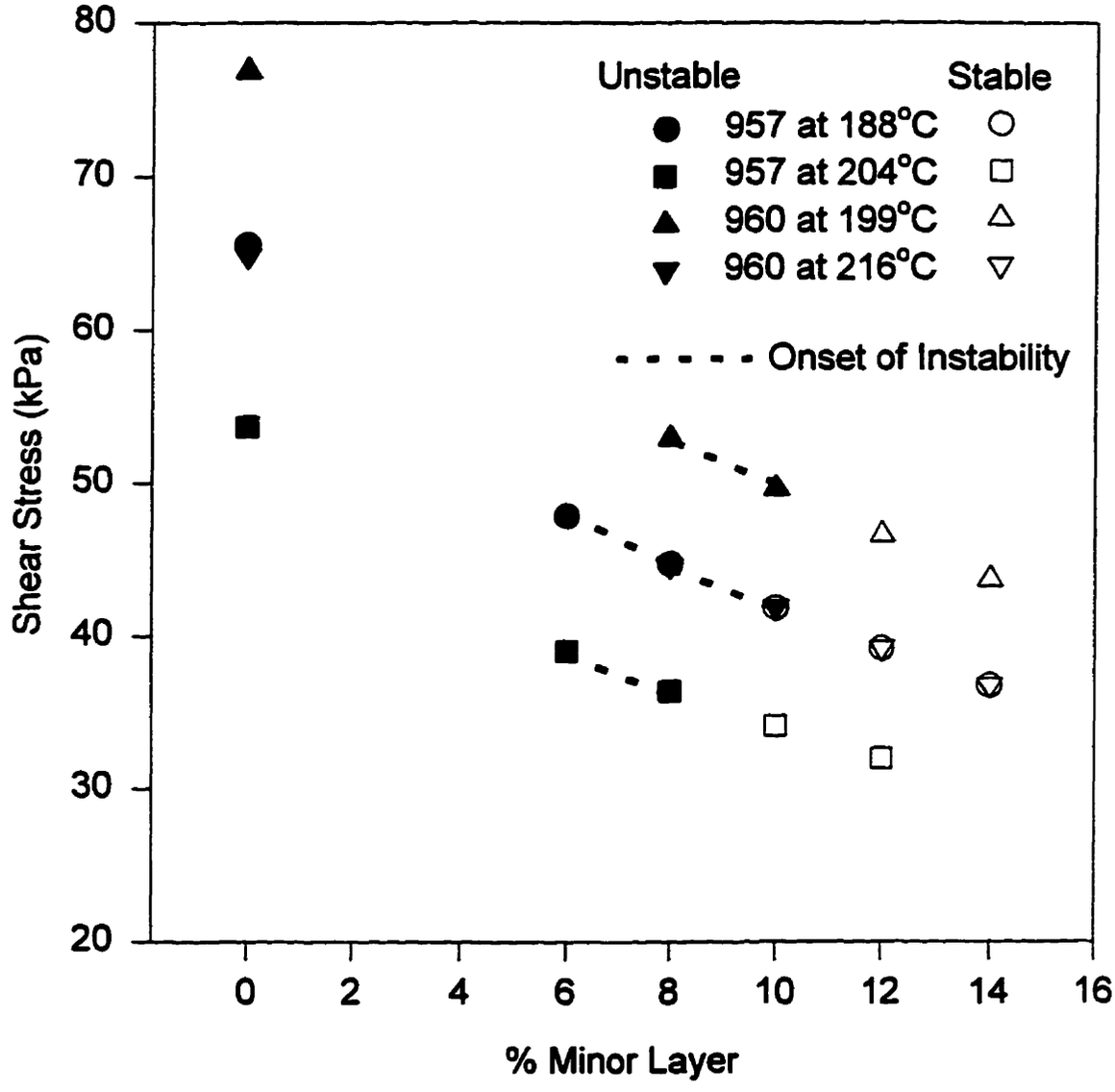


Figure 6.3.2 Exit shear stress versus layer ratio for broad MWD materials.

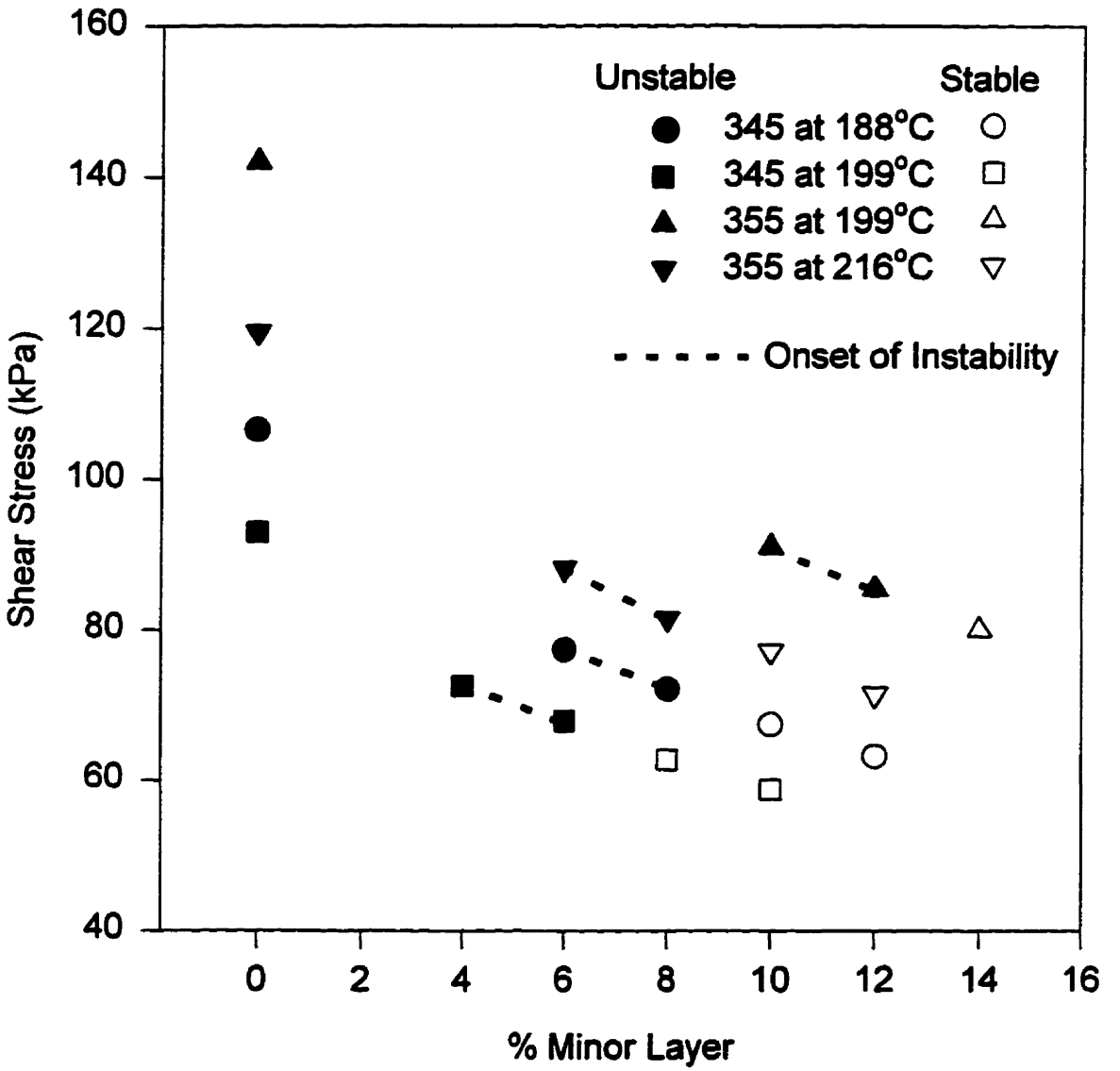


Figure 6.3.3 Exit shear stress versus layer ratio for narrow MWD materials

The observations also suggest that the 'wave' type of interfacial instability occurs when the interface moves closer to the wall (or the layer gets thinner), however, there is still no explanation as to the reason for the interface to go unstable. What is the driving force? It stands to reason that the initial perturbation to the flow field must occur at the merge point of the two layers. This area was investigated in more detail using a 2-D finite element method analysis. Figures 6.3.4 and 6.3.5 show the velocity contours and streamlines, respectively, at the merge point using NA960 with a 12% 'A' layer and a 88% 'B' layer. The velocity contour (Figure 6.3.4) shows the relatively high velocity of the 'B' layer material prior to combining. Figures 6.3.6 and 6.3.7 are the corresponding results for an 8% 'A' layer and a 92% 'B' layer. As the throughput rate of the 'A' layer is reduced and the 'B' layer is increased, the streamlines follow more abrupt changes. In fact a small vortex begins to appear on the left side of the 'B' layer at the merge point. Similar simulations were made representing the second set of experiments in which the 'B' layer was the minor component. Figures 6.3.8 and 6.3.9 show velocity contours and streamlines, respectively, for a 12% 'B' layer and a 88% 'A' layer. Figures 6.3.10 and 6.3.11 are the corresponding Figures for a 8% 'B' layer and a 92% 'A' layer. Despite the fact that the velocity contours and streamlines appear to be better under these conditions, an interfacial instability was observed. In fact, the 'wave' type of interfacial instability was observed at almost the same flow ratio under both conditions.

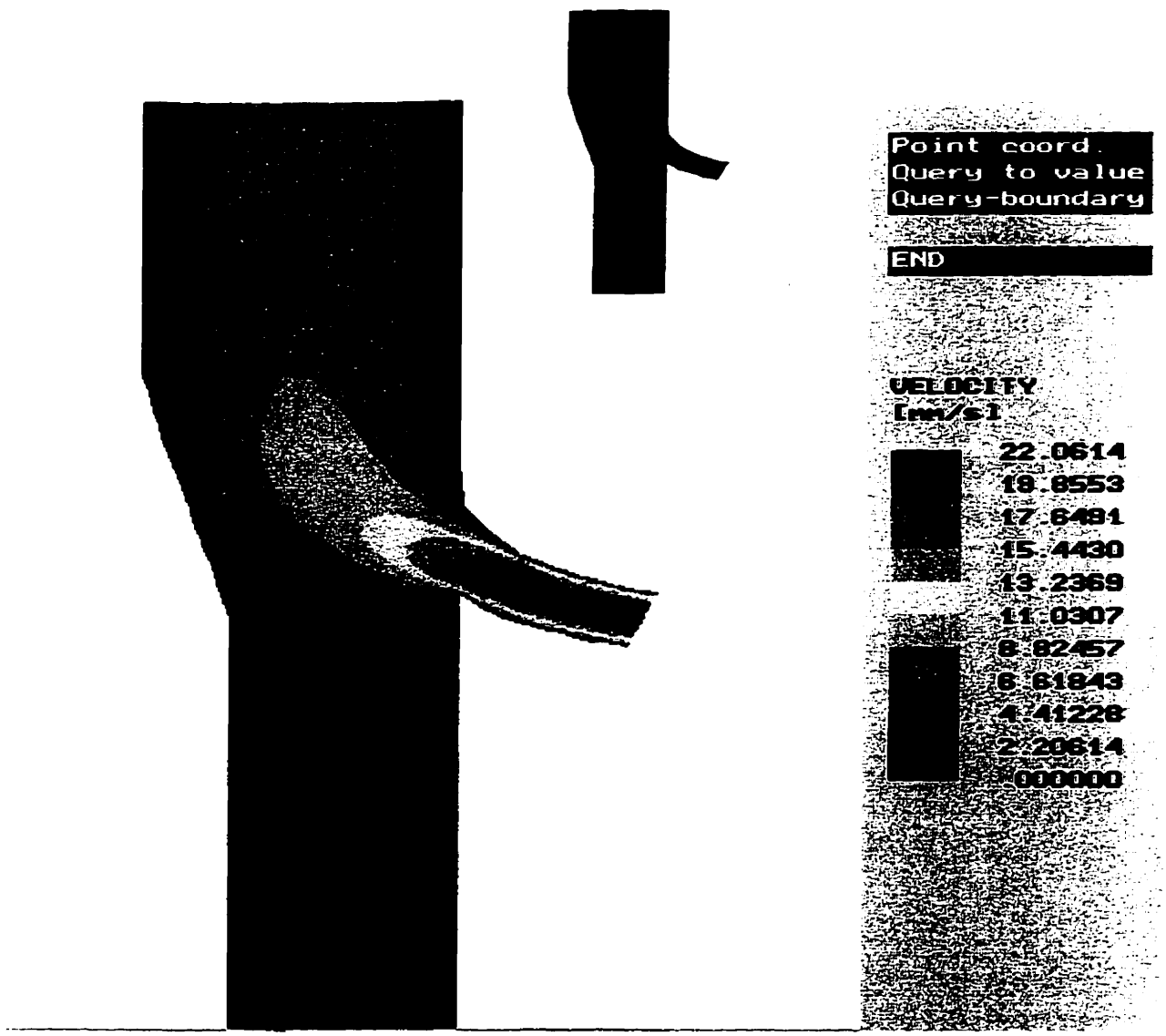


Figure 6.3.4 Velocity contours for an A:B ratio of 12:88 for NA960 in both layers.

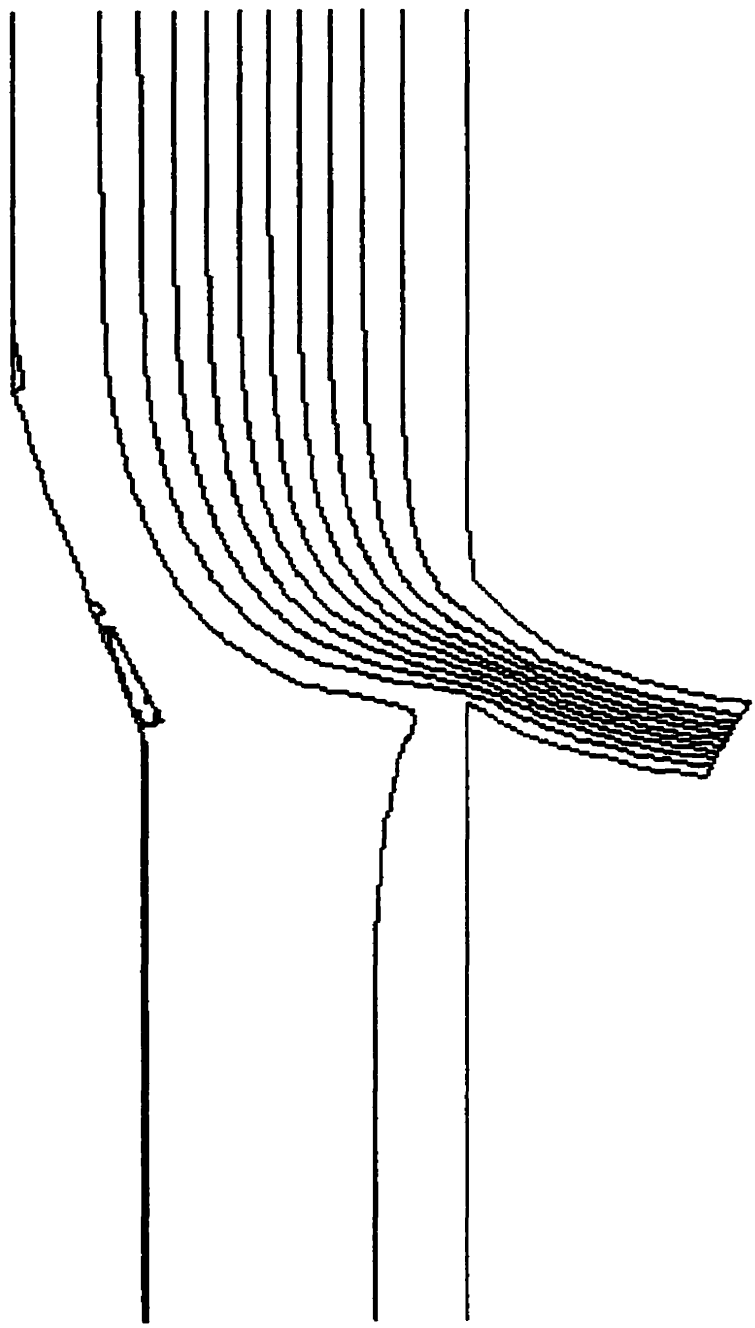


Figure 6.3.5 Streamlines for an A:B ratio of 12:88 for NA960 in both layers.

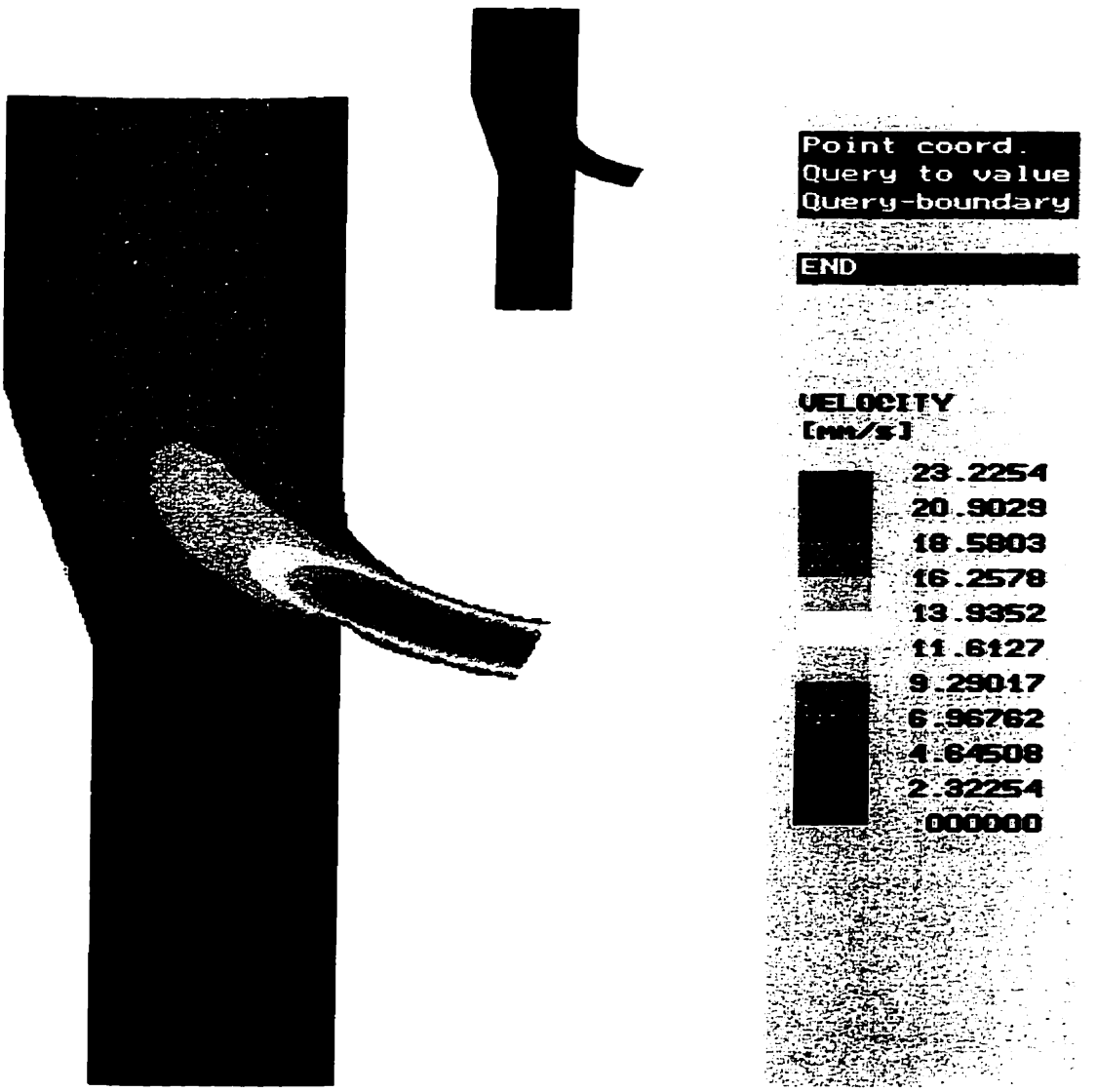


Figure 6.3.6 Velocity contours for an A:B ratio of 8:92 for NA960 in both layers.

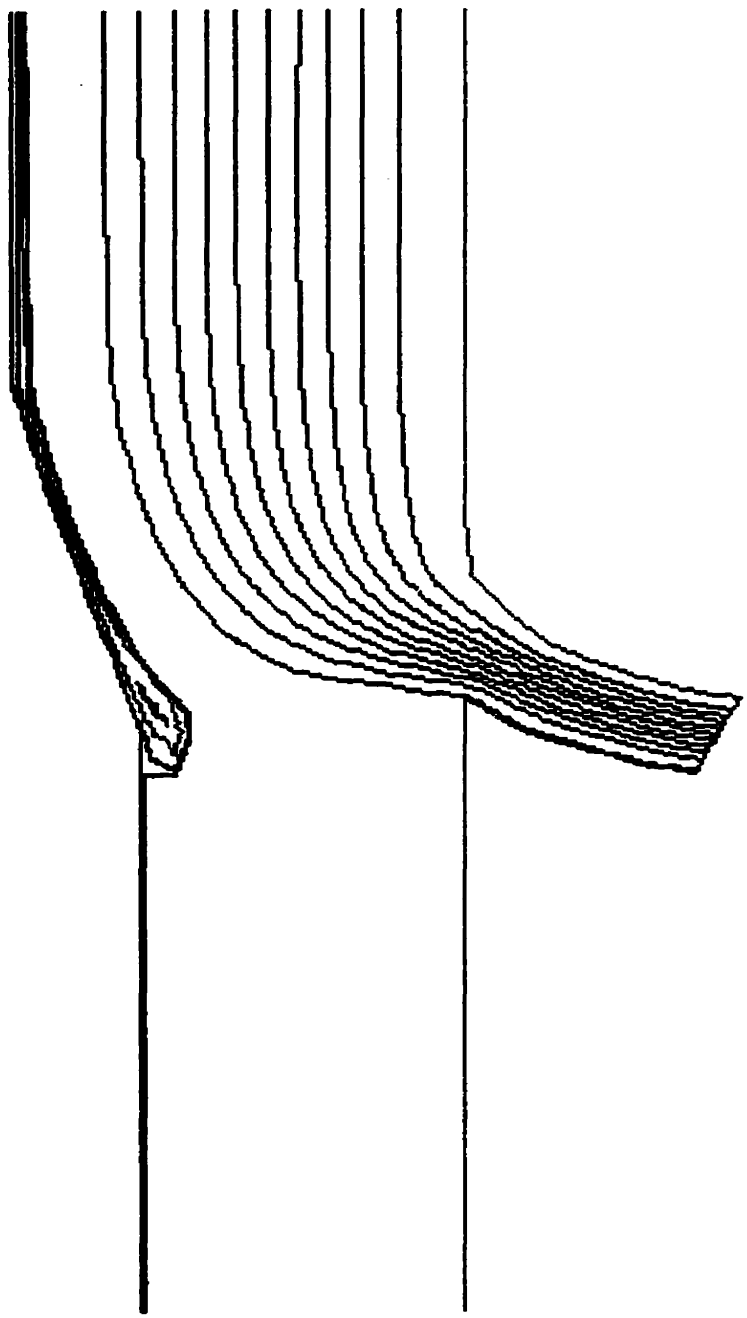


Figure 6.3.7 Streamlines for an A:B ratio of 8:92 for NA960 in both layers.

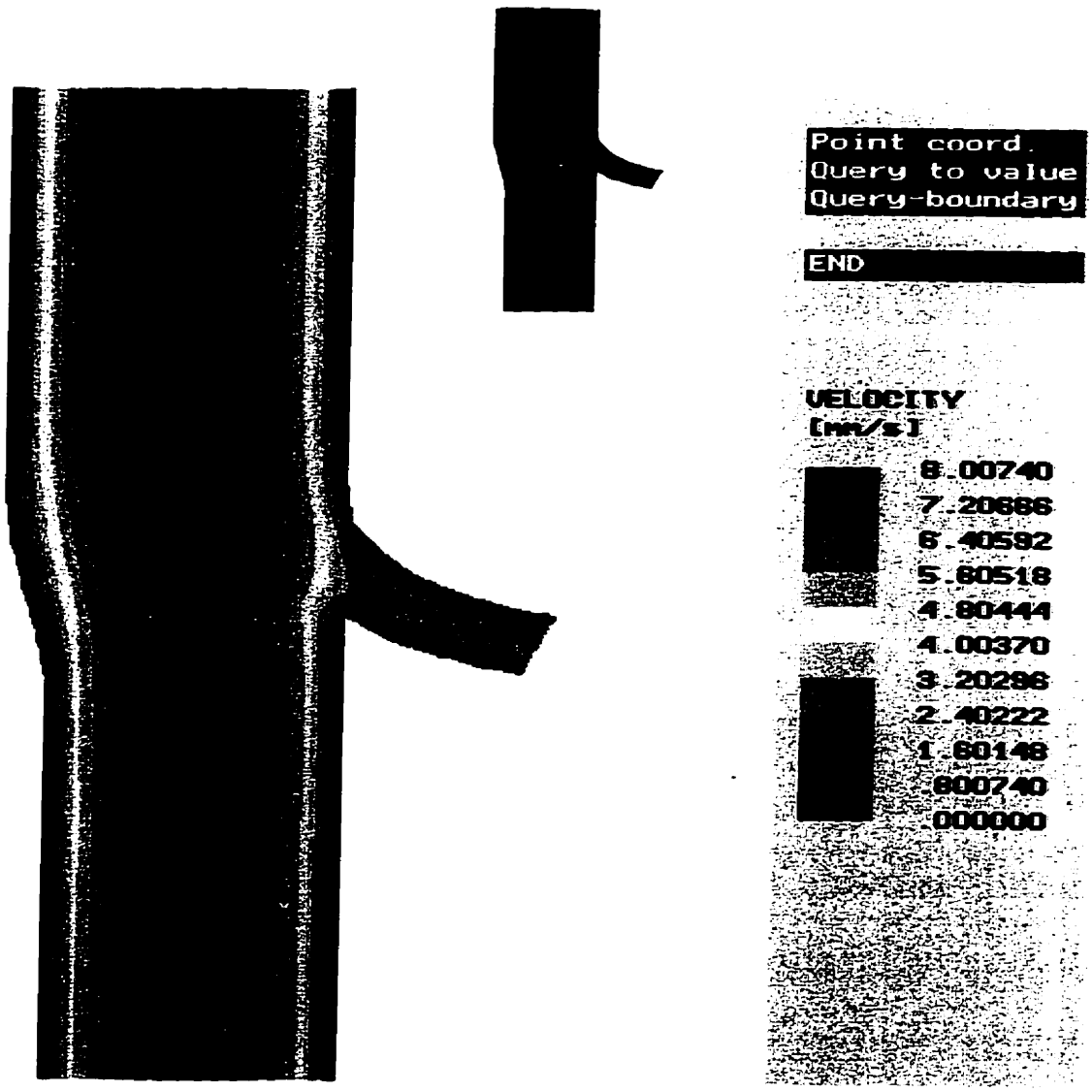


Figure 6.3.8 Velocity contours for an A:B ratio of 88:12 for NA960 in both layers

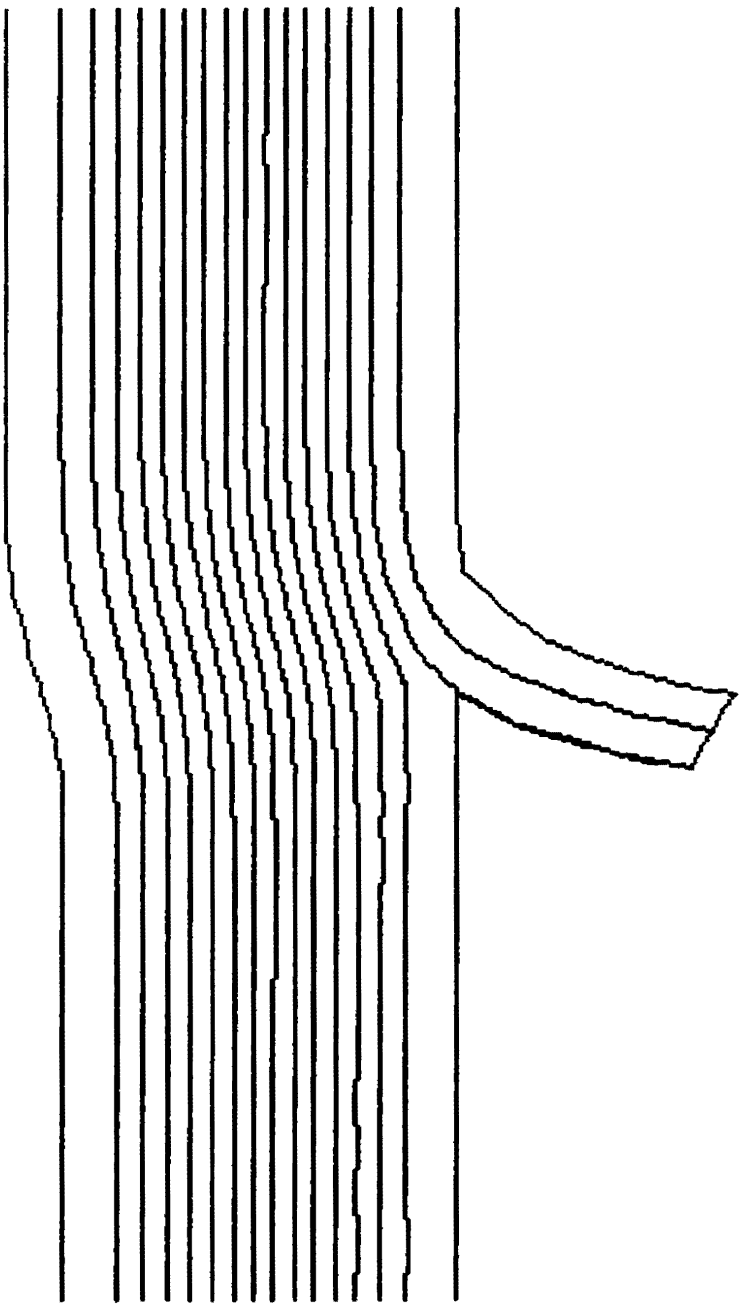


Figure 6.3.9 Streamlines for an A:B ratio of 88:12 for NA960 in both layers

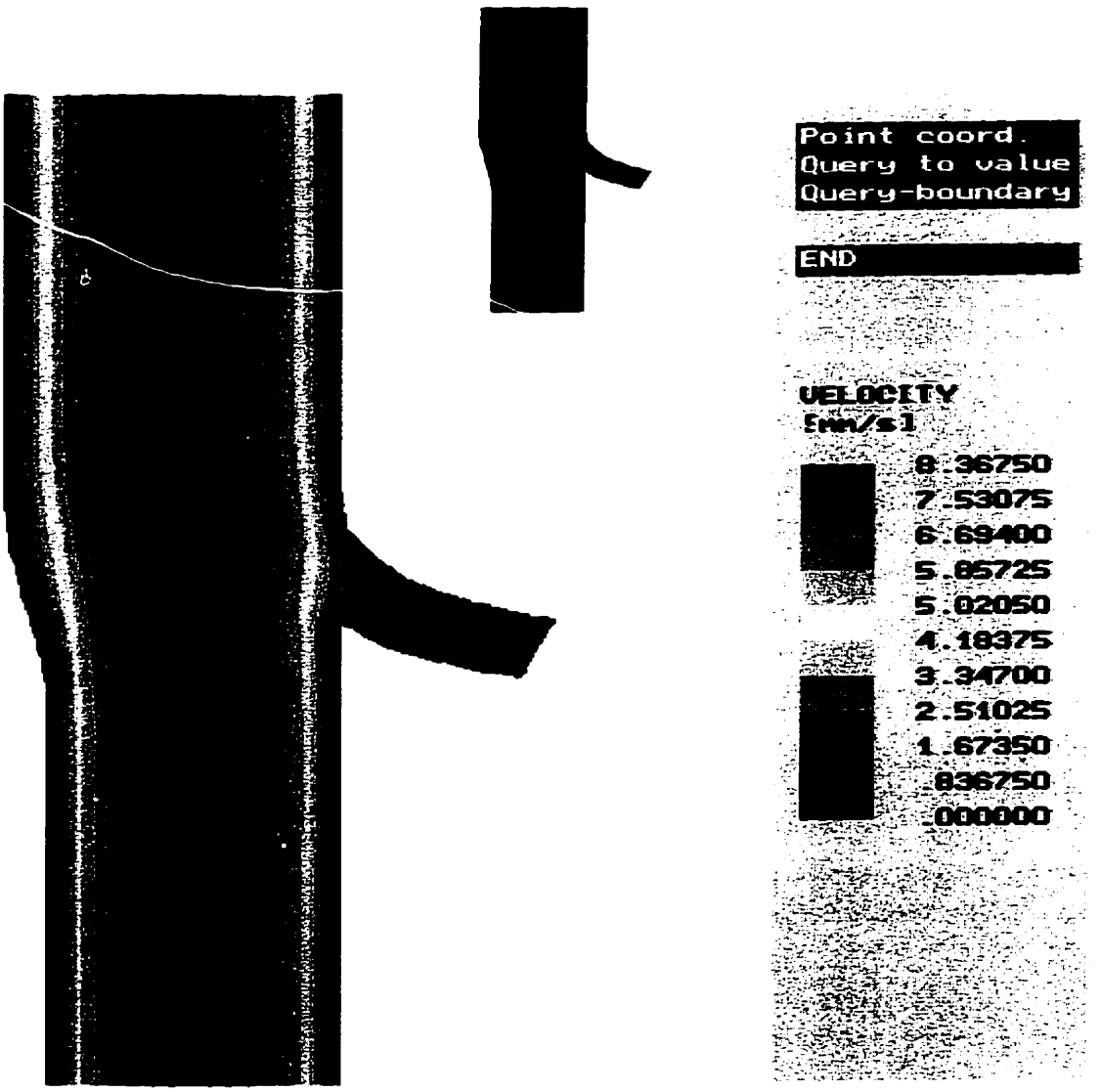


Figure 6.3.10 Velocity contours for an A:B ratio of 92:8 for NA960 in both layers

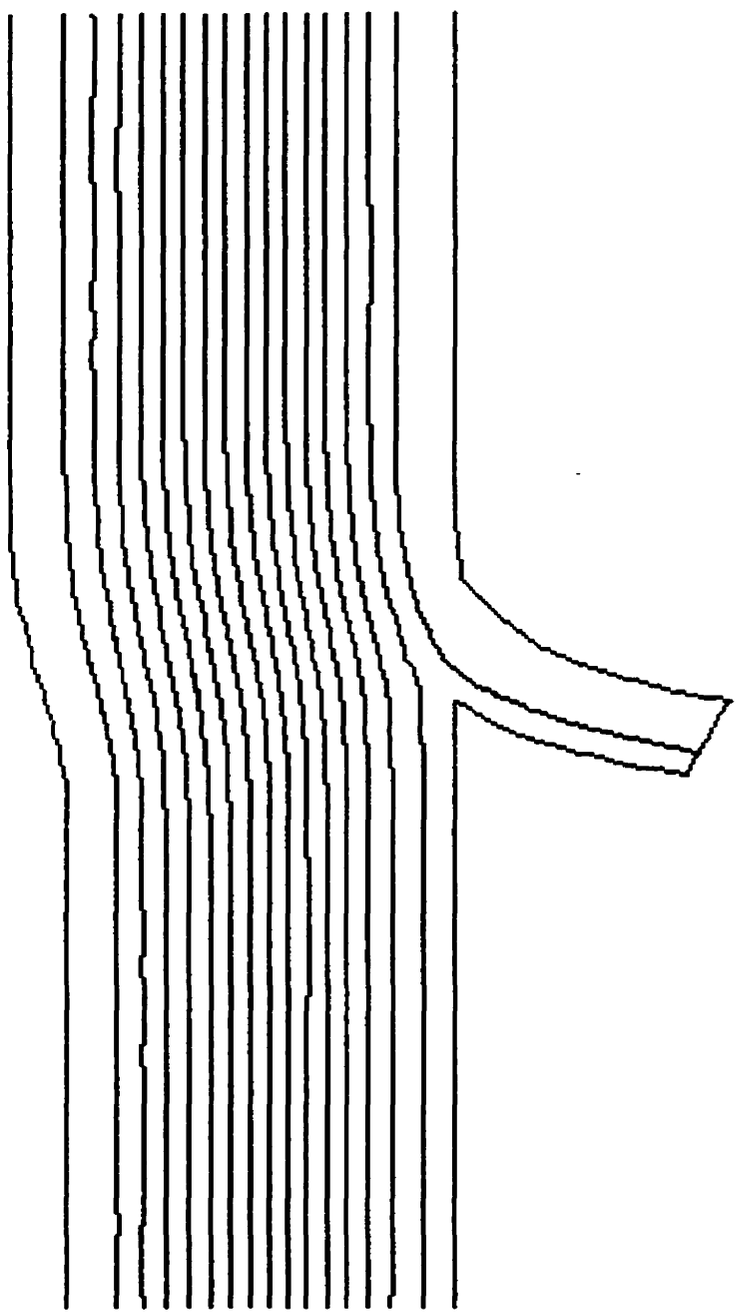


Figure 6.3.11 Streamlines for an A:B ratio of 92:8 for NA960 in both layers

Since the observations also indicate that the 'wave' type interfacial instability occurs more readily in broad MWD materials, and these materials tend to exhibit stronger elastic behaviour, it stands to reason that the 'wave' instability is strongly influenced by the elastic properties of the materials. However, since the extrusion of the same materials results in an instability, it is unlikely that the instability is due to elastic differences in the materials as some researchers have suggested. It is more likely that the instability is due to the total deformation of the flow stream. This was investigated by comparing the average velocity of the individual layers before and after combining. A velocity ratio was calculated as follows:

$$Velocity\ Ratio = \frac{Average\ Layer\ Velocity\ Prior\ To\ Combining}{Average\ Layer\ Velocity\ after\ Combining} \qquad (6.3.1)$$

This was determined for the various flow rate ratios used in the experiments and is plotted in Figures 6.3.12 and 6.3.13. Figure 6.3.12 relates to the first set of experiments where the large channel (A) transported the minor component while Figure 6.3.13 represents the experiment in which the large channel (A) transported the major component. In both figures the same material, NA960, is used in each layer. The graphs shows that the velocity ratio of the minor component increases dramatically as the percentage of the minor component gets smaller. In other words, the acceleration of the minor layer ,at the merge point, increases as the layer becomes thinner.

However, there is a marked difference in velocity ratio at which the interfacial instability occurs for the first two sets of experiments. This difference is believed to be due to the orientation of the minor layer. In the first set of experiments the minor layer is always

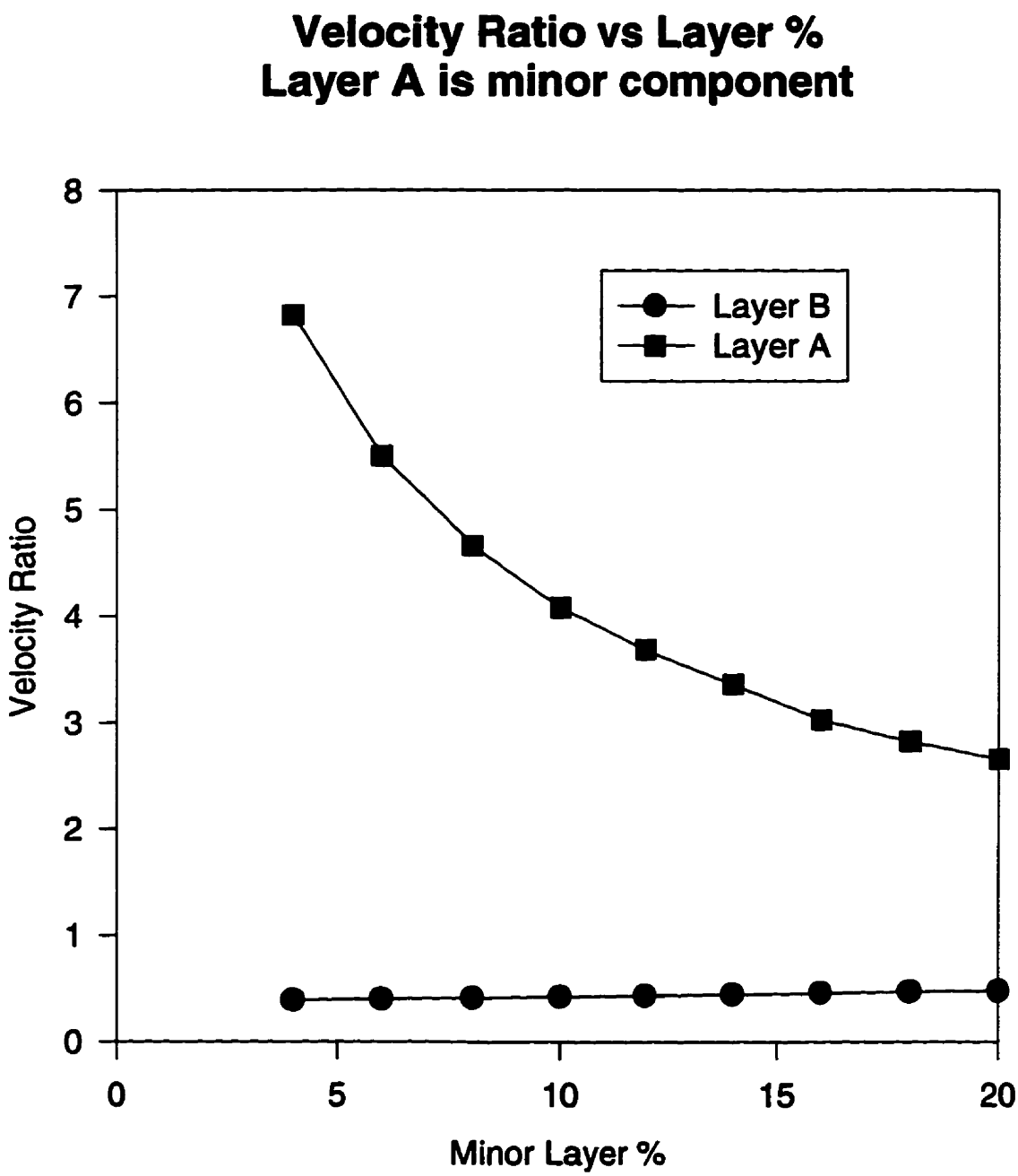


Figure 6.3.12 Velocity ratio versus layer ratio with A as the minor layer.

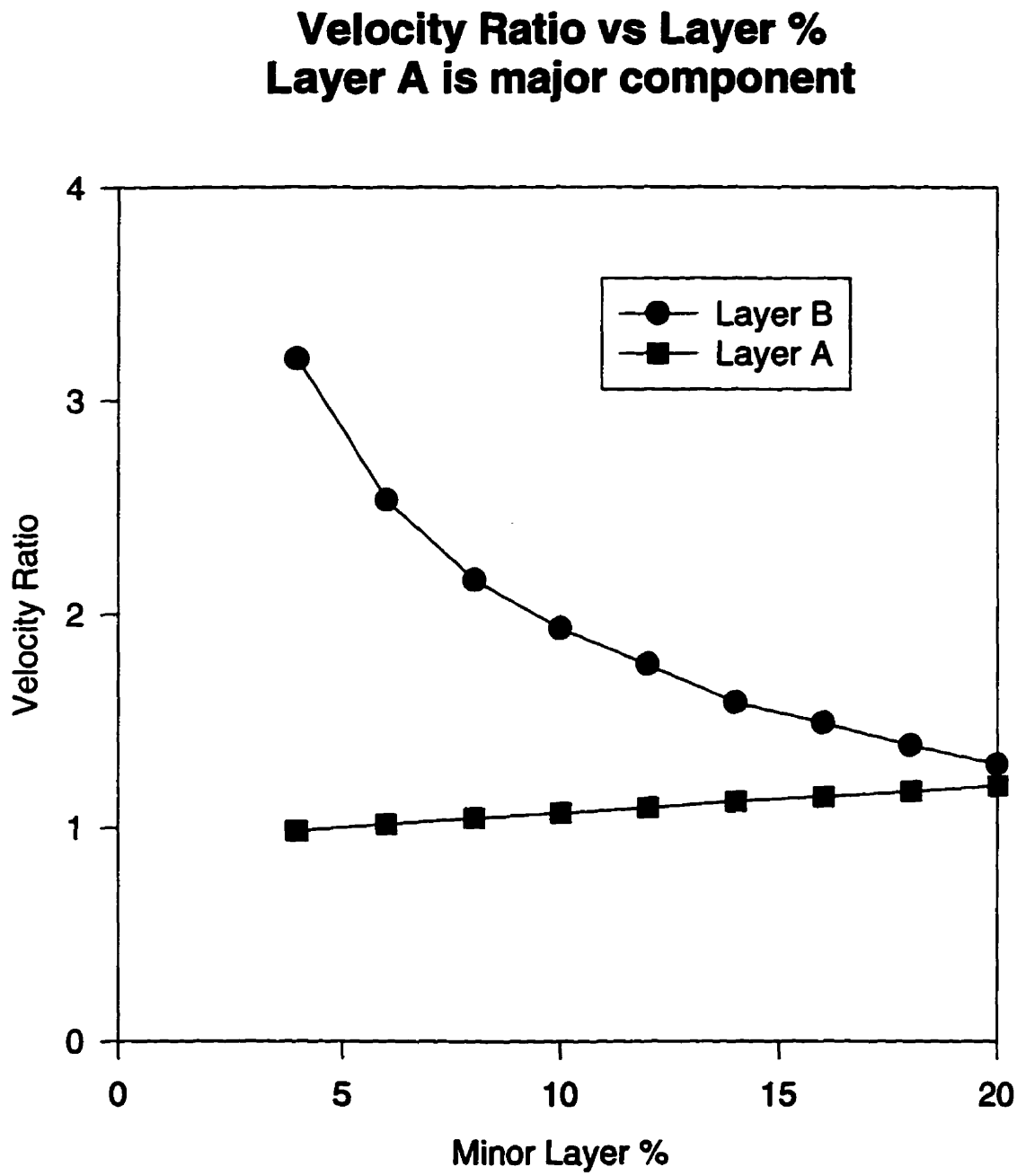


Figure 6.3.13 Velocity ratio versus layer ratio with A as the major layer.

moving in the axial direction while in the second set of experiments, the minor layer is forced to turn from the radial direction to the axial direction. This results in an additional acceleration effect that is not accounted for in the simple calculation presented above. Regardless of the actual values, the minor layer does experience an increased acceleration or elongation as it becomes thinner. It is speculated that this acceleration (or elongation rate) combined with the visco-elastic behaviour of the material is the source of the 'wave' instability.

Figure 6.3.14 compares the elongational viscosity of the materials used in this experiment a 190°C. These are estimated by the method developed by Cogswell (1972) and clearly show a difference among the materials. Furthermore, the broad molecular weight materials (NA960 and NA957) show a gradual increase and a sharp decrease while the narrow molecular weight materials (NA355 and NA345) exhibit a more rounded maximum. Now consider the increasing portion (to the left of the maximum) of the elongational viscosity curve for each material. As the elongation rate increases, so does the resistance to elongation. This elongational viscosity difference appears to be a more likely explanation for the occurrence of the interfacial instability during coextrusion including the case where both layers are the same material. If the material is elongated too much at the merge point it will try and resist this deformation once it joins the other material. Whether it succeeds or not will depend on the relative viscoelastic properties of each stream. If the major layer has a higher resistance to deformation than the minor layer, then the flow field will be more stable than if the reverse situation were to exist.

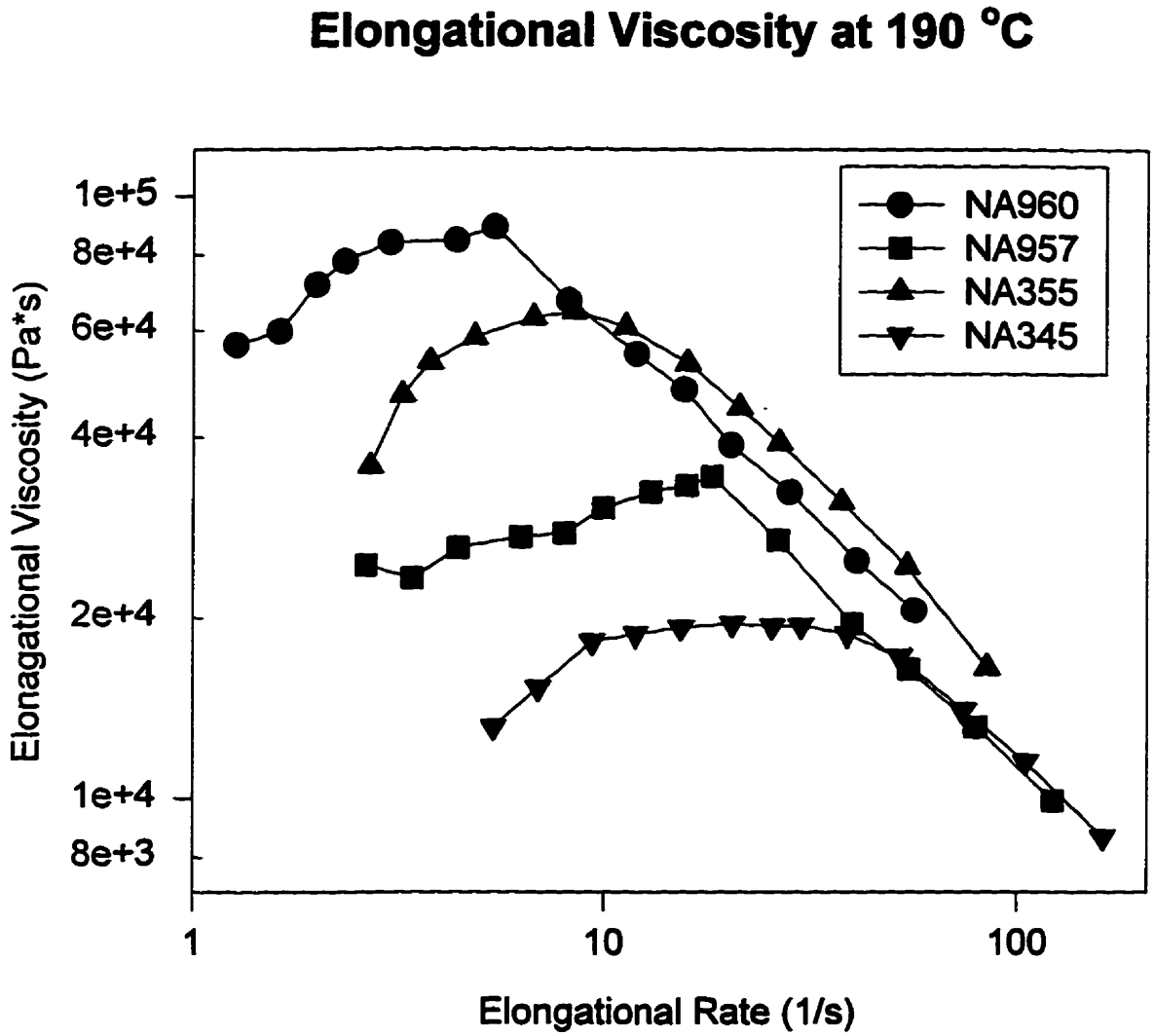


Figure 6.3.14 A comparison of the elongational viscosity of the materials used in this study.

6.4 Discussion

The experiments performed in this study indicate that broad MWD materials have a greater tendency to exhibit interfacial instability and that these interfacial instabilities are more due to layer ratio than processing conditions or die geometries. In contrast, materials with narrower MWDs tend to exhibit an interfacial instability which appears to be related to the stress at the interface and, hence, can be affected by whatever affects the interfacial stress. This would include increasing the melt temperature, increasing the die gap or reducing the flow rate. The broad MWD materials also exhibit an interfacial instability that appears to be caused during the merging of the layers.

Wilson and Komami's (1993) results only consider the wave instability but assume that the instability is initiated by a periodic variation in the flow field (such as the extruder screw rpm) and the material combination determines whether the instability is dampened or amplified. Furthermore, they did not study the effect using the same material in both layers. While the choice of materials and flow conditions may dampen or amplify the effect, it is unlikely that the initiation is due to an external source. This is deduced by the fact that the frequency of the instability increased while the rpm of the screw decreased.

Ramanathan et al(1996) have concluded that the wave instability begins in the area where the materials combine but they attempt to correlate the instability to an elasticity ratio and a critical skew. The skew is basically defined as the layer thickness ratio with an equal layer thickness having a skew of 1.0. The problem with this approach is that it does not explain the observation of interfacial instability with the same materials. On the other hand,

the results, presented here, are quite complementary to the research performed by Ramanathan et al(1996) in that similar observations are made in two types of extrusion processes with different materials.

The results obtained here would suggest that the wave interfacial instability should be correlated to both the shear viscosity and the elongational viscosity ratios of the materials being coextruded. The velocity ratio analysis presented in section 6.3 clearly showed that each layer may undergo a different deformation depending on the flow rate ratios and the geometry of the flow field. Since the shear viscosity and the elongational viscosity depend on the shear rate and elongation rate, respectively, each layer will behave somewhat differently. This provides a possible explanation for the observation of an instability during the coextrusion of the same material in each layer. However, due to the periodic nature of the instability, any theoretical analysis would need to account for this transient behaviour. Past studies have attempted to do this by assuming that one of the layers has a periodic flow variation but there does not appear to be a physical explanation for this variation. Mathematical modelling of this phenomenon should use models in which the elastic behaviour of the materials, coupled with the deformation that they undergo when they combine can result in a periodic interface position. It is believed that this will lead to the development models that can be used to predict this phenomenon during the design of the extrusion dies.

CHAPTER 7

CONCLUDING REMARKS and RECOMMENDATIONS

7.1 Die Design

The main objective of this work was to obtain a better understanding of the fundamental requirements of a blown film extrusion die and apply this knowledge towards the creation of an improved design. This section will summarize how the results of this study are applied from an engineering viewpoint.

The analysis of the conventional style of coextrusion die used in the tubular film process has led to the development of a new style of die with distinct advantages. First, the new design has reduced the wetted surface area of the polymer flow channels, thereby, reducing the potential for degradation. This benefit has been confirmed by other designers of commercial coextrusion dies who have also proposed improvements to the design presented here (Mavridis, 1996). Reducing the wetted surface area also reduces the pressure requirements of the die providing the designer with a little more flexibility in the design process. The designer does not have to compromise the minimum velocity criterion in order to satisfy the maximum pressure limitations of the system.

The construction of the die is also much simpler than that of the conventional systems in that each layer now consists of 2 plates that combine to form an individual module. The flow channels are machined on the surface of these disks with large radius

turns rather than drilled holes that are commonly used in conventional dies. This has significant advantages from a maintenance standpoint. When cleaning the die, the modular construction allows for the disassembly of one layer at a time. Once the two pieces that form the module are separated, all of the flow passages are completely visible and accessible for easy cleaning. On the conventional dies, it is very difficult to clean out any drilled passages or even the cylindrical surfaces for that matter.

Of course these benefits are obtained with essentially any stacked type of die including those shown in patents of the late 50's. However, the application of the stacked type of die design to the tubular film process has been hampered by the inadequate polymer distribution systems of the past. The fundamental problem was to create a uniform annular flow from a stream of polymer entering the die from one side (a side fed die). This was the purpose of the distribution systems designed and tested in Chapter 4. The new flat spiral system maintains the homogenizing advantages of the standard spiral mandrel concept while providing the mechanical construction benefits of a side fed system.

One of the milestones in making the system work was the development of an accurate modelling technique. The Control Volume Method of modelling the flow provided an accurate prediction of the final flow distribution and a means of calculating the pressure requirements of the die. A uniform flow distribution is probably the single most important function of an annular die. This is especially true in multi-layer barrier applications which require a relatively expensive barrier material to be uniformly distributed into a thin annular layer. This layer can ultimately be drawn to an average thickness below 5 microns and since this layer controls the functionality of the package, the uniformity of the distribution is

critical. The pressure information is important in terms of the mechanical construction in that it provides the data that the mechanical engineer requires to ensure that there is no excessive deflection of the components.

The visualization experiments facilitated the understanding of the flow behaviour within the new flat spiral distribution system and provided data that could be used to validate Finite Element Method modelling techniques. The visualization experiments also helped to point out some asymmetries in the binary distribution system which were not initially apparent.

The Finite Element Method analysis, presented in Chapter 5, is in good agreement with the observations made during the visualization experiments. The analysis showed that a relatively crude grid can provide reasonable accuracy. The comparison between the FEM results and the CVM results indicate that the CVM approximations tend to under predict the pressure drop through the distribution system. It is believed that the rapid advances being made in computer technology will make the FEM flow analysis a standard part of spiral die design in the next few years.

The coextrusion experiments are believed to be the first fundamental study of coextrusion instability involving identical polymers in both layers. The observations confirmed that the 'zig-zag' instability is due to excessive stress at the interface and occurs a stress levels over 70 kPa for the narrow MWD materials used in this study. The observations made in this study would also tend to support some recent findings of other researchers in that the origin of the 'wave' instability is at the point where the two layers combine and depends on the elongational behaviour of each layer. Furthermore, the bulk

elongation of each layer would appear to be a more likely factor in the origin of the 'wave' type of interfacial instability. From a design standpoint, the results suggest that the acceleration of the materials at the merge point needs to be controlled in order to minimize the potential for a 'wave' instability. This is especially true for materials with broad molecular weight distributions and/or high viscosities. Maintaining a low velocity ratio (as defined in chapter 6) would be appear to be a good starting point for a design criterion here. The 'zig-zag' instability resulting from a high stress region in the flow field can be eliminated by reducing the interfacial stress. Since the product structure or layer ratios are defined by the package requirements, the solution would be to increase the material temperature, decrease the total flow rate or modify the equipment to reduce the stress.

7.2 Recommendations

The control volume method model of the flat spiral system appears to be sufficiently accurate to be applied to a design procedure for these types of dies. However, further work should be done on improving the accuracy of the analytical expressions used to determine the resistance of the channels.

The new flat spiral distribution system appears to be very capable of distributing the polymer melt uniformly and can be applied to the development of multi-layer dies for the tubular film process.

The visualization experiments provided valuable insight into the behaviour of the flat spiral flow field as well as some data for verifying the FEM analysis. It is recommended

that future work should include fluids with non-Newtonian viscosity behaviours to verify the predictions presented in this study.

The FEM analysis should be used during the development of new complex flow fields in order to improve the designer's understanding of the flow behaviour. A more refined FEM grid is required in order to perform a non-isothermal analysis or even a more accurate isothermal analysis. The particle path analysis can be extremely useful in determining the homogenizing (or mixing) capability of the spirals and can be used to improve this function of the die.

Future work on interfacial instability should focus on the elongation rate of each layer at the merge point and should including the effect of the elongational viscosity of the materials. A transient analysis of this area without any externally applied fluctuations would be preferable. Of particular interest to die designers would be the determination of design parameters which help to minimize the occurrence of an instability for a wide range of materials.

REFERENCES

Brydson,J.A. Flow properties of polymer melts 2nd edition, George Godwin Ltd. (1981)

Benkhouch,K. And Sebastian,D.H.,"Design and analysis of spiral mandrel blown film dies", SPE Antec, pp1774-1778 (1989).

Butler,T.I., 'The influence of extruder residence time distribution on polymer degradation', TAPPI Polymers Laminations & Coatings conference proceedings, pp.401-416, 1989

Chen, J.H. and Ren, H.L. "Research of instable interface mechanism in coextrusion", SPE ANTEC, 1989

Cheng,C.Y., "Screw and die design for HDPE blown film", Polym. Plast. Technol. Eng., 17, 45-58 (1981)

Cogswell,F.N., Polym.Eng.Sci., 12, 64 (1972)

Colombo, R. U.S. Patent, 2,820,249 (1958)

Coyle,D.J. and Perdikoulias, J. "Mathematical modelling of flow in extrusion dies", 7th Annual PPS meeting (1991a)

Coyle,D.J. and Perdikoulias, J., "Flow simulation and visualization in spiral mandrel dies", SPE ANTEC, 2445-2447 (1991b)

Dealy,J.M. and Wissbrun,K.F., Melt rheology and its role in plastics processing: Theory and Applications, Van Nostrand and Reinhold, New York (1990).

Dooley,J. and Hilton,B.T., "Coextrusion layer rearrangement in different channel geometries", SPE ANTEC, 3354-3364, (1993)

Fahy,E.J. and Gilmour,P.W.,"A finite element analysis of generalized newtonian fluids through spiral mandrel dies", International Journal for Numerical Methods in Engineering, 23, 1-11 (1986)

Fredrickson,A.G. and Bird,R.B., Ind.Eng.Chem., 50, 347 (1958)

FIDAP v7.5: Fluid Dynamics Analysis Package, Fluid Dynamics International Inc.,Evanston, Illinois, USA, 1995

Foster, R.T., personal communications, 1989

Gates, P.C., "Optimizing the coextrusion process", TAPPI 1990 Coextrusion Seminar Notes, pp.13-15.

Halle, R.W., "Thermal Stability - A key polymer processing parameter - A comparative study of ethylene copolymers", TAPPI PL&C Conference Proceedings, pp.585-598 (1989)

Han,C.D., Multiphase flow in polymer processing, Academic Press (1981)

Han,C.D. and Shetty, R., "Studies on Multilayer film coextrusion II. Interfacial Instability in two layer flat film coextrusion", Polym.Eng.Sci., 18, 180 (1978)

Helmy,H.A.A. and Worth,R.A.,"Design of polymer melt extrusion dies to avoid non-uniformity of flow",Rheology Vol. 3: App. lications, Eds. G.Astarita, GT.Marrucci and L.Nicolais, 8th International Congress on Rheology, Naples Italy, Sept 1-5, pp. 69-75 (1980)

Himmelblau, D.M. and Bischoff, K.B., Process Analysis and Simulation: Deterministic Systems, John Wiley, New York (1968)

Hinsken, H. , Kunststoffe 77, 461 (1987)

Johnston, R.T., 'Degradation and stabilization of Linear Low Density Polyethylene during melt processing', Eighth International Conference on Advances in the Stabilization and Controlled Degradation of Polymers.

Karagiannis, A., Modelling of Single Component and Bicomponent Extrusion Flows , PhD Thesis, McMaster University, Hamilton, Ontario, Canada (1989)

Kemblowski,Z. and Sek,J., "Residence time distribution in a real single screw extruder", Polym.Eng.Sci., 21, 1194-1202 (1981)

Kurzbuch,W., "Control melt temperature with die design", Plastics Engneering, 43-46 (August 1974)

LAYERCAD: Coextrusion Flow Simulation Software, POLYDYNAMICS INC. Hamilton, Ontario, Canada. COMPUPLAST International Inc, Zlin, Czech Republic

Levenspiel, O., Chemical Reaction Engineering, Wiley-Interscience, 2nd Ed., New York (1972)

Lin, S.H., Chem.Eng.Sci., 35, 1477 (1980)

Mavridis, H. " Modular Coextrusion Stacked Dies for Blown Film", Antec p 101-105, May 1996.

Mavridis,H., and Shroff,R.N.,'Multilayer Extrusion: Experiments and computer simulation', Polym.Eng.Sci. Vol. 34, 559-569, (1994)

Menges,G.,Mayer,A.,Bartilla,T. and Wortberg,J., "A new concept for the design of spiral mandrel dies", Advances in Polymer Technology, 4 , 177-185 (1984)

Michaeli,W., Extrusion dies, Carl Hanser Verlag, Munich (1984)

Middleman,S., Fundamentals of polymer processing, McGraw-Hill Inc. New York (1977)

Mirshra, P. and Mirshra, I., AIChE J 22, 617 (1976)

Mitsoulis,E. and Hannachi,A. "Analysis and Design for Multi-layer Parison Coextrusion in Blow Molding", SPE Antec , pp.747-750, (1990)

Munstedt,H. And Wolter,H.-J., "Low-Density Polyethelyne (PE-LD ,PE-LLD), Kunststoffe, German Plastics 83, 10 p3-5 (1993)

Nauman,E.B. and Buffham,A.B., Mixing in Continuous Flow Systems, John Wiley, New York (1983)

Nordberg, M.E. and Winter ,H.H., Polym. Eng. Sci, 28, 444-452, (1988)

O'Brien,K.T. (Ed.), Computer Modeling for Extrusion and Other Continuous Polymer Processes, Carl Hanser Verlag, Munich (1992)

Parnaby,J., Hassan,G.A., Helmy,A.A. and Ali,A., "Design of plastics machinary using lumped parameters methods", Plastics and Rubber Processing and Applications, 1 , 303-315 (1981)

Perdikoulias,J., Polymer flow through spiral mandrel dies: Analysis and Design, Master's Thesis, McMaster University, Hamilton, Ontario, Canada (1988)

Perdikoulias,J., Richard,C., Vlcek,J. and Vlachopoulos,J.,'A study of coextrusion flows in polymer processing', SPE ANTEC, pp.2461-2464 (1991)

Perdikoulias,J. and Tzoganakis,C.,"Flow visualization in spiral mandrel dies", McMaster University/Brampton Engineering video tape (1987)

Perdikoulias,J., Tzoganakis,C. and Vlachopoulos,J., 'Flow visualization and residence time distribution in spiral mandrel dies', Plastics and Rubber Processing and Applications, 11, 1 (1989)

Perdikoulias,J.,Tzoganakis,C. and Vlachopoulos,J., "Molten polymer flow through spiral mandrel dies", Proceedings of the Canadian Chemical Engineering Graduate Students Conference, Kingston (1987)

Perdikoulias,J.,Vlcek,J. and Vlachopoulos,J.,"Polymer flow through spiral mandrel dies: A comparison of models", Advances in Polymer Technology, 7, 333-341 (1987)

Perdikoulias,J.,Vlcek,J. and Vlachopoulos,J., "Investigating interfacial instability in Coextrusion", SPE Antec , pp3365-3369, (1993)

Pinto, G. and Tadmor, Z., "Mixing and RTD in melt screw extruders", Polym.Eng.Sci., 10, 279-288 (1970)

POLYCAD 2D: FEM Flow Simulation Software, POLYDYNAMICS Inc. Hamilton, Ontario, Canada. COMPUPLAST International Inc., Zlin, Czech Republic

Proctor,B.,"Flow analysis in extrusion dies", SPE Journal, 28, 34-41 (1972)

Ramamurthy,A.V.,"LLDPE rheology and blown film fabrication", Advances in Polymer Technology, 6 ,489-499 (1986)

Ramamurthy,A.V., U.S. Patent No. 4,522,776

Ramanathan, R. and Schrenk, W.J., "Flow Visualization: A contemporary experimental toll to decifer stability of multilayer coextrusion flows", Engineering Plastics, 6, 73-86 (1993)

Ramanathan,R. and Dooley,J. "Dynamics of Mulitlayer Polymer Melt Flow: An experimental and numerical investigation", SPE ANTEC, 426-430 (1992)

Ramanathan, R. et al, " 'Wave' pattern instability in multilayer coextrusion-An experimental investigation", SPE ANTEC, 224-228, (1996)

Rauwendaal,C.,"Flow distribution in spiral mandrel dies", SPE ANTEC , 917-923,(1986) see also Polym.Eng.Sci.,27,pp. 186-191, (1987)

Rauwendaal,C., Polymer extrusion, Carl Hanser Verlag, Munich (1986)

Richardson,P.N., Introduction to extrusion, Society of Plastics Engineers, Inc., Connecticut (1974)

Rincon, A.J., "Transient simulation of coextrusion flows", PhD Proposal, McMaster University,Hamilton, Ontario, (1995).

Saillard,P. and Agassant,J.F.,"Polymer flow in a spiral mandrel die for tubular films", Polym.Proc.Eng., 2, 37-52,(1984)

Saillard,P."Les phenomenes thermiques dans les outillages d'extrusion des matieres plastiques", These Docteur - Ingenieur, Sophia Antipolis, Valbonne, France (1982)

Saini,D.R. and Shenoy,A.V.,"Melt rheology of some specialty polymers", Journal of Elastomers and Plastics, 17, 189-217 (1985)

Schott,N.R. adn Saleh, D.V., "Effect of RTD on extruded LDPE foam", SPE Antec, 526-539 (1978)

Schrenk,W.J. and Alfrey, T. Coextruded multilayer polymer films and sheets in Polymer Blends, Vol 2, Paul, D.R. and Seymour,N.(eds.), Academic Press, New York (1978)

Schrenk, W.J., U.S. Patent 3,308,508 (1967)

Shanker, R. and Ramanathan, R. "Effect of die geometry on flow kinematics in extrusion dies", SPE Antec 65-68, (1995)

Shenoy,A.V. and Saini,D.R.,"Melt Flow Index: More than just a quality control rheological parameter. Part 1", Advances in Polymer Technology, 6, 1-58 (1986)

Shenoy,A.V.,Chattopadhyay,S.and Nadkarni,V.M.,"From melt flow index to rheogram", Rheol.Acta, 22, 90-101 (1983)

Sneller, J.R., "Coex commodity films are alive and growing", Modern Plastics, pp 54-55, September (1987)

Stamato,H.J. and Weiss, R.A., Determination of the RTD in a plasticating extruder using ionomer tracer", SPE ANTEC, 42-44 (1985)

Stevens,M.J.,Extruder principles and operation, Elsevier Applied Science Publishers Ltd., New York (1985)

Tadmor,Z and Gogos,C.G.,Principles of Polymer Processing, John Wiley & Sons, New York (1979)

Torres, A., Hrymak,A., and Vlachopoulos,J., "Thermal effects in coextrusionof polymer melts", SPE ANTEC, 58-64 (1995)

Veazey,E.W., SPE News Letter, p.4 (Feb. 1988)

Vergnes,B. and Agassant,J.F.,"Die flow computations: A method to solve industrial problems in polymer processing", Advances in Polymer Processing, 6, 441-455 (1986)

Vlachopoulos,J., Behncke,P. and Vlcek, J., "Polycad: A finite element package for polymer process analysis and design", Adv.Polym.Tech., 9, 147-156 (1989)

Vlcek,J.,Kral.V. and Kouba,K.,"The calculation of the form of a spiral mandrel", Plast. Rubber Proc. App. , 4, 309-315 (1984)

Vlcek,J.,Perdikoulias,J.and Vlachopoulos,J.,"Computer aided design of spiral mandrel dies", Proceedings of the 37th Canadian Chemical Engineering Conference, Montreal (1987 B)

Vlcek,J.,Perdikoulias,J. and Vlachopoulos,J.,"Determination of output uniformity from spiral mandrel dies", Intern.Polym.Proc., 2, 174-181 (1988)

Vlcek,J.,Perdikoulias,J. and Vlachopoulos,J., "Investigating interface instabilities in coextrusion", SPE ANTEC, 3365-3369 (1993)

Volungus, R., personal communication, May 1991

Whelan,A. and Dunning,D.J., Developments in plastics technology-I, Applied science publishers, London, (1982)

Wilson, G.M. and Khomami, B., J. Rheol. 37(2) (1993)

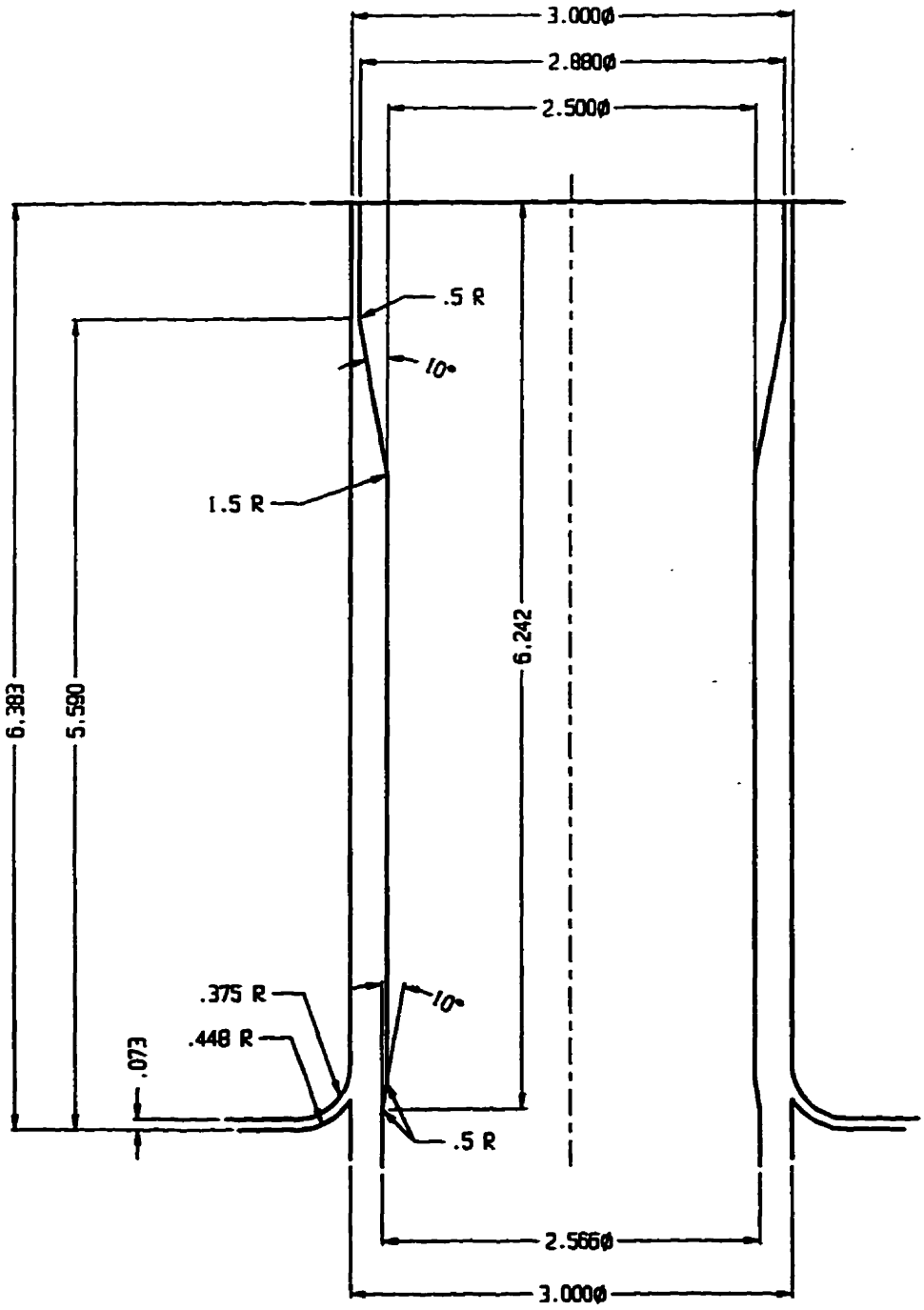
Wolf,D and White, D.H., "Experimental study of the RTD in plasticating screw extruders" AIChE J., 22, 122-131 (1976)

Wortberg,J and Schmitz,K.P.,"Design and optimisation of a spiral mandrel die", Kunststoffe, 72, 198-205 (1982)

APPENDICES

Appendix A

Detailed Dimensions


3.000Ø
2.880Ø
2.500Ø
.5 R
10°
1.5 R
6.383
5.590
6.242
.375 R
.448 R
.073
10°
.5 R
2.566Ø
3.000Ø

Appendix B

Additional Material Data

Petrothene®

RECEIVED NOV 3 0 1992
RECEIVED 3 0 1992

NA 355

355-196

High Molecular Weight Low Density Polyethylene Blown Film Grade Melt Index 0.5 Density 0.925

Petrothene NA 355 is a high molecular weight, low density polyethylene homopolymer or use in producing tough, clear film for packaging items such as heavy textiles and he roduce (e.g. potatoes, apples, etc.); drum liners and any clarity application where owngauging is needed. The low melt index and stiffness of this resin make it excellen hrink film. It can also be used for coextrusion and blending.

Petrothene NA 355 is designed to be blown with a long-stalk bubble shape when films han 1.5 mils are extruded. In long-stalk extrusion, the extrudate above the die is main t the same diameter as the die until the bubble expands to its final diameter just belov ost line. The rapid expansion of the bubble just below the frost line creates an orienta he melt which optimizes the film's impact strength.

the film being extruded has a gauge of more than 1.5 mils, either a long-stalk or a onventional bubble shape can be used with little or no resulting difference in the film's hysical properties.

is recommended that NA 355 be extruded at a melt temperature of 370 to 380°F, abo 100°F lower that that used for LLDPE or HMW/HDPE. A 3:1 blow-up ratio and a 30 n arger die gap are also recommended. Exact recommendations can be made only if quipment, operating conditions and required end product properties are known. Pleas ontact your Quantum polyolefins sales representative if you have further questions.

Petrothene NA 355, when extruded with a long stalk, can be drawn down to 0.5 mils ar naintain its high strength and high clarity. It is comparable in impact strength to HMW/I nd LLDPE. NA 355 contains medium levels of slip and antiblock additives.

uantum Chemical Corporation
SI Division
500 Northlake Drive
incinnati, OH 45249
13/530-6500

Quantu

93

Petrothene®

NA 355

operty	Nominal Value with Long Stalk*	Units	AS Me
Resin			
ınsity	0.925	g/cm³	D
ılt Index	0.5	g/10 min.	D
Film			
ıze	5.8	%	D
oss, 45°	69		D
ırt Drop, F_{50}	300	g	D
DD, Body	2.0	ft-lb	D
Crease	1.9	ft-lb	D
ıtron Puncture Strength			
Force	24	newtons	
Energy	0.42	joules	
nsile Strength			
@ Break, MD	5400	psi	D
TD	5200	psi	D
@ Yield, MD	1840	psi	D
TD	1860	psi	D
ngation, MD	200	%	D
TD	340	%	D
Secant Modulus,			
MD	32,400	psi	D
TD	36,400	psi	D

film properties obtained on 1 mil film extruded with a long stalk and 3:1 blow-up ratio

aterial Safety Data Sheet (MSDS) is available for this product. Users of this product are urged to study and use this in

information on this data sheet is, to our best knowledge, true and accurate. However, since conditions of use are trol, all recommendations or suggestions are presented without guarantee or responsibility on our part. We disclaim nection with the use of information contained herein or otherwise. All risks of such use are assumed by the user. F ing contained herein shall be construed as an inducement or recommendation to use any process or to manufactur luct in conflict with existing or future patents.

u have any questions, please contact your Quantum polyolefins sales representative.

ıntum Chemical Corporation
Division
)0 Northlake Drive
cinnati, OH 45249
/530-6500

Quant

Petrothene®
NA 957

Low Density Polyethylene
Film Extrusion Grade
Melt Index 2.6 Density 0.924

Applications
PETROTHENE NA 957 is a series of highly uniform resins specifically developed for the multi-wall bag market. NA 957 produces films with exceptional drawdown, outstanding toughness, high dart drop impact strength and excellent heat sealing characteristics. Other applications include general packaging, industrial liners, food containers and trash bags.

Certification
The basic resin PETROTHENE NA 957 meets the requirements of the Food and Drug Administration, Code of Federal Regulations, Title 21, Part 177.1520. This regulation allows the use of this olefin polymer in "articles or components of articles intended for use in contact with food." Specific limitations or conditions of use may apply. Contact your Quantum polyolefins sales representative for more information regarding the suitability of specific products for specific applications.

Processing Techniques
PETROTHENE NA 957 extrudes at high output rates with good bubble stability over a wide temperature range. Best results are obtained at melt temperatures between 310-350°F (154-176°C) and blow-up ratio of 1.5-2.4:1. Using proper techniques, the resin can be drawn to 0.5 mil at commercial production rates.

Specific recommendations for processing NA 957 can be made only when the end use application, required properties and the processing equipment are known. For exact recommendations, please contact your Quantum polyolefins sales representative.

Typical Properties*

Property	Value	Units	ASTM Test Method
Density	0.924	g/cm³	D 1505
Melt Index	2.6	g/10 min.	D 1238
Vicat Softening Point	80	°C	D 1525
Low Temperature Brittleness, F_{50}	-75	°C	D 746
Tensile Strength @ Yield	1,400	psi	D 638
@ Break	1,800	psi	
Elongation @ Yield	100	%	D 638
@ Break	650	%	
Hardness, Shore D	42		D 2240
Film**			
Haze	15	%	D 1003
Gloss, 45°	40		D 2457
Dart Drop Impact Strength, F_{50}	120	g	D 1709
Tensile Strength, MD	2,500	psi	D 882
TD	2,200	psi	
Elongation, MD	300	%	
TD	500	%	
1% Secant Modulus, MD	21,000	psi	D 882
TD	25,000	psi	

Products	NA 957-000	NA 957-061	NA 957-097
Slip	None	None	Low
Antiblock	None	High	High

*These are typical values and not to be construed as specific product limits.
**Data obtained from film produced in a 3½" (89 mm) blown film line, commercially available 8" (203 mm) die, 325°F (163°C) melt extrusion temperature, 2.2:1 BUR, 1.25 mil (32 micron) gauge.

A Material Safety Data Sheet is available for this product. Users of this product are urged to study and use this information.

The information on this data sheet is, to our best knowledge, true and accurate. However, since conditions of use are beyond our control, all recommendations or suggestions are presented without guarantee or responsibility on our part. We disclaim all liability in connection with the use of information contained herein or otherwise. All risks of such use are assumed by the user. Furthermore, nothing contained herein shall be construed as an inducement or recommendation to use any process or to manufacture or use any product in conflict with existing or future patents.

Quantum Chemical Corporation
USI Division
11500 Northlake Drive
Cincinnati, OH 45249
(513) 530-6500

Quantum

6723-19/891

This paper is made from recycled fibers and can be recycled.

Petrothene®
NA 960

Low Density Polyethylene
Film Extrusion Grade
Melt Index 0.9 Density 0.919

Applications

PETROTHENE NA 960 is a series of resins designed for a wide variety of industrial film applications where high impact strength and excellent drawdown are needed. NA 960 exhibits good uniformity, ease of processing and good tensile strength.

Certification

The basic resin PETROTHENE NA 960 meets the requirements of the Food and Drug Administration, Code of Federal Regulations, Title 21, Part 177.1520. This regulation allows the use of this olefin polymer in "...articles or components of articles intended for use in contact with food." Specific limitations or conditions of use may apply. Contact your Quantum polyolefin sales representative for further information regarding the suitability of specific products for specific applications.

Processing Techniques

Specific recommendations for processing NA 960 can only be made when the processing conditions, equipment and end use are known. For further suggestions, please contact your Quantum polyolefins sales representative.

Typical Properties*

Property		Value	Units	ASTM Test Method
Resin				
Density		0.919	g/cm³	D 1505
Melt Index		0.9	g/10 min.	D 1238
Tensile Strength**		2,100	psi	D 638
Elongation @ Break		660	%	D 638
Dart Drop Impact Strength, F_{50}***		170	gms	D 1709
Vicat Softening Point		94	°C	D 1525
Products	**NA 960-000**	**NA 960-050**	**NA 960-055**	**NA 960-057**
Slip	None	Low	Medium	High
Antiblock	None	Medium	Medium	High
Products	**NA 960-062**	**NA 960-086**	**NA 960-186**	
Slip	Medium	None	None	
Antiblock	High	Medium	Medium	

*These are typical values and not to be construed as specific product limits.
**Data derived from type IV specimen, 75 mil plaque @ 20" min.
***Data derived from 1.5 mil specimen, 26" drop.

A Material Safety Data Sheet is available for this product. Users of this product are urged to study and use this information.

The information on this data sheet is, to our best knowledge, true and accurate. However, since conditions of use are beyond our control, all recommendations or suggestions are presented without guarantee or responsibility on our part. We disclaim all liability in connection with the use of information contained herein or otherwise. All risks of such use are assumed by the user. Furthermore, nothing contained herein shall be construed as an inducement or recommendation to use any process or to manufacture or use any product in conflict with existing or future patents.

Quantum Chemical Corporation
USI Division
11500 Northlake Drive
Cincinnati, OH 45249
(513) 530-6500

6723-20/891

This paper is made from recycled fibers and can be recycled.

Quantum

Petrothene®
NA 345

Low Density Polyethylene
Film Extrusion Grade
Density 0.922 Melt Index 1.8

Applications

PETROTHENE NA 345 is a series of homopolymer resins combining premium clarity with strength and stiffness. In addition, NA 345 exhibits good impact strength on both flat and creased film. NA 345 is recommended for textile packaging, light produce, bread bags and other thin packaging films enhanced by clarity and sparkle.

The optical values of NA 345 actually improve with decreases in film gauge and are maintained at wide die gap settings. This fact leads to important cost savings. Film can be drawn down to a minimum gauge consistent with required physical properties, with the assurance that optical properties will not suffer, but improve. With wider die gaps, back pressures are reduced as are extrusion costs.

Certification

The basic resin PETROTHENE NA 345 meets the requirements of the Food and Drug Administration, Code of Federal Regulations, Title 21, Part 177.1520. This regulation allows the use of this olefin polymer in "...articles or components of articles intended for use in contact with food." Specific limitations or conditions of use may apply. Contact your Quantum polyolefins sales representative for further information.

Processing Techniques

Specific recommendations for processing NA 345 can only be made when the processing conditions, equipment and end use are known. For further suggestions please contact your Quantum polyolefins sales representative.

Typical Properties*

Property	Value	Units	ASTM Test Method
Resin			
Density	0.922	g/cm³	D 1505
Melt Index	1.8	g/10 min.	D 1238
Film**			
Haze	5.0	%	D 1003
Gloss, 45°	70	units	D 2457
Dart Drop Impact Strength, F_{50}	90	g	D 1709
TEDD	0.90	ft-lb.	D 4272
Tensile Strength @ Yield, TD	1,600	psi	D 882
@ Break, MD	3,800		
TD	3,000		
Elongation, MD	300	%	D 882
TD	500	%	
1% Secant Modulus, MD	26,000	psi	D 882
TD	30,000	psi	
Elmendorf Tear Strength, MD	280	g	D 1922
TD	240		

Product	NA 345-009	NA 345-013	NA 345-166	NA 345-195
Slip	None	None	None	Medium
Antiblock	None	None	High	Medium

Product	NA 345-196
Slip	Medium
Antiblock	Medium

*These are typical values and not to be construed as specific product limits.
**Film properties obtained on 1.25 mil film.

A Material Safety Data Sheet is available for this product. Users of this product are urged to study and use this information.

The information on this data sheet is, to our best knowledge, true and accurate. However, since conditions of use are beyond our control, all recommendations or suggestions are presented without guarantee or responsibility on our part. We disclaim all liability in connection with the use of information contained herein or otherwise. All risks of such use are assumed by the user. Furthermore, nothing contained herein shall be construed as an inducement or recommendation to use any process or to manufacture or use any product in conflict with existing or future patents.

Quantum Chemical Corporation
USI Division
11500 Northlake Drive
Cincinnati, OH 45249
(513) 530-6500

Quantum

6723-36/891

This paper is made from recycled fibers and can be recycled.

ROSAND PRECISION CAPILLARY RHEOMETER

25th Feb 1994 1:09pm **TEST INFORMATION**

Polymer type ..... LDPE
Trade name ..... USI LDPE
Grade ..... NA 345-000
Batch number I2WL31

Lab code number A94-00153
Molecular weight Mw 2-25-94
Filler percentage .....
Filler types .....
Sample origin ..... H.MAVRIDIS
Additional information ..... FC,SIDE B,190C,1.5mm DIES

Operator's initials ..... RBM
Mw/Mn .....
Drying temperature .....
Drying atmosphere .....
Drying hours .....

TEST TEMPERATURE

Top zone temp (°C) 190
Middle zone temp (°C) 190
Bottom zone temp (°C) 190
Bottom actual temp (°C) 192.5

TEST GEOMETRY

Long die length (mm) 24
Long die diameter (mm) .. 1.5
Short die length (mm) 0.25
Short die diameter (mm) .. 1.5
Die entry angle (deg) 180

RUN SCHEDULE - Piston Speeds mm/min

0.7,1,1.5,2,3,5,7,10,15,20,25,35,50,70,100,150

PRESSURE TRANSDUCERS

Transducer at long die .....
Max pressure (psi) 3000
Information .....
Transducer at short die ....
Max pressure (psi) 500
Information .....

PREHEAT SEQUENCE

Initial pressure long die (MPa) 0
Initial pressure short die (MPa) 0
Time before 2nd compression (min) ... 0
Final pressure long die (MPa) 0
Final pressure short die (MPa) 0
Preheat time (min) 5

CONTROL FACTORS

Variation on standard sample rate 0.5
Max no. of samples at any speed 75
Endpoint filter time constant 3.5
Allowable deviation at end point 0.15
Disc title LDPE3
File title 9 88

(Rabinowitsch corrected) - CURRENT TEST RESULTS

	Shear rate /s	Time s	Pl MPa	Ps MPa	Po MPa	Shear Stress kPa	Shear Visc Pa.s	Exten Stress kPa	Elong Visc kPa.s	n
N	6.22	186	1.18	0.05	0.04	17.8	2861	0	0	1.00
N	8.89	299	1.50	0.08	0.06	22.4	2519	0	0	1.00
N	13.33	421	2.04	0.12	0.10	30.4	2280	0	0	1.00
	21.74	461	2.40	0.15	0.13	35.5	1634	71.3	13.17	0.51
	33.15	493	3.02	0.22	0.19	44.2	1334	105.8	15.29	0.49
	56.49	515	3.92	0.35	0.31	56.3	996.8	170.3	18.23	0.46
	80.34	534	4.66	0.46	0.41	66.4	826.1	223.5	18.74	0.44
	116.8	550	5.54	0.61	0.56	77.9	667.0	296.1	19.26	0.42
	179.1	562	6.66	0.83	0.77	92.1	514.3	401.4	19.53	0.40
	242.8	575	7.67	1.03	0.96	104.8	431.7	496.2	19.34	0.38
	307.7	585	8.44	1.21	1.13	114.1	370.8	583.5	19.40	0.37
	440.1	596	9.79	1.53	1.45	130.4	296.2	733.6	18.76	0.35
	644.5	606	11.30	1.91	1.81	148.2	230.0	907.0	17.22	0.33
	925.3	615	12.80	2.22	2.11	167.0	180.4	1041.1	14.03	0.31
	1361	623	14.43	2.62	2.49	186.6	137.1	1209.9	11.53	0.29
	2117	631	16.55	3.07	2.93	212.8	100.5	1395.9	8.65	0.27

ROSAND PRECISION CAPILLARY RHEOMETER

25th Feb 1994 12:32pm **TEST INFORMATION**

Polymer type ..... LDPE
Trade name ..... USI LDPE
Grade ..... NA 355-196
Batch number I2VF32

Lab code number A94-00151
Molecular weight Mw 2-25-94
Filler percentage .....
Filler types .....
Sample origin ..... H.MAVRIDIS
Additional information ..... FC,SIDE B,190C,1.5mm DIES

Operator's initials ..... RBM
Mw/Mn .....
Drying temperature .....
Drying atmosphere .....
Drying hours .....

TEST TEMPERATURE

Top zone temp (°C) 190
Middle zone temp (°C) 190
Bottom zone temp (°C) 190
Bottom actual temp (°C) 191.3

TEST GEOMETRY

Long die length (mm) 24
Long die diameter (mm) .. 1.5
Short die length (mm) 0.25
Short die diameter (mm) .. 1.5
Die entry angle (deg) 180

RUN SCHEDULE - Piston Speeds mm/min

0.7,1,1.5,2,3,5,7,10,15,20,25,35,50,70,100,150

PRESSURE TRANSDUCERS

Transducer at long die .....
Max pressure (psi) 3000
Information .....
Transducer at short die .....
Max pressure (psi) 500
Information .....

PREHEAT SEQUENCE

Initial pressure long die (MPa) 0
Initial pressure short die (MPa) 0
Time before 2nd compression (min) 0
Final pressure long die (MPa) 0
Final pressure short die (MPa) 0
Preheat time (min) 5

CONTROL FACTORS

Variation on standard sample rate 0.5
Max no. of samples at any speed 75
Endpoint filter time constant 3.5
Allowable deviation at end point 0.15
Disc title LDPE3
File title 2 87

(Rabinowitsch corrected) - CURRENT TEST RESULTS

	Shear rate /s	Time s	Pl MPa	Ps MPa	Po MPa	Shear Stress kPa	Shear Visc Pa.s	Exten Stress kPa	Elong Visc kPa.s	n
N	6.22	152	2.55	0.14	0.11	38.1	6128	0	0	1.00
	11.47	226	3.12	0.21	0.18	46.0	4009	97.1	35.77	0.45
	17.45	294	3.90	0.32	0.28	56.6	3242	152.2	46.92	0.43
	23.52	339	4.50	0.42	0.38	64.4	2737	200.7	53.21	0.42
	35.85	380	5.47	0.59	0.54	77.0	2147	284.2	58.54	0.40
	61.06	405	6.83	0.88	0.82	93.9	1539	425.1	63.01	0.38
	86.78	422	7.87	1.13	1.06	106.4	1226	545.7	64.49	0.37
	126.1	440	9.19	1.43	1.35	122.5	971.5	685.6	60.88	0.36
	193.0	455	10.74	1.77	1.68	141.5	733.1	845.0	52.29	0.34
	261.3	468	11.96	2.03	1.92	156.8	600.2	957.5	44.74	0.33
	330.7	478	12.91	2.25	2.11	168.8	510.3	1044.4	39.09	0.32
	472.2	488	14.50	2.55	2.41	189.0	400.4	1179.4	31.17	0.31
	689.6	498	16.35	2.96	2.75	212.4	308.0	1335.6	24.36	0.29
	987.1	506	18.17	3.07	2.91	238.5	241.6	1394.6	16.52	0.28
N	888.9	507	18.08	3.01	2.85	238.0	267.7	0	0	1.00
N	1333	508	16.90	2.74	2.59	223.6	167.7	0	0	1.00

ROSAND PRECISION CAPILLARY RHEOMETER

25th Feb 1994 10:38am **TEST INFORMATION**

Polymer type ..... LDPE
Trade name ..... USI LDPE
Grade ..... NA 957-000
Batch number M2UN4A

Lab code number A94-00149
Molecular weight Mw 2-25-94
Filler percentage .....
Filler types .....
Sample origin ..... H.MAVRIDIS
Additional information ..... PC,SIDE B,190C,1.5mm DIES

Operator's initials ..... RBM
Mw/Mn .....
Drying temperature .....
Drying atmosphere .....
Drying hours .....

TEST TEMPERATURE
Top zone temp (°C) 190
Middle zone temp (°C) 190
Bottom zone temp (°C) 190
Bottom actual temp (°C) 192.3

TEST GEOMETRY
Long die length (mm) 24
Long die diameter (mm) .. 1.5
Short die length (mm) 0.25
Short die diameter (mm) .. 1.5
Die entry angle (deg) 180

RUN SCHEDULE - **Piston Speeds mm/min**
0.7,1,1.5,2,3,5,7,10,15,20,25,35,50,70,100,150

PRESSURE TRANSDUCERS
Transducer at long die .....
Max pressure (psi) 3000
Information .....
Transducer at short die ....
Max pressure (psi) 500
Information .....

PREHEAT SEQUENCE
Initial pressure long die (MPa) 0
Initial pressure short die (MPa) 0
Time before 2nd compression (min) ... 0
Final pressure long die (MPa) 0
Final pressure short die (MPa) 0
Preheat time (min) 5

CONTROL FACTORS
Variation on standard sample rate 0.5
Max no. of samples at any speed 75
Endpoint filter time constant 3.5
Allowable deviation at end point 0.15
Disc title LDPE3
File title 9 86

(Rabinowitsch corrected) - CURRENT TEST RESULTS

	Shear rate /s	Time s	Pl MPa	Ps MPa	Po MPa	Shear Stress kPa	Shear Visc Pa.s	Exten Stress kPa	Elong Visc kPa.s	n
N	6.22	118	0.92	0.06	0.05	13.5	2178	0	0	1.00
N	8.89	263	1.18	0.09	0.08	17.3	1943	0	0	1.00
	16.57	321	1.45	0.13	0.12	20.8	1254	64.9	24.47	0.49
	22.26	357	1.71	0.16	0.14	24.6	1103	79.8	23.29	0.48
	33.78	392	2.14	0.23	0.21	30.1	891.3	115.4	26.16	0.47
	57.17	409	2.71	0.34	0.31	37.5	656.2	170.8	27.22	0.45
	80.88	422	3.21	0.44	0.41	43.7	540.8	221.0	27.61	0.44
	116.9	439	3.86	0.60	0.57	51.5	441.0	302.8	30.44	0.43
	177.8	457	4.74	0.84	0.80	61.7	347.0	421.6	32.41	0.41
	239.5	470	5.47	1.05	1.00	69.8	291.3	526.9	33.22	0.40
	301.9	483	6.09	1.25	1.20	76.3	252.9	629.4	34.39	0.40
	428.1	500	7.03	1.43	1.38	88.4	206.5	713.8	26.93	0.38
	620.4	515	8.05	1.60	1.53	101.9	164.2	786.2	19.56	0.37
	880.9	528	9.13	1.86	1.79	114.7	130.2	911.2	16.44	0.36
	1278	542	10.36	2.15	2.07	129.6	101.4	1044.2	13.16	0.35
	1954	557	12.12	2.59	2.43	151.5	77.55	1212.8	9.93	0.33

ROSAND PRECISION CAPILLARY RHEOMETER

25th Feb 1994 9:13am **TEST INFORMATION**

Polymer type ..... LDPE
Trade name ..... USI LDPE
Grade ..... NA 960-000
Batch number H2VK32

Lab code number A94-00147
Molecular weight Mw 2-25-94
Filler percentage .....
Filler types .....
Sample origin ..... H.MAVRIDIS
Additional information ..... FC,SIDE B,190C,1.5mm DIES

Operator's initials ..... RBM
Mw/Mn .....
Drying temperature .....
Drying atmosphere .....
Drying hours .....

TEST TEMPERATURE

Top zone temp (°C) 190
Middle zone temp (°C) 190
Bottom zone temp (°C) 190
Bottom actual temp (°C) 190.3

TEST GEOMETRY

Long die length (mm) 24
Long die diameter (mm) .. 1.5
Short die length (mm) 0.25
Short die diameter (mm) .. 1.5
Die entry angle (deg) 180

RUN SCHEDULE - Piston Speeds mm/min

0.7,1,1.5,2,3,5,7,10,15,20,25,35,50,70,100,150

PRESSURE TRANSDUCERS

Transducer at long die .....
Max pressure (psi) 3000
Information .....
Transducer at short die .....
Max pressure (psi) 500
Information .....

PREHEAT SEQUENCE

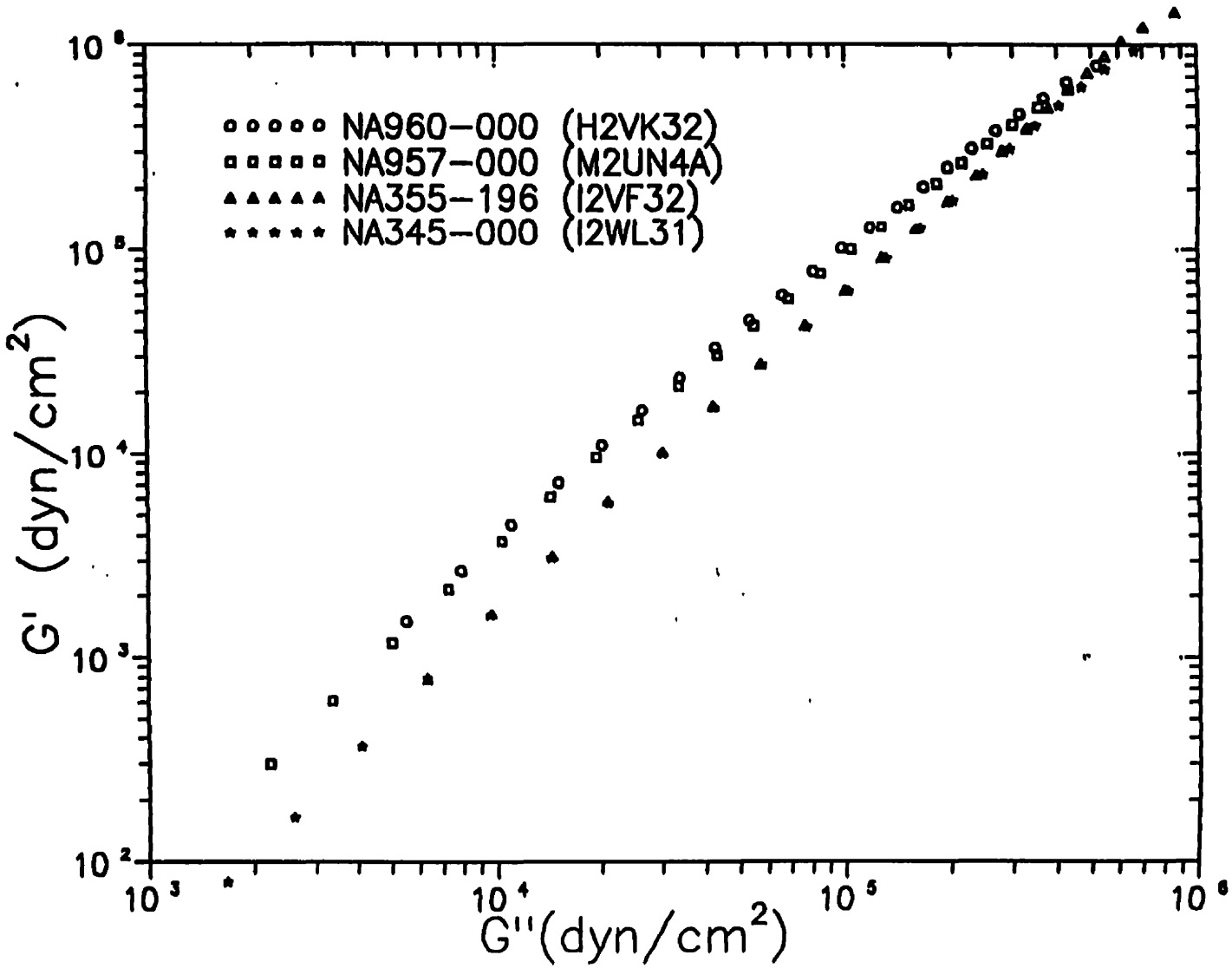
Initial pressure long die (MPa) 0
Initial pressure short die (MPa) 0
Time before 2nd compression (min) ... 0
Final pressure long die (MPa) 0
Final pressure short die (MPa) 0
Preheat time (min) 5

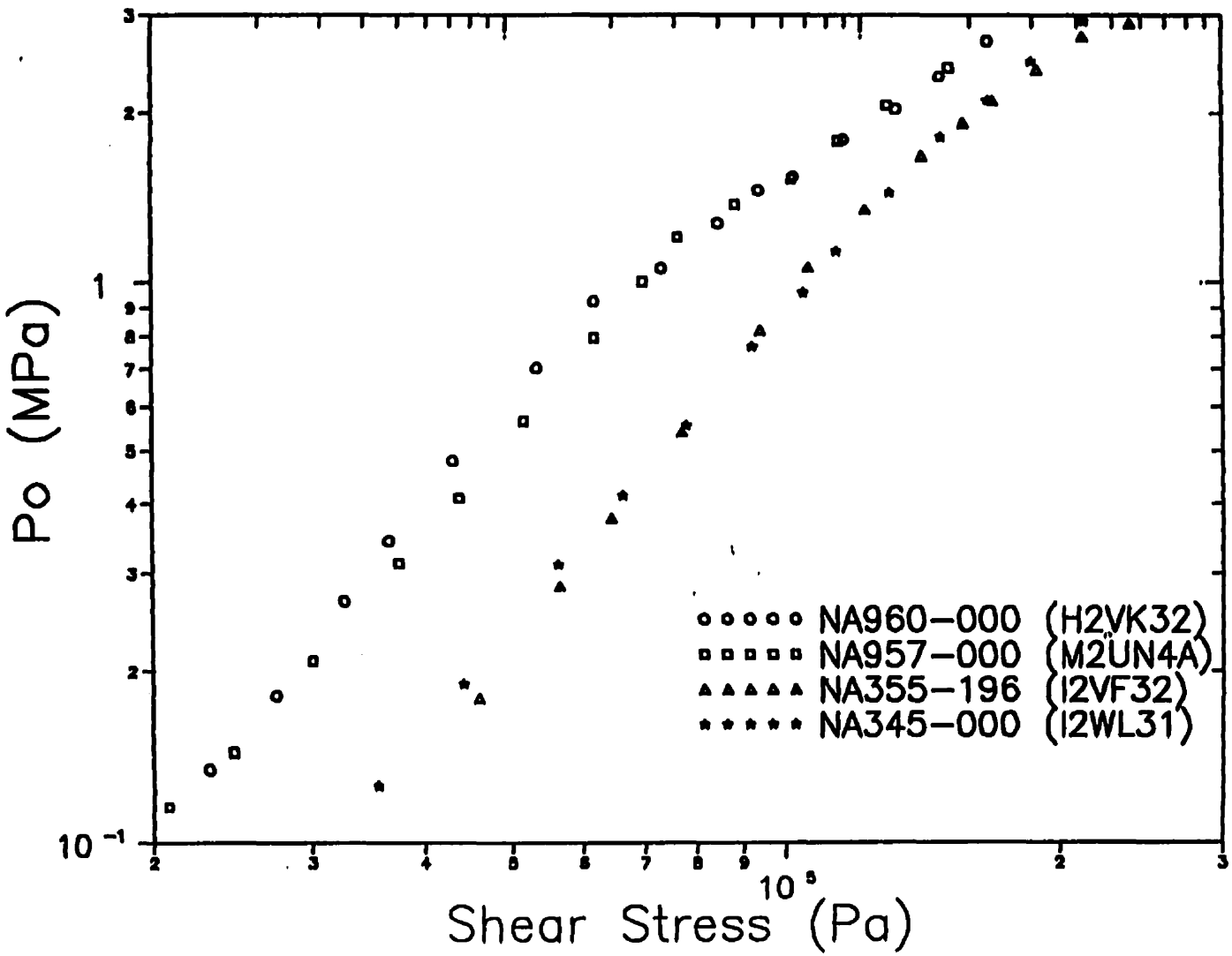
CONTROL FACTORS

Variation on standard sample rate 0.5
Max no. of samples at any speed 75
Endpoint filter time constant 3.5
Allowable deviation at end point 0.15
Disc title LDPE5
File title 4 15

(Rabinowitsch corrected) - CURRENT TEST RESULTS

	Shear rate /s	Time s	Pl MPa	Ps MPa	Po MPa	Shear Stress kPa	Shear Visc Pa.s	Exten Stress kPa	Elong Visc kPa.s	n
	8.07	308	1.61	0.15	0.13	23.1	2855	72.7	56.83	0.45
	11.62	405	1.93	0.20	0.18	27.4	2356	97.6	59.86	0.44
	17.59	468	2.36	0.29	0.27	32.6	1856	143.3	71.53	0.43
	23.60	517	2.69	0.37	0.34	36.6	1550	183.7	78.15	0.42
	35.74	553	3.23	0.51	0.48	43.1	1205	254.0	83.88	0.41
	60.30	575	4.12	0.74	0.70	53.4	884.9	369.1	84.67	0.40
	85.13	593	4.87	0.97	0.93	61.7	724.8	483.9	89.16	0.39
	122.7	617	5.74	1.11	1.08	73.2	596.7	549.6	67.23	0.39
	186.1	631	6.69	1.33	1.27	84.6	454.6	657.1	54.86	0.38
	250.1	649	7.45	1.52	1.46	93.7	374.5	749.2	47.93	0.37
	314.6	662	8.10	1.61	1.51	102.4	325.5	790.3	38.79	0.37
	444.7	678	9.22	1.87	1.78	116.0	260.9	913.8	32.37	0.36
	642.0	688	10.51	2.12	2.03	132.5	206.4	1029.0	24.90	0.35
	908.1	697	11.80	2.43	2.34	147.8	162.8	1175.4	20.58	0.34
	1312	708	13.40	2.82	2.71	167.1	127.3	1354.1	16.73	0.33
N	1333	711	14.35	2.94	2.82	180.1	135.1	0	0	1.00


NA960-000 (H2VK32)
NA957-000 (M2UN4A)
NA355-196 (I2VF32)
NA345-000 (I2WL31)
G' (dyn/cm²)
G''(dyn/cm²)
10⁶
10⁵
10⁴
10³
10²
10³
10⁴
10⁵
10⁶


Po (MPa)
Shear Stress (Pa)
10 -1
1
2
3
10 5
NA960-000 (H2VK32)
NA957-000 (M2UN4A)
NA355-196 (I2VF32)
NA345-000 (I2WL31)

NA957-000 A94-00149 190C 20% 50mm LD620

STO MOD	LOSS MOD	ETA'	TANDEL	TORQUE	G*	ETA*	RAD FREQ
6.04E+05	4.30E+05	1.08E+03	.712	7.17E+02	7.42E+05	1.86E+03	3.98E+02
4.93E+05	3.53E+05	1.40E+03	.716	5.57E+02	6.06E+05	2.41E+03	2.51E+02
4.05E+05	2.99E+05	1.89E+03	.740	4.99E+02	5.03E+05	3.18E+03	1.59E+02
3.29E+05	2.54E+05	2.54E+03	.772	4.98E+02	4.15E+05	4.15E+03	1.00E+02
2.66E+05	2.15E+05	3.41E+03	.811	5.59E+02	3.42E+05	5.42E+03	6.31E+01
2.12E+05	1.82E+05	4.56E+03	.855	6.93E+02	2.80E+05	7.02E+03	3.98E+01
1.68E+05	1.52E+05	6.06E+03	.908	8.56E+02	2.26E+05	9.02E+03	2.51E+01
1.31E+05	1.27E+05	7.98E+03	.966	8.45E+02	1.82E+05	1.15E+04	1.59E+01
1.01E+05	1.04E+05	1.04E+04	1.032	7.05E+02	1.45E+05	1.45E+04	1.00E+01
7.68E+04	8.52E+04	1.35E+04	1.109	5.56E+02	1.15E+05	1.82E+04	6.31E+00
5.75E+04	6.88E+04	1.73E+04	1.197	4.32E+02	8.96E+04	2.25E+04	3.98E+00
4.22E+04	5.49E+04	2.19E+04	1.301	3.34E+02	6.93E+04	2.76E+04	2.51E+00
3.05E+04	4.33E+04	2.73E+04	1.420	2.55E+02	5.29E+04	3.34E+04	1.59E+00
2.14E+04	3.36E+04	3.36E+04	1.574	1.93E+02	3.98E+04	3.98E+04	1.00E+00
1.46E+04	2.57E+04	4.08E+04	1.769	1.44E+02	2.96E+04	4.69E+04	6.31E-01
9.57E+03	1.94E+04	4.86E+04	2.022	1.05E+02	2.16E+04	5.43E+04	3.98E-01
6.08E+03	1.43E+04	5.68E+04	2.345	7.59E+01	1.55E+04	6.17E+04	2.51E-01
3.70E+03	1.03E+04	6.50E+04	2.785	5.37E+01	1.09E+04	6.90E+04	1.59E-01
2.14E+03	7.25E+03	7.25E+04	3.390	3.71E+01	7.56E+03	7.56E+04	1.00E-01
1.17E+03	5.00E+03	7.92E+04	4.276	2.52E+01	5.13E+03	8.14E+04	6.31E-02
6.06E+02	3.37E+03	8.46E+04	5.550	1.68E+01	3.42E+03	8.59E+04	3.98E-02
2.99E+02	2.22E+03	8.84E+04	7.417	1.10E+01	2.24E+03	8.92E+04	2.51E-02

C(1)	C(2)	C(3)	C(0)	COR.COEFF.	LN W VS. LN GPP
1.880E+00	-2.065E-01	1.295E-02	-1.181E+01	9.999E-01	

C(1)	C(2)	C(3)	C(0)	COR.COEFF.	TAND VS. LN G*
-3.461E+00	6.883E-01	-4.593E-02	1.462E+01	9.949E-01	

C(1)	C(0)	COR.COEFF.	LN GP=C1*LN GPP+C0
1.676E+00	-7.453E+00	9.997E-01	

C(1)	C(2)	C(0)	COR.COEFF	LN GP=C1*LN GPP +C2*LN(GPP**2)+C0
2.402E+00	-4.623E-02	-1.005E+01	1.000E+00	

C(1)	C(2)	C(0)	Mean-Err	LN GP=C1*LN Gs +C2*LN(Gs**2)+C0
2.507E+00	-5.691E-02	-1.021E+01	1.963E-02	

RDI= 2.27E+00 ER= 1.63E+00 SLOPE= 1.68E+00 GCOM= 1.10E+05 COW= 1.15E+01
ET= 1.99E+01

ETA*1000 = 1.074E+03 , Mean-%Error = 2.38E-01 (ETA* extrapolation)
ETA'1000 = 6.120E+02 , Mean-%Error = 4.89E-01 (G" extrapolation)
PDL = 2.27E+01 , Mean-%Error = 4.28E+00
PDR = 3.164E+01, PDH = 2.158E+01, Visc: 1.000E+05 2.784E+04 1.290E+03
PI= 1.21E+01 Modsep= 3.57E+00
NO OF POINTS = 22 NIMIN= 2 AB = .81800
SLOPE OF ETA ZERO-GAMMA DOT ZERO = .8820

RHEOLOGICAL PARAMETERS
AB = .818 A = 3.000 B = .273 D = 1.574E+00
RDR = 7.556E+00 ETA ZERO = 1.666E+05 GAMMA DOT ZERO = 3.816E+00
STD ERROR, FIT = 2.827E-02

RHEOLOGICAL PARAMETERS
AB = .818 A = 2.836 B = .288 D = 1.771E+00
RDR = 8.489E+00 ETA ZERO = 1.500E+05 GAMMA DOT ZERO = 3.764E+00
STD ERROR, FIT = 2.575E-02
RDR_new = 6.598E+00 (at ETA/ETA0= .1375)

NA355-196 A94-00151 190C 20% 50mm LD619

STO MOD	LOSS MOD	ETA'	TANDEL	TORQUE	G*	ETA*	RAD FREQ
1.46E+06	8.70E+05	2.18E+03	.597	8.09E+02	1.70E+06	4.26E+03	3.98E+02
1.23E+06	7.08E+05	2.82E+03	.575	6.52E+02	1.42E+06	5.65E+03	2.51E+02
1.05E+06	6.13E+05	3.87E+03	.586	5.81E+02	1.21E+06	7.66E+03	1.59E+02
8.83E+05	5.49E+05	5.48E+03	.621	6.09E+02	1.04E+06	1.04E+04	1.00E+02
7.37E+05	4.89E+05	7.75E+03	.664	7.11E+02	8.84E+05	1.40E+04	6.31E+01
6.06E+05	4.32E+05	1.09E+04	.713	9.01E+02	7.44E+05	1.87E+04	3.98E+01
4.91E+05	3.78E+05	1.51E+04	.771	1.24E+03	6.19E+05	2.47E+04	2.51E+01
3.90E+05	3.28E+05	2.07E+04	.840	1.57E+03	5.09E+05	3.21E+04	1.59E+01
3.05E+05	2.80E+05	2.80E+04	.918	1.60E+03	4.14E+05	4.14E+04	1.00E+01
2.34E+05	2.36E+05	3.74E+04	1.010	1.39E+03	3.32E+05	5.26E+04	6.31E+00
1.75E+05	1.96E+05	4.91E+04	1.117	1.13E+03	2.63E+05	6.59E+04	3.98E+00
1.28E+05	1.59E+05	6.34E+04	1.241	9.06E+02	2.04E+05	8.14E+04	2.51E+00
9.20E+04	1.27E+05	8.02E+04	1.382	7.11E+02	1.57E+05	9.90E+04	1.59E+00
6.37E+04	9.97E+04	9.96E+04	1.566	5.47E+02	1.18E+05	1.18E+05	1.00E+00
4.25E+04	7.65E+04	1.21E+05	1.798	4.13E+02	8.75E+04	1.39E+05	6.31E-01
2.75E+04	5.73E+04	1.44E+05	2.084	3.04E+02	6.36E+04	1.60E+05	3.98E-01
1.71E+04	4.20E+04	1.67E+05	2.454	2.19E+02	4.54E+04	1.81E+05	2.51E-01
1.02E+04	3.01E+04	1.90E+05	2.944	1.55E+02	3.18E+04	2.00E+05	1.59E-01
5.82E+03	2.10E+04	2.10E+05	3.616	1.07E+02	2.18E+04	2.18E+05	1.00E-01
3.15E+03	1.44E+04	2.28E+05	4.561	7.21E+01	1.47E+04	2.33E+05	6.31E-02
1.62E+03	9.61E+03	2.41E+05	5.947	4.79E+01	9.75E+03	2.45E+05	3.98E-02
7.76E+02	6.30E+03	2.51E+05	8.111	3.12E+01	6.35E+03	2.53E+05	2.51E-02

C(1)	C(2)	C(3)	C(0)	COR.COEFF.	LN W VS. LN GPP
1.506E+01	-1.491E+00	5.324E-02	-5.694E+01	9.996E-01	

C(1)	C(2)	C(3)	C(0)	COR.COEFF.	TAND VS. LN G*
-2.467E+00	4.276E-01	-2.556E-02	1.467E+01	9.969E-01	

C(1)	C(0)	COR.COEFF.	LN GP=C1*LN GPP+C0
1.697E+00	-8.439E+00	9.998E-01	

C(1)	C(2)	C(0)	COR.COEFF	LN GP=C1*LN GPP +C2*LN(GPP**2)+C0
2.003E+00	-2.037E-02	-9.274E+00	9.999E-01	

C(1)	C(2)	C(0)	Mean-Err	LN GP=C1*LN Gs +C2*LN(Gs**2)+C0
2.671E+00	-5.741E-02	-1.230E+01	9.237E-03	

RDI= 1.89E+00 ER= 7.26E-01 SLOPE= 1.70E+00 GCOM= 2.29E+05 COW= 6.25E+00
ET= 7.18E+00
ETA*1000 = 2.294E+03 , Mean-%Error = 4.61E-01 (ETA* extrapolation)
ETA'1000 = 1.209E+03 , Mean-%Error = 1.24E+00 (G" extrapolation)
PDL = 2.25E+01 , Mean-%Error = 9.32E+00
PDR = 6.339E+00, PDH = 6.616E+00, Visc: 3.821E+05 2.094E+05 3.165E+04
PI= 5.42E+00 Modsep= 4.71E+00
NO OF POINTS = 22 NIMIN= 2 AB = .81800
SLOPE OF ETA ZERO-GAMMA DOT ZERO = .8820

RHEOLOGICAL PARAMETERS
AB = .818 A = 3.000 B = .273 D = 6.934E-01
RDR = 3.197E+00 ETA ZERO = 5.328E+05 GAMMA DOT ZERO = 2.707E+00
STD ERROR, FIT = 6.352E-02

RHEOLOGICAL PARAMETERS
AB = .818 A = 2.366 B = .346 D = 1.062E+00
RDR = 4.895E+00 ETA ZERO = 3.503E+05 GAMMA DOT ZERO = 2.687E+00
STD ERROR, FIT = 1.446E-02
RDR_new = 1.945E+00 (at ETA/ETA0= .1375)

NA345-009 A94-00153 190C 20% 50mm LD618

STO MOD	LOSS MOD	ETA'	TANDEL	TORQUE	G*	ETA*	RAD FREQ
9.39E+05	6.66E+05	1.67E+03	.710	7.45E+02	1.15E+06	2.89E+03	3.98E+02
7.66E+05	5.48E+05	2.18E+03	.715	5.95E+02	9.42E+05	3.75E+03	2.51E+02
6.24E+05	4.70E+05	2.97E+03	.753	5.34E+02	7.82E+05	4.93E+03	1.59E+02
5.03E+05	4.04E+05	4.04E+03	.804	5.53E+02	6.46E+05	6.46E+03	1.00E+02
4.00E+05	3.47E+05	5.50E+03	.868	6.36E+02	5.29E+05	8.39E+03	6.31E+01
3.11E+05	2.94E+05	7.39E+03	.945	8.08E+02	4.28E+05	1.08E+04	3.98E+01
2.37E+05	2.46E+05	9.80E+03	1.037	1.08E+03	3.42E+05	1.36E+04	2.51E+01
1.77E+05	2.03E+05	1.28E+04	1.146	1.18E+03	2.69E+05	1.70E+04	1.59E+01
1.29E+05	1.64E+05	1.64E+04	1.278	1.00E+03	2.09E+05	2.09E+04	1.00E+01
9.14E+04	1.31E+05	2.07E+04	1.430	7.71E+02	1.59E+05	2.53E+04	6.31E+00
6.28E+04	1.02E+05	2.56E+04	1.620	5.78E+02	1.20E+05	3.00E+04	3.98E+00
4.19E+04	7.76E+04	3.09E+04	1.852	4.26E+02	8.82E+04	3.51E+04	2.51E+00
2.71E+04	5.79E+04	3.65E+04	2.133	3.10E+02	6.40E+04	4.03E+04	1.59E+00
1.68E+04	4.22E+04	4.22E+04	2.513	2.22E+02	4.55E+04	4.55E+04	1.00E+00
9.99E+03	3.01E+04	4.77E+04	3.014	1.55E+02	3.17E+04	5.03E+04	6.31E-01
5.67E+03	2.10E+04	5.27E+04	3.701	1.07E+02	2.17E+04	5.46E+04	3.98E-01
3.07E+03	1.43E+04	5.70E+04	4.659	7.19E+01	1.46E+04	5.83E+04	2.51E-01
1.59E+03	9.57E+03	6.04E+04	6.036	4.77E+01	9.70E+03	6.12E+04	1.59E-01
7.83E+02	6.29E+03	6.29E+04	8.038	3.12E+01	6.34E+03	6.34E+04	1.00E-01
3.64E+02	4.08E+03	6.46E+04	11.190	2.01E+01	4.09E+03	6.49E+04	6.31E-02
1.64E+02	2.61E+03	6.57E+04	15.992	1.29E+01	2.62E+03	6.58E+04	3.98E-02
8.04E+01	1.67E+03	6.64E+04	20.744	8.21E+00	1.67E+03	6.65E+04	2.51E-02

C(1)	C(2)	C(3)	C(0)	COR.COEFF.	LN W VS. LN GPP
8.523E+00	-8.611E-01	3.304E-02	-3.305E+01	9.999E-01	

C(1)	C(2)	C(3)	C(0)	COR.COEFF.	TAND VS. LN G*
-1.272E+00	1.027E-01	-2.657E-03	1.361E+01	9.876E-01	

C(1)	C(0)	COR.COEFF.	LN GP=C1*LN GPP+C0
1.770E+00	-9.068E+00	9.998E-01	

C(1)	C(2)	C(0)	COR.COEFF	LN GP=C1*LN GPP +C2*LN(GPP**2)+C0
2.209E+00	-3.043E-02	-1.034E+01	1.000E+00	

C(1)	C(2)	C(0)	Mean-Err	LN GP=C1*LN Gs +C2*LN(Gs**2)+C0
2.681E+00	-5.800E-02	-1.236E+01	1.186E-02	

RDI= 1.84E+00 ER= 7.23E-01 SLOPE= 1.77E+00 GCOM= 2.64E+05 COW= 3.09E+01
ET= 6.62E+00
ETA*1000 = 1.629E+03 , Mean-%Error = 3.85E-01 (ETA* extrapolation)
ETA'1000 = 9.175E+02 , Mean-%Error = 7.94E-01 (G" extrapolation)
PDL = 1.56E+01 , Mean-%Error = 4.32E+00
PDR = 7.465E+00, PDH = 7.795E+00, Visc: 8.047E+04 4.177E+04 5.359E+03
PI= 5.69E+00 Modsep= 4.93E+00
NO OF POINTS = 22 NIMIN= 2 AB = .81800
SLOPE OF ETA ZERO-GAMMA DOT ZERO = .8820

RHEOLOGICAL PARAMETERS
AB = .818 A = 3.000 B = .273 D = 4.805E-01
RDR = 2.787E+00 ETA ZERO = 1.100E+05 GAMMA DOT ZERO = 1.892E+01
STD ERROR, FIT = 7.588E-02

RHEOLOGICAL PARAMETERS
AB = .818 A = 2.285 B = .358 D = 1.024E+00
RDR = 5.636E+00 ETA ZERO = 8.077E+04 GAMMA DOT ZERO = 1.209E+01
STD ERROR, FIT = 2.321E-02
RDR_new = 2.013E+00 (at ETA/ETA0= .1375)

NA960-000 A94-00147 190C 20% 50mm LD621

STO MOD	LOSS MOD	ETA'	TANDEL	TORQUE	G*	ETA*	RAD FREQ
7.95E+05	5.22E+05	1.31E+03	.656	8.01E+02	9.51E+05	2.39E+03	3.98E+02
6.59E+05	4.27E+05	1.70E+03	.649	6.28E+02	7.85E+05	3.13E+03	2.51E+02
5.49E+05	3.66E+05	2.31E+03	.667	5.63E+02	6.60E+05	4.16E+03	1.59E+02
4.58E+05	3.13E+05	3.13E+03	.683	5.69E+02	5.54E+05	5.54E+03	1.00E+02
3.79E+05	2.69E+05	4.26E+03	.709	6.40E+02	4.65E+05	7.37E+03	6.31E+01
3.12E+05	2.30E+05	5.79E+03	.739	8.01E+02	3.88E+05	9.74E+03	3.98E+01
2.54E+05	1.96E+05	7.82E+03	.774	1.03E+03	3.21E+05	1.28E+04	2.51E+01
2.05E+05	1.67E+05	1.05E+04	.815	1.10E+03	2.64E+05	1.67E+04	1.59E+01
1.64E+05	1.41E+05	1.41E+04	.858	9.82E+02	2.16E+05	2.16E+04	1.00E+01
1.30E+05	1.18E+05	1.87E+04	.906	8.10E+02	1.76E+05	2.78E+04	6.31E+00
1.02E+05	9.81E+04	2.46E+04	.964	6.55E+02	1.41E+05	3.55E+04	3.98E+00
7.87E+04	8.10E+04	3.22E+04	1.029	5.26E+02	1.13E+05	4.49E+04	2.51E+00
6.01E+04	6.61E+04	4.17E+04	1.100	4.19E+02	8.93E+04	5.64E+04	1.59E+00
4.49E+04	5.35E+04	5.35E+04	1.192	3.31E+02	6.99E+04	6.99E+04	1.00E+00
3.29E+04	4.28E+04	6.79E+04	1.303	2.58E+02	5.40E+04	8.56E+04	6.31E-01
2.35E+04	3.38E+04	8.50E+04	1.442	1.98E+02	4.12E+04	1.03E+05	3.98E-01
1.63E+04	2.63E+04	1.05E+05	1.611	1.50E+02	3.09E+04	1.23E+05	2.51E-01
1.10E+04	2.01E+04	1.27E+05	1.823	1.12E+02	2.29E+04	1.45E+05	1.59E-01
7.17E+03	1.51E+04	1.51E+05	2.100	8.15E+01	1.67E+04	1.67E+05	1.00E-01
4.47E+03	1.10E+04	1.75E+05	2.470	5.83E+01	1.19E+04	1.89E+05	6.31E-02
2.65E+03	7.89E+03	1.98E+05	2.981	4.09E+01	8.33E+03	2.09E+05	3.98E-02
1.49E+03	5.51E+03	2.20E+05	3.710	2.80E+01	5.71E+03	2.27E+05	2.51E-02

C(1)	C(2)	C(3)	C(0)	COR.COEFF.	LN W VS. LN GPP
-3.807E+00	3.137E-01	-2.439E-03	7.432E+00	9.999E-01	

C(1)	C(2)	C(3)	C(0)	COR.COEFF.	TAND VS. LN G*
-6.393E+00	2.203E+00	-2.680E-01	1.612E+01	9.973E-01	

C(1)	C(0)	COR.COEFF.	LN GP=C1*LN GPP+C0
1.613E+00	-6.829E+00	9.998E-01	

C(1)	C(2)	C(0)	COR.COEFF	LN GP=C1*LN GPP +C2*LN(GPP**2)+C0
2.445E+00	-4.849E-02	-1.016E+01	1.000E+00	

C(1)	C(2)	C(0)	Mean-Err	LN GP=C1*LN Gs +C2*LN(Gs**2)+C0
2.310E+00	-4.875E-02	-8.992E+00	1.389E-02	

RDI= 2.45E+00 ER= 1.79E+00 SLOPE= 1.61E+00 GCOM= 8.59E+04 COW= 2.98E+00
ET= 2.53E+01
ETA*1000 = 1.350E+03 , Mean-%Error = 2.77E-01 (ETA* extrapolation)
ETA'1000 = 7.419E+02 , Mean-%Error = 5.51E-01 (G" extrapolation)
PDL = 3.55E+01 , Mean-%Error = 6.43E+00
PDR = 3.574E+01, PDH = 2.680E+01, Visc: 3.332E+05 9.191E+04 3.429E+03
PI= 1.32E+01 Modsep= 3.34E+00
NO OF POINTS = 22 NIMIN= 2 AB = .81800
SLOPE OF ETA ZERO-GAMMA DOT ZERO = .8820
RHEOLOGICAL PARAMETERS
AB = .818 A = 3.000 B = .273 D = 2.046E+00
RDR = 8.319E+00 ETA ZERO = 5.247E+05 GAMMA DOT ZERO = 9.314E-01
STD ERROR, FIT = 2.400E-02
RHEOLOGICAL PARAMETERS
AB = .818 A = 3.133 B = .261 D = 1.928E+00
RDR = 7.788E+00 ETA ZERO = 5.888E+05 GAMMA DOT ZERO = 8.809E-01
STD ERROR, FIT = 2.293E-02
RDR_new = 9.623E+00 (at ETA/ETA0= .1375)